Novel particles for image-guided cancer therapy

Chris Oerlemans

Dissertation, Utrecht University, The Netherlands

ISBN: 978-90-902-7430-0

Cover design	Kerry Randolph, Phoenix, Arizona, USA
Lay out	Karin van Rijnbach
Printed by	Ipskamp Drukkers BV, Enschede, The Netherlands

Financial support for the reproduction of this thesis was generously provided by:

ALV, Avanti Polar Lipids, Büchi, GeniaLab, Guerbet, Ina Veenstra-Rademaker Stichting, Mallinckrodt Nederland BV, Lipiod, Metall Rare Earth, Röntgenstichting, Laboratoires SERB SAS.

Novel particles for image-guided cancer therapy

Nieuwe partikels voor beeldgestuurde kankertherapie
(met een samenvatting in het Nederlands)

Proefschrift

ter verkrijging van de graad van doctor
aan de Universiteit Utrecht
op gezag van rector magnificus, prof. dr. G.J. van der Zwaan,
ingevolge het besluit van het college voor promoties
in het openbaar te verdedigen
op donderdag 23 mei 2013 des middags te 2:30

door

Chris Oerlemans

geboren op 31-07-1983 te Kapelle

Promotoren:	Prof. dr. ir. W.E. Hennink Prof. dr. ir. P.R. Luijten
Copromotor:	Dr. J.F.W. Nijsen

Voor mijn ouders

Luctor et Emergo (Ik worstel en kom boven)

Provincie Zeeland (1586)

CONTENTS

Chapter 1

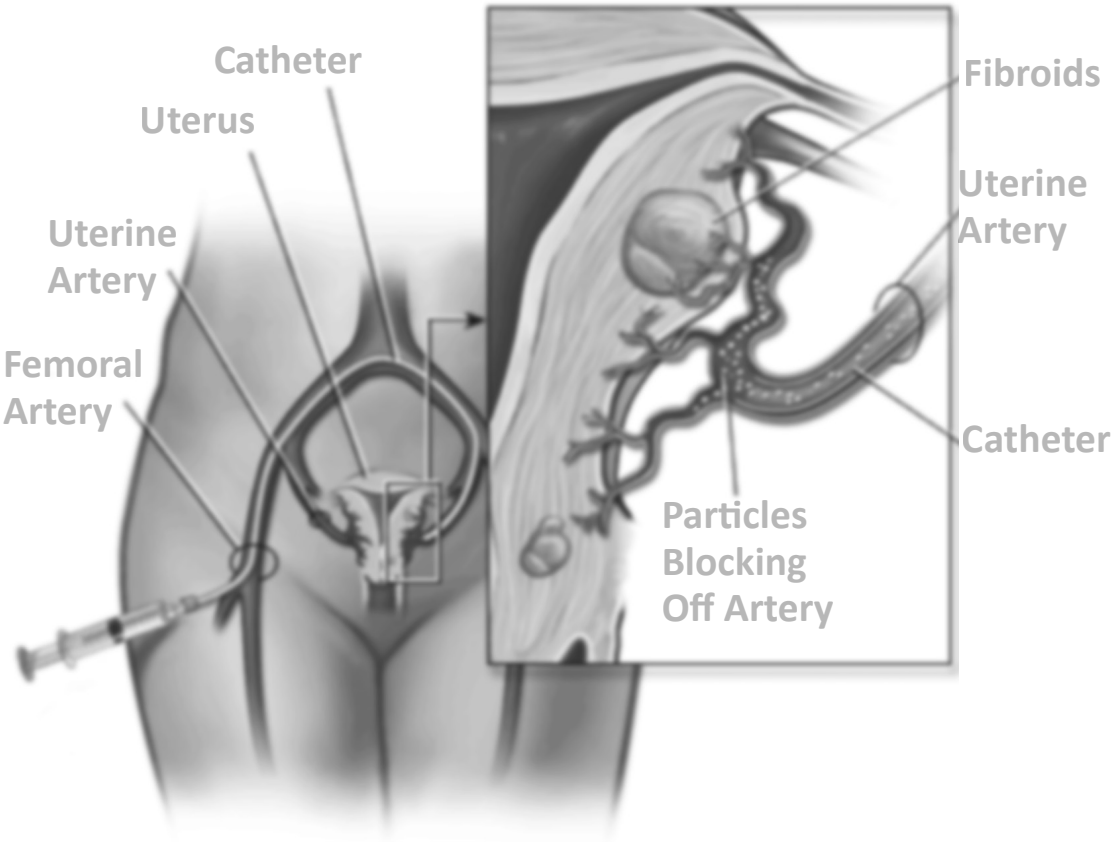
Catheter
Uterus
Uterine Artery
Femoral Artery
Fibroids
Uterine Artery
Catheter
Particles Blocking Off Artery

General introduction and outline of thesis

GENERAL INTRODUCTION

Tumor resection, external beam radiation therapy and chemotherapy are still the most frequently applied treatments options for cancer treatment. However, these conventional therapies are often not able to cure the patient. Tumor resection and external beam radiation are regularly hindered by tumor location, tumor size and blood supply, while the presence of metastases further complicates removal of all tumor tissue. Furthermore, resection may lead to mutilation of the body and comorbidity, for instance in radical mastectomy and extensive lymph node resections, where partial or complete breast removal is regularly accompanied by the removal of the overlying skin, the muscles beneath the breast and the axillary lymph nodes. Parenteral administration of chemotherapeutic drugs does not only affect the tumor tissue, but also results in systemic toxicity, often resulting in side effects and low efficacy. The knowledge concerning tumor pathology has significantly increased over the last decades. Currently, it is known that the susceptibility of tumor tissue to chemotherapeutic agents is dependent on tumor origin, genetics and biological diversity. Therefore, a great extent of research is conducted to develop new treatment options aimed at personalized therapies and local drug delivery to tumors. Ideally, successful tumor targeting will lead to a high tumor-to-normal-tissue ratio, enhancing treatment efficacy while toxicity and side effects are reduced [1, 2].

NANOPARTICLES

One of the most promising developments for local cancer therapy is drug delivery with small particles containing a therapeutic agent. Nanoparticles have an average size from a few nanometer (nm) up to several hundred nm. In 1986, Matsumura and Maeda discovered that nano-sized particles accumulated in tumor tissue much more as compared to normal tissue [3]. Diffusion of nutrients and oxygen is hampered when the tumor reaches a size of around 2-3 mm; therefore the formation of neovasculature is necessary for the tumor tissue to grow beyond the diffusion threshold. Tumor angiogenesis usually results in neovasculature made of poorly aligned defective endothelial cells containing wide fenestrations and lacking smooth muscle innervations. Additionally, solid tumors usually produce extensive amounts of various vascular permeability factors. Therefore, most solid tumors exhibit enhanced vascular permeability, which will ensure a sufficient supply of nutrients

and oxygen to the tumor tissue, allowing rapid growth. The 'leaky' vasculature of tumor tissue allows particles up to 700 nm to extravasate and lodge in and around the tumor tissue (Fig. 1) [3], which is called the enhanced permeability and retention (EPR) effect [4-6]. Well-known examples of nanoparticles are micelles and liposomes. Micelles are colloidal particles with a size usually between 5-100 nm [8]. Micelles consist of amphiphiles or surface-active agents (surfactants), which exist of two distinct regions: mostly a hydrophilic head-group and a hydrophobic tail. At low concentrations in an aqueous medium, the amphiphiles exist as monomers, but when the concentration increases, aggregation and self-assembly above a certain concentration (referred to as the CMC, critical micelle concentration) occurs, and micelles are formed [9]. Hydrophobic drugs can be loaded within the hydrophobic core of micelles. Liposomes are spherical particles, usually within the range of 50-200 nm, and consist of a phospholipid bilayer surrounding an aqueous core [10]. Hydrophilic drugs can be dissolved in the aqueous core, while lipophilic drugs can be solubilized in the phospholipid bilayer. Both micelles and liposomes protect the

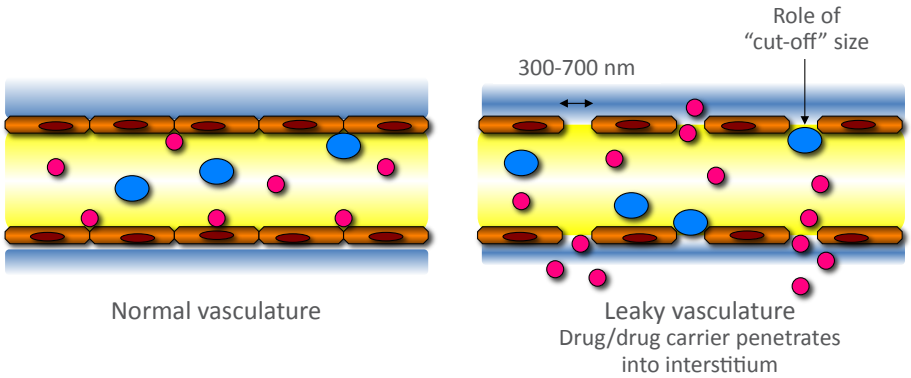

Fig. 1. The enhanced permeability and retention (EPR) effect. Healthy vasculature displays a regular shape with finely aligned endothelial cells. In tumor vessels, a defective architecture, wide fenestrations between the endothelial cells and impaired drainage is observed, providing an increased permeability to macromolecules and nanoparticles such as liposomes and polymeric micelles, enabling particle accumulation within the tumor tissue [7].

encapsulated drugs from exposure to its environment, slowing down degradation and increasing local drug delivery [11-15]. Moreover, targeting ligands and imaging moieties can be encapsulated in or chelated to micelles and liposomes, making them versatile drug delivery systems [11, 16, 17]. Targeting ligands enable specific binding to the tumor tissue, hence aiming at increased drug delivery. Imaging modalities such as computed tomography (CT), magnetic resonance imaging (MRI) and nuclear imaging techniques such as single photon emission computed tomography (SPECT), positron emitting tomography (PET), and optical imaging techniques such as bioluminescence with fluorescent or near-infrared fluorophores allow real-time monitoring of nanoparticles loaded with contrast agents in the body.

TRIGGERED RELEASE

A more recent development of advanced local drug delivery to obtain high drug concentrations at the tumor site and subsequent increase in efficacy of the therapy

is triggered release from drug-loaded particles. A promising technique for triggered drug release is high-intensity focused ultrasound (HIFU). Ultrasound is a sound pressure wave with a frequency higher than 20 kHz. This ultrasound beam can be focused in a small spatial region in tissue. Consequently, high levels of acoustic energy are generated which are absorbed by the tissue, resulting in a local temperature increase up to 60 °C in clinical practice. HIFU is already clinically used for the ablation of uterine fibroids. Clinical trials are underway for the treatment of several benign and malignant tumors of the prostate, breast, uterus, liver, kidney, pancreas, bone, and brain [18]. For these therapies, HIFU can be combined with magnetic resonance imaging (MRI). This way, real-time patient imaging and thermometry for temperature feedback is merged, which enables a safer and more efficient treatment. Moreover, HIFU also enables triggered release of drugs from thermosensitive particles due to the temperature elevation produced by the ultrasound beam. However, temperature elevation up to 60 °C is undesired for HIFU-triggered drug release, because it may result in thermal damage of healthy tissue. Exposure of tissue to pulsed wave- (PW) HIFU, in which shorter pulses are given in combination with short duty cycles (i.e. repeatedly 100 μs 'on-time' and 900 μs 'off-time'), results in lower temperature elevation (from 37 °C to 42 °C) as compared to continuous wave- (CW) HIFU and therefore circumvents thermal damage [19]. Liposomes can be rendered thermosensitive by the introduction of phospholipids displaying a gel-to-liquid transition temperature (T_m) around 42 °C, such as 1,2-dipalmitoyl-*sn*-glycero-3-phosphocholine (DPPC). When the T_m of the thermosensitive liposomes is exceeded due to (PW-)HIFU exposure, their water-soluble content is released as a consequence of conformational changes in the alkyl chains of the phospholipids [20, 21], resulting in local drug delivery to the tumor tissue. Beside temperature elevation, also non-thermal effects are associated with HIFU exposure, for instance acoustic cavitation, which is the formation and/or activation of gas-filled bubbles in a medium [22]. The sustained growth of bubbles and their oscillations over several acoustic cycles is known as non-inertial cavitation, whereas the violent growth and immediate collapse of bubbles is called inertial cavitation [23]. Cavitation can result in the formation of transient pores in the plasma membrane of individual cells and alter the permeability of blood vessels and, therefore, improve drug or gene delivery to the targeted tissue [24].

MICROSPHERES

Another promising treatment modality for efficient tumor targeting is embolotherapy. This therapy has gained an important position for the treatment of a wide variety of conditions affecting different organs of the human body, such as uterine fibroids, arteriovenous malformations (AVM), kidney and liver tumors [25, 26]. This therapy involves the administration of particles with a size between 15-1200 μm into the tumor-feeding artery by catheterization [27]. Embolization particles preferably have a spherical shape with a narrow size distribution to ensure uniform artery occlusion with a predictable penetration depth [28, 29]. During an embolization procedure, a catheter is advanced intra-arterially to the desired location under fluoroscopy-guidance using radiopaque contrast medium. Next, the particles are infused which results in a reduction or complete obstruction of the blood flow. This causes a lack of nutrients and oxygen and finally to necrosis of the affected tissue. An embolization procedure for the treatment of uterine fibroids is illustrated in Fig. 2. Beside bland

embolization, embolization particles can be loaded with chemotherapeutic agents to increase the efficacy of the therapy. Different drug-eluting beads (DEB) [30] loaded with doxorubicin [31] or irinotecan have been developed [32]. Once the beads are administered and occlude the artery, a local release of the drug from the beads occurs, resulting in exposure of the tumors to the drug. The currently developed DEB are mainly used for the treatment of hepatocellular carcinoma (HCC). A different application of embolotherapy is radioembolization, which is currently used to treat HCC and colorectal liver metastasis [33]. Radioembolization combines lodging of the particles in the tumor vasculature, with radioactivity, resulting in internal radiation of tumor tissue. The hepatic artery supplies 80-100% of the blood to liver tumors, while over 70% of blood to the normal liver parenchyma is delivered by the portal system [34]. Embolization of the hepatic artery, therefore, allows selective targeting of the tumor tissue. Several types of radioactive microspheres have been developed for selective internal radiation therapy (SIRT), such as glass or resin microspheres bearing the radioactive element yttrium-90 (^{90}Y) [35, 36] and holmium-166 (^{166}Ho) poly(L-lactic acid) (PLLA) microspheres [37]. The ^{166}Ho-PLLA microspheres, which were developed at University Medical Center Utrecht, the Netherlands, can be visualized with MRI, as opposed to the ^{90}Y microsphere formulations, which enables post-procedural feedback and dosimetry calculations for a more safe and controlled therapy. For radioactive embolization particles, it is imperative that the microspheres lodge around the tumor with great proximity, due to the mean tissue range of the radioactive isotopes (3-4 mm) [33], to maximize the radiation effect while minimizing toxicity to the surrounding healthy tissue. Therefore, the mean size of these microspheres is around 30 μm, considerably smaller than several bland embolotherapy agents of which the size can be selected depending on the treatment strategy.

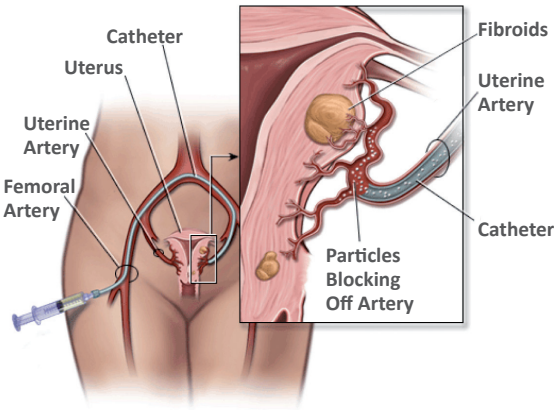

Fig. 2. Bland embolization of uterine fibroids using microparticles. A catheter is introduced into the femoral artery and advanced to the tumor feeding artery. Next, the microparticles are injected which occlude the artery leading to obstruction of the blood flow and subsequent necrosis of the afferent tissue.

MULTIMODALITY IMAGING

For preclinical research, it is essential that newly developed particles can be visualized using medical imaging techniques to study the particle characteristics *in vitro* and to allow biodistribution studies *in vivo*. For patient care, different medical imaging techniques are used mainly for differential diagnosis. However, for safe and successful local treatment, i.e. during embolization procedures, real-time intra-procedural and post-procedural follow-up is crucial. Several medical imaging techniques are

available to meet these demands, such as magnetic resonance imaging (MRI), X-ray based imaging, i.e. fluoroscopy, computed tomography (CT), ultrasound imaging (ultrasonography) and nuclear imaging techniques like single photon emission computed tomography (SPECT) and positron emission tomography (PET). MR imaging is based on the detection of magnetization of hydrogen nuclei (^{1}H) in a strong magnetic field after application of radiofrequency pulses. Contrast agents used for ^{1}H MRI are usually (para)magnetic elements, such as iron, manganese, gadolinium and holmium. These elements locally alter the magnetization of hydrogen nuclei, thereby enhancing the contrast [38, 39]. For X-ray imaging, a generator is used to produce a beam of X-rays which is projected towards an object. The detector captures the radiation behind the object, resulting in a 2-D projection image. The X-ray absorbance within the object depends on its density and composition and allows the discrimination of different structures. Fluoroscopy is frequently used to obtain real-time images of the internal structures of a patient during a clinical intervention to provide the surgeon with direct feedback. CT uses radiation to generate a 3-D reconstruction of the object or patient and is regularly utilized for the diagnosis of cancer, but can also be used for post-procedural follow-up. Contrast enhancement to outline structures in the body with CT can be achieved using radiopaque contrast agents such as iodine, bromine and barium [40]. Nuclear imaging exploits the increased metabolism associated with tumor tissue to locate malignant tissue in the patient and allows for the visualization of diminutive amounts of gamma-emitting isotopes [14], i.e. technetium-99m (^{99m}Tc), indium-111 (^{111}In) and iodine-125 (^{125}I) for SPECT imaging or positron-emitting isotopes for PET imaging, such as fluorine-18 (^{18}F), copper-64 (^{64}Cu) and zirconium-89 (^{89}Zr). Different particles loaded with contrast agents are currently under development or already in clinical trials. Examples of preclinically investigated imageable micelles are discussed in Chapter 2 of this dissertation [11]. Until now, no micelle formulation with imaging possibilities has yet entered clinical trials. Chelation of gadolinium to the liposomal bilayer or introduction of gadolinium in the aqueous core of the liposomes enabled MR imaging of liposomes [41-43]. Inclusion of iodine allowed *in vivo* CT imaging of liposomes [44]. The use of gas-filled (e.g. air or perfluorocarbon) microbubbles allows contrast-enhanced ultrasound (CEUS) imaging [45]. Due to a high degree of echogenicity (the ability to reflect ultrasound waves), utilization of microbubbles result in a contrast-enhanced image of the area of interest. Preclinical research demonstrated that ultrasound exposure can result in microbubble disruption and subsequently enhanced drug or gene delivery, as was shown for example with paclitaxel and different drug model compounds, plasmid DNA and synthetic oligonucleotides, such as antisense or siRNA [46, 47]. For SPECT imaging, ^{111}In-, ^{67}Ga- and ^{99m}Tc-loaded liposomes were developed [48-50]. Liposomes containing ^{18}F were developed for PET imaging [51]. However, in addition to micelles, only preclinical studies have yet been performed for imageable liposomes. Preclinical research has been conducted with alginate microspheres crosslinked with different lanthanide elements for MR imaging [52]. Moreover, preclinical research on holmium-alginate microspheres containing a lipiodol emulsion allowing additional CT visualization beside MR imaging is described in Chapter 6 of this dissertation. Other examples of preclinical microsphere formulations that can be visualized with MR and/or CT imaging include microspheres loaded with iron oxide (MRI), barium and iodine (CT) [53-56]. One microsphere formulation, ^{166}Ho-PLLA microspheres, which allow visualization by MRI and SPECT [57, 58], has now reached a clinical phase 2 trial for the treatment of unresectable liver metastases [37].

OUTLINE

The aim of the work described in this thesis is the development of novel particles for image-guided cancer therapy. The development, characterization and evaluation of micelles, liposomes and microspheres for advanced targeted cancer treatment, combining imaging with therapy and/or triggered release, is described. Following this introductory chapter, **Chapter 2** provides an overview of the current clinical status of polymeric micelles in cancer therapy and discusses the possibilities to optimize the micelle composition by the introduction of targeting ligands, imaging moieties and modifications of the micelles which enable triggered release of the encapsulated compounds. In **Chapter 3**, new insights into triggered release of a lipophilic compound (Nile red) from non-crosslinked (NCL) and core-crosslinked (CCL) micelles upon exposure to continuous wave- (CW) HIFU and pulsed wave- (PW) HIFU high-intensity focused ultrasound (HIFU) are provided. Moreover, evidence for a new mechanism behind HIFU-triggered release of both hydrophilic and lipophilic compounds from thermosensitive as well as non-thermosensitive liposomes is presented. **Chapter 4** describes the development of thermosensitive liposomes containing a fluorescent label, which is released after the application of magnetic resonance-guided (MR-)HIFU. These liposomes can be exploited as a new tool for efficient surgical resection of non-palpable breast tumor lesions by enabling proper discrimination between tumor tissue and adjacent healthy tissue. **Chapter 5** reports on the development and characterization of different alginate-lanthanide microsphere formulations and discusses the implementation of these microspheres for MRI-guided embolotherapy, which was assessed both *in vitro* and *ex vivo*. In **Chapter 6**, a novel holmium-alginate microsphere formulation containing lipiodol for multimodality image-guided embolotherapy is described. The microspheres can be visualized during an embolization procedure with fluoroscopy and post-procedural the biodistribution of the microspheres can be assessed with X-ray imaging and MRI. **Chapter 7** presents a summary of the previous chapters and considers future directions of the particles developed and studied in this dissertation and discusses the benefits of a combined approach when merging targeted drug delivery, triggered drug release and multimodality imaging in cancer therapy.

REFERENCES

1. Varde NK, Pack DW. Microspheres for controlled release drug delivery. Expert Opin Biol Ther. 2004;4:35-51.
2. Peer D, Karp JM, Hong S, Farokhzad OC, Margalit R, Langer R. Nanocarriers as an emerging platform for cancer therapy. Nat Nanotechnol. 2007;2:751-60.
3. Matsumura Y, Maeda H. A new concept for macromolecular therapeutics in cancer chemotherapy: mechanism of tumoritropic accumulation of proteins and the antitumor agent smancs. Cancer Res. 1986;46:6387-92.
4. Torchilin V. Tumor delivery of macromolecular drugs based on the EPR effect. Adv Drug Deliv Rev. 2011;63:131-35.
5. Maeda H. Macromolecular therapeutics in cancer treatment: The EPR effect and beyond. J Control Release. 2012:164:138-44.
6. Greish K. Enhanced permeability and retention of macromolecular drugs in solid tumors: a royal gate for targeted anticancer nanomedicines. J Drug Target. 2007;15:457-64.
7. Lembo D, Cavalli R. Nanoparticulate delivery systems for antiviral drugs. Antivir Chem Chemother. 2010;21:53-70.
8. Oerlemans C, Bult W, Bos M, Storm G, Nijsen JF, Hennink WE. Polymeric micelles in anticancer therapy: targeting, imaging and triggered release. Pharm Res. 2010;27:2569-89.
9. Torchilin VP. Micellar nanocarriers: pharmaceutical perspectives. Pharm Res. 2007;24:1-16.
10. Torchilin VP. Recent advances with liposomes as pharmaceutical carriers. Nat Rev Drug Discov. 2005;4:145-60.
11. Maeda H, Wu J, Sawa T, Matsumura Y, Hori K. Tumor vascular permeability and the EPR effect in macromolecular therapeutics: a review. J Control Release. 2000;65:271-84.
12. Allen TM, Hansen C, Martin F, Redemann C, Yau-Young A. Liposomes containing synthetic lipid derivatives of poly(ethylene glycol) show prolonged circulation half-lives in vivo. Biochim Biophys Acta. 1991;1066:29-36.
13. Papahadjopoulos D, Allen TM, Gabizon A, Mayhew E, Matthay K, Huang SK, Lee KD, Woodle MC, Lasic DD, Redemann C. Sterically stabilized liposomes: improvements in pharmacokinetics and antitumor therapeutic efficacy. Proc Natl Acad Sci USA. 1991;88:11460-4.
14. Torchilin VP. PEG-based micelles as carriers of contrast agents for different imaging modalities. Adv Drug Deliv Rev. 2002;54:235-52.
15. Klibanov AL, Maruyama K, Torchilin VP, Huang L. Amphipathic polyethyleneglycols effectively prolong the circulation time of liposomes. FEBS Lett. 1990;268:235-7.
16. Torchilin VP. Multifunctional nanocarriers. Adv Drug Deliv Rev. 2006;58:1532-55.
17. Torchilin VP. Targeted pharmaceutical nanocarriers for cancer therapy and imaging. AAPS J. 2007;9:E128-47.
18. Al-Bataineh O, Jenne J, Huber P. Clinical and future applications of high intensity focused ultrasound in cancer. Cancer Treat Rev. 2012;38:346-53.
19. Dromi S, Frenkel V, Luk A, Traughber B, Angstadt M, Bur M, Poff J, Xie J, Libutti SK, Li KC, Wood BJ. Pulsed-high intensity focused ultrasound and low temperature-sensitive liposomes for enhanced targeted drug delivery and antitumor effect. Clin Cancer Res. 2007;13:2722-7.
20. Papahadjopoulos D, Jacobson K, Nir S, Isac T. Phase transitions in phospholipid vesicles. Fluorescence polarization and permeability measurements concerning the effect of temperature and cholesterol. Biochim Biophys Acta. 1973;311:330-48.
21. Yatvin MB, Weinstein JN, Dennis WH, Blumenthal R. Design of liposomes for enhanced local release of drugs by hyperthermia. Science. 1978;202:1290-3.
22. Apfel RE. Acoustic cavitation: a possible consequence of biomedical uses of ultrasound. Br J Cancer Suppl. 1982;5:140-6.
23. Wu J, Nyborg WL. Ultrasound, cavitation bubbles and their interaction with cells. Adv Drug Deliv Rev. 2008;60:1103-16.

24. Yudina A, Moonen C. Ultrasound-induced cell permeabilisation and hyperthermia: strategies for local delivery of compounds with intracellular mode of action. Int J Hyperthermia. 2012;28:311-9.
25. Ginat DT, Saad WE, Turba UC. Transcatheter renal artery embolization: clinical applications and techniques. Tech Vasc Interv Radiol. 2009;12:224-39.
26. Spies JB, Allison S, Flick P, McCullough M, Sterbis K, Cramp M, Bruno J, Jha R. Polyvinyl alcohol particles and tris-acryl gelatin microspheres for uterine artery embolization for leiomyomas: results of a randomized comparative study. J Vasc Interv Radiol. 2004;15:793-800.
27. Biosphere medical, http://www.biospheremed.com/publication_files/MR02-033-RevF-Embosphere.pdf, accessed on 10-30-12.
28. Rasuli P, Hammond I, Al-Mutairi B, French GJ, Aquino J, Hadziomerovic A, Goulet D, Jolly EE. Spherical versus conventional polyvinyl alcohol particles for uterine artery embolization. J Vasc Interv Radiol. 2008;19:42-6.
29. Chiesa AG, Hart WR. Uterine artery embolization of leiomyomas with trisacryl gelatin microspheres (TGM): pathologic features and comparison with polyvinyl alcohol emboli. Int J Gynecol Pathol. 2004;23:386-92.
30. Biocompatibles Ltd., http://www.biocompatibles.com/products/dcbead, accessed on 10-30-12.
31. Lewis AL, Holden RR. DC Bead embolic drug-eluting bead: clinical application in the locoregional treatment of tumours. Expert Opin Drug Deliv. 2011;8:153-69.
32. Lewis AL, Holden RR, Chung ST, Czuczman P, Kuchel T, Finnie J, Porter S, Foster D. Feasibility, safety and pharmacokinetic study of hepatic administration of drug-eluting beads loaded with irinotecan (DEBIRI) followed by intravenous administration of irinotecan in a porcine model. J Mater Sci: Mater Med. 2013;34:115-27.
33. Vente MA, Hobbelink MG, van het Schip AD, Zonnenberg BA, Nijsen JF. Radionuclide liver cancer therapies: from concept to current clinical status. Anticancer Agents Med Chem. 2007;7:441-59.
34. Breedis C, Young G. The blood supply of neoplasms in the liver. Am J Pathol. 1954;30:969-77.
35. Kennedy AS, Salem R. Radioembolization (yttrium-90 microspheres) for primary and metastatic hepatic malignancies. Cancer J. 2010;16:163-75.
36. Murthy R, Nunez R, Szklaruk J, Erwin W, Madoff DC, GuptaS, Ahrar K, Wallace MJ, Cohen A, Coldwell DM, Kennedy AS, Hicks ME. Yttrium-90 microsphere therapy for hepatic malignancy: devices, indications, technical considerations, and potential complications. Radiographics. 2005;25:S41-55.
37. Smits ML, Nijsen JF, van den Bosch MA, Lam MG, Vente MA, Mali WP, van het Schip AD, Zonnenberg BA. Holmium-166 radioembolisation in patients with unresectable, chemorefractory liver metastases (HEPAR trial): a phase 1, dose-escalation study. Lancet Oncol. 2012;13:1025-34.
38. Fossheim SL, Colet JM, Mansson S, Fahlvik AK, Muller RN, Klaveness J. Paramagnetic liposomes as magnetic resonance imaging contrast agents. Assessment of contrast efficacy in various liver models. Invest Radiol. 1998;33:810-21.
39. Seevinck PR, Seppenwoolde JH, de Wit TC, Nijsen JF, Beekman FJ, van het Schip AD, Bakker CJ. Factors affecting the sensitivity and detection limits of MRI, CT, and SPECT for multimodal diagnostic and therapeutic agents. Anticancer Agents Med Chem. 2007;7:317-34.
40. Zielhuis SW, Nijsen JF, Seppenwoolde JH, Zonnenberg BA, Bakker CJ, Hennink WE, van Rijk PP, van het Schip AD. Lanthanide bearing microparticulate systems for multi-modality imaging and targeted therapy of cancer. Curr Med Chem Anticancer Agents. 2005;5303-13.
41. Zielhuis SW, Seppenwoolde JH, Mateus VA, Bakker CJ, Krijger GC, Storm G, Zonnenberg BA, van het Schip AD, Koning GA, Nijsen JF. Lanthanide-loaded liposomes for multimodality imaging and therapy. Cancer Biother Radiopharm. 2006;21:520-27.

42. Grange C, Geninatti-Crich S, Esposito G, Alberti D, Tei L, Bussolati B, Aime S, Camussi G. Combined delivery and magnetic resonance imaging of neural cell adhesion molecule-targeted doxorubicin-containing liposomes in experimentally induced Kaposi's sarcoma. Cancer Res. 2010;70:2180-90.
43. Erdogan S, Medarova ZO, Roby A, Moore A.,Torchilin VP, Enhanced tumor MR imaging with gadolinium-loaded polychelating polymer-containing tumor-targeted liposomes. J Magn Reson Imaging. 2008;27:574-80.
44. Zheng J, Allen A, Serra S, Vines D, Charron M, Jaffray DA. Liposome contrast agent for CT-based detection and localization of neoplastic and inflammatory lesions in rabbits: validation with FDG-PET and histology. Contrast Media Mol Imaging. 2010;5:147-54.
45. Wilson SR, Greenbaum LD, Goldberg BB. Contrast-enhanced ultrasound: what is the evidence and what are the obstacles? AJR Am J Roentgenol. 2009;193:55-60.
46. Ferrara K, Pollard R, Borden M. Ultrasound microbubble contrast agents: fundamentals and application to gene and drug delivery. Annu Rev Biomed Eng. 2007;9:415-47.
47. Hernot JS, Klibanov AL. Microbubbles in ultrasound-triggered drug and gene delivery. Adv Drug Deliv Rev. 2008;60:1153-66.
48. Erdogan S, Ozer AY, Ercan MT, Hincal AA. Scintigraphic imaging of infections with ^{99m}Tc-labelled glutathione liposomes. J Microencapsul. 2000;17:459-65.
49. Erdogan S, Roby A, Torchilin VP. Enhanced tumor visualization by gamma-scintigraphy with ^{111}In-labeled polychelating-polymer-containing immunoliposomes. Mol Pharm. 2006;3:525-30.
50. Ogihara I, Kojima S, Jay M. Tumor uptake of ^{67}Ga-carrying liposomes. Eur J Nucl Med. 1986;11:405-11.
51. Oku N, Tokudome Y, Tsukada H, Kosugi T, Namba Y, Okada S. In vivo trafficking of long-circulating liposomes in tumour-bearing mice determined by positron emission tomography. Biopharm Drug Dispos. 1996;17:435-41.
52. Oerlemans C, Seevinck PR, van de Maat GH, Boulkhrif H, Bakker CJ, Hennink WE, Nijsen JF. Alginate-lanthanide microspheres for MRI-guided embolotherapy. Acta Biomater. 2013;9:4681-7.
53. Stampfl U, Sommer CM, Bellemann N, Holzschuh M, Kueller A, Bluemmel J, Gehrig T, Shevchenko M, Kenngott H, Kauczor HU, Radeleff B. Multimodal visibility of a modified polyzene-F-coated spherical embolic agent for liver embolization: feasibility study in a porcine model. J Vasc Interv Radiol. 2012;23:1225-31.
54. Bartling SH, Budjan J, Aviv H, Haneder S, Kraenzlin B, Michaely H, Margel S, Diehl S, Semmler W, Gretz N, Schonberg SO, Sadick M. First multimodal embolization particles visible on x-ray/computed tomography and magnetic resonance imaging, Invest Radiol. 2011;46:178-86.
55. Sharma KV, Dreher MR, Tang Y, Pritchard W, Chiesa OA, Karanian J, Peregoy J, Orandi B, Woods D, Donahue D, Esparza J, Jones G, Willis SL, Lewis AL, Wood BJ. Development of "imageable" beads for transcatheter embolotherapy. J Vasc Interv Radiol. 2010;21:865-76.
56. Saralidze K, Knetsch ML, van der MC, Koole LH. Versatile polymer microspheres for injection therapy: aspects of fluoroscopic traceability and biofunctionalization. Biomacromolecules. 2010;11:3556-62.
57. Vente MA, de Wit TC, van den Bosch MA, Bult W, Seevinck PR, Zonnenberg BA, de Jong HW, Krijger GC, Bakker CJ, van het Schip AD, Nijsen JF. Holmium-166 poly(L-lactic acid) microsphere radioembolisation of the liver: technical aspects studied in a large animal model. Eur Radiol. 2010;20:862-9.
58. Seevinck PR, Seppenwoolde JH, Zwanenburg JJ, Nijsen JF, Bakker CJ. FID sampling superior to spin-echo sampling for T_2*-based quantification of holmium-loaded microspheres: theory and experiment. Magn Reson Med. 2008;60:1466-76.

Chapter 2

Chris Oerlemans
Wouter Bult
Mariska Bos
Gert Storm
Frank Nijsen
Wim Hennink

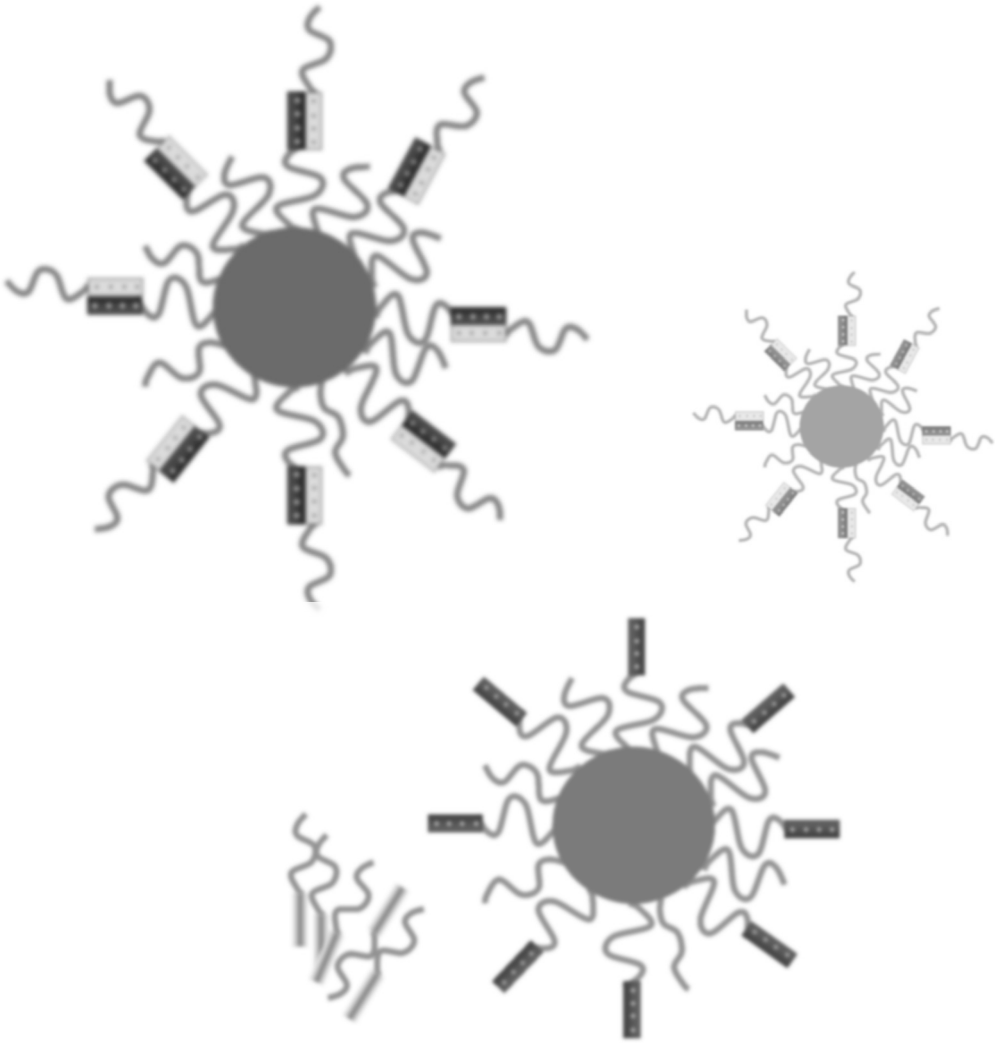

Polymeric Micelles in Anticancer Therapy: Targeting, Imaging and Triggered Release

Pharmaceutical Research 27, 2569-2589
2010

ABSTRACT

Micelles are colloidal particles with a size around 5-100 nm which are currently under investigation as carriers for hydrophobic drugs in anticancer therapy. Currently, five micellar formulations for anticancer therapy are under clinical evaluation, of which Genexol-PM has been FDA-approved for use in patients with breast cancer. Micelle-based drug delivery, however, can be improved in different ways. Targeting ligands can be attached to the micelles which specifically recognize and bind to receptors overexpressed in tumor cells, and chelation or incorporation of imaging moieties enables tracking micelles *in vivo* for biodistribution studies. Moreover, pH-, thermo-, ultrasound-, or light-sensitive block copolymers allow for controlled micelle dissociation and triggered drug release. The combination of these approaches will further improve specificity and efficacy of micelle-based drug delivery and brings the development of a 'magic bullet' a major step forward.

INTRODUCTION

Cancer is a leading cause of death world-wide and is responsible for approximately 13% of all deaths, according to the World Health Organization [1]. In Europe alone, Ferlay *et al.* recently estimated that in 2008 1.7 million cancer deaths occurred, and 3.2 million cancer cases were diagnosed [2]. Although prognosis is better now, the large variety of cancer types and metastases makes treatment very difficult. Surgical resection is the treatment of choice, since this treatment is usually curative. Surgery, however, is not an option in many patients due to the tumor size, location and presence of metastases. External beam radiotherapy is also considered a curative treatment option. However, not all tumors are eligible for this therapy due to motion of the tumor-bearing tissue or the adjacency of radiosensitive organs. Another frequently used therapy is systemic chemotherapy, but although chemotherapeutic agents are becoming more and more specific, many of the clinically used chemotherapeutics require high tissue concentrations, which are frequently associated with systemic toxicity. A very promising approach to overcome systemic toxicity is the application of drug-loaded nanosized drug carriers, such as liposomes, polymeric nanoparticles, dendrimers and micelles [3-5]. The incorporation of chemotherapeutic agents into nanosized drug carriers has several advantages compared to systemic chemotherapy. First, low-molecular weight drugs are mostly rapidly eliminated by liver and/or kidneys. By loading them in stealth nanoparticles, their bioavailability substantially increases [6]. Second, due to their small size, nanosized drug carriers are passively targeted to the tumors by the enhanced permeability and retention (EPR) effect, leading to a higher drug concentration at the tumor site and decreased toxicity compared with systemic administration [7]. Third, hydrophobic drugs can only be administered intravenously (i.v.) after addition of solubilizing adjuvants like ethanol or Cremophor EL, which is often accompanied with toxic side effects [8, 9]. Incorporation of these drugs in micelles avoids the use of adjuvants [10]. This review will focus on micelles as a nanosized drug carrier system for cancer therapy and their modifications for tumor targeting, multimodality imaging and triggered release (Fig. 1).

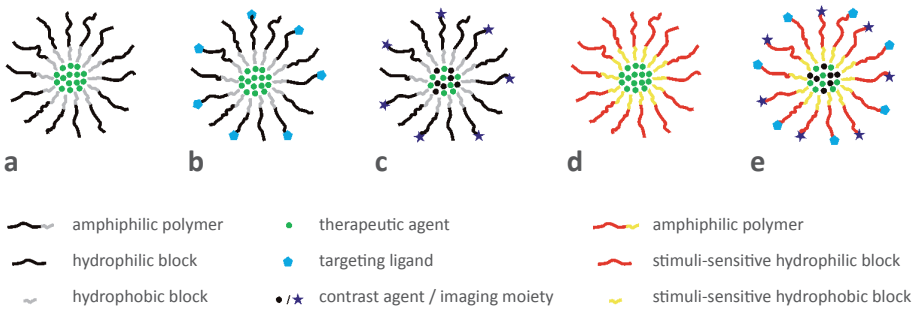

Fig. 1. Schematic drawing of polymeric micelle (a). Micelle conjugated with a targeting ligand (b). Micelle containing an incorporated contrast agent or chelated imaging moieties (c). Micelle modified for triggered drug release (d). Either the hydrophilic or hydrophobic polymer can be rendered thermo/pH/light/ultrasound-sensitive. Optimized micelle for anticancer therapy, bearing targeting ligands, contrast agents or imaging moieties, therapeutic drugs and polymers suitable for triggered, controlled release (e).

MICELLES

Micelles are colloidal particles with a size usually within a range of 5-100 nm. Micelles consist of amphiphiles or surface-active agents (surfactants), which exist of two distinct regions: mostly a hydrophilic head-group and a hydrophobic tail. At low concentrations in an aqueous medium, the amphiphiles exist as monomers in true solution, but when the concentration increases, aggregation and self-assembly take place within a narrow concentration window, and micelles are formed [3]. The concentration at which micelles are formed is referred to as the critical micelle concentration (CMC). The formation of micelles above their CMC is driven by dehydration of the hydrophobic tails, leading to a favorable state of entropy. Additionally, the formation of Van der Waals bonds allow the hydrophobic polymers to join and to form the micelle core [3]. The resulting hydrophilic shell re-establishes hydrogen bond networks with the surrounding water [3, 11]. Amphiphilic copolymers usually exhibit a CMC much lower compared to low-molecular-weight surfactants. The CMC of polymeric micelles is typically in the order of 10^{-6} to 10^{-7} M, while 10^{-3} to 10^{-4} M is common for low molecular weight surfactants [12]. Due to the low CMC, polymeric micelles remain stable at very low polymer concentrations, which makes them relatively insensitive to dilution, resulting in an enhanced circulation time compared to surfactant micelles [12].

Polymeric Micelles as Drug Delivery Systems

The bioavailability of anticancer drugs after oral administration is usually low due to reduced absorption [3]. Additionally, intravenous administration of these drugs is challenging and requires a formulation with organic solvents and classical surfactants (e.g. the Taxol formulation of paclitaxel from Bristol-Myers Squibb). Solubilization of hydrophobic drugs in the core of micelles can overcome this problem. Polymeric micelles have several advantages over other nanosized drug delivery systems, such as a smaller size as compared to, for instance, liposomes, which is important for, e.g., percutaneous lymphatic delivery or extravasation from blood vessels into the tumor tissue [13]. Polymeric micelles are based on block-copolymers with hydrophilic and hydrophobic units that self-assemble in an aqueous environment into structures composed of a hydrophobic core stabilized by a hydrophilic shell. These blocks can be arranged in different ways: A-B type copolymers (diblock copolymer), A-B-A type copolymers (triblock copolymer), and grafted copolymers [3, 11]. Grafted polymers are branched polymers consisting of one hydrophilic backbone and one to multiple hydrophobic polymer side chains or vice versa. Polymer selection for micelles is based on the characteristics of both the hydrophilic and the hydrophobic block copolymer. The hydrophilic shell of the micelle provides steric stability and once properly selected avoids rapid uptake by the reticuloendothelial system (RES), resulting in a prolonged circulation time in the body [12]. Poly(ethylene glycol) (PEG) is the most commonly used hydrophilic polymer. PEG is water-soluble, highly hydrated, an efficient steric protector, and biocompatible, and it has low toxicity [3, 11, 12, 14, 15]. The hydrophobic block copolymer should possess a high drug loading capacity and good compatibility of the hydrophobic core with the incorporated drug. One of the possibilities to calculate drug-polymer interactions is the Flory-Huggins theory, which accounts for the forces of interaction between the polymer and the drug and quantifies the difference in the intermolecular interactions of the components in a binary mixture, thereby predicting the compatibility of the drug and polymer

[16]. Most commonly used polymers for hydrophobic core formation are polyesters, polyethers, and polyamino acids [15, 17]. Frequently used core-forming molecules are poly(propylene oxide) (PPO), poly(D,L-lactic acid) (PDLLA), poly(ε-caprolactone) (PCL), poly(L-aspartate) and poloxamers [18]. The stability (CMC) of polymeric micelles depends on the type and molecular weight of the hydrophobic block. Generally, the more hydrophobic and the higher the molecular weight, the lower the CMC [14, 19]. In addition, Carstens *et al.* demonstrated that end-group modification of the coreforming block can be used to stabilize polymeric micelles and to increase drug compatibility and loading, as was shown for mPEG-*b*-oligo(ε-caprolactone) derivatized with aromatic groups [20, 21]. Poloxamers exist of a triblock polymer of PEG-PPO-PEG and are commercially available in various compositions under the name Pluronics (BASF Corp.) [12]. Different micellar formulations containing these core-forming molecules will be discussed in the next sections.

Polymeric Micelles in Clinical Trials

Currently, many drug-loaded polymeric micelles for anticancer therapy are under investigation in preclinical studies to improve drug efficacy. Five micellar formulations have been tested in clinical trials (Table 1) and will be discussed in more detail.

Table 1: Polymeric micelles in clinical trials [20]

Polymeric micelle	Block copolymer	Drug	Diameter	Indication	Clinical phase	Ref.
NK012	PEG-PGlu(SN-38)	SN-38	20 nm	Breast cancer	II	[20, 21]
NK105	PEG-P(aspartate)	Paclitaxel	85 nm	Advanced stomach cancer	II	[6, 22]
SP1049C	Pluronic L61 and F127	Doxorubicin	22-27 nm	Adenocarcinoma of oesophagus, gastroesophageal junction and stomach	III	[15, 23]
NC-6004	PEG-PGlu(cisplatin)	Cisplatin	30 nm	Solid tumors	I/II	[24, 25]
Genexol-PM	PEG-P(D,L-lactide)	Paclitaxel	20-50 nm	Breast cancer	IV	[21, 26, 27]
				Pancreatic cancer	II	[28, 29]
				Non-small-cell lung cancer in combination with carboplatin	II	[30]
				Pancreatic cancer in combination with gemcitabine	I/II	[21]
				Ovarian cancer in combination with carboplatin	I/II	[21]

NK012

NK012 is a polymeric micellar formulation that consists of a block copolymer of PEG and polyglutamate (PGlu) conjugated with 7-ethyl-10-hydroxy-camptothecin (SN-38) [6]. SN-38 is a camptothecin analog and acts as a DNA topoisomerase I inhibitor, but cannot be administered i.v. due to its water-insolubility and high toxicity. SN-38 is covalently coupled to the PGlu segment by the condensation reaction between the carboxylic acid of PGlu and the phenol of SN-38 using 1,3-diisopropylcarbodiimide and *N,N*-dimethylaminopyridine as coupling agent and catalyst, respectively. Consequently, the PGlu segment is rendered hydrophobically to induce micelle formation (Fig. 2) [26, 33]. Preclinical *in vivo* studies with NK012 showed potent antitumor activity in mice. A pharmacokinetic study revealed that the plasma area under the curve (AUC) of micellar SN-38 after i.v. administration (30 mg kg^{-1}) to HT-29 tumor-cell-bearing mice was around 200 times higher as compared to CPT-11 (which is hydrolyzed to SN-38 in the circulation) at a dose of 66.7 mg kg^{-1}. The IC_{50} values of NK012 were up to 5.8 times higher than those of free SN-38. In addition, the clearance of NK012 in the HT-29 tumors was significantly slower compared to CPT-11 and SN-38. The highest tumor-to-plasma concentration ratio of micellar SN-38 was up to 10 times higher compared to free SN-38. Moreover, NK012 clearance was significantly lower compared to CPT-11 [33, 34]. Furthermore, a combination of NK012 with 5-fluoruracil (5-FU) showed a significantly higher antitumor effect in human colon cancer xenografts compared to CPT-11/5-FU [35]. From a phase I study with NK012, it was concluded that 37 mg m^{-2} as a SN-38 equivalent every 3 weeks was the maximum tolerated dose (MTD) in which neutropenia was found to be the dose-limiting toxicity (DLT) [26, 36, 37]. Currently, the efficacy and safety of NK012 are evaluated in phase II studies in breast cancer patients [22, 23].

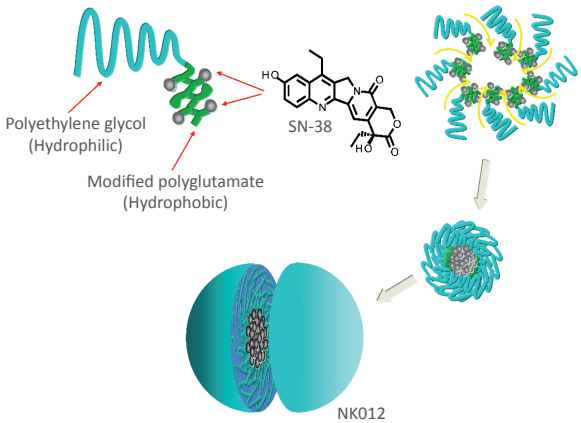

Fig. 2. Schematic structure of NK012, consisting of PEG and partially modified polyglutamate. PEG is used to form the hydrophilic segment, and SN-38 was incorporated into the hydrophobic core of the micelle [33].

NK105

Paclitaxel (PTX) is frequently used for the treatment of various cancer types, including lung, ovarian and breast cancer [38, 39]. However, systemically administered PTX causes serious side effects, such as neutropenia and peripheral sensory neuropathy. Additionally, Cremophor EL and ethanol, which are used to solubilize PTX, resulted in a hypersensitive reaction or anaphylaxis in 2-4% of the

patients treated with systemic PTX [8, 22, 40]. Therefore, new PTX formulations are being investigated, such as the NK105 micellar formulation that consists of PEG and modified polyaspartate as hydrophobic block. Half of the carboxylic groups of the polyaspartate block were esterified with 4-phenyl-1-butanol after treatment with the condensing agent 1,3-diisopropylcarbodiimide to increase its hydrophobicity and improve drug incorporation [6, 41]. PTX is physically incorporated in the core by hydrophobic interactions with the hydrophobic block. NK105 showed similar cytotoxicity in 12 human tumor cell lines (lung, gastric, oesophagus, colon, breast and ovarian) compared to PTX [41]. In preclinical *in vivo* studies with colon 26-bearing CDF1 mice, the AUC of NK105 was over 50 times higher, while the maximum plasma concentration (C_{max}) in the tumors was three times higher compared to PTX [22]. In BALB/c mice bearing subcutaneous HT-29 colon cancer tumors, NK105 administered as a PTX-equivalent dose of 25 mg kg^{-1} showed comparable antitumor activity with 100 mg kg^{-1} of free PTX. Additionally, a significant reduction of side effects, caused by Cremophor EL and ethanol after systemic PTX administration, occurred with NK105 [41]. In a phase I study with NK105, less hypersensitivity reactions occurred in patients suffering from pancreatic, bile duct, gastric, and colonic cancers compared to systemic PTX treatment [24]. NK105 was administered intravenously for 1 h every 3 weeks, and the recommended dose of 150 mg m^{-2} was well-tolerated [22, 24]. Currently, a phase II study in patients with advanced stomach cancer is underway [6].

SP1049C

SP1049C consists of a mixture (1:8 w/w ratio) of non-ionic Pluronic block copolymers: Pluronic L61 and F127. Doxorubicin is physically encapsulated by noncovalent bonds in the hydrophobic core of the micelles [42]. *In vitro*, it was shown that SP1049C exhibited greater efficacy than doxorubicin against a variety of tumor cell lines [43]. In preclinical *in vivo* studies, SP1049C demonstrated superior antitumor activity, efficacy and an increased AUC in tumor tissue in multiple animal tumor models and in doxorubicin-resistant tumors compared to free doxorubicin [44, 45]. AUC and C_{max} in liver, kidney, heart, lung and plasma were similar for SP1049C and free doxorubicin. The MTD of SP1049C was determined at 70 mg m^{-2} in a phase I study, around the same as systemic doxorubicin, but SP1049C showed significantly higher antitumor activity and a favorable safety profile compared to doxorubicin. Despite the occurrence of neutropenia as DLT [42], a phase II study concluded that SP1049C was effective as monotherapy in patients suffering from adenocarcinoma of the oesophagus [46, 47]. SP1049C is currently investigated in phase III in patients with metastatic adenocarcinoma of the oesophagus, gastroesophageal junction and stomach.

NC-6004 (NANOPLATIN™)

Cisplatin (cis-dichlorodiamineplatinum[II] or CDDP) is a widely used anticancer agent for treatment of various cancers. However, the use of cisplatin is limited because of severe adverse effects like nephro- or neurotoxicity and drug resistance [22, 48]. To reduce these side effects and improve efficacy, the micellar formulation NC-6004 was developed. NC-6004 is composed of PEG and a poly(γ-benzyl L-glutamate)/CDDP complex. In BALB/c mice bearing a human gastic cell line (MKN-4), significant antitumor activity was observed after NC-6004 administration as compared to the control group, but no difference in antitumor activity was observed between

the NC-6004 and CDDP administration groups at equivalent dose. However, in Sprague-Dawley rats, a 65-fold increase of the AUC and an 8-fold increase of the C_{max} compared to systemic CDDP was found. In tumor tissue, an increase in C_{max} of 2.5 times was found, and, importantly, NC-6004 was found to significantly reduce nephro- and neurotoxicity, the dose-limiting factors of CDDP [49]. In a small phase I study, it was shown that NC-6004 was well-tolerated by patients suffering from colorectal carcinoma, upper gastrointestinal cancers, non-small-cell lung carcinoma (NSCLC), melanoma and other tumor types [26, 27]. Although a small number of patients (17 in total) was included in this study, a DLT phase I/II study with NC-6004 in combination with gemcitabine is in progress with patients suffering from locally advanced pancreatic cancer and metastatic pancreatic cancer [23].

GENEXOL-PM

Genexol-PM is a micellar paclitaxel formulation consisting of PEG and poly(D,L-lactic acid) (PDLLA) [28]. Preclinical *in vivo* studies with Genexol-PM demonstrated a 3-fold increase in the MTD and a significantly increased antitumor efficacy compared with free PTX [50]. The AUC of Genexol-PM was similar to PTX, but the concentration of PTX was 2-3 times higher in tissues, including liver, spleen, kidneys, lungs, heart and tumor [50]. In phase I studies, a MTD 390 mg m^{-2} every 3 weeks or 120 mg m^{-2} every week was determined without the occurrence of hypersensitivity reactions [28, 51]. In phase II studies, Genexol-PM was found to be effective and safe with high response rates in patients suffering from metastatic breast cancer and advanced pancreatic cancer [29-31, 52]. In patients with metastatic breast cancer, however, hypersensitivity reactions occurred in 8 out of 41 patients (19.5%) [29]. Moreover, Genexol-PM in combination with cisplatin showed significant antitumor activity and allowed administration of higher dose compared with the Cremophor EL-based formulation in patients with advanced NSCLC. Furthermore, no significant toxicity was found, although hypersensitivity reactions occurred as well [32]. Several studies are currently underway, including a phase III and IV study in patients with recurrent breast cancer [23].

POLYMERIC MICELLAR SYSTEMS FOR ENHANCED DRUG DELIVERY

Active Targeting of Polymeric Micelles

In addition to passive targeting, micelles can be modified with ligands for active targeting to increase the selectivity for tumor cells and enhance intracellular drug delivery while reducing systemic toxicity and adverse side effects compared to untargeted micelles and systemic chemotherapy [53]. The concept behind this approach is based on receptor-mediated endocytosis. When the ligands conjugated to the micelles bind to their specific receptors on the cell membrane, the micelles are internalized by endocytosis [54]. In this way, higher intracellular drug concentrations are obtained. Active targeting can be achieved by conjugation of specific ligands, like monoclonal antibodies (mAbs) or their Fab fragments, oligosaccharides or peptides to the shell-forming block [53]. This allows micelles to specifically bind to antigens or receptors that are overexpressed on the tumor cells. Kabanov *et al.* were one of the first to report an actively targeted micelle-based drug delivery system by developing micelles consisting of Pluronic P85 and murine polyclonal antibodies against α2-glycoprotein to deliver the neuroleptic agent haloperidol to the

brain [55]. The antibodies were anchored to the micelles using a pluronic analog, butylpoly (25)(oxypropylene)poly(20)(oxyethylene) ether of 2-hydroxyacetaldehyde (BPEA). Vega *et al.* addressed mAb-based targeting of micelles in anticancer therapy [56]. The epidermal growth factor receptor (EGFR), a transmembrane glycoprotein with an intracellular tyrosine kinase domain, which is overexpressed on the cells of more than one-third of all solid tumors, was targeted with the mAb C225 [57]. This mAb specifically binds to the external domain of EGFR and is therefore suitable for active targeting of micelles to a variety of tumors [58]. Next to monoclonal antibodies, folate is an important ligand for active targeting of cancer cells. The folate receptor is overexpressed in many types of cancer, including malignancies of the ovary, brain, kidney, breast, myeloid cells and lung, as folate is an essential vitamin for the biosynthesis of nucleotide bases and is consumed in elevated quantities by proliferating cells [53, 59, 60]. Another interesting possibility of micelle-based active targeting is based on ligand-receptor interactions with angiogenesis regulators [61]. When tumor cells cluster and reach a size of around 2-3 mm, diffusion of oxygen and nutrients to the tumor is repressed. This induces tumor angiogenesis, which allows tumors to grow beyond their diffusion limit [62]. The regulators of this process can be exploited for drug targeting to inhibit angiogenesis and prevent further tumor growth. Integrins represent a large group of structurally related receptors for extracellular matrix (ECM) proteins and immunoglobulin superfamily molecules and are regarded as key regulators of tumor angiogenesis. Active targeting to $\alpha_v\beta_3$ integrin with the micelle conjugated cyclic pentapeptide c(Arg-Gly-Asp-d-Phe-Lys) (cRGDfK) is explored by Nasongkla *et al.* [63]. Currently, several micelle compositions for active targeting in anticancer therapy are investigated *in vitro* and *in vivo*, as stated in Table 2. The research on micelles modified with targeting ligands has shown superior results compared to non-targeted micelles. Higher cellular uptake, cytotoxicity and tumor regression was demonstrated, making active targeting an important additional value to passively targeted polymeric micelles for anticancer therapy. However, these systems are more complicated since multiple modifications need to be made in one carrier type. Every single modification needs to be optimized, making it difficult and time-consuming to prepare these micelles under GMP conditions which will result in high costs. Furthermore, the circulation half-life might be decreased due to the presence of targeting ligands on the outer shell of the micelles, leading to lower drug concentrations. Consequently, clinical implementation of these systems remains challenging.

Imaging Systems Based on Polymeric Micelles

IMAGING MODALITIES

Nuclear imaging, magnetic resonance imaging (MRI) and X-ray computed tomography (CT) play an important role in the diagnosis of cancer and therapy response evaluation. The administration of contrast agents for these imaging modalities greatly enhances the specificity by highlighting the area of interest. Nuclear imaging allows for the visualization of minute amounts of gamma-emitting isotopes, such as technetium-99m (^{99m}Tc), indium-111 (^{111}In) and iodine-125 (^{125}I), for single photon emission computed tomography (SPECT) imaging or positron-emitting isotopes for positron emission tomography (PET) imaging, such as fluorine-18 (^{18}F), copper-64 (^{64}Cu) and zirconium-89 (^{89}Zr). Nuclear imaging is the most sensitive imaging modality, requiring an isotope concentration of around 10^{-10} M at the site of interest

Table 2: Micelles for active targeting for anti-cancer therapy in preclinical models

Block copolymers	Drug	Active ligand	Target	Results
PEG-*b*-PE	PTX	mAb 2C5	Nucleosome-restricted specificity for different cancer cells	Enhanced accumulation in tumor tissue and significant tumor weight decrease in C57BL/6J mice [61]
PEG-*b*-PG	Dox	mAb C225	EGF receptor	More potent than free doxrubicin in inhibiting the growth of A431 cells after a 6 h exposure period [53]
PEG-*b*-PCL	Dox	$\alpha_v\beta_3$ ligand (cRGDfK)	$\alpha_v\beta_3$ integrin	Greatly enhanced internalization in tumor endothelial cells (human Kaposi's sarcoma) [60]
PLGA-*b*-PEG	Dox	Folate	Folate receptor	Significant increase in cellular uptake in human squamous cell carcinoma cell line of the oral cavity (KB cells) Increased tumor uptake and significant regression of tumor volume in a nude mice xenograft model (Fig. 3) [62]
mPEG-*b*-PCL	PTX	Folate	Folate receptor	Endocytosis in MCF-7 cells and increased cytotoxicity in MCF-7 and HeLa cells [63]
PEG_{3350}-DSPE : $mPEG_{2300}$-DSPE (1:100)	9-NC	Folate	Folate receptor	Enhanced folate receptor-mediated endocytosis and increased cytotoxicity in HeLa and SGC7901 cells [64]
P105 and P105/L101	PTX	Folate	Folate receptor	Increased internalization explained the improved cytotoxicity of the FOL-micellar PTX to tumor cells in MCF-7 and MCF-7 cells pre-exposed to doxorubicin (to induce drug resistance) [65]
DSPE-PEG_{3400}-SPA	17-AAG	VIP	$VPAC_1$ receptors	Cytotoxicity was similar to free drug and significant higher than non-targeted micelles [66]

PE, phosphatidylethanolamine; PG, Poly(L-Glu); PCL, poly(ε-caprolactone); cRGDfK, cyclic(Arg-Gly-Asp-d-Phe-Lys); 9-NC, 9-nitrocamptothecin; PTX, paclitaxel, Dox, doxorubicin; [m]PEG-DSPE, [methoxy-]poly(ethylene glycol)-distearoylphosphatidylethanolamine; P, Pluronic; 17-AAG, 17-allylamino-17-demethoxy geldanamycin; VIP, vasoactive intestinal peptide; SPA, succinimidyl propionate.

[70]. However, the specificity of nuclear imaging has its drawbacks: it does not allow visualization of the surrounding anatomy, and the temporal resolution is limited [71]. Another imaging modality is MRI, which detects changes in magnetization of hydrogen nuclei (^{1}H) in the body in a strong magnetic field after application of radiofrequency pulses. Contrast agents used for ^{1}H MRI are usually paramagnetic

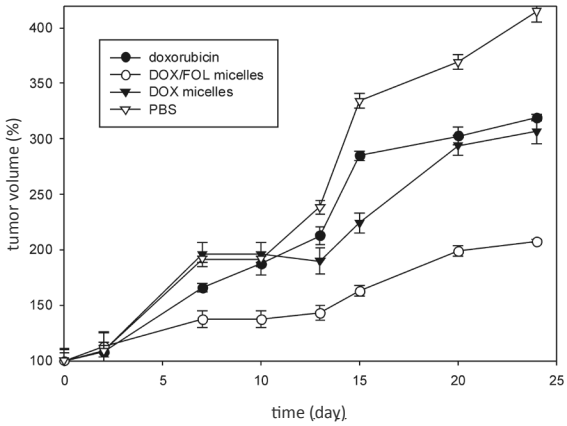

Fig. 3. Tumor volume growth in a nude mice xenograft model after i.v. administration of free doxorubicin, doxorubicin-loaded PLGA-*b*-PEG micelles and doxorubicin/folate PLGA-*b*-PEG micelles [65].

elements, such as iron, manganese, gadolinium and holmium, that locally alter the magnetization of hydrogen nuclei, thereby enhancing the contrast [72, 73]. Moreover, fluorine-19 (^{19}F) is increasingly gaining attention, since it is a MR-sensitive atom with very low biological abundance. The gyromagnetic ratio of ^{19}F differs by only about 6% from ^{1}H, while the relative sensitivity is 0.83, which avoids the need for drastic hardware modifications [74]. CT imaging utilizes differences in absorption of X-rays between different tissues in the body to discriminate between structures in the body. Contrast agents that are used for CT are heavy elements such as iodine, bromine and barium [75]. The concentration of contrast agent required at the site of interest is approximately 10^{-2} M [70]. The latter two imaging modalities, MRI and CT, allow for simultaneous visualization of both anatomy and the contrast agent. MRI is more suitable for imaging of soft tissue and requires a lower concentration of the contrast agent at the site of interest than CT [76]. The development of delivery systems for contrast agents is appropriate for nuclear imaging, CT and MRI, since the contrast agent must selectively reach the site of interest. The development of carrier devices is especially required for MRI and CT contrast agents due to their lower sensitivity compared to nuclear imaging.

POLYMERIC MICELLES FOR NUCLEAR IMAGING

Micelles loaded with gamma emitters have been investigated in detail for non-invasive biodistribution studies [77, 78]. Frequently used nuclides for this purpose are ^{99m}Tc and ^{111}In, since these isotopes are easily available, require straightforward labeling procedures and exhibit half-lives that allow for prolonged *in vivo* imaging [79]. ^{99m}Tc can be coupled using a selective *N*-(*N*-(3-diphenylphosphinopropionyl) glycyl) cysteine linker [80]. Coupling of ^{111}In to micelles can be achieved by chelating molecules like diethylenetriaminepentaacetic acid (DTPA) or 1,4,7,10-tetraazacyclododecane-1,4,7,10-tetraacetic acid (DOTA), that are conjugated to the polymers. Recently, a biodistribution study using micro-SPECT/CT was performed with ^{111}In-loaded DTPA-PEG-*b*-PCL micelles after i.v. injection in tumor-bearing mice [77]. Interestingly, the authors observed increased uptake in tumors with large vessels, which was attributed to the EPR effect. In recent years, the use of PET isotopes with a relatively long half-life such as ^{64}Cu ($T_{½}$=12.7 h), ^{89}Zr ($T_{½}$=78.4 h) and gallium-67 (^{67}Ga, $T_{½}$=3.2 days) has increased. These metals can be coupled in a

straightforward fashion using chelators like DTPA and DOTA. The biodistribution of ^{64}Cu-containing micelles was investigated *in vivo* with PET imaging by Pressly *et al.* using a DOTA-conjugated poly (methyl methacrylate-*co*-methacryloxysuccinimide-graftpoly(ethylene glycol)) (PMMA-*co*-PMASI-*g*-PEG) micellar formulation chelated with ^{64}Cu, which demonstrated increased blood circulation and low accumulation in excretory organs [81, 82].

POLYMERIC MICELLES FOR MRI

A lot of work has been conducted for the development of micellar MRI contrast agents. Two approaches that have been frequently used are the incorporation of iron oxide particles in micelles or the use of chelators for complexation of paramagnetic metals to the hydrophilic block of micelle-forming block copolymers. The complexation of paramagnetic ions is commonly performed through a chelating moiety, such as DTPA and DOTA. A recent example of this approach is the work of Shiraishi *et al.*, who prepared DOTA-grafted PEG-*b*-poly(L-lysine) micelles with gadolinium and showed a 2-fold relative signal intensity increase in tumor-bearing mice which was maintained for 48 h [83]. Hydrophobic iron oxide particles have been encapsulated in a number of different micellar formulations to enhance their circulation time. Talelli *et al.* used micelles consisting of a hydrophobic domain of biodegradable block copolymers of mPEG-*b*-poly[*N*-(2-hydroxypropyl) methacrylamide dilactate] to encapsulate superparamagnetic iron oxide nanoparticles (SPIONs with a size around 5 nm) (Fig. 4) [84]. The particles were stable, and the MRI characteristics of the iron oxide particles were retained. Khemtong *et al.* incorporated SPIONs (size around 10 nm) in PEG-*b*-PLA micelles and proposed an off-resonance saturation method for MRI as a useful tool to enhance contrast effects of the superparamagnetic polymeric micelles [85]. Lu *et al.* prepared mPEG-*b*-PCL micelles to encapsulate manganese-doped SPIONs (size around 10 nm). It was found that the T_2-weighted signal intensity in mouse liver decreased about 80% at 5 min after i.v. administration in a time window of 36 h for enhanced-MRI, which can strongly improve the contrast between small lesions and normal tissues [86]. A relatively new class of MRI contrast agents are fluorine-19 (^{19}F)-containing contrast agents. ^{19}F nuclei behave similar to ^{1}H nuclei in a magnetic field and can be visualized on clinical MRI systems [87]. The advantage of ^{19}F MRI is the near absence of a background signal, since the endogenous ^{19}F concentration in the body is very low. The use of ^{19}F-loaded particulate systems for contrast enhancement on MRI has emerged within recent years, since the specific ^{19}F hardware has become increasingly available on clinical MR scanners [87], allowing clinical evaluation of fluorine particulate systems. Currently, perfluorocarbons like perfluorooctylbromide and perfluoropolyether are the most commonly used ^{19}F contrast agents [88, 89]. These compounds, however, have a poor aqueous solubility and are administered as emulsions. As an alternative, self-assembling fluorinated block copolymers have been synthesized. These block copolymers composed of a hydrophilic PEG and a hydrophobic block containing ^{19}F form micelles in aqueous solution and showed promising imaging results *in vitro* [90, 91], but need to be further investigated *in vivo*.

MICELLES FOR CT IMAGING

The relatively high concentration of contrast agent required for CT makes this imaging modality less suitable for molecular imaging. However, by extending the

circulation time of contrast agents and/or by targeting them to the tissue of interest, this drawback might be overcome. Torchilin *et al.* developed micelle-based CT iodine-containing micelles (mPEG-*b*-iodolysine, iodolysine is iodine-substituted poly-L-

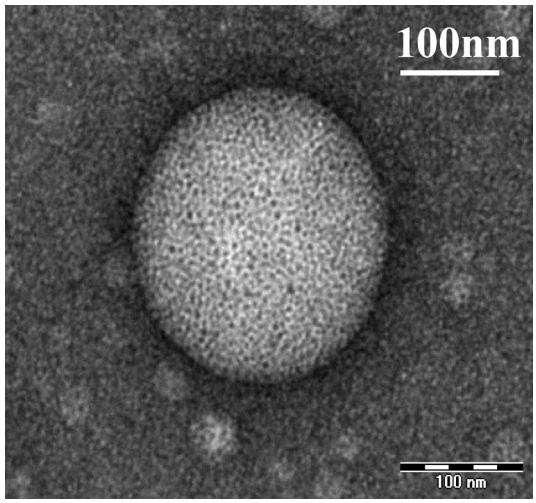

Fig. 4. TEM image of SPION-loaded micelles containing 1 mg mL^{-1} SPIONs and 0.9 mg mL^{-1} mPEG-*b*-p(HPMAm-Lac_2) at high magnification [84].

lysine) which were used as so-called blood pool agents [92]. Clinical applications like minimally invasive angiography and image guidance of minimally invasive procedures could benefit from a long-circulation intravascular contrast agent. Micelles modified for tumor imaging using CT have not been reported to date. Nevertheless, CT is particularly suitable to merge with SPECT or PET images. This combines the specificity of nuclear medicine with the anatomical information from CT and will significantly increase the applicability of nuclear imaging [71].

Triggered Release of Polymeric Micelles

Drug release from micelles is governed by the rate of drug diffusion, the partition coefficient, micelle stability and rate of biodegradation of the copolymers [93]. Other factors that influence the release are the drug concentration within the micelles, the length of the hydrophobic polymer, the molecular weight, the physicochemical characteristics of the drug and the localization of the drug within the micelles [94]. Drug release from micelles at the targeted area can be enhanced by applying an internal or external trigger. Several methods for triggered release have been described, including pH-sensitive, thermosensitive, ultrasound-sensitive and light-sensitive micelles [95].

pH-SENSITIVE MICELLES

Differences in pH between healthy tissue and tumor tissue, as well as the acidic environment in endosomal and lysosomal compartments, can be exploited as an internal stimulus for triggered drug release [96, 97]. The pH in healthy extracellular compartments (pH_e) is 7.4, while the intracellular (pH_i) is around 7.2. The pH in tumor

tissue is slightly lower, around pH 6.8, due to the high rate of aerobic and anaerobic glycolysis in cancer cells [17, 98]. Lactate and carbon dioxide, metabolic acid products, diffuse from the cancer cell into the interstitial fluid. However, due to the impaired vasculature, impaired lymphatic drainage, and elevated interstitial pressure, the excretion is retarded, and the metabolic products consequently accumulate [99]. In the endosomal and lysosomal compartments the pH is even lower, around 5-6, which can be utilized for triggered drug release directly into the cells. The pH-triggered release of drugs can be established by protonation of pH-sensitive polymers that form the hydrophobic core of polymeric micelles at physicological pH. Destabilization occurs when the protonatable groups become charged below the pKa, leading to repulsion between the polymer chains, which results in micelle dissociation. Many examples of protonation of polymers that trigger micelle destabilization have been reported, including poly(L-histidine), polypyridines, and polysulfonamides [10]. Poly(L-histidine) is the most commonly used pH-sensitive component in micelle-based pH-triggered release systems since this polymer contains an imidazole ring endowing it with pH-dependent amphoteric properties [100]. It has a pK_a around 6.5, is biodegradable and has low toxicity [98, 101-106]. Lee *et al.* prepared micelles, respectively, based on a triblock copolymer PLA-*b*-PEG-*b*-polyHis, which showed triggered release of doxorubicin when the pH was lowered from 7.4 to 6.0. After 5 h, 40-50% of doxorubicin was released at pH 6.8-6.0, while 60-70% was released after 24 h. Cytotoxicity was 60% at pH 6.8 and 74% at pH 6.0, while only minimal release and cytotoxicity were observed at pH 7.4 [107]. Polypyridines like poly(2-vinylpyridine) (P2VP) and poly(4-vinylpyridine) (P4VP) are water-insoluble at neutral or alkalic pH, but become protonated and thus soluble at pH<5 [10, 108]. A recently developed micellar formulation containing P2VP has been described by Karanikolas *et al.* [109]. A triblock copolymer of PEO-*b*-P2VP-*b*-PEO was used to demonstrate pH-triggered micelle destabilization. No drug release studies concerning this micelle formulation, however, have been reported yet. Another mechanism of pH-triggered release is based on the use of acid-labile bonds (pH-sensitive polymer-drug conjugates) [18, 110]. Different acid labile bonds such as orthoesters, hydrazones, cis-acotinyl and acetal have been positioned either in the main chain, at the side chain, or at the terminal of the core-forming block [111-113]. For example, Bae *et al.* prepared micelles based on mPEG-*b*-poly(aspartate hydrazone doxorubicin) where doxorubicin was conjugated to the hydrophobic segments through acid-sensitive hydrazone linkers. Selective release of the drug at endosomal pH and suppressed tumor growth in mice with enhanced therapeutic efficacy and decreased systemic toxicity compared to free doxorubicin was reported [114]. Chen *et al.* prepared micelles with PEG and an acid-labile polycarbonate [96], and demonstrated that the acetal groups of the polycarbonate were hydrolyzed, resulting in paclitaxel or doxorubicin release of 60-70% after exposure to mildly acidic conditions (pH 5.0-4.0), respectively, for 10 h. Huang *et al.* prepared PEG-*b*-PtNEA micelles based on the orthoester-containing monomer poly(trans-*N*-(2-ethoxy-1,3-dioxan-5-yl)acrylamide) (PtNEA) containing Nile red dye. The micelles remained stable at pH 7.4 but destabilized in mildly acidic media due to the acid-triggered hydrolysis of the orthoester groups, which increased the hydrophilicity of PtNEA, resulting in Nile red release [115]. Tang *et al.* used polymethacrylamide derivative (PMYM)-bearing orthoester side chains as pH-sensitive hydrophobic block to prepare PEG-*b*-PMYM micelles capable of drug release after exposure to mildly acidic conditions [113].

THERMOSENSITIVE MICELLES

Thermosensitive micelles are based on the lower critical solution temperature (LCST) or cloud point (CP) of the thermosensitive block of the block copolymer forming micelle. Below the LCST, a thermosensitive polymer is water-soluble, but above this temperature the polymer becomes insoluble due to disruption of hydrogen bonds between water and the polymer chains. The LCST of a polymer can be modulated by introduction of hydrophobic or hydrophilic comonomers. Hydrophobic monomers decrease the LCST, while it is increased by hydrophilic comonomers [10]. A frequently studied polymer for the preparation of thermosensitive micelles is poly(*N*-isopropylacrylamide) (PNIPAAm), which has a reversible and sharp phase transition. It switches from a water-soluble hydrophilic polymer to a hydrophobic insoluble polymer around 32 °C [116, 117]. PNIPAAm can be used either as a hydrophilic segment or as a hydrophobic segment of polymeric micelles. As hydrophobic fragment, PNIPAAm is often conjugated to PEG to form stable micelles [118, 119]. The micelles can be prepared by heating the solution above the LCST of PNIPAAm [10, 120]. By copolymerizing with hydrophilic monomers the LCST of PNIPAAm can be increased, making it suitable as hydrophilic segment for heat-triggered release. Three monomers that have been investigated in combination with PNIPAAm are acrylamide (AAm), hydroxymethylacrylamide (HMAAm), and dimethylacrylamide (DMAAm). It was found that that copolymers of PNIPAAm with these hydrophilic monomers can have an LCST above body temperature [121]. Various preclinical studies have been conducted with thermosensitive micelles, as shown in Table 3. Additionally, thermosensitive micelles have been developed which are not based on PNIPAAm as thermosensitive segment. For instance, micelles based on poly(*N*-vinylcaprolactam)-*b*-poly(ethylene glycol)-folic acid (PNVCL-*b*-PEG-FA) micelles with a LCST of 33 °C were prepared. At 37 °C, the micelles showed a slow sustained release profile of the entrapped 5-FU up to 30 h (around 80% was released) [128]. Poly(*N*-(2-hydroxypropyl)methacrylamide) (PHPMAm) is a hydrophilic, non-immunogenic and biocompatible polymer which can be hydrophobically rendered by esterification with lactic acid [129]. Soga *et al.* demonstrated that the lower critical solution temperature (LCST) of PHPMAm-lactate can be well-controlled between 10 °C and 65 °C by the length of the lactate side group and copolymer composition [130]. It was shown that polymeric micelles composed of PEG-*b*-PHPMAm-dilactate gradually dissolved due to hydrolysis of the lactic acid side groups [131]. PEG-*b*-PHPMAm-Lac micelles containing 2 mg mL^{-1} paclitaxel which destabilized after around 1 week at physiological conditions were developed [132]. *In vivo*, the antitumor efficacy of this micelle formulation in B16F10 tumor-bearing mice after i.v. administration was comparable with the Cremophor EL formulation of paclitaxel but evaded the toxicological side effects originating from Cremophor EL [8, 9]. However, no significant accumulation of micelles in tumor tissue was observed after 24 h, probably caused by premature micelle destabilization. Low stability in the systemic circulation is one of the problems that may arise after i.v. administration of polymeric micelles. *In vitro* studies showed that the addition of either human albumin or serum to drug-loaded micelles substantially decreased their stability, leading to rapid release of the encapsulated drug [133, 134]. Additionally, the micelles may be diluted below their CMC after i.v. administration, which also leads to premature micelle destabilization [135, 136]. An increased micellar stability can be established by either physical or chemical crosslinking of the shell, the intermediate layer or the core of the micelles [137, 138]. This way, the circulation time of the micelles can be enhanced. Crosslinking also enables controlled release of the entrapped drug,

Table 3: Overview of thermosensitive polymeric micelles, which contain PNIPAAm as thermosensitive fragment

Micelle type	LCST	Results preclinical studies
P(NIPAAm-*co*-DMAAm)-*b*-PDLLA	40 °C	At 37 °C slow doxorubicin release, at 42.5 °C triggered release *in vitro* [119]
P(NIPAAm-*co*-DMAAm)-*b*-PLGA	39 °C	Below the LCST stable micelles, enhanced paclitaxel release *in vitro* at 39.5 °C compared to 37 °C [120] Higher cytotoxicity *in vitro* at 39.5 °C compared to free paclitaxel [120] or free doxorubicin [121] above LCST
P(NIPAAm-*co*-AAm)-*b*-PDLLA	41 °C	Enhanced cytotoxicity at 43 °C compared to free docetaxel, and lower cytotoxicity at 37 °C, higher LD_{50} and higher efficacy *in vivo* [122]
PMMA-*b*-P(NIPAAm-*co*-PEGMEMA)-*b*-PMMA	39 °C	Below the LCST the micelles expand, while above the LCST the hydrophilic block shrinks. Release of folic acid (used as model drug) increased at 41 °C compared to 37 °C *in vitro* [123]
P(NIPAAm-*co*-DMAAm)-*b*-(PDLLA-*co*-PCL)	40 °C	Significant increased doxorubicin release *in vitro* after 10 h exposure to 41 °C compared to temperatures below the LCST [124]

PDLLA, poly(D,L-lactic acid); PLGA, poly(D,L-lactide-*co*-glycolide); MEMA, methyl ether methacrylate; PMMA, poly(methyl methacrylate); PCL, poly(ε-caprolactone).

whereas the stimuli responsiveness of the micelles is not affected [139, 140]. Rijcken *et al.* prepared core-crosslinked thermosensitive micelles based on *N*-(2-hydroxyethyl) methacrylamide (HEMAm) block copolymers which were derivatized with various monodisperse oligolactates (HEMAm-Lac_n). Part of the hydroxyl end groups of the lactic acid groups were derivatized with methacrylic acid to allow crosslinking of the micellar core by radical polymerization [137]. These core-crosslinked micelles showed an excellent physical stability and a superior circulation profile compared to non-crosslinked micelles. More than 50% of the micelles still resided in the circulation 6 h post-injection, and an increased tumour accumulation was observed. Hence, two promising approaches have been developed regarding thermosensitive micelles. First, micelles consisting of a hydrophilic block copolymer with an LCST above 37 °C are able to release their content after the induction of mild hyperthermia, which, for instance, can be induced by (focused) ultrasound. Second, stabilized, crosslinked micelles derivatized with lactate side chains are very attractive for controlled release of anticancer drugs at 37 °C upon i.v. administration.

ULTRASOUND-RESPONSIVE MICELLES

Ultrasound with a frequency higher than 20 kHz can be used to generate ultrasonic waves in tissue [141]. In general, exposure of tissue to ultrasound results in two effects: hyperthermia (thermal effects by absorption of energy), and non-thermal effects associated with oscillating or cavitating bubbles [142]. A favorable characteristic of ultrasound is noninvasive deep penetration in the body which can be focused and controlled. Additionally, ultrasound can facilitate absorption and membrane passage of drugs [141-144]. Exposure of micelles to ultrasound has been reported for triggered drug release in tumor tissue [142]. Several studies suggest that drug release

is triggered due to disruption of the carrier and the formation of micropores in cell membranes, facilitating passive diffusion and intracellular accumulation of the drug [145]. The abrupt compression and expansion of the fluid in the shockwave caused by the collapse of microscopic gas bubbles that are present in the body results in shear stress which in turn disrupts micelles and permeabilizes cell membranes [143]. The increased permeability of the cell membrane is induced by cavitation, defined as the oscillation of bubbles in an acoustic field, and allows direct passage of the therapeutics into the cytosol [146]. When ultrasound is applied, several factors should be considered: time of application, application procedure (continuous or pulsed with different exposure times), lipophilicity and concentration of the drug, ultrasound frequency, and power density [145, 147]. The appropriate frequency, power density and pulse duration depend on the location of the tumor. High frequencies (1-3 MHz) have higher power densities and can be more narrowly focused, making them suitable for small superficial tumors. Low frequencies (20-100 kHz), on the other hand, are able to penetrate deeper into the body and are therefore more appropriate for deeply located tumors, but can also damage healthy tissue and organs due to a strong cavitation effect [148-150]. The most frequently studied micelles for ultrasound-triggered release are based on Pluronic P105, a $(PEO)_{37}$-$(PPO)_{56}$-$(PEO)_{37}$ block copolymer [150]. These micelles showed increased drug release upon exposure to ultrasound [142, 151], which makes them attractive drug delivery systems for triggered release. However, upon administration, Pluronic P105-based micelles dissociated quickly, which resulted in micelle disintegration and premature drug release [152]. Therefore, it is important to increase their stability, which can be achieved by adding stabilizing agents. PluroGel is an example of Pluronic P105 micelles stabilized with the crosslinking agent *N,N*-diethylacrylamide (NNDEA) [149, 153]. The formed interpenetrating network is a thermally reversible nanogel which expands below 31 °C and enables drug loading at room temperature. When the temperature increases above 31 °C, the network contracts and collapses into a tight hydrophobic core in which the drug is entrapped. Husseini *et al.* demonstrated that although the micellar formulation was stabilized with NNDEA, the release of doxorubicin in response to 70 kHz ultrasound was similar compared to non-stabilized P105 micelles [148, 151, 154-157]. Nelson *et al.* introduced a colon carcinogen tumor cell (DHD/K12/TRb) into the hind limbs of BDIX rats which were then treated weekly with stabilized micelles or free doxorubicin by i.v. administration [153]. Application of 20 and 70 kHz low-frequency ultrasound significantly reduced the tumor size as compared to noninsonated controls. Additionally, a significant reduction was also found in tumors treated with free doxorubicin, which can be ascribed to the enhancement of passive diffusion as this is associated with the use of ultrasound [145]. Micelles based on Pluronic P105 can also be stabilized by introducing a PEG-diacylphospholipid like 1,2-distearoyl-*sn*-glycero-3-phosphoethanolamine-*N*-[methoxy-(polyethylene glycol)-2000] ($mPEG_{2000}$-DSPE) in a 1:1 ratio to decrease the CMC, as was demonstrated by Gao *et al.* [142, 149, 153, 158-160]. *In vivo* studies demonstrated that exposure of both stabilized and non-stabilized Pluronic P105 micelles loaded with doxorubicin or 5-FU to low-frequency ultrasound resulted in enhanced drug concentrations in tumor tissue and a significant decrease in tumor volume compared to mice which were not treated with ultrasound. However, the release of doxorubicin from non-stabilized Pluronic P105 micelles was around 3 times higher as compared to stabilized micelles (10% and 3%, respectively), and they were more susceptible to the shearing forces associated with cavitation [142, 159, 161, 162]. Nevertheless, drug release was observed each

Table 4: Overview of non-Pluronic ultrasound responsive micelles

Micelle type	Characteristics and results
PEG-*b*-PBLA	8-fold increase of intracellular doxorubicin uptake after 30 s ultrasound application (1 MHz) in mice bearing ovarian cancer (A2780) cells [156]
PEO-*b*-PNHL	Micelle half-life in the systemic circulation can be tailored by composition modifications [139, 158] Lactate esters are hydrolyzed and the PNHL block becomes hydrophilic and doxorubicin was released after 70 kHz application [139, 158]
PEO-*b*-PTHPMA	Ultrasound (1 MHz) application resulted in hydrolysis of acetal bonds and cleavage of THP groups [160]
PEG-*b*-PLLA	Irreversible break of PEG and PLA linkage after ultrasound application (1.1 MHz) by cavitation and subsequent Nile red release [161]
PEG-*co*-PLA-tocopherol	Improved drug uptake after 30 s ultrasound application (1 MHz) in tumor in mice and regression of drug-resistant breast cancer (MCF7/AD_m tumors) [143, 146]

PBLA, poly(*β*-benzyl-L-aspartate); PNHL, copolymer of poly(*N*-isopropylacrylamide) and polylactate esters of hydroxyethyl metacrylate (HEMA-lactate); PTHPMA, poly(tetrahydropyranyl-2-methacrylate); PLLA, poly(L-lactic acid).

time ultrasound was applied. Therefore, pulsed ultrasound can theoretically release all of the encapsulated drug from the stabilized micelles, while their stability in the circulation is much better as compared to non-stabilized micelles [146]. Non-Pluronic micelles have also been investigated for ultrasound-triggered release, as summarized in Table 4. Although promising studies have been performed with low-frequency ultrasound-sensitive micelles, low-frequency ultrasound cannot be focused and results in damage of healthy tissues due to cavitation, which restricts its practical clinic use [164]. Cavitation also occurs with high ultrasonic intensities, although this effect is less prominent than low-frequency ultrasound. High-intensity focused ultrasound (HIFU) has been studied extensively in combination with MRI, and, importantly, recent studies have shown that ultrasound-induced hyperthermia can be controlled using MRI thermometry [165, 166], which makes this technique suitable for triggered drug release from both thermo- and ultrasound-sensitive micelles. We therefore consider high-frequency focused ultrasound preferable over low-frequency ultrasound for triggered drug release.

LIGHT-RESPONSIVE MICELLES

Light can be used as an external stimulus for micelle disintegration and offers the possibility to locally destabilize micelles in the body [167]. This increases the specificity of drug delivery. Particularly, ultraviolet (UV) and near-infrared (NIR) light can be used to trigger release. However, UV light is not able to penetrate deeply into the body because of absorption by the skin, yet it can trigger drug release for topical treatment of the skin and mucosa. NIR is able to penetrate deeper, up to 10 cm, in the body, because hemoglobin (the principal absorber of visible light), water and lipids (the principal absorbers of infrared light) have low absorption in the NIR region (650-900 nm) [167-169]. Micelles can be rendered light-sensitive and thus deliver drugs in response to light by incorporation and/or conjugation of a chromophore structure

in/to the hydrophobic polymer [167]. When light-sensitive micelles are illuminated, the hydrophilic/hydrophobic balance changes and the micelles dissociate. In general, there are two types of reactions associated with light-induced micelle destabilization. First, the photoreaction of a chromophore can change the polarity of the hydrophobic polymer reversibly, which causes subsequent micellar destabilization. When the photoreaction stops, the initial polarity is returned and the micelles are re-established (Table 5) [167, 170]. A second photoreaction that might occur upon illumination of light-sensitive micelles with UV or NIR is established by the irreversible cleavage of a photolabile group from the hydrophobic block, converting it into a hydrophilic polymer leading to micellar destabilization [167]. Table 6 summarizes irreversible light-response micelles that have been investigated. Although promising results have been achieved with destabilization of micelles upon light exposure, no *in vivo* studies with drug-loaded micelles have yet been performed.

Table 5: Overview of light-sensitive chromophores, which enable reversible light response

Chromophore	Light response
Cinnamoyl	Ionization: isomerization to more hydrophilic species due to the electric charge generation or dimerization [168, 169]
Azobenzene	Isomerization: upon UV irradiation, the compound in the *trans* conformation, having no dipole moment, is reversibly converted to the *cis* conformation with a dipole moment [164, 167, 170] Examples are: NNDMA, MOAB and the light-sensitive micellar formulation with hydrophilic P(*t*BA-*co*-AA) and hydrophobic PAzoMA [164, 170]
Spirobenzopyran	Zwitterion: colorless spiropyran is converted into colored merocyanin upon UV (365 nm) irradiation and re-established under visible light (620 nm) [168]
Diarylethenes	Photocyclization: configuration of a ring system as a result of the formation of one new single bond [171]
Fulgides	Photochromism: switch from open colorless state to colored cyclic state [172]
Overcrowded alkenes	Chiroptical switch: switch to another conformation [173]

NNDMA, *N*,*N*-dimethylacrylamide; MOAB, methacryloyloxyazobenzene; P(*t*BA-*co*-AA), poly(*tert*-butyl acrylate-*co*-acrylic acid); PAzoMA, poly(azobenzene methacrylate).

MULTIFUNCTIONAL POLYMERIC MICELLES

Currently, increasing attention in micelle-based anticancer therapy is given to multifunctional micelles containing at least two out of three features regarding targeting ligands, imaging agents or triggered release. The combination of imaging agents and triggered release enables micelle tracking in the body and on-command triggered release once the micelles reach their target area, while combining active targeting and triggered release results in more efficient drug delivery. For multifunctional micelles, only pH-sensitivity as triggered release mechanism has been investigated in combination with active targeting. Kataoka *et al.* prepared doxorubicin-loaded, pH-sensitive polymeric micelles equipped with folate-ligands.

Table 6: Overview of irreversible light-responsive micelles and their cleavage mechanism

Micelle composition	Photolabile group	Light source	Cleavage mechanism
PEG-PPyMA	1-pyrenylmethyl	UV	Pyrenylmethyl ester is cleaved: PPyMA → PMA + 1-pyrenemethanol [164, 174]
PEG-*b*-PNBMA	2-nitrobenzylmethyl	UV/ NIR	PNBMA → PMA + 2-nitrosobenzoldeyde [164]
PEG-*b*-P(MA-DEACM)	DEACM	UV/ NIR	Cleavage DEACM [175]
n/a	3,5-DMB	UV	Cleavage ester of 3,5-DMB [176]

PPyMA, poly(1-pyrenylmethyl methacrylate); PMA, poly(methacrylic acid); PNBMA, poly(2-nitrobenzylmethyl methacrylate); DEACM, coumarin chromophore (7-[diethylamino]coumarin-4-yl) methyl; 3,5-DMB, 3,5-dimethoxybenzoin; n/a, not applicable.

In an *in vitro* study with human pharyngeal cancer cells, cytotoxicity of folate-bound micelles was 8-fold higher than that of non-targeted pH-sensitive micelles [180]. An *in vivo* study with mice showed that after i.v. administration the folate-equipped micelles resulted in a therapy that was substantially better than that of free doxorubicin and micelles without folate conjugation [181]. The research group of Bae successfully prepared pH-sensitive micelles bearing targeting ligands. For example, doxorubicin-loaded poly(L-histidine)-*b*-PEG-*b*-PLLA micelles were conjugated with folic acid for active targeting to overcome multidrug resistance [182]. It was shown that when the micelles were internalized by folate receptor-mediated endocytosis, the poly(L-histidine) block became protonated at endosomal pH, resulting in micelle destabilization and subsequent release of the drug into the cytosol by disruption of the endosomal membrane [104, 182]. In this way, drug interaction with the P-glycoprotein transporter, present in the cellular membrane and the major cause of multidrug resistance, is minimized [98]. In mice, these pH-sensitive micelles had significantly better antitumor effects as compared to pH-insensitive micelles [104, 182]. The same group also developed a pH-dependent doxorubicin-loaded poly(L-histidine)-*b*-PEG-*b*-PLLA micelle formulation by conjugating biotin, an example of a non-specific cell-penetrating peptide, to the hydrophilic shell of the micelles [101]. In MCF-7 cells, internalization of biotin-conjugated micelles was significantly higher at pH 7.0 as compared to pH 7.4. At pH 6.8, micelle destabilization and enhanced doxorubicin release was observed. A more advanced approach is defined by an active targeting micellar system shielded with a pH-sensitive compound. Bae's group conjugated trans-acting activator of transcription (TAT) peptide to PLLA-*b*-PEG-*b*-PSD micelles for intracellular delivery of drugs in tumor cells. At pH 7.4, the anionic PSD (poly(methacryloyl sulfadimethoxine)) is complexed with cationic TAT coupled to the distal end of the PEG block. When the pH decreases below 6.8, the sulfonamide groups lose their charge and detach, resulting in micelles which expose TAT at their surface, which subsequently facilitates cellular uptake of the micelles. This is referred as the 'pop-up' mechanism (Fig. 5) [183] and reduces the circulation half-life problems as observed with active targeting systems, since the micelles only expose the TAT peptides at the tumor site. *In vitro* studies with MCF-7 cells and *in vivo* studies in BALB/c mice with drug-resistant solid tumors resulted in effective treatment and significant tumor regression [184]. Yang *et al*. investigated folate-based active targeting

of PEG-*b*-poly(malic acid)-*co*-poly(ε-caprolactone) (PEG-*b*-PMA-*co*-PCL) micelles in combination with pH responsiveness. In mouse mammary carcinoma cells, doxorubicin uptake by tumor cells and cytotoxicity were enhanced compared to non-targeted micelles [185]. Wu *et al.* prepared pH-sensitive polymeric micelles which were conjugated with AP peptide (CRKRLDRN, which has a very specific binding

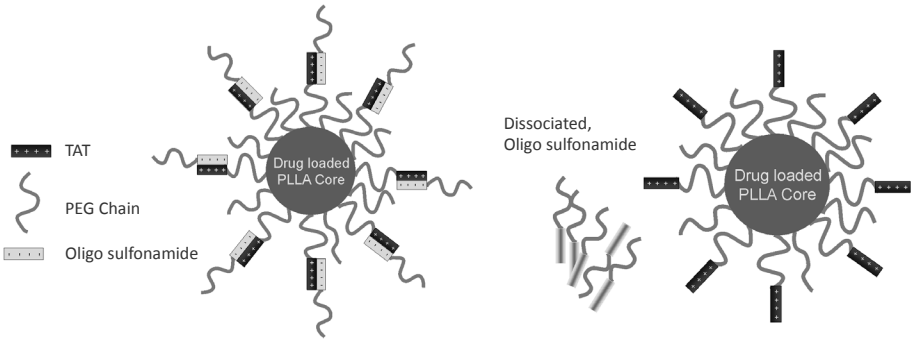

Fig. 5. Schematic model of the 'pop-up' mechanism-based micelle formulation. The carrier system consists of two components, a PLLA-*b*-PEG micelle conjugated to TAT and a pH-sensitive diblock polymer PSD-*b*-PEG. At normal blood pH, the sulfonamide groups are negatively charged, binding via electrostatic interactions to the TAT units, thereby shielding these groups (a). When the system experiences a decrease in pH (near tumor) sulphonamide looses charge and detaches, thus exposing TAT for interaction with tumor cells (b) [183].

affinity to IL-4 receptors of atherosclerotic plaques and breast tumor tissue), and demonstrated a significant increase in delivery of doxorubicin and tumor reduction in MDA-MB231 human breast tumor-bearing mice compared to non-targeted micelles and free doxorubicin [186]. As was shown in these studies, the combination of active targeting and triggered release resulted in superior cytotoxicity and antitumor activity as compared to non-multifunctional micelles. However, it would be interesting to also include other options for triggered release in combination with active targeting. For instance, temperature- or ultrasound-sensitive micelles can be triggered to release their content after exposure to HIFU and, if combined with active targeting, would result in an efficient, well-controlled drug delivery system. Another combination of strategies in micelle-based drug delivery is active targeting and imaging. In this way, the micelles can be tracked throughout the body, and the micelle deposition at the target site can be determined. Rossin *et al.* tracked the biodistribution of poly(acrylic acid-*b*-methyl acrylate) (PEG-*b*-PAA-*b*-PMA) shell-crosslinked micelles (SCKs) with autoradiography of the ^{64}Cu-labeled micelles, but did not find any significant higher uptake of folate-conjugated micelles compared to non-targeted micelles in KB tumor cell xenograft-bearing mice. This was ascribed to the presence of necrotic areas in big, fast-growing tumors, which hampered extravasation of the micelles into tumor tissue [187]. However, folate receptor-mediated uptake of the SCKs in very small tumors was observed, suggesting the possible use of radiolabeled SCKs as drug delivery systems for imaging and treatment of early-stage tumors. EGF-receptor-targeted PEG-*b*-PCL micelles labeled with ^{111}In were developed by Lee *et al.* [77]. Images taken with micro-SPECT/CT showed that the intratumoral distribution of both targeted and non-targeted micelles was heterogeneous and positively correlated with tumor

Table 7: Multifunctional micellar formulations

Block copolymer	Targeting ligand	Imaging agent	Trigger	Drug	Ref.
PEG-*b*-PBLA	Folate	n/a	pH	Dox	[177, 178]
poly(L-histidine)-*b*-PEG-*b*-PLLA	Folate	n/a	pH	Dox	[179]
poly(L-histidine)-*b*-PEG-*b*-PLLA	TAT	n/a	pH	Dox	[98, 180, 181]
PEG-*b*-PMA-*co*-PCL	Folate	n/a	pH	Dox	[182]
PEG-*b*-PDLLA	CRKRLDRN	n/a	pH	Dox	[183]
PEG-*b*-PAA-*b*-PMA	Folate	^{64}Cu (autoradiography)	n/a	n/a	[184]
PEG-*b*-PCL	EGF	^{111}In (SPECT/CT)	n/a	n/a	[74]
PEG-*b*-PDLLA	LCP	SPIO (MRI)	n/a	Dox	[185]
PEG-*b*-PDLLA	CRGD	SPIO (MRI)	n/a	Dox	[186]
PEG-*b*-PCL	Folate	SPIO (MRI)	n/a	Dox	[187]

PBLA, poly(β-benzyl-L-aspartate); n/a, not applicable; TAT, trans-acting activator of transcription; PCL, poly(ε-caprolactone); PMA, poly(malic acid); PAA-*b*-PMA, poly(acrylic acid-*b*-methyl acrylate); LCP, lung cancer-targeting peptide.

vascularization. Enhanced accumulation in tumor tissue was observed with the targeted micelles (T-BCM) compared to non-targeted micelles (NT-BCM) (Fig. 6). In a recent *in vitro* study, Guthi *et al.* described a multifunctional methoxy-terminated PEG-*b*-PDLLA micelle system that is encoded with a lung cancer-targeting peptide (LCP) and loaded with SPIONs together with doxorubicin for MR imaging and therapeutic delivery, respectively [188]. A significantly increased cell targeting, micelle uptake, superb T_2 relaxivity for ultrasensitive MR detection and cell cytotoxicity in $\alpha_v\beta_6$-expressing lung cancer cells were shown. Previously, the same micelles were conjugated with a cRGD ligand that can target $\alpha_v\beta_3$ integrins on tumor endothelial (SLK) cells [189], resulting in ultrasensitive detection by MRI and growth inhibition of tumor SLK cells. Hong *et al.* prepared a micellar formulation consisting of folate-conjugated PEG-*b*-PCL loaded with doxorubicin and SPIONs. *In vitro* studies with human hepatic carcinoma cells (Bel 7402 cells, which over-express surface receptors for folic acid) showed a significant inhibition in proliferation compared to non-targeted micelles [190]. Moreover, MR imaging revealed detection of the targeted micelles in the cells. These studies indicated the advantages of image-guided drug delivery. Diagnostics are considerably improved and drug delivery efficiency is significantly enhanced by the combination of active tumor targeting and imaging. Table 7 summarizes the micellar formulation characteristics combining different approaches.Despite the promising results in multifunctional micellar drug delivery research, the combination of all three features has not been investigated yet. Upcoming research should be focused on the development of even more advanced micellar systems to improve their efficacy. The aim is to get the highest drug concentration to the tumor tissue as possible which can be monitored by imaging to verify the absolute

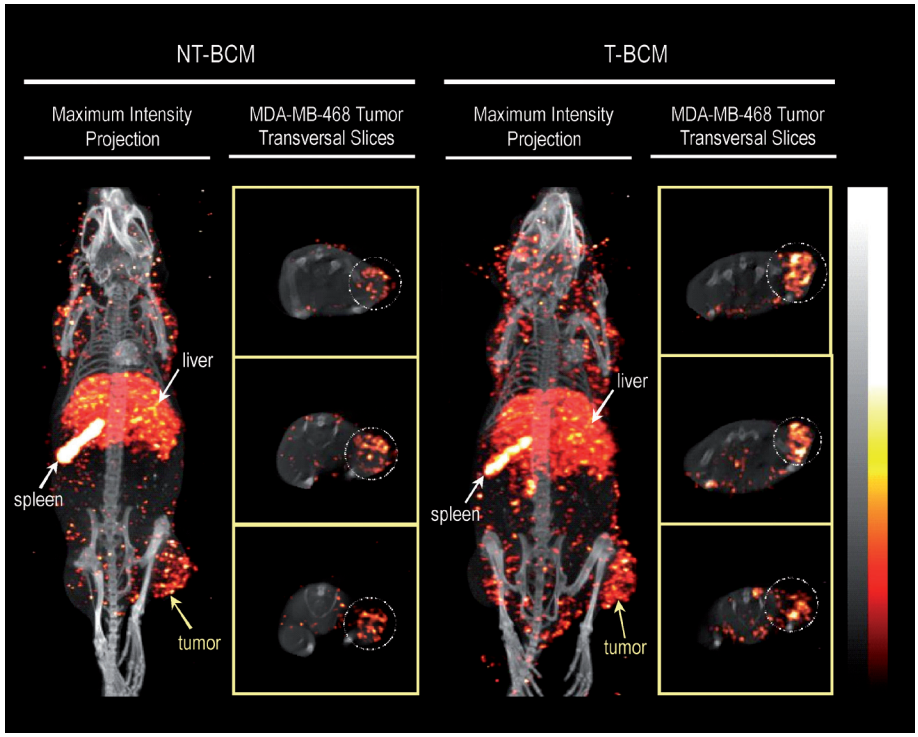

Fig. 6. MicroSPECT/CT images illustrating the whole-body biodistribution of the non-targeted block copolymer micelles (NT-BCM) and targeted block copolymer micelles (T-BCM) labeled with ^{111}In, in MDA-MB-468 tumor-bearing mice that were injected intravenously at a dose of 250 mg kg^{-1} of PEG-*b*-PCL copolymer. The maximum intensity projection and the tumor transverse slice images were acquired at 48 h post injection. The tumor transverse slices shown represent consecutive sections of the tumor at an approximate thickness of 4 mm section^{-1} [77].

released drug concentration at the target site. This will result in personalized systems which are guided by multimodality imaging techniques.

CONCLUSION AND FUTURE PERSPECTIVES

A multitude of preclinical studies on multifunctional micelles has been published, which showed that micelle-based drug delivery is advantageous over free drug delivery in laboratory animals, resulting in less adverse effects and toxicity in non-targeted areas. Until now, five (passively targeted) micelle products for anticancer therapy have been investigated in clinical trials, of which one has been granted FDA-approval (Genexol-PM) to be used in patients with breast cancer. To fully exploit the clinical possibilities of this new generation of nanomedicines, further development is required regarding drug loading and retention, circulation kinetics, tumor accumulation, target cell uptake and intracellular drug release. Additionally, the combination of multiple mechanisms for micelle-based drug delivery in anticancer therapy, characterized by active targeting, imaging and triggered release offers challenging opportunities to improve therapeutic efficacy. Despite

the interesting approaches for multifunctional drug-loaded micellar formulations, many opportunities have not been explored yet. Frequently used anticancer drugs like paclitaxel, cisplatin and 5-FU have to be investigated for multifunctional micelle-based anticancer therapy. Moreover, no multifunctional micelles based on light- or ultrasound-triggered release have been prepared yet, and only a few multifunctional micelle formulations which are able to release their content after being exposed to mild hyperthermia have been evaluated. Since imaging is an important tool to investigate biodistribution and release profiles, imaging agents should be included in the new generation of multifunctional micelles. The next step is to implement these micellar formulations in clinical anticancer therapies. Therefore, it is important that the micellar formulations comply with the Pharmacopeia and that preparation of the micelles can be performed under GMP conditions. Clinical studies require multidisciplinary expertise at different levels in which a close corporation between researchers and clinicians is essential. Labeling of micelles with a radioactive tracer allows tracking of the administered dose. For that reason, it is not only an attractive tool for *in vivo* biodistribution studies, but it can also be exploited as theranostics in patient treatment to develop individual-based therapy. Dosimetry can be used to adjust the dose to the patient since the amount of radioactivity in the tumor tissue then correlates linearly with the local drug concentration, provided that both drug and contrast agent are stably associated in the micelle during circulation. A scout dose can be administered to the patient to investigate the tumor-to-non-tumor ratio, and depending on factors like tumor type, size and responsiveness, an optimal treatment dose can be calculated. Next to conventional MRI and nuclear imaging, also the chemical exchange saturation transfer (CEST) modality can be exploited for imaging purposes in micelle-based drug delivery. The CEST modality is a recently introduced MR-derived imaging procedure which is based on the use of CEST agents containing one or more exchangeable proton pools [191, 192]. Radiofrequency irradiation of the resonance of the mobile protons results in a saturated magnetization. Due to chemical exchange, the saturated magnetization is transferred to the water signal. The major advantage of CEST agents over conventional MRI is that the signal can be generated locally. Once CEST agents are encapsulated into micelles, the coating will initially prevent signal enhancement, but after release the contrast agents will come into contact with their surroundings and exchange protons with the bulk water protons, which reduces the signal intensity, resulting in negative contrast [193]. At this moment, no micelle-based CEST agents have been developed, but the hopeful prospect will certainly lead to the exploration of this research area. The versatility of micelle-based drug delivery and the large number of promising preclinical studies describing numerous approaches to optimize these nanomedicines will bring the development of a 'magic bullet' a major step forward. Now it is time to bring this potential into clinical practice.

ACKNOWLEDGEMENTS

The authors thank dr. Cristianne Rijcken from the Department of Pharmaceutics, Utrecht Institute for Pharmaceutical Sciences (UIPS), Utrecht University, the Netherlands, for valuable discussions. The authors would like to acknowledge Meditrans (an Integrated Project funded by the European Commission) for the financial support.

REFERENCES

1. WorldHealthOrganization: fact sheet cancer. http://www.who.int/mediacentre/factsheets/fs297/en/index.html, accessed on 10-12-09.
2. Ferlay J, Parkin DM, Steliarova-Foucher E. Estimates of cancer incidence and mortality in Europe in 2008. Eur J Cancer. 2010;46:765-81.
3. Torchilin VP. Micellar nanocarriers: pharmaceutical perspectives. Pharm Res. 2007;24:1-16.
4. Torchilin VP. Targeted pharmaceutical nanocarriers for cancer therapy and Imaging. AAPS J. 2007;9:E128-47.
5. Mishra B, Patel BB, Tiwari S. Colloidal nanocarriers: a review on formulation technology, types and applications toward targeted drug delivery. Nanomedicine. 2010;6:9-24.
6. Matsumura Y. Poly (amino acid) micelle nanocarriers in preclinical and clinical studies. Adv Drug Deliv Rev. 2008;60:899-914.
7. Maeda H, Wu J, Sawa T, Matsumura Y, Hori K. Tumor vascular permeability and the EPR effect in macromolecular therapeutics: a review. J Control Release. 2000;65:271-84.
8. Weiss RB, Donehower RC, Wiernik PH, Ohnuma T, Gralla RJ, Trump DL. Hypersensitivity reactions from taxol. J Clin Oncol. 1990;8:1263-8.
9. Kloover JS, den Bakker MA, Gelderblom H, van Meerbeeck JP. Fatal outcome of a hypersensitivity reaction to paclitaxel: a critical review of premedication regimens. Br J Cancer. 2004;90:304-5.
10. Rijcken CJ, Soga O, Hennink WE, van Nostrum CF. Triggered destabilisation of polymeric micelles and vesicles by changing polymers polarity: an attractive tool for drug delivery. J Control Release. 2007;120:131-48.
11. Jones MC, Leroux JC. Polymeric micelles - a new generation of colloidal drug carriers. Eur J Pharm Biopharm. 1999;48:101-11.
12. Adams ML, Lavasanifar A, Kwon GS. Amphiphilic block copolymers for drug delivery. J Pharm Sci. 2003;92:1343-55.
13. Trubetskoy VS. Polymeric micelles as carriers of diagnostic agents. Adv Drug Deliv Rev. 1999;37:81-8.
14. Torchilin VP. Structure and design of polymeric surfactant-based drug delivery systems. J Control Release. 2001;73:137-72.
15. Sutton D, Nasongkla N, Blanco E, Gao J. Functionalized micellar systems for cancer targeted drug delivery. Pharm Res. 2007;24:1029-46.
16. Patel S, Lavasanifar A, Choi P. Application of molecular dynamics simulation to predict the compatability between water-insoluble drugs and self-associating poly(ethylene oxide)-*b*-poly(epsilon-caprolactone) block copolymers. Biomacromolecules. 2008;9:3014-23.
17. Gaucher G, Dufresne MH, Sant VP, Kang N, Maysinger D, Leroux JC. Block copolymer micelles: preparation, characterization and application in drug delivery. J Control Release. 2005;109:169-88.
18. Blanco E, Kessinger CW, Sumer BD, Gao J. Multifunctional micellar nanomedicine for cancer therapy. Exp Biol Med (Maywood). 2009;234:123-31.
19. Kabanov AV, Batrakova EV, Alakhov VY. Pluronic block copolymers as novel polymer therapeutics for drug and gene delivery. J Control Release. 2002;82:189-212.
20. Carstens MG, van Nostrum CF, Ramzi A, Meeldijk JD, Verrijk R, de Leede LL. Poly(ethylene glycol)-oligolactates with monodisperse hydrophobic blocks: preparation, characterization, and behavior in water. Langmuir. 2005;21:11446-54.
21. Carstens MG, de Jong PH, van Nostrum CF, Kemmink J, Verrijk R, de Leede LG. The effect of core composition in biodegradable oligomeric micelles as taxane formulations. Eur J Pharm Biopharm. 2008;68:596-606.
22. Matsumura Y, Kataoka K. Preclinical and clinical studies of anticancer agent-incorporating polymer micelles. Cancer Sci. 2009;100:572-9.
23. United States National Library of Medicine, overview of clinical trials available via www.clinicaltrials.org, accessed on 01-27-10.

24. Hamaguchi T, Kato K, Yasui H, Morizane C, Ikeda M, Ueno H. A phase I and pharmacokinetic study of NK105, a paclitaxel-incorporating micellar nanoparticle formulation. Br J Cancer. 2007;97:170-6.
25. Supratek Pharm Inc. Pipepline available via www.supratek.com, accessed on 10-12-09.
26. Matsumura Y. Polymeric micellar delivery systems in oncology. Jpn J Clin Oncol. 2008;38:793-802.
27. Wilson RH, Plummer R, Adam J, Eatock M, Boddy AV, Griffin M. Phase I and pharmacokinetic study of NC-6004, a new platinum entity of cisplatin-conjugated polymer forming micelles. J Clin Oncol. 26: 2008 (May 20 suppl; abstr 2573).
28. Kim TY, Kim DW, Chung JY, Shin SG, Kim SC, Heo DS. Phase I and pharmacokinetic study of Genexol-PM, a cremophor-free, polymeric micelle-formulated paclitaxel, in patients with advanced malignancies. Clin Cancer Res. 2004;10:3708-16.
29. Lee KS, Chung HC, Im SA, Park YH, Kim CS, Kim SB. Multicenter phase II trial of Genexol-PM, a Cremophor-free, polymeric micelle formulation of paclitaxel, in patients with metastatic breast cancer. BreastCancer Res Treat. 2008;108:241-50.
30. Podoltsev NA, Rubin M, Figueroa J, Lee MY, Kwonj J, Yu J. Phase II clinical trial of paclitaxel loaded polymeric micelle (GPM) in patients (pts) with advanced pancreatic cancer (APC): J Clin Oncol. 26: 2008 (May 20 suppl; abstr 4627).
31. Saif MW, Rubin M, Figueroa J, Kerr RO. Multicenter phase II trial of Genexol-PM (GPM), a novel Cremophor-free, polymeric micelle formulation of paclitaxel in patients with advanced pancreatic cancer (APC): Final results. Gastrointestinal Cancers Symposium 2008.
32. Kim DW, Kim SY, Kim HK, Kim SW, Shin SW, Kim JS. Multicenter phase II trial of Genexol-PM, a novel Cremophorfree, polymeric micelle formulation of paclitaxel, with cisplatin in patients with advanced non-small-cell lung cancer. Ann Oncol. 2007;18:2009-14.
33. Koizumi F, Kitagawa M, Negishi T, Onda T, Matsumoto S, Hamaguchi T. Novel SN-38-incorporating polymeric micelles, NK012, eradicate vascular endothelial growth factorsecreting bulky tumors. Cancer Res. 2006;66:10048-56.
34. Saito Y, Yasunaga M, Kuroda J, Koga Y, Matsumura Y. Enhanced distribution of NK012, a polymeric micelle-encapsulated SN-38, and sustained release of SN-38 within tumors can beat a hypovascular tumor. Cancer Sci. 2008;99:1258-64.
35. Nakajima TE, Yasunaga M, Kano Y, Koizumi F, Kato K, Hamaguchi T. Synergistic antitumor activity of the novel SN-38-incorporating polymeric micelles, NK012, combined with 5-fluorouracil in a mouse model of colorectal cancer, as compared with that of irinotecan plus 5-fluorouracil. Int J Cancer. 2008;122:2148-53.
36. Burris HA, Infante JR, Spigel DR, Greco FA, Thompson DS, Matsumoto S. A phase I dose-escalation study of NK012. J Clin Oncol. 26: 2008 (May 20 suppl; abstr 2538).
37. Kato K, Hamaguchi T, Shirao K, Shimada Y, Doi T, Ohtsu A. Interim analysis of phase I study of NK012, polymer micelle SN-38, in patients with advanced cancer. Gastrointestinal Cancers Symposium 2008.
38. Khayat D, Antoine EC, Coeffic D. Taxol in the management of cancers of the breast and the ovary. Cancer Invest. 2000;18:242-60.
39. Carney DN. Chemotherapy in the management of patients with inoperable non-small cell lung cancer. Semin Oncol. 1996;23:71-5.
40. Rowinsky EK, Donehower RC. Paclitaxel (taxol). N Engl J Med. 1995;332:1004-14.
41. Hamaguchi T, Matsumura Y, Suzuki M, Shimizu K, Goda R, Nakamura I. NK105, a paclitaxel-incorporating micellar nanoparticle formulation, can extend *in vivo* antitumour activity and reduce the neurotoxicity of paclitaxel. Br J Cancer. 2005;92:1240-6.
42. Danson S, Ferry D, Alakhov V, Margison J, Kerr D, Jowle D. Phase I dose escalation and pharmacokinetic study of pluronic polymer-bound doxorubicin (SP1049C) in patients with advanced cancer. Br J Cancer. 2004;90:2085-91.
43. Venne A, Li S, Mandeville R, Kabanov A, Alakhov V. Hypersensitizing effect of pluronic L61 on cytotoxic activity, transport, and subcellular distribution of doxorubicin in multiple drug-resistant cells. Cancer Res. 1996;56:3626-9.

44. Batrakova EV, Dorodnych TY, Klinskii EY, Kliushnenkova EN, Shemchukova OB, Goncharova ON. Anthracycline antibiotics non-covalently incorporated into the block copolymer micelles: *in vivo* evaluation of anti-cancer activity. Br J Cancer. 1996;74:1545-52.
45. Alakhov V, Klinski E, Li SM, Pietrzynski G, Venne A, Batrakova E. Block copolymer-based formulation of doxorubicin. From cell screen to clinical trials. Colloids Surf B-Biointerfaces. 1999;16:113-34.
46. Armstrong A, Brewer J, Newman C, Alakhov V, Pietrzynski G, Campbell S. SP1049C as first-line therapy in advanced (inoperable or metastatic) adenocarcinoma of the oesophagus: A phase II window study. J Clin Oncol. 24: 2006 (June 20 suppl; abstr. 4080).
47. Valle JW, Lawrence J, Brewer J, Clayton A, Corrie P, Alakhov Vl. A phase II, window study of SP1049C as first-line therapy in inoperable metastatic adenocarcinoma of the oesophagus. J Clin Oncol. 22: 2004 (July 15 suppl; abstr. 4195).
48. Nishiyama N, Okazaki S, Cabral H, Miyamoto M, Kato Y, Sugiyama Yl. Novel cisplatin-incorporated polymeric micelles can eradicate solid tumors in mice. Cancer Res. 2003;63:8977-83.
49. Uchino H, Matsumura Y, Negishi T, Koizumi F, Hayashi T, Honda T. Cisplatin-incorporating polymeric micelles (NC-6004) can reduce nephrotoxicity and neurotoxicity of cisplatin in rats. Br J Cancer. 2005;93:678-87.
50. Kim SC, Kim DW, Shim YH, Bang JS, Oh HS, Wan KS. *In vivo* evaluation of polymeric micellar paclitaxel formulation: toxicity and efficacy. J Control Release. 2001;72:191-202.
51. Tan E, Leong SS, Lim WT, Toh CK, Chowbay B. Weekly administration of a cremophor-free, polymeric micelle formulation of paclitaxel to Asian patients with advanced solid tumor: Phase I study results. Gastrointestinal Cancers Symposium 2007.
52. Kim C, Bae S, Lee N, Lee K, Park S, Kim D. Phase II study of Genexol (paclitaxel) and carboplatin as first-line treatment of advanced or metastatic non-small-cell lung cancer (NSCLC). J Clin Oncol. 24: 2006 (June 20 suppl.; abstr. 17049).
53. Mahmud A, Xiong XB, Aliabadi HM, Lavasanifar A. Polymeric micelles for drug targeting. J Drug Target. 2007;15:553-84.
54. Torchilin VP. Cell penetrating peptide-modified pharmaceutical nanocarriers for intracellular drug and gene delivery. Biopolymers. 2008;90:604-10.
55. Kabanov AV, Chekhonin VP, Alakhov VY, Batrakova EV, Lebedev AS, Melik-Nubarov NS. The neuroleptic activity of haloperidol increases after its solubilization in surfactant micelles. Micelles as microcontainers for drug targeting. FEBS Lett. 1989;258:343-5.
56. Vega J, Ke S, Fan Z, Wallace S, Charsangavej C, Li C. Targeting doxorubicin to epidermal growth factor receptors by site-specific conjugation of C225 to poly(L-glutamic acid) through a polyethylene glycol spacer. Pharm Res. 2003;20:826-32.
57. Wen X, Wu QP, Ke S, Ellis L, Charnsangavej C, Delpassand AS. Conjugation with (111)In-DTPA-poly(ethylene glycol) improves imaging of anti-EGF receptor antibody C225. J Nucl Med. 2001;42:1530-7.
58. Mendelsohn J. Epidermal growth factor receptor inhibition by a monoclonal antibody as anticancer therapy. Clin Cancer Res. 1997;3:2703-7.
59. Leamon CP, Reddy JA. Folate-targeted chemotherapy. Adv Drug Deliv Rev. 2004;56:1127-41.
60. Lu Y, Low PS. Immunotherapy of folate receptor-expressing tumors: review of recent advances and future prospects. J Control Release. 2003;91:17-29.
61. Avraamides CJ, Garmy-Susini B, Varner JA. Integrins in angiogenesis and lymphangiogenesis. Nat Rev Cancer. 2008;8:604-17.
62. Greish K. Enhanced permeability and retention of macromolecular drugs in solid tumors: a royal gate for targeted anticancer nanomedicines. J Drug Target. 2007;15:457-64.
63. Nasongkla N, Shuai X, Ai H, Weinberg BD, Pink J, Boothman DA, cRGD-functionalized polymer micelles for targeted doxorubicin delivery. Angew Chem Int Ed Engl. 2004;43:6323-7.

64. Torchilin VP, Lukyanov AN, Gao Z, Papahadjopoulos-Sternberg B. Immunomicelles: targeted pharmaceutical carriers for poorly soluble drugs. Proc Natl Acad Sci USA. 2003;100:6039-44.
65. Yoo HS, Park TG. Folate receptor targeted biodegradable polymeric doxorubicinmicelles. J Control Release. 2004;96:273-83.
66. Park EK, Lee SB, Lee YM. Preparation and characterization of methoxy poly(ethylene glycol)/poly(epsilon-caprolactone) amphiphilic block copolymeric nanospheres for tumor-specific folate-mediated targeting of anticancer drugs. Biomaterials. 2005;26:1053-61.
67. Han X, Liu J, Liu M, Xie C, Zhan C, Gu B. 9-NC-loaded folate-conjugated polymer micelles as tumor targeted drug delivery system: preparation and evaluation *in vitro*. Int J Pharm. 2009;372:125-31.
68. Wang Y, Yu L, Han L, Sha X, Fang X. Difunctional Pluronic copolymer micelles for paclitaxel delivery: synergistic effect of folate-mediated targeting and Pluronic-mediated overcoming multidrug resistance in tumor cell lines. Int J Pharm. 2007;337:63-73.
69. Onyuksel H, Mohanty PS, Rubinstein I. VIP-grafted sterically stabilized phospholipid nanomicellar 17-allylamino-17-demethoxy geldanamycin: a novel targeted nanomedicine for breast cancer. Int J Pharm. 2009;365:157-61.
70. Torchilin VP. PEG-based micelles as carriers of contrast agents for different imaging modalities. Adv Drug Deliv Rev. 2002;54:235-52.
71. Nijsen JF, Krijger GC. and A.D.van het Schip. The bright future of radionuclides for cancer therapy. Anticancer Agents Med Chem. 2007;7:271-90.
72. Fossheim S, Johansson C, Fahlvik AK, Grace D, Klaveness J. Lanthanide-based susceptibility contrast agents: assessment of the magnetic properties. Magn Reson Med. 1996;35:201-6.
73. Seevinck PR, Seppenwoolde JH, de Wit TC, Nijsen JF, Beekman FJ, van het Schip AD. Factors affecting the sensitivity and detection limits of MRI, CT, and SPECT for multimodal diagnostic and therapeutic agents. Anticancer Agents Med Chem. 2007;7:317-34.
74. Janjic JM, Ahrens ET. Fluorine-containing nanoemulsions for MRI cell tracking. Wiley Interdiscip Rev Nanomed Nanobiotechnol. 2009;1:492-501.
75. Zielhuis SW, Nijsen JFW, Seppenwoolde JH, Zonnenberg BA, Bakker CJG, Hennink WE. Lanthanide bearing microparticulate systems for multi-modality imaging and targeted therapy of cancer. Curr Med Chem Anti-Canc Agents. 2005;5:303-13.
76. Coenegrachts K, De Greeter F, ter Beek L, Walgraeve N, Bipat S, Stoker J. Comparison of MRI (including SS SE-EPI and SPIO-enhanced MRI) and FDG-PET/CT for the detection of colorectal liver metastases. Eur Radiol. 2009;19:370-9.
77. Lee H, Hoang B, Fonge H, Reilly RM, Allen C. *In vivo* distribution of polymeric nanoparticles at the whole-body, tumor, and cellular levels. Pharm Res (2010).
78. Hoang B, Lee H, Reilly RM, Allen C. Noninvasive monitoring of the fate of 111In-labeled block copolymer micelles by high resolution and high sensitivity microSPECT/CT imaging. Mol Pharm. 2009;6:581-92.
79. Shokeen M, Fettig NM, Rossin R. Synthesis, *in vitro* and *in vivo* evaluation of radiolabeled nanoparticles. Q J Nucl Med Mol Imaging. 2008;52:267-77.
80. Visentin R, Pasut G, Veronese FM, Mazzi U. Highly efficient technetium-99 m labeling procedure based on the conjugation of *N*-[*N*-(3-diphenylphosphinopropionyl)glycyl] cysteine ligand with poly(ethylene glycol). Bioconjug Chem. 2004;15:1046-54.
81. Pressly ED, Rossin R, Hagooly A, Fukukawa K, Messmore BW, Welch MJ. Structural effects on the biodistribution and positron emission tomography (PET) imaging of well-defined (64)Cu-labeled nanoparticles comprised of amphiphilic block graft copolymers. Biomacromolecules. 2007;8:3126-34.
82. Fukukawa K, Rossin R, Hagooly A, Pressly ED, Hunt JN, Messmore BW. Synthesis and characterization of core-shell star copolymers for *in vivo* PET imaging applications. Biomacromolecules. 2008;9:1329-39.
83. Shiraishi K, Kawano K, Minowa T, Maitani Y, Yokoyama M. Preparation and *in vivo* imaging of PEG-poly(L-lysine)-based polymeric micelle MRI contrast agents. J Control Release. 2009;136:14-20.

84. Talelli M, Rijcken CJ, Lammers T, Seevinck PR, Storm G, van Nostrum CF. Superparamagnetic iron oxide nanoparticles encapsulated in biodegradable thermosensitive polymeric micelles: toward a targeted nanomedicine suitable for image-guided drug delivery. Langmuir. 2009;25:2060-7.
85. Khemtong C, Kessinger CW, Togao O, Ren J, Takahashi M, Sherry AD. Off-resonance saturation magnetic resonance imaging of superparamagnetic polymeric micelles. Conf Proc IEEE Eng Med Biol Soc. 2009;2009:4095-7.
86. Lu J, Ma S, Sun J, Xia C, Liu C, Wang Z. Manganese ferrite nanoparticle micellar nanocomposites as MRI contrast agent for liver imaging. Biomaterials. 2009;30:2919-28.
87. Lanza GM, Winter PM, Neubauer AM, Caruthers SD, Hockett FD, Wickline SA. $^{1}H/^{19}F$ magnetic resonance molecular imaging with perfluorocarbon nanoparticles. Curr Top Dev Biol. 2005;70:57-76.
88. Caruthers SD, Neubauer AM, Hockett FD, Lamerichs R, Winter PM, Scott MJ. *In vitro* demonstration using ^{19}F magnetic resonance to augment molecular imaging with paramagnetic perfluorocarbon nanoparticles at 1.5 Tesla. Invest Radiol. 2006;41:305-12.
89. Soman NR, Lanza GM, Heuser JM, Schlesinger PH, Wickline SA. Synthesis and characterization of stable fluorocarbon nanostructures as drug delivery vehicles for cytolytic peptides. Nano Lett. 2008;8:1131-6.
90. Peng H, Blakey I, Dargaville B, Rasoul F, Rose S, Whittaker AK. Synthesis and evaluation of partly fluorinated block copolymers as MRI imaging agents. Biomacromolecules. 2009;10:374-81.
91. Du W, Nystrom AM, Zhang L, Powell KT, Li Y, Cheng C. Amphiphilic hyperbranched fluoropolymers as nanoscopic ^{19}F magnetic resonance imaging agent assemblies. Biomacromolecules. 2008;9:2826-33.
92. Torchilin VP, Frank-Kamenetsky MD, Wolf GL. CT visualization of blood pool in rats by using long-circulating, iodine-containing micelles. Acad Radiol. 1999;6:61-5.
93. Kwon GS, Okano T. Polymeric micelles as new drug carriers. Adv Drug Deliv Rev. 1996;21:107-16.
94. Teng Y, Morrison ME, Munk P, Webber SE, Prochazka K. Release kinetics studies of aromatic molecules into water from block polymer micelles. Macromolecules. 1998;31:3578-87.
95. Rapoport N. Physical stimuli-responsive polymeric micelles for anticancer drug delivery. Prog Polym Sci. 2007;32:962-90.
96. Chen W, Meng F, Li F, Ji SJ, Zhong Z. pH-responsive biodegradable micelles based on acid-labile polycarbonate hydrophobe: synthesis and triggered drug release. Biomacromolecules. 2009;10:1727-35.
97. Engin K, Leeper DB, Cater JR, Thistlethwaite AJ, Tupchong L, McFarlane JD. Extracellular pH distribution in human tumours. Int J Hyperthermia. 1995;11:211-6.
98. Lee ES, Gao Z, Bae YH. Recent progress in tumor pH targeting nanotechnology. J Control Release. 2008;132:164-70.
99. Stubbs M, McSheehy PM, Griffiths JR, Bashford CL. Causes and consequences of tumour acidity and implications for treatment. Mol Med Today. 2000;6:15-9.
100. Lee ES, Gao Z, Bae YH. Recent progress in tumor pH targeting nanotechnology. J Control Release. 2008;132:164-70.
101. Lee ES, Na K, Bae YH. Super pH-sensitive multifunctional polymeric micelle. Nano Lett. 2005;5:325-9.
102. Yin H, Bae YH. Physicochemical aspects of doxorubicin-loaded pH-sensitive polymeric micelle formulations from a mixture of poly(L-histidine)-*b*-poly(L-lactide)-*b*-poly(ethylene glycol). Eur J Pharm Biopharm. 2009;71:223-30.
103. Yin H, Lee ES, Kim D, Lee KH, Oh KT, Bae YH. Physicochemical characteristics of pH-sensitive poly(L-histidine)-*b*-poly(ethylene glycol)/poly(L-lactide)-*b*-poly(ethylene glycol) mixed micelles. J Control Release. 2008;126:130-8.
104. Kim D, Lee ES, Park K, Kwon IC, Bae YH. Doxorubicin loaded pH-sensitive micelle: antitumoral efficacy against ovarian A2780/DOXR tumor. Pharm Res. 2008;25:2074-82.

105. Lee ES, Shin HJ, Na K, Bae YH. Poly(L-histidine)-PEG block copolymer micelles and pH-induced destabilization. J Control Release. 2003;90:363-74.
106. Lee ES, Na K, Bae YH. Doxorubicin loaded pH-sensitive polymeric micelles for reversal of resistant MCF-7 tumor. J Control Release. 2005;103:405-18.
107. Lee ES, Oh KT, Kim D, Youn YS, Bae YH. Tumor pH-responsive flower-like micelles of poly(L-lactic acid)-*b*-poly(ethylene glycol)-*b*-poly(L-histidine). J Control Release. 2007;123:19-26.
108. Borchert U, Lipprandt U, Bilang M, Kimpfler A, Rank A, Peschka-Suss R. pH-induced release from P2VP-PEO block copolymer vesicles. Langmuir. 2006;22:5843-7.
109. Karanikolas A, Tsolakis P, Bokias G, Tsitsilianis C. Stimuli-responsive poly(ethylene oxide)-*b*-poly(2-vinylpyridine)-*b*-poly(ethylene oxide) triblock copolymers and complexation with poly(acrylic acid) at low p H. Eur Phys J E Soft Matter (2008).
110. Filippov S, Hruby M, Konak C, Mackova H, Spirkova M, Stepanek P. Novel pH-responsive nanoparticles. Langmuir. 2008;24:9295-301.
111. Du FS, Huang XN, Chen GT, Lin SS, Liang DH, Li ZC. Aqueous solution properties of the acid-labile thermoresponsive poly(meth)acrylamides with pendent cyclic orthoester groups. Macromolecules. 2010;43:2474-83.
112. Gillies ER, Frechet JMJ. Development of acid-sensitive copolymer micelles for drug delivery. Pure Appl Chem. 2004;76:1295-307.
113. Tang RP, Ji WH, Wang C. Amphiphilic block copolymers bearing ortho ester side-chains: pH-dependent hydrolysis and self-assembly in water. Macromol Biosci. 2010;10:192-201.
114. Bae Y, Nishiyama N, Fukushima S, Koyama H, Yasuhiro M, Kataoka K. Preparation and biological characterization of polymeric micelle drug carriers with intracellular pH-triggered drug release property: tumor permeability, controlled subcellular drug distribution, and enhanced *in vivo* antitumor efficacy. Bioconjug Chem. 2005;16:122-30.
115. Huang XN, Du FS, Cheng J, Dong YQ, Liang DH, Ji SP. Acid-sensitive polymeric micelles based on thermoresponsive block copolymers with pendent cyclic orthoester groups. Macromolecules. 2009;42:783-90.
116. Pelton R. Temperature-sensitive aqueous microgels. Adv Colloid Interface Sci. 2000;85:1-33.
117. Schild HG. Poly (*N*-Isopropylacrylamide)-experiment, theory and application. Prog Polym Sci. 1992;17:163-249.
118. Topp MDC, Dijkstra PJ, Talsma H, Feijen J. Thermosensitive micelle-forming block copolymers of poly(ethylene glycol) and poly(*N*-isopropylacrylamide). Macromolecules. 1997;30:8518-20.
119. Wei H, Cheng SX, Zhang XZ, Zhuo RX. Thermo-sensitive polymeric micelles based on poly(*N*-isopropylacrylamide) as drug carriers. Prog Polym Sci. 2009;34:893-910.
120. Chung JE, Yokoyama M, Okano T. Inner core segment design for drug delivery control of thermo-responsive polymeric micelles. J Control Release. 2000;65:93-103.
121. Chung JE, Yokoyama M, Yamato M, Aoyagi T, Sakurai Y, Okano T. Thermo-responsive drug delivery from polymeric micelles constructed using block copolymers of poly(*N*-isopropylacrylamide) and poly(butylmethacrylate). J Control Release. 1999;62:115-27.
122. Kohori F, Sakai K, Aoyagi T, Yokoyama M, Yamato M, Sakurai T. Control of adriamycin cytotoxic activity using thermally responsive polymeric micelles composed of poly(*N*-isopropylacrylamide-*co*-*N*,*N*-dimethylacrylamide)-*b*-poly(D,L-lactide). Colloids Surf B Biointerfaces. 1999;16:195-205.
123. Liu SQ, Tong YW, Yang YY. Thermally sensitive micelles self-assembled from poly(*N*-isopropylacrylamide-*co*-*N*,*N*-dimethylacrylamide)-*b*-poly(D,L-lactide-*co*-glycolide) for controlled delivery of paclitaxel. Mol Biosyst. 2005;1:158-65.
124. Liu SQ, Tong YW, Yang YY. Incorporation and *in vitro* release of doxorubicin in thermally sensitive micelles made from poly(*N*-isopropylacrylamide-co-*N*,*N*-dimethylacrylamide)-*b*-poly(D, L-lactide-*co*-glycolide) with varying compositions. Biomaterials. 2005;26:5064-74.
125. Liu B, Yang M, Li R, Ding Y, Qian X, Yu L. The antitumor effect of novel docetaxel-loaded thermosensitive micelles. Eur J Pharm Biopharm. 2008;69:527-34.

126. Qu T, Wang A, Yuan J, Shi J, Gao Q. Preparation and characterization of thermo-responsive amphiphilic triblock copolymer and its self-assembled micelle for controlled drug release. Colloids Surf B Biointerfaces. 2009;72:94-100.
127. Nakayama M, Okano T, Miyazaki T, Kohori F, Sakai K, Yokoyama M. Molecular design of biodegradable polymeric micelles for temperature-responsive drug release. J Control Release. 2006;115:46-56.
128. Prabaharan M, Grailer JJ, Steeber DA, Gong S. Thermosensitive micelles based on folate-conjugated poly(*N*-vinylcaprolactam)-block-poly(ethylene glycol) for tumor-targeted drug delivery. Macromol Biosci. 2009;9:744-53.
129. Talelli M, Rijcken CJF, van Nostrum CF, Storm G, Hennink WE. Micelles based on HPMA copolymers. Adv Drug Deliv Rev. 2010;62:231-9.
130. Soga O, van Nostrum CF, Hennink WE. Poly(*N*-(2-hydroxypropyl) methacrylamide mono/di lactate): a new class of biodegradable polymers with tuneable thermosensitivity. Biomacromolecules. 2004;5:818-21.
131. Soga O, van Nostrum CF, Ramzi A, Visser T, Soulimani F, Frederik PM. Physicochemical characterization of degradable thermosensitive polymeric micelles. Langmuir. 2004;20:9388-95.
132. Soga O, van Nostrum CF, Fens M, Rijcken CJ, Schiffelers RM, Storm G. Thermosensitive and biodegradable polymeric micelles for paclitaxel delivery. J Control Release. 2005;103:341-53.
133. Opanasopit P, Yokoyama M, Watanabe M, Kawano K, Maitani Y, Okano T. Influence of serum and albumins from different species on stability of camptothecin-loaded micelles. J Control Release. 2005;104:313-21.
134. Liu JB, Zeng FQ, Allen C. Influence of serum protein on polycarbonate-based copolymer micelles as a delivery system for a hydrophobic anti-cancer agent. J Control Release. 2005;103:481-97.
135. Savic R, Azzam T, Eisenberg A, Maysinger D. Assessment of the integrity of poly(caprolactone)-*b*-poly(ethylene oxide) micelles under biological conditions: a fluorogenic-based approach. Langmuir. 2006;22:3570-8.
136. Zhang J, Wang LQ, Wang HJ, Tu KH. Micellization phenomena of amphiphilic block copolymers based on methoxy poly(ethylene glycol) and either crystalline or amorphous poly(caprolactone-*b*-lactide). Biomacromolecules. 2006;7:2492-500.
137. Rijcken CJ, Snel CJ, Schiffelers RM, van Nostrum CF, Hennink WE. Hydrolysable core-crosslinked thermosensitive polymeric micelles: synthesis, characterisation and *in vivo* studies. Biomaterials. 2007;28:5581-93.
138. O'Reilly RK, Hawker CJ, Wooley KL. Cross-linked block copolymer micelles: functional nanostructures of great potential and versatility. Chem Soc Rev. 2006;35:1068-83.
139. Hu FQ, Ren GF, Yuan H, Du YZ, Zeng S. Shell cross-linked stearic acid grafted chitosan oligosaccharide self-aggregated micelles for controlled release of paclitaxel. Colloids Surf B Biointerfaces. 2006;50:97-103.
140. Lokitz BS, Convertine AJ, Ezell RG, Heidenreich A, Li YT, McCormick CL. Responsive nanoassemblies via interpolyelectrolyte complexation of amphiphilic block copolymer micelles. Macromolecules. 2006;39:8594-602.
141. Marin A, Muniruzzaman M, Rapoport N. Mechanism of the ultrasonic activation of micellar drug delivery. J Control Release. 2001;75:69-81.
142. Husseini GA, Pitt WG. Ultrasonic-activated micellar drug delivery for cancer treatment. J Pharm Sci. 2009;98:795-811.
143. Husseini GA, Runyan CM, Pitt WG. Investigating the mechanism of acoustically activated uptake of drugs from Pluronic micelles. BMC Cancer. 2002;2:20.
144. Bohmer MR, Klibanov AL, Tiemann K, Hall CS, Gruell H, Steinbach OC. Ultrasound triggered image-guided drug delivery. Eur J Radiol. 2009;70:242-53.
145. Husseini GA, Myrup GD, Pitt WG, Christensen DA, Rapoport NY. Factors affecting acoustically triggered release of drugs from polymeric micelles. J Control Release. 2000;69:43-52.

146. Husseini GA, Pitt WG. Micelles and nanoparticles for ultrasonic drug and gene delivery. Adv Drug Deliv Rev. 2008;60:1137-52.
147. Husseini GA, Pitt WG, Christensen DA, Dickinson DJ. Degradation kinetics of stabilized Pluronic micelles under the action of ultrasound. J Control Release. 2009;138:45-8.
148. Marin A, Sun H, Husseini GA, Pitt WG, Christensen DA, Rapoport NY. Drug delivery in pluronic micelles: effect of high-frequency ultrasound on drug release from micelles and intracellular uptake. J Control Release. 2002;84:39-47.
149. Husseini GA, Pitt WG. The use of ultrasound and micelles in cancer treatment. J Nanosci Nanotechnol. 2008;8:2205-15.
150. Munshi N, Rapoport N, Pitt WG. Ultrasonic activated drug delivery from Pluronic P-105 micelles. Cancer Lett. 1997;118:13-9.
151. Husseini GA, Christensen DA, Rapoport NY, Pitt WG. Ultrasonic release of doxorubicin from Pluronic P105 micelles stabilized with an interpenetrating network of *N*,*N*-diethylacrylamide. J Control Release. 2002;83:303-5.
152. Pruitt JD, Husseini G, Rapoport N, Pitt MG. Stabilization of pluronic P-105 micelles with an interpenetrating network of *N*,*N*-diethylacrylamide. Macromolecules. 2000;33:9306-9.
153. Nelson JL, Roeder BL, Carmen JC, Roloff F, Pitt WG. Ultrasonically activated chemotherapeutic drug delivery in a rat model. Cancer Res. 2002;62:7280-3.
154. Husseini GA, O'Neill KL, Pitt WG. The comet assay to determine the mode of cell death for the ultrasonic delivery of doxorubicin to human leukemia (HL-60 Cells) from Pluronic P105 micelles. Technol Cancer Res Treat. 2005;4:707-11.
155. Husseini GA, El-Fayoumi RI, O'Neill KL, Rapoport NY, Pitt WG. DNA damage induced by micellar-delivered doxorubicin and ultrasound: comet assay study. Cancer Lett. 2000;154:211-6.
156. Rapoport N. Combined cancer therapy by micellar-encapsulated drug and ultrasound. Int J Pharm. 2004;277:155-62.
157. Pruitt JD, Pitt WG. Sequestration and ultrasound-induced release of doxorubicin from stabilized Pluronic P105 micelles. Drug Deliv. 2002;9:253-8.
158. Gao Z, Fain HD, Rapoport N. Ultrasound-enhanced tumor targeting of polymeric micellar drug carriers. Mol Pharm. 2004;1:317-30.
159. Gao ZG, Fain HD, Rapoport N. Controlled and targeted tumor chemotherapy by micellar-encapsulated drug and ultrasound. J Control Release. 2005;102:203-22.
160. Rapoport NY, Christensen DA, Fain HD, Barrows L, Gao Z. Ultrasound-triggered drug targeting of tumors *in vitro* and *in vivo*. Ultrasonics. 2004;42:943-50.
161. Husseini GA, Diaz de la Rosa MA, Gabuji T, Zeng Y, Christensen DA, Pitt WG. Release of doxorubicin from unstabilized and stabilized micelles under the action of ultrasound. J Nanosci Nanotechnol. 2007;7:1028-33.
162. Myhr G, Moan J. Synergistic and tumour selective effects of chemotherapy and ultrasound treatment. Cancer Lett. 2006;232:206-13.
163. Wang J, Pelletier M, Zhang H, Xia H, Zhao Y. High-frequency ultrasound-responsive block copolymer micelle. Langmuir. 2009;25:13201-5.
164. Zhang H, Xia H, Wang J, Li Y. High intensity focused ultrasound-responsive release behavior of PLA-*b*-PEG copolymer micelles. J Control Release. 2009;139:31-9.
165. Enholm JK, Kohler MO, Quesson B, Mougenot C, Moonen CT, Sokka SD. Improved volumetric MR-HIFU ablation by robust binary feedback control. IEEE Trans Biomed Eng. 2010;57:103-13.
166. Kohler MO, Mougenot C, Quesson B, Enholm J, Le BB, Laurent C. Volumetric HIFU ablation under 3D guidance of rapid MRI thermometry. Med Phys. 2009;36:3521-35.
167. Zhao Y. Rational design of light-controllable polymer micelles. Chem Rec. 2007;7:286-94.
168. Wu G, Mikhailovsky A, Khant HA, Fu C, Chiu W, Zasadzinski JA. Remotely triggered liposome release by near-infrared light absorption via hollow gold nanoshells. J Am Chem Soc. 2008;130:8175-7.
169. Goodwin AP, Mynar JL, Ma Y, Fleming GR, Frechet JM. Synthetic micelle sensitive to IR light via a two-photon process. J Am Chem Soc. 2005;127:9952-3.

170. Lee HI, Wu W, Oh JK, Mueller L, Sherwood G, Peteanu L. Light-induced reversible formation of polymeric micelles. Angew Chem Int Ed Engl. 2007;46:2453-7.
171. varez-Lorenzo C, Bromberg L, Concheiro A. Light-sensitive intelligent drug delivery systems. Photochem Photobiol. 2009;85:848-60.
172. Mayer G, Heckel A. Biologically active molecules with a "light switch". Angew Chem Int Ed Engl. 2006;45:4900-21.
173. Tong X, Wang G, Soldera A, Zhao Y. How can azobenzene block copolymer vesicles be dissociated and reformed by light? J Phys Chem B. 2005;109:20281-7.
174. Irie M. Diarylethenes for memories and switches. Chem Rev. 2000;100:1685-716.
175. Yokoyama Y. Fulgides for memories and switches. Chem Rev. 2000;100:1717-40.
176. Feringa BL, van Delden RA, Koumura N, Geertsema EM. Chiroptical molecular switches. Chem Rev. 2000;100:1789-816.
177. Jiang J, Tong X, Zhao Y. A new design for light-breakable polymer micelles. J Am Chem Soc. 2005;127:8290-1.
178. Babin J, Pelletier M, Lepage M, Allard JF, Morris D, Zhao Y. A new two-photon-sensitive block copolymer nanocarrier. Angew Chem Int Ed Engl. 2009;48:3329-32.
179. McCoy CP, Rooney C, Edwards CR, Jones DS, Gorman SP. Light-triggered molecule-scale drug dosing devices. J Am Chem Soc. 2007;129:9572-3.
180. Bae Y, Jang WD, Nishiyama N, Fukushima S, Kataoka K. Multifunctional polymeric micelles with folate-mediated cancer cell targeting and pH-triggered drug releasing properties for active intracellular drug delivery. Mol Biosyst. 2005;1:242-50.
181. Bae Y, Nishiyama N, Kataoka K. *In vivo* antitumor activity of the folate-conjugated pH-sensitive polymeric micelle selectively releasing adriamycin in the intracellular acidic compartments. Bioconjug Chem. 2007;18:1131-9.
182. Kim D, Gao ZG, Lee ES, Bae YH. I *In vivo* evaluation of doxorubicin-loaded polymeric micelles targeting folate receptors and early endosomal pH in drug-resistant ovarian cancer. Mol Pharm. 2009;6:1353-62.
183. Sethuraman VA, Bae YH. TAT peptide-based micelle system for potential active targeting of anti-cancer agents to acidic solid tumors. J Control Release. 2007;118:216-24.
184. Lee ES, Gao Z, Kim D, Park K, Kwon IC, Bae YH. Super pH-sensitive multifunctional polymeric micelle for tumor $pH_{(e)}$ specific TAT exposure and multidrug resistance. J Control Release. 2008;129:228-36.
185. Yang X, Grailer JJ, Pilla S, Steeber DA, Gong S. Tumor targeting, pH-responsive, and stable unimolecular micelles as drug nanocarriers for targeted cancer therapy. Bioconjug Chem. 2010;21:496-504.
186. Wu XL, Kim JH, Koo H, Bae SM, Shin H, Kim MS. Tumor-targeting peptide conjugated pH-responsive micelles as a potential drug carrier for cancer therapy. Bioconjug Chem. 2010;21:208-13.
187. Rossin R, Pan D, Qi K, Turner JL, Sun X, Wooley KL. ^{64}Cu-labeled folate-conjugated shell cross-linked nanoparticles for tumor imaging and radiotherapy: synthesis, radiolabeling, and biologic evaluation. J Nucl Med. 2005;46:1210-8.
188. Guthi JS, Yang SG, Huang G, Li S, Khemtong C, Kessinger CW. MRI-visible micellar nanomedicine for targeted drug delivery to lung cancer cells. Mol Pharm. 2010;7:32-40.
189. Nasongkla N, Bey E, Ren J, Ai H, Khemtong C, Guthi JS. Multifunctional polymeric micelles as cancer-targeted, MRI-ultrasensitive drug delivery systems. Nano Lett. 2006;6:2427-30.
190. Hong G, Yuan R, Liang B, Shen J, Yang X, Shuai X. Folate-functionalized polymeric micelle as hepatic carcinoma-targeted, MRI-ultrasensitive delivery system of antitumor drugs. Biomed Microdevices. 2008;10:693-700.
191. Woods M, Donald EWC, Sherry AD. Paramagnetic lanthanide complexes as PARACEST agents for medical imaging. Chem Soc Rev. 2006;35:500-11.
192. Ward KM, Aletras AH, Balaban RS. A new class of contrast agents for MRI based on proton chemical exchange dependent saturation transfer (CEST). J Magn Reson. 2000;143:79-87.
193. Terreno E, Stancanello J, Longo D, Castelli DD, Milone L, Sanders HM. Methods for an improved detection of the MRI-CEST effect. Contrast Media Mol Imaging. 2009;4:237-47.

Chapter 3

Roel Deckers
Agnes Paradissis
Chris Oerlemans
Marina Talelli
Gert Storm
Wim Hennink
Frank Nijsen

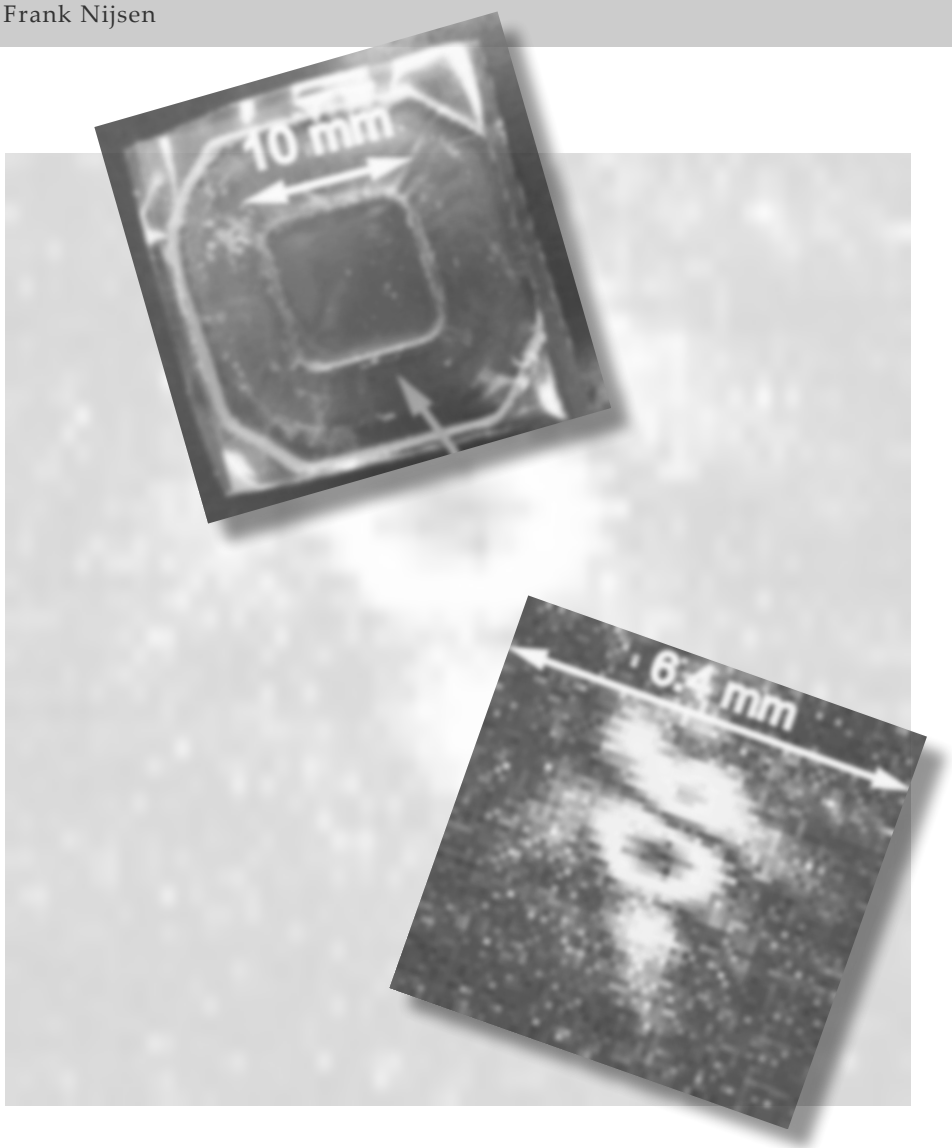

I New insights into the HIFU-triggered release from polymeric micelles

Submitted

ABSTRACT

Continuous wave- (CW), low frequency, high intensity focused ultrasound (HIFU) is a promising modality to trigger release of active compounds from polymeric micelles. The aim of the present study was to investigate whether high frequency CW- as well as pulsed wave- (PW) HIFU can induce the release of a hydrophobic agent from non-crosslinked (NCL) and core crosslinked (CCL) poly(ethylene glycol)-*b*-poly[*N*-(2-hydroxypropyl) methacrylamide-lactate] (mPEG-*b*-p(HPMAm-Lac_n)) micelles. It was shown that high frequency CW- as well as PW-HIFU was able to trigger the release (up to 85%) of the hydrophobic compound Nile red (NR) from NCL and CCL micelles. No changes in size distribution of the micelles after CW- and PW-HIFU exposure were observed and no degradation of the polymer chain had occurred. We therefore hypothesize that the polymeric micelles are temporally destabilized upon HIFU exposure due to radiation force induced shear forces, leading to NR release on demand.

INTRODUCTION

In recent years, there is a growing interest in using nanosized drug-loaded carriers ('nanomedicines') to improve (cancer) treatment [1-3]. These drug carriers aim for a reduced systemic toxicity and an improved efficacy of particularly chemotherapeutic drugs. Among the different drug carriers such as liposomes, polymeric micelles are one of the most promising drug carrier systems. The water solubility of hydrophobic drugs can be increased by loading them into the hydrophobic core of micelles, resulting in improved bioavailability. In addition, premature degradation of the drug is minimized. Furthermore, their submicron size (10-200 nm) allows them to accumulate in the tumor tissue via the enhanced permeability and retention (EPR) effect [4-10]. Triggered release of micelle-loaded drugs may lead to a high local drug concentration at the aimed site. Over the past decades, several types of internal and external triggers have been investigated to release drugs from their nanosized carrier systems, including light, temperature and pH [11-15]. Recently, high intensity focused ultrasound (HIFU) has been proposed as a modality for triggered release of active compounds from polymeric micelles as well as other nanocarriers [16-18]. Ultrasound is a mechanical wave that transports energy through a medium and which can be focused within a volume of about 10 mm^3 in deep tissue (~10 cm). The interactions of the ultrasound waves with tissue may lead to local heating and mechanical stress (i.e. cavitation, radiation force) depending on characteristics of the ultrasound wave (i.e. continuous wave versus pulsed wave ultrasound, frequency and intensity) [19-21]. Husseini *et al.* and Rapoport *et al.* have shown that low frequency (20-90 kHz) continuous wave- (CW) ultrasound can be used to release hydrophobic agents from non-stabilized as well as stabilized pluronic micelles [22, 23]. Ultrasound-induced release of chemotherapeutic agents from pluronic micelles has shown to be effective in killing cancer cells *in vitro* as well as *in vivo* [24, 25]. However, low frequency ultrasound is associated with unwanted cavitation in healthy tissue and can be less focused in one point, therefore clinical applications are restricted to some extent [26-28]. Recently, it has been shown that high frequency CW ultrasound (1.1 MHz) might also be used for triggering drug release from block copolymer micelles [29-31]. It was reported that cavitation caused the accelerated degradation of the micelle forming PLA-*b*-PEG copolymer resulting in destabilization of the micelles and release of the hydrophobic payload. Although the use of high frequency HIFU reduces the possibility of unwanted cavitation, the use of CW-HIFU can lead to tissue heating *in vivo*. In contrast, when using pulsed wave- (PW) HIFU, the ultrasound wave is only transmitted repetitively during a short period of time, followed by a long time period of no transmission thereby evading tissue heating. The aim of the present study is to investigate whether high frequency CW- as well as PW-HIFU can induce the release of the hydrophobic model compound Nile red (NR) from non-crosslinked (NCL) and core crosslinked (CCL) poly(ethylene glycol)-*b*-poly[*N*-(2-hydroxypropyl) methacrylamide-lactate] (mPEG-*b*-p(HPMAm-Lac_n)) micelles.

MATERIALS AND METHODS

MATERIALS

Tetrahydrofuran (THF) and methanol (MeOH), both of analytical grade, were purchased from Biosolve Ltd. (Valkenswaard, the Netherlands). THF was purified by reflux distillation over sodium and stored with molecular sieves. Triethylamine was obtained from Merck (Darmstadt, Germany). Nile red (NR), potassium persulfate (KPS) and tetramethylethylenediamine (TEMED) were purchased from Sigma Aldrich (Zwijndrecht, the Netherlands). All buffers were filtered through a 0.22 μm filter prior to use.

BLOCK COPOLYMER SYNTHESIS

Block copolymers composed of pHPMAm-Lac$_n$ (various mono- and dilactate ratios) as thermosensitive block and mPEG$_{5000}$ as hydrophilic block were synthesized by radical polymerization using (mPEG$_{5000}$)$_2$-ABCPA as macroinitiator (ratio of monomer : initiator was 150 : 1) as described previously [32]. The percentage of pHPMAmLac$_2$ in the block copolymer was determined based on the ^{1}H-NMR spectra. ^{1}H NMR spectra of the polymers were recorded with a Gemini 300 MHz spectrometer (Varian Associates Inc. NMR Instruments, Palo Alto, CA, USA) before and after HIFU exposure. NCL micelles (polymer concentration of 10 mg mL^{-1}) in phosphate buffer (pH 7.4) were freeze dried. The obtained samples were dissolved in DMSO d6. ^{1}H-NMR (DMSO, d6): 7.5 (b, CO-NH-CH$_2$), 5.5 (b, CH-OH (HPMAmLac$_2$), 5.3 (b, CH-OH (HPMAmLac$_1$), 5.0 (b, CO-CH (CH$_3$)-O), 4.1 (b, CO-CH-(CH$_3$)-OH), 3.6 (b, PEG methylene protons, O-CH$_2$-CH$_2$), 3.4 (b, NH-CH$_2$-CH$_2$), 1.4, (b, CO-CH-CH$_3$), 1.3 (b, HO-CH-CH$_3$), 1.0-0.6 (pHPMAmLac$_n$ main chain protons). The percentage of pHPMAmLac$_2$ in the block copolymer was determined based on the ^{1}H-NMR spectra: L2 / (L1 + L2) x 100%; 'L1' and 'L2' are assigned as the protons peaks of the hydroxyl group of pHPMAmLac$_1$ and pHPMAmLac$_2$, respectively.

METHACRYLATION

Methacrylate groups were coupled to the thermosensitive block of mPEG-*b*-p((HPMAm-Lac$_1$)-*co*-(HPMAm-Lac$_2$)) by reaction of methacrylic anhydride with part of the terminal hydroxyl groups of the lactate side chains. The block copolymer (50 mg mL^{-1}) was dissolved in distilled and dried THF. Next, methacrylic anhydride, triethylamine (equal molar amount relative to methacrylic anhydride), as well as DMAP (4 eq, relative to polymer), were added. After reaction at room temperature for 16 h, the reaction mixture was dialyzed (membrane with a weight cut-off of 12-14 kDa) against water and freeze dried. The percentage of -OH groups in the polymer derivatized with methacrylate groups was determined with ^{1}H NMR in DMSO-d6 as follows: (((m + n) / 2) / ((m + n) / 2) + L1 + L2) × 100% in which 'm' and 'n' correspond with the two protons of the double bond of methacrylate groups attached either to pHPMAm-Lac$_1$ or pHPMAm-Lac$_2$ chains. 'L1' is the proton of the free alcohol functionality of pHPMAm-Lac$_1$, 'L2' is the proton of the free alcohol functionality of pHPMAm-Lac$_2$, and '(m + n) / 2' the number of derivatized pHPMAm-Lac$_1$ and pHPMAm-Lac$_2$ chains [33]. The number average molecular weight (M_n) before HIFU exposure of the block copolymer was determined by ^{1}H NMR from the ratio of the

integral of the peak at 3.6 ppm (PEG methylene protons) to the integral of the peak at 4.1 ppm (methine proton (CO-CH (CH_3)-OH). Furthermore, the possible hydrolysis of the lactic acid side groups due to HIFU exposure was studied using ^{1}H NMR by comparing the integral of the peak at 5.5 (CH-O<u>H</u> ($HPMAmLac_2$) before and after HIFU exposure.

DETERMINATION OF CRITICAL MICELLE TEMPERATURE (CMT)

The critical micelle temperature (CMT) of the synthesized block copolymers in aqueous solution was measured by light scattering using a Shimadzu UV 2450 UV/Vis spectrometer as described previously [33]. The polymers were dissolved overnight at 4 °C in ammonium acetate buffer (120 mM, pH 5) at a concentration of 2 mg mL^{-1}.

NON-CROSSLINKED (NCL) MICELLE FORMATION

NCL polymeric micelles were formed via the 'rapid heating' procedure at pH 5 and pH 7.4 as described previously [34]. In brief, mPEG-*b*-p(HPMAm-Lac_2) was dissolved in ammonium acetate buffer (pH 5, 120 mM) or phosphate buffer (pH 7.4, 100 mM) at an initial concentration of 2 mg mL^{-1} or 10 mg mL^{-1} (for the GPC study and ^{1}H NMR study) and stored overnight at 4 °C. The solutions were incubated at 0 °C for at least 15 min in glass vials. Next, Nile red (NR), a hydrophobic fluorescent dye, was dissolved in THF at a concentration of 5 μg mL^{-1} and mixed with mPEG-*b*-p(HPMAm-Lac_2), volume ratio 1 to 9. The mixture was rapidly heated to 50 °C in a water bath under vigorous shaking for 1 min. The obtained dispersions contained 0.5 μg mL^{-1} NR and 1.8 or 9 mg mL^{-1} polymer. THF was evaporated under nitrogen flow for 30 min. Finally, the NCL micelles were filtrated through a 0.45 μm filter, stored at room temperature and used within one day for the HIFU experiments.

CORE CROSSLINKED (CCL) MICELLE FORMATIONS

CCL micelles (with methacrylation percentages of 4% and 13%) were formed via the same 'rapid heating' procedure as described above. In brief, mPEG-*b*-p((50% HPMAm-Lac_1)-*co*-(50% HPMAm-Lac_2)) block copolymer (2 mg mL^{-1}) was dissolved overnight at 4 °C in ammonium acetate buffer (pH 5, 120 mM) or in phosphate buffer (pH 7.4, 100 mM). Next, 75 μL of TEMED solution (120 mg mL^{-1}, in ammonium acetate buffer 120 mM, pH 5 or in phosphate buffer 100 mM, pH 7.4) was added to 2.49 mL of polymer solution, followed by the addition of 300 μL of NR solution in THF (5 μg mL^{-1}). The mixture was rapidly heated at 50 °C and subsequently slowly cooled down to room temperature, and 135 μL of KPS solution (30 mg mL^{-1} in ammonium acetate buffer 120 mM, pH 5 or in phosphate buffer 100 mM, pH 7.4) was added. The polymerization was performed by incubating the mixture under a nitrogen atmosphere for 1 h. The resulting formulation (3 mL) contained 1.6 μg mL^{-1} polymer and 0.5 μg mL^{-1} NR. THF was evaporated under nitrogen flow for 30 min. To remove possible aggregates as well as non-encapsulated, precipitated NR, the micellar dispersions were filtered using a 0.45 μm filter (regenerated cellulose syringe filter, Grace Davison Discovery Science, Breda, the Netherlands). The CCL micelles were stored at room temperature and used for the HIFU experiments within 24 h.

HIFU EQUIPMENT

To expose a small volume (0.5 mL) of micellar dispersion to HIFU, an in-house developed sample-holder was built (Fig. 1a). The sample-holder was made from a silicone-like gasket (Thermo Fisher Scientific, Landsmeer, the Netherlands) sealed on both sides with an ultrasound transparent polyester heat seal membrane (Waters, Acquity UPLC Consumables, Etten-Leur, the Netherlands), see Fig 1b. The sample-holder was submerged in water at room temperature and placed in the focal point of a mono-element focused ultrasound transducer (Imasonic, Besançon, France), see Fig. 1a. The transducer had an external radius aperture of 120 mm and a focal length of 80 mm. The sinusoidal signal (1.5 MHz) was generated by using a AG 1006 amplifier/generator. The dimensions of the focal point were 2 x 2 x 5 mm^3 (at -3 dB). The small size of the sample holder together with the ultrasound induced convection in the sample holder ensured that the complete sample volume was sonicated during the chosen exposure times (Fig. 1c). The acoustic output power of the HIFU system was calibrated with a balance measurement [35]. Acoustic powers in the range of 2.5-20 W were used, which corresponds to a spatial peak, temporal peak intensity (I_{SPTP}) of 0.8-6.7 W mm^2 and peak negative pressure of 1.6-4.5 MPa. The SonoVue microbubbles were obtained from Bracco (Milan, Italy) and the suspension was prepared according to the manufacturer's instructions, resulting in 1-5 x 10^8 microbubbles mL^{-1} [36]. The microbubbles were mixed with the micelles (7% v/v) before injection in the sample holder.

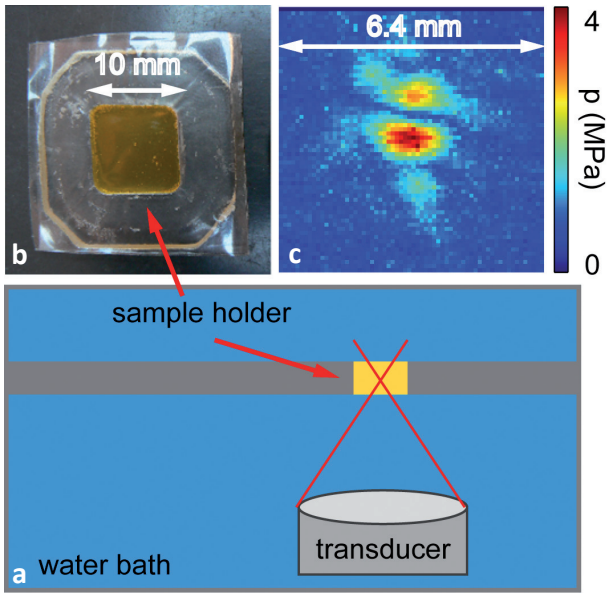

Fig. 1. Schematic overview of HIFU set-up (a). Photo of the in-house developed sample holder with a volume of 0.5 mL (b). Pressure map (in MPa) in focal point at 20 W acoustic power (c).

ANALYTICAL METHODS

The measurements of the amount of release are based on the decrease of NR fluorescence upon the release of NR from the core of the micelle into the aqueous solution. The fluorescence of NR depends strongly on the polarity of its environment. Releasing the

NR from the hydrophobic core of the micelles into the buffer solution causes a larger increase in polarity, which leads to a substantial red shift of the emission spectrum as well as significant decrease of the quantum yield and fluorescence lifetime. After HIFU exposure, the micellar dispersions were collected and the fluorescence emission spectrum (570-700 nm) was recorded on a spectrophotometer with an excitation wavelength of 550 nm. To calculate the percentage of released NR the following equation was used: NR released (%) = (NR_0 - NR_{HIFU} / (NR_0 - NR_{aa}) x 100%, where NR_0 is the fluorescence emission peak intensity at ~600 nm recorded before ultrasound exposure. NR_{HIFU} is the fluorescence emission peak intensity at ~600 nm recorded after exposing the NR-loaded micelles to HIFU. NR_{aa} is the fluorescence emission peak intensity at ~600 nm of NR (0.5 μg mL^{-1}) in ammonium acetate buffer in the absence of polymer. The average size and polydispersity index (PDI) of the NR-loaded NCL and CCL micelles were determined by dynamic light scattering (DLS) using a Malvern CGS-3 multi-angle goniometer (Malvern Ltd., Malvern, UK) equipped with a JDS Uniphase 22 mW HeNe 632-nm laser, an optical fiber-based detector and a digital LV/LSE-5003 correlator. Autocorrelation functions were analyzed by the cumulants method (fitting a single exponential to the correlation function to obtain the mean size and the PDI) and the CONTIN routine (fitting a multiple exponential to the correlation function to obtain the distribution of particle sizes). The measurements were performed in triplicate at 25 °C and at a 90° angle. The molecular weight of the polymers was measured using gel permeation chromatography (GPC) before and after HIFU exposure. In short, two serial PLgel 3 μm MIXED-D columns (Polymer Laboratories, UK) were used with a Waters System (Waters Associates Inc., Milford, MA) with a differential refractometer model 410. DMF containing 10 mM LiCl was used as the eluent at a flow rate of 0.7 mL min^{-1} at 40 °C. The samples were dissolved overnight at a concentration of 5 mg mL^{-1} in the eluent and filtered through a 0.45 μm filter prior to analysis. The molecular weights were calibrated with poly(ethylene glycol) standards.

EXPERIMENTAL PROTOCOLS

To investigate the relationship between duration and power of the HIFU exposure and the release of NR, all micelle formulations (polymer concentration 2 mg mL^{-1}, pH 7.4 and pH 5 (only NCL)) were subjected to continuous wave- (CW) HIFU exposure (*f* = 1.5 MHz) for different durations (1, 2, 3 and 4 min) at constant acoustic power (20 W) and different acoustic powers (2.5, 5, 10 and 20 W) with constant exposure time (4 min). Before and directly after CW-HIFU exposure the size distribution of the micelles was measured using DLS. In addition, ^1H NMR spectra were recorded and GPC analyses were performed after exposing NCL micelles (polymer concentration 10 mg mL^{-1}, pH 7.4) during 4 min to 20 W of HIFU. Furthermore, the relationship between duration and power of PW-HIFU exposure (*f* = 1.5 MHz, Pulse Repetition Frequency (PRF) = 1 kHz, Duty Cycle (DC) = 10%) and the release of NR from NCL micelles (polymer concentration 2 mg mL^{-1}, pH 5) was investigated. NCL micelles (0.5 mL) with and without microbubbles (7% v/v) were subjected to PW-HIFU exposure for different durations (1, 2, 5 and 10 min) at constant acoustic power (10 W) and different acoustic powers (2.5, 5, 10 and 20 W) with constant exposure time (10 min). Note that the effective HIFU-on time for the PW-HIFU experiments is only 10% of the exposure time mentioned above. In Table 1, the HIFU experiments and analyses as performed in this study are summarized. To verify that the observed decrease

Table 1: Overview of experiments performed with different micelle formulations

Polymer concentration	Micelle formulation	pH = 5	pH = 7.4	DLS	GPC	^{1}H NMR
2 mg mL^{-1}	NCL	CW^1	CW^1	pre, post	-	-
	CCL 4%	-	CW^1	pre, post	-	-
	CCL 13%	-	CW^1	pre, post	-	-
	NCL	PW	-	pre, post	-	-
	NCL	PW+MB	-	pre, post	-	-
	NCL	HT	HT	pre, post	-	-
	CCL 4%	HT	HT	pre, post	-	-
	CCL 13%	HT	HT	pre, post	-	-
10 mg mL^{-1}	NCL	-	CW^2	-	pre, post	pre, post

Abbreviations: CCL 4%, core crosslinked micelles, 4% methacrylation; CCL 13%, core crosslinked micelles, 13% methacrylation; CW^1, continuous wave HIFU, exposure time: 1-4 min, acoustic power: 2.5-20 W; CW^2, continuous wave HIFU, exposure time: 4 min, power: 20 W; HT, hyperthermia; MB, microbubbles; NCL, non-crosslinked micelles; post, after HIFU/hyperthermia exposure; pre, before HIFU/hyperthermia exposure; PW, pulsed wave HIFU, exposure time: 1-4 min, power: 2.5-20 W; PW + MB, pulsed wave HIFU + MB. Exposure time: 1-4 min, power: 2.5-20 W.

in fluorescence intensity is not due to HIFU-induced degradation of NR, control experiments were performed whereby NR (0.5 μg mL^{-1}) in MeOH was exposed to CW-HIFU (4 min, 20 W). Furthermore, to exclude temperature-induced release of the NR from the micelles, the temperature at the position of the focal point was measured at the highest exposure condition (i.e. CW-HIFU, 4 min, 20 W) with a Ni(Cr)-NiK thermocouple (Thermodig N800, AIS, France) fixed in the in-house developed US-permeable sample-holder (filled with 0.5 mL micelle dispersion). In addition, NCL and CCL micelles (4% and 13% methacrylation) were incubated during 1 h in a water bath at different temperatures (20 °C, 37 °C and 45 °C) and every 3 min a sample was taken to determine the particle size with DLS and the release of NR using fluorescence spectroscopy. All experiments were performed in triplicate.

RESULTS

CHARACTERIZATION OF SYNTHESIZED BLOCK COPOLYMERS, NCL MICELLES AND CCL MICELLES

The block copolymer composed of a thermosensitive block of pHPMAm-Lac$_2$ and a hydrophilic mPEG$_{5000}$ block was obtained by radical polymerization using a mPEG-macroinitiator, resulting in a yield of ~80%. The number average molecular weight (M_n) of the resulting block copolymer mPEG-*b*-p(HPMAm-Lac$_2$) was 26,000 g mol^{-1} (M_w/M_n = 1.4) as determined by GPC analysis. The critical micelle temperature (CMT)

Table 2: Characteristics of the synthesized block copolymers

Polymer	M_n (kDa, GPC)	M_w/M_n (GPC)	M_n (kDa, NMR)	Lac_2 (%)	Methacrylation (%)	CMT (°C)
mPEG-*b*-p(HPMAm-Lac_2)	26	1.4	23	100	-	4
mPEG-*b*-p(HPMAm-Lac_1)-*co*-HPMAm-Lac_2)	22	1.9	18	45.7	4	25*
mPEG-*b*-p(HPMAm-Lac_1)-*co*-HPMAm-Lac_2)	22	1.9	18	45.7	13	9*

*before methacrylation CMT was 29 °C. Abbreviations: CMT, critical micelle temperature; GPC, gel permeation chromatography; M_n, number average molecular weight; M_w, weight average molecular weight; NMR, ^{1}H NMR.

Table 3: Size and size distribution of NCL and CCL micelles (polymer concentration 2 mg mL^{-1}) before and after CW-HIFU (20 W, 4 min). Results are presented as mean ± SD.

Micelle type	Z_{AVE} before (nm)	Z_{AVE} after (nm)	PDI before	PDI after
NCL (pH 5)	72 ± 5	82 ± 11	0.1 ± 0.0	0.2 ± 0.1
NCL (pH 7.4)	91 ± 11	99 ± 8	0.2 ± 0.1	0.2 ± 0.0
CCL 4% (pH 7.4)	96 ± 1	98 ± 1	0.1 ± 0.0	0.2 ± 0.0
CCL 13% (pH 7.4)	67 ± 7	70 ± 11	0.1 ± 0.0	0.2 ± 0.0

Abbreviations: CCL 4%, core crosslinked micelles, 4% methacrylation; CCL 13%, core crosslinked micelles, 13% methacrylation; NCL, non-crosslinked micelles; PDI, polydispersity; Z_{AVE}, Z-average.

was 4 °C, which was in agreement with previous studies [39, 40]. The block copolymer composed of a random block of pHPMAm-Lac_1/Lac_2 and a hydrophilic $mPEG_{5000}$ block also resulted in a yield ~80% using the same method described above. The number average molecular weight (M_n) of this mPEG-*b*(HPMAm-Lac_1)-*co*-p(HPMAm-Lac_2) was 22,000 g mol^{-1} (M_w/M_n = 1.9). The co-monomer composition of the thermosensitive block was 54.3 mol% HPMAm-Lac_1 and 45.7 mol% HPMAm-Lac_2, as determined by ^{1}H NMR, which is close to the feed ratio of 1:1. Part of the lactate groups (4% and 13%) of this block copolymer was derivatized with methacrylate groups. Similar to previous data, introduction of methacrylate groups rendered the block copolymer more hydrophobic, resulting in a decrease of the CMT from 29 °C to 25 °C and to 9 °C for 4% and 13% methacrylation, respectively, which was in line with previous data [32, 41]. The characteristics of the synthesized polymers are summarized in Table 2. The average size of the NR-loaded NCL and CCL micelles formulations before HIFU exposure, as measured by DLS, was between 72 and 96 nm (PDI ≤ 0.2) (Table 3).

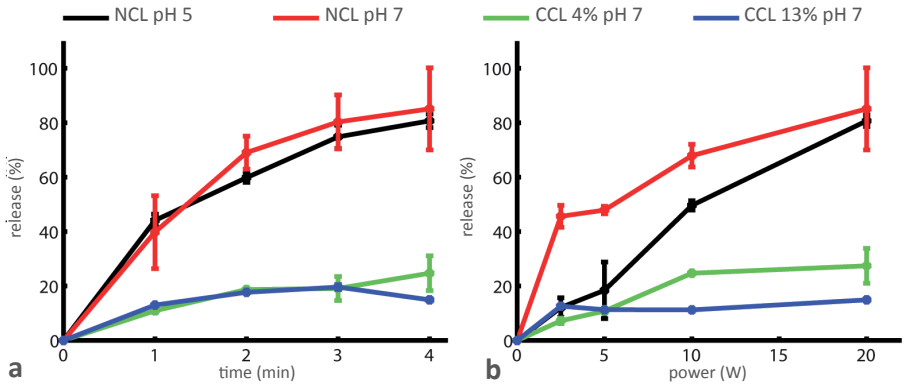

Fig. 2. Release of NR from polymeric micelles upon CW-HIFU exposure as function of exposure time with acoustic power set at 20 W (a) and as function of acoustics power with exposure time set at 4 min (b). NCL micelles were exposed to CW-HIFU at pH 5 and 7.4. CCL micelles with two different extents of crosslinking (4% and 13% methacrylation) were exposed to CW-HIFU at pH 7.4. All experiments were performed at room temperature and in triplicate.

HIFU-TRIGGERED RELEASE OF NR FROM mPEG-*b*-P(HPMAM-LAC$_N$) MICELLES

Fig. 2 shows that the release of NR from NCL micelles increased with increasing exposure time at constant power (Fig. 2a) as well as with increasing acoustic power at constant exposure time (Fig. 2b) at pH 5 and 7.4. Almost all of the loaded NR (~85%) was released from the NCL micelle samples after 20 W of CW-HIFU exposure during 4 min. No differences in release of NR from NCL micelles were observed at pH 5 and 7.4 after CW-HIFU exposure at 20 W with increasing exposure time (Fig. 2a). However, the release kinetics of NR from NCL micelles as a function of power was different for pH 5 and pH 7.4 (Fig. 2b). At low powers less release of NR from NCL micelles at pH 5 than at pH 7.4 was observed, but at 20 W the release was equal. In contrast to NCL, the CCL micelles (4% and 13% methacrylation) responded substantially less to CW-HIFU exposure and showed only 15-20% release of the payload with both increasing exposure time and with increasing acoustic power. At pH 7.4 there was no significant difference in NR release from 4% and 13% CCL micelles at constant acoustic power and increasing exposure duration (Fig. 2a). However, at constant exposure time and increasing acoustic power slightly more NR release was observed from the CCL micelles with 4% methacrylation compared to the CCL micelles with 13% methacrylation (27% and 15% respectively at 20 W and 4 min). For both NCL micelles and NCL micelles in the presence of microbubbles, a small increase of NR release with increasing exposure time was observed (Fig. 3a) upon PW-HIFU exposure at constant acoustic power (10 W, pH 5). However, in the presence of microbubbles the release was about 10% lower. A similar release profile was observed for NCL micelles at pH 5 with and without the presence of microbubbles with increasing acoustic power at constant exposure time, i.e. 10 min (Fig. 3b). Again, a 10% lower NR release in the presence of microbubbles was observed. The percentage of NR released (around 40% in the absence of microbubbles) is comparable for CW- and PW-HIFU at equal amounts of energy deposit, i.e. 1 min CW- and 10 min PW-HIFU exposure at 20 W.

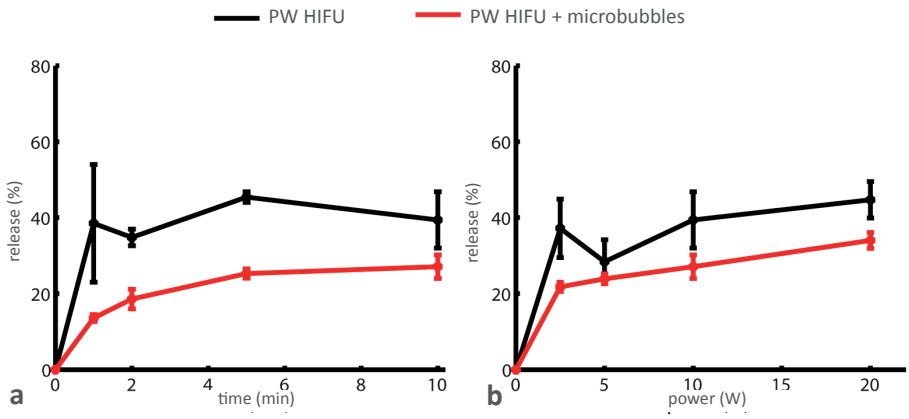

Fig 3. Release of NR from NCL polymeric micelles (pH 5) using PW-HIFU with and without microbubbles as function of exposure time with acoustic power set at 10 W (a) and as function of acoustic power with exposure time set at 10 min (b). All experiments were performed at room temperature and in triplicate.

CONTROL EXPERIMENTS

No fluorescence was measured in spectrophotometric control experiments using empty NCL micelles. Furthermore, in these control experiments it was shown that the fluorescence emission spectrum of NR (0.5 μg mL^{-1}) in buffer is red shifted and has a very low quantum yield. Finally, it was shown that the fluorescence emission spectrum of NR dissolved in MeOH does not changed upon HIFU exposure (Fig. 4a). A maximum temperature increase of ~9 °C (so actual temperature was ~29 °C) was measured when applying 20 W CW-HIFU during 4 min. However, after 60 min of exposure to temperatures of 20 °C, 37 °C or 45 °C in a warm water bath the maximum

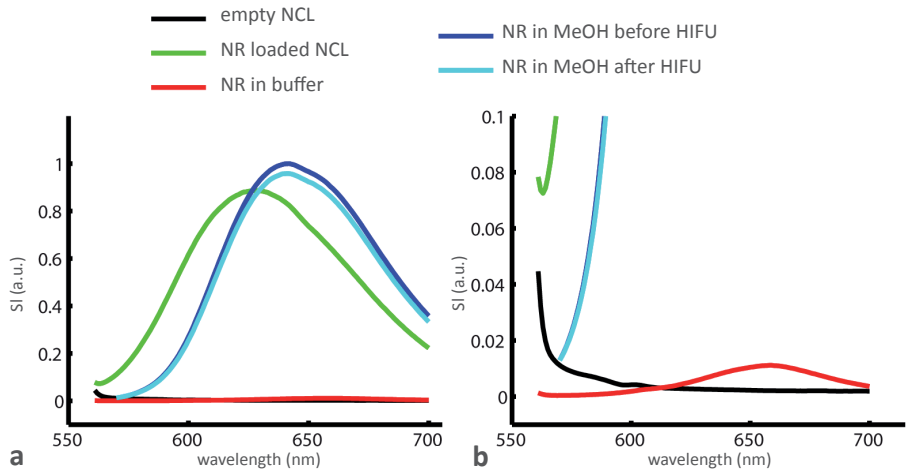

Fig. 4. Fluorescence emission spectra of empty NCL micelles, NR loaded NCL micelles, NR (0.5 μg mL^{-1}) in buffer and NR (0.5 μg mL^{-1}) in MeOH before and after HIFU (a). Y-axis zoom of same spectra (b).

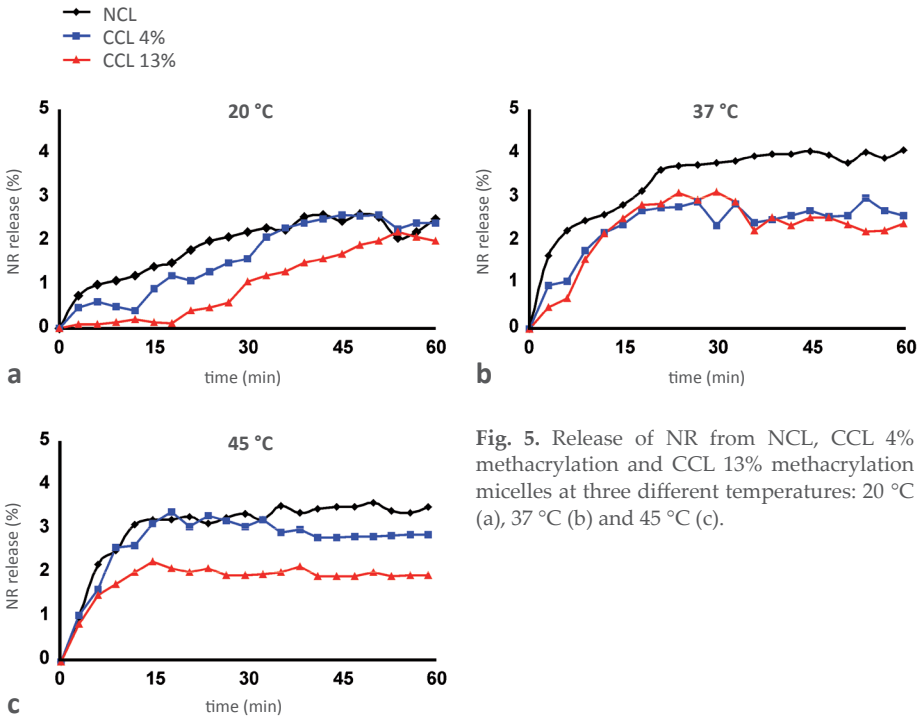

Fig. 5. Release of NR from NCL, CCL 4% methacrylation and CCL 13% methacrylation micelles at three different temperatures: 20 °C (a), 37 °C (b) and 45 °C (c).

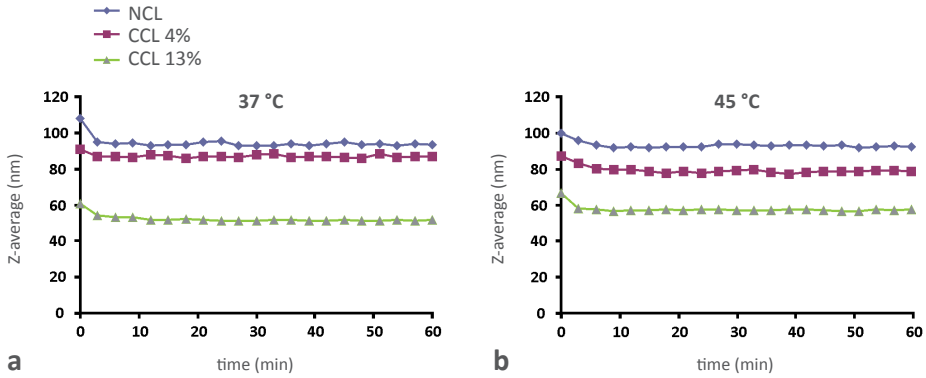

Fig. 6. Stability of NR-loaded NCL and CCL micelles as determined by DLS at pH 7.4 incubated over time at 37 °C (a) and 45 °C (b). Figure shows Z-average (in nm) of different micellar formulations as function of time at 2 different temperatures.

measured release of NR from NCL was 5%, 5% and 7%, respectively (Fig. 5). The maximum NR release from the CCL micellar formulations was comparable or slightly lower than the release from NCL micelles. Furthermore, no change in Z-average was observed for all formulations at all temperatures (Fig. 6).

CHARACTERIZATION OF MICELLES AFTER HIFU EXPOSURE

DLS measurements of the NCL micelles at pH 5 and 7.4 and CCL micelles (4% and 13% methacrylation) at pH 7.4 before and after HIFU exposure (20 W, 4 min) showed a nearly unchanged Z-average with a PDI of ≤ 0.2 (Table 3). Similar results were obtained for NCL micelles at pH 5 before and after PW-HIFU with and without microbubbles at four different exposure times and four different acoustic powers. GPC analysis of the block copolymer before and after CW-HIFU exposure (20 W, 4 min) of NCL micelles at pH 7.4, revealed an unchanged M_n 19,000 g mol^{-1} (M_w/M_n = 1.5). ^{1}H NMR data of NCL micelles before and after HIFU exposure did not show detectable hydrolysis of the HPMA side chains (Fig. 7).

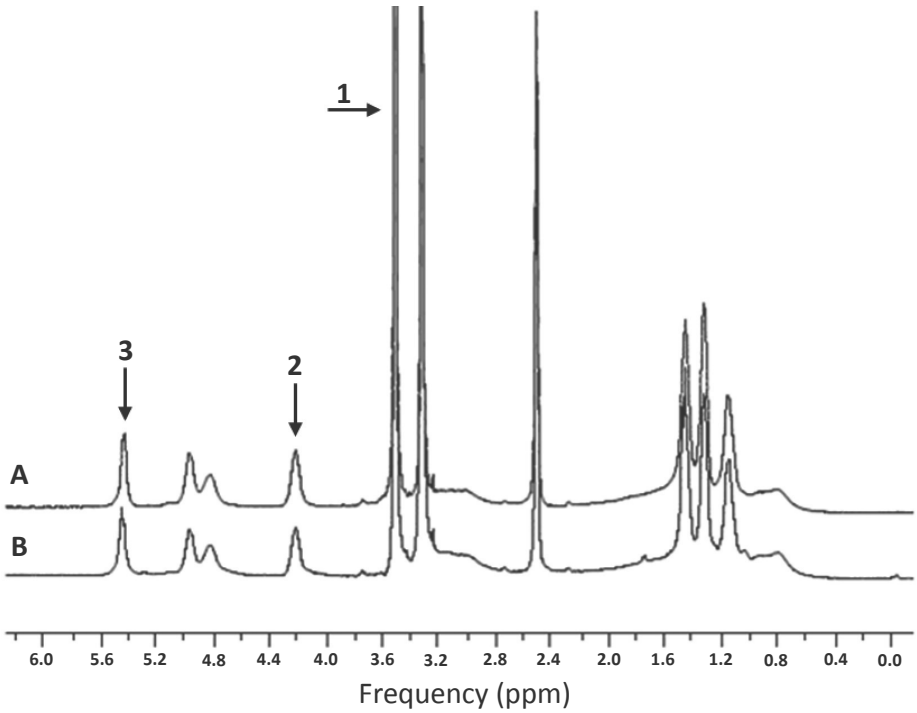

Fig. 7. ^{1}H-NMR spectra of mPEG-*b*-p(HPMAm-Lac_2) before (a) and after CW-HIFU for 4 min at 20 W (b). Arrow 1 indicates the PEG methylene proton resonance peak, arrow 2 indicates the methine proton (CO-CH(CH_3)-OH) resonance peak and arrow 3 indicates the (CH-O<u>H</u> ($HPMAmLac_2$)) resonance peak.

DISCUSSION

Several groups have investigated the ability of using CW-HIFU for triggered (drug) release from micelles [42]. However, the *in vivo* use of CW-HIFU for inducing the non-thermal release of drugs from micelles is not feasible because of the high acoustic absorption of tissue leading to temperature increase. In the present study, it has been shown that CW- as well as PW-high frequency (1.5 MHz) focused ultrasound (HIFU) has the ability to induce the release of a hydrophobic agent (NR) from NCL and CCL

micelles. After 20 W of CW-HIFU exposure for 4 min an almost complete release (~85 %) of the loaded NR from NCL micelles was achieved. Zhang *et al.* also achieved substantial NR release (~70%) from PLA-*b*-PEG micelles using high frequency ultrasound, but only after applying 150 min CW-HIFU at 160 W [29]. In contrast, Marin *et al.* and Husseini *et al.* only found up to 10% release from pluronic micelles, though lower ultrasound intensities (up to 8 W cm^2) were used as compared to our study [23, 43]. Furthermore, it was observed that the same CW-HIFU settings lead to less release from CCL micelles than from NCL micelles, which can be ascribed to the covalent crosslinking of the core. Moreover, at low acoustic power settings (up to ~10 W), NCL micelles at pH 7.4 released more NR than NCL micelles at pH 5. This can be explained by the fact that at pH 5 the lactic acid side groups have the highest stability against hydrolysis [44]. However, it does not explain the acoustic power dependency. Finally, a slightly higher NR release was observed from CCL micelles with 4% methacrylation compared to CCL micelles with 13% methacrylation. From these findings, it can be concluded that micelles with a densely crosslinked core show less NR release with the same ultrasound settings. Similar observations were made by Husseini *et al.* for unstabilized and stabilized micelles using low frequency HIFU [23]. No differences in NR release from NCL micelles at pH 5 were observed between PW- and CW-HIFU when equal amounts of acoustic energy were deposited. In contrast, the release of NR from NCL after PW-HIFU exposure in the presence of microbubbles was slightly less than in their absence which is most probably due to absorption of part of the ultrasound energy by the oscillating microbubbles [45]. The differences in release kinetics of hydrophobic agents from micelles in our study and other published studies can be attributed to the different micellar formulations, to the ultrasound set-up and exposure parameters and to the underlying mechanisms causing the release. In literature, several mechanisms are proposed to explain the ultrasound-induced release from micelles. In a recent study, Wang *et al.* hypothesized that the combined thermal and mechanical effect, related to a relatively weak cavitation effect, of high frequency CW-HIFU induces the hydrolysis of 2-tetrahydropyranyl methacrylate (THPMA) side groups of the PEO-*b*-PTHPMA diblock copolymer leading to the destabilization of the micelles. This claim was based on pH, infrared spectroscopy, DLS and atomic force microscopy data. However, quantitative analysis of the polymer before and after HIFU exposure was not performed [31]. In another study, the same group confirmed these results by performing a comparative study on the ultrasound-induced disruption of four different block copolymer micelles [30]. Using significant lower ultrasound powers and shorter exposure times as compared to the previous study, the authors claim that disruption of all micelle formulations was due to chemical degradation of the polymers. However, the extent of micellular disruption and thus release depended on the diblock copolymer used. Also for PLA-*b*-PEG based micelles, the ultrasound-induced degradation of the PLA-*b*-PEG copolymer was pointed out as micelle disrupting force by Zhang *et al.* [29]. Although high frequency CW-HIFU was used in this study, the authors argued that cavitation causes the chemical disruption of the PLA-*b*-PEG micelles. Interestingly, with the exact same HIFU exposure parameters they did not observe NR release from pluronic micelles, which is in contrast with the work done by the group of Husseini *et al.* who showed that low as well as high frequency HIFU can disrupt pluronic micelles by cavitation-induced high shear forces [43, 46]. In their early study they suggest that transient cavitation (i.e. oscillating microbubbles) was responsible for the release, because they found a linear relationship between acoustic power and the degree of drug

release [43]. However, in a more recent paper they found a non-linear relationship between the acoustic intensity and the amount of release, which indicates that inertial cavitation (i.e. exploding microbubbles) is probably the mechanism that causes the release [46]. In the present study, none of the above mentioned mechanisms are likely to contribute to the observed ultrasound-induced release. The DLS results after CW- as well as PW-HIFU exposure of micelle samples with and without microbubbles did not result in a significant change in micelle size after HIFU exposure. However, it cannot be excluded that the NCL micelles are temporarily destabilized during HIFU and reform after stopping HIFU exposure. Likely, CCL are (more) resistant towards the destabilizing forces, which might explain the lower amount of release from CCL compared to NCL micelles with the same ultrasound settings. Furthermore, no differences in the GPC and ^{1}H NMR data before and after CW-HIFU were observed, which exclude chemical degradation such as hydrolysis of the lactate side groups and/or the ester bond connecting the PEG and the thermosensitive block. Finally, the equal release of NR from NCL micelle at pH 5 (at which the polymers have the highest stability [44] and pH 7.4 at fixed power of 20 W (Fig. 2a) demonstrates that chemical degradation is not the driving force for HIFU-triggered release from NCL micelles. The use of high frequency ultrasound, the absence of increased release by adding microbubbles and the absence of a threshold intensity for ultrasound-induced release suggest that (inertial) cavitation is not the (main) mechanism for the observed ultrasound-triggered release. Furthermore, it can be excluded that heat development during CW- or PW-HIFU exposure caused the NR release from the micelles because micelles exposed during 1 h to temperatures that are reached during CW-HIFU treatment did only lead to 8% NR release (Fig. 5). It is suggested that radiation force induced convection of the micelle solution causes shear forces, which leads to a temporary physical destabilization of the micelles and thus release of NR. Similar shear forces may be expected *in vivo* when micelles are pushed against vessel walls or through the extravascular space [47]. This theory also explains why micelles with a higher percentage of crosslinking of the forming blocks release less of the entrapped hydrophobic compound upon HIFU sonication. The crosslinking of forming blocks stabilizes micelles and thus diminishes the release upon HIFU sonication. The present study demonstrates that high frequency CW- as well as PW-HIFU is able to trigger the release of a hydrophobic (i.e. NR) compound from mPEG-*b*-p(HPMAm-Lac$_n$) micelles. Up to 85% of the NR was released from micelles depending on micelle formulation as well as ultrasound parameters. It was demonstrated that release was not triggered due to chemical degradation of the block copolymer but rather likely due to radiation force induced convection that cause shear forces. Overall, (PW-) HIFU is a highly promising technique to destabilize mPEG-*b*-p(HPMAm-Lac$_n$) micelles on demand and spatiotemporally control the release of hydrophobic compounds.

ACKNOWLEDGEMENTS

The authors gratefully acknowledge dr. Holger Rehmann for providing the Varian Cary Eclipse fluorescence spectrophotometer for the fluorescence imaging measurements, dr. Albert de Graaf for his support in the ^{1}H NMR measurement, mr. Willem van Doesum for the help with HIFU experiments and mr. Mies J. van Steenbergen for his overall contribution in this study.

REFERENCES

1. Allen TM, Cullis PR. Drug delivery systems: entering the mainstream. Science. 2004;303:1818-22.
2. Davis MR, Chen ZG, Shin DM. Nanoparticle therapeutics: an emerging treatment modality for cancer. Nat Rev Drug Discov. 2008;7:771-82.
3. Parveen S, Misra R, Sahoo SK. Nanoparticles: a boon to drug delivery, therapeutics, diagnostics and imaging. Nanomedicine: nanotechnology, biology, and medicine. 2012;8:147-66.
4. Gaucher G, Dufresne MH, Sant VP, Kang N, Maysinger D, Leroux JC. Block copolymer micelles: preparation, characterization and application in drug delivery. J Control Release. 2005;109:169-88.
5. Lavasanifar A, Samuel J, Kwon GS. Poly(ethylene oxide)-block-poly(L-amino acid) micelles for drug delivery. Adv Drug Deliv Rev. 2002;54:169-90.
6. Nishiyama N, Kataoka K. Current state, achievements, and future prospects of polymeric micelles as nanocarriers for drug and gene delivery. Pharmacol Ther. 2006;112:630-48.
7. Oerlemans C, Bult W, Bos M, Storm G, Nijsen JF, Hennink WE. Polymeric micelles in anticancer therapy: targeting, imaging and triggered release. Pharm Res. 2010;27:2569-89.
8. Torchilin VP. Micellar nanocarriers: pharmaceutical perspectives. Pharm Res. 2007;24:1-16.
9. Gong J, Chen M, Zheng Y, Wang D, Wang Y. Polymeric micelles drug delivery system in oncology. J Control Release. 2012;159:312-23.
10. Kedar U, Phutane P, Shidhaye S, Kadam V. Advances in polymeric micelles for drug delivery and tumor targeting, Nanomedicine: nanotechnology, biology, and medicine. 2010;6:714-29.
11. Bae Y, Fukushima S, Harada A, Kataoka K. Design of environment-sensitive supramolecular assemblies for intracellular drug delivery: polymeric micelles that are responsive to intracellular pH change. Angew Chem Int Ed Engl. 2003;42:4640-3.
12. Chung JE, Yokoyama M, Yamato M, Aoyagi T, Sakurai Y, Okano T. Thermo-responsive drug delivery from polymeric micelles constructed using block copolymers of poly(*N*-isopropylacrylamide) and poly(butylmethacrylate). J Control Release. 1999;62:115-27.
13. Gillies ER, Frechet JM. A new approach towards acid sensitive copolymer micelles for drug delivery. Chem Commun (Camb). 2003;14:1640-1.
14. Zhao Y. Light-Responsive Block Copolymer Micelles. Macromolecules. 2012;45:3647-57.
15. Rijcken CJ, Soga O, Hennink WE, van Nostrum CF. Triggered destabilisation of polymeric micelles and vesicles by changing polymers polarity: an attractive tool for drug delivery. J Control Release. 2007;120:131-48.
16. Ranjan S, Jacobs GC, Woods DL, Negussie AH, Partanen A, Yarmolenko PS, Gacchina CE, Sharma KV, Frenkel V, Wood BJ, Dreher MR. Image-guided drug delivery with magnetic resonance guided high intensity focused ultrasound and temperature sensitive liposomes in a rabbit Vx2 tumor model. J Control Release. 2012;158:487-94.
17. Staruch R, Chopra R, Hynynen K. Localised drug release using MRI-controlled focused ultrasound hyperthermia. Int J Hyperthermia. 2011;27:156-71.
18. de Smet M, Heijman E, Langereis S, Hijnen NM, Gruell H. Magnetic resonance imaging of high intensity focused ultrasound mediated drug delivery from temperature-sensitive liposomes: an *in vivo* proof-of-concept study. J Control Release. 2011;150:102-10.
19. Deckers R, Moonen CT. Ultrasound triggered, image guided, local drug delivery. J Control Release. 2010;148:25-33.
20. Frenkel V. Ultrasound mediated delivery of drugs and genes to solid tumors. Adv Drug Deliv Rev. 2008;60:1193-208.
21. O'Brien Jr. WD. Ultrasound-biophysics mechanisms. Prog Biophys Mol Biol. 2007;93:212-55.
22. Husseini GA, Christensen DA, Rapoport NY, Pitt WG. Ultrasonic release of doxorubicin from Pluronic P105 micelles stabilized with an interpenetrating network of *N*,*N*-diethylacrylamide. J Control Release. 2002;83:303-5.

23. Husseini GA, Diaz de la Rosa MA, Gabuji T, Zeng Y, Christensen DA, Pitt WG. Release of doxorubicin from unstabilized and stabilized micelles under the action of ultrasound. J Nanosci Nanotechnol. 2007;7:1028-33.
24. Husseini GA, El-Fayoumi RI, O'Neill KL, Rapoport NY, Pitt WG. DNA damage induced by micellar-delivered doxorubicin and ultrasound: comet assay study. Cancer Lett. 2000;154:211-16.
25. Nelson JL, Roeder BL, Carmen JC, Roloff F, Pitt WG. Ultrasonically activated chemotherapeutic drug delivery in a rat model. Cancer Res. 2002;62:7280-3.
26. Ahmadi F, McLoughlin IV, Chauhan S, ter-Haar G. Bio-effects and safety of low-intensity, low-frequency ultrasonic exposure. Prog Biophys Mol Biol. 2012;108:119-38.
27. Dalecki D. Mechanical bioeffects of ultrasound. Annu Rev Biomed Eng. 2004;6:229-48.
28. Hynynen K. The threshold for thermally significant cavitation in dog's thigh muscle *in vivo*. Ultrasound Med Biol. 1991;17:157-69.
29. Zhang H, Xia H, Wang J, Li Y. High intensity focused ultrasound-responsive release behavior of PLA-*b*-PEG copolymer micelles. J Control Release. 2009;139:31-9.
30. Xuan JA, Pelletier M, Xia HS, Zhao Y. Ultrasound-Induced disruption of amphiphilic block copolymer micelles. Macromol Chem Phys. 2011;212:498-506.
31. Wang J, Pelletier M, Zhang H, Xia H, Zhao Y. High-frequency ultrasound-responsive block copolymer micelle. Langmuir. 2009;25:13201-5.
32. Rijcken CJ, Veldhuis TF, Ramzi A, Meeldijk JD, van Nostrum CF, Hennink WE. Novel fast degradable thermosensitive polymeric micelles based on PEG-block-poly(*N*-(2-hydroxyethyl)methacrylamide-oligolactates). Biomacromolecules. 2005;6:2343-51.
33. Rijcken CJ, Snel CJ, Schiffelers RM, van Nostrum CF, Hennink WE. Hydrolysable core-crosslinked thermosensitive polymeric micelles: synthesis, characterisation and *in vivo* studies. Biomaterials. 2007;28:5581-93.
34. Neradovic D, Soga O, van Nostrum CF, Hennink WE. The effect of the processing and formulation parameters on the size of nanoparticles based on block copolymers of poly(ethylene glycol) and poly(*N*-isopropylacrylamide) with and without hydrolytically sensitive groups. Biomaterials. 2004;25:2409-18.
35. Madelin G, Hosten B, Biateau C, Mougenot C, Franconi JM, Thiaudiere E. Comparison of laser interferometry and radiation force method of measuring ultrasonic power. Ultrasonics. 2005;43:769-74.
36. Schneider M. SonoVue, a new ultrasound contrast agent. Eur Radiol. 1999;9:347-8.
37. Dutta AK, Kamada K, Ohta K. Spectroscopic studies of nile red in organic solvents and polymers. J Photoch Photobio A. 1996;93:57-64.
38. Sarkar N, Das K, Nath DN, Bhattacharyya K. Twisted Charge-Transfer Process of Nile Red in Homogeneous Solution and in Faujasite Zeolite. Langmuir. 1994;10:326-9.
39. Soga O, van Nostrum CF, Hennink WE. Poly(*N*-(2-hydroxypropyl) methacrylamide mono/di lactate): a new class of biodegradable polymers with tuneable thermosensitivity. Biomacromolecules. 2004;5:818-21.
40. Soga O, van Nostrum CF, Ramzi A, Visser T, Soulimani F, Frederik PM, Bomans PH, Hennink WE. Physicochemical characterization of degradable thermosensitive polymeric micelles. Langmuir. 2004;20:9388-95.
41. Talelli M, Iman M, Rijcken CJ, van Nostrum CF, Hennink WE. Targeted core-crosslinked polymeric micelles with controlled release of covalently entrapped doxorubicin. J Control Release. 2010;148:121-2.
42. Rapoport N. Ultrasound-mediated micellar drug delivery. Int J Hyperthermia. 2012;28:374-85.
43. Marin A, Sun H, Husseini GA, Pitt WG, Christensen DA, Rapoport NY. Drug delivery in pluronic micelles: effect of high-frequency ultrasound on drug release from micelles and intracellular uptake. J Control Release. 2002;84:39-47.
44. Neradovic D, van Steenbergen MJ, Vansteelant L, Meijer YJ, van Nostrum CF, Hennink WE. Degradation mechanism and kinetics of thermosensitive polyacrylamides containing lactic acid side chains. Macromolecules. 2003;36:7491-8.

45. Leighton TG. The acoustic bubble. London: Academic Press. 1994.
46. Husseini GA, Diaz de la Rosa MA, Richardson ES, Christensen DA, Pitt WG. The role of cavitation in acoustically activated drug delivery. J Control Release. 2005;107:253-61.
47. Hancock HA, Smith LH, Cuesta J, Durrani AK, Angstadt M, Palmeri ML, Kimmel E, Frenkel V. Investigations into pulsed high-intensity focused ultrasound-enhanced delivery: preliminary evidence for a novel mechanism. Ultrasound Med Biol. 2009;35:1722-36.

Chapter 3

Chris Oerlemans
Roel Deckers
Gert Storm
Wim Hennink
Frank Nijsen

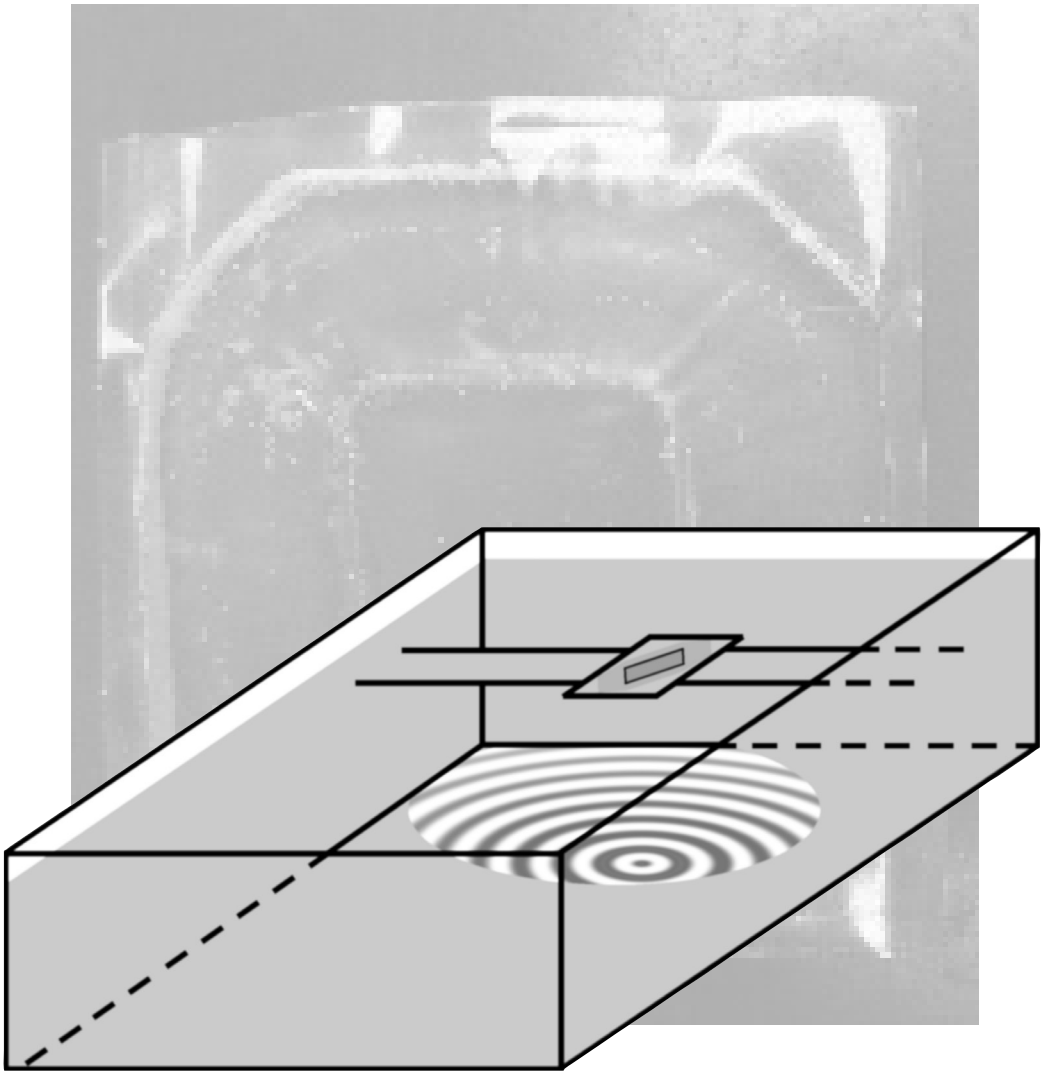

II Evidence for a new mechanism behind HIFU-triggered release from liposomes

Journal of Controlled Release
in press

ABSTRACT

A promising approach for local drug delivery is high-intensity focused ultrasound (HIFU)-triggered release of drugs from stimuli-responsive nanoparticles such as liposomes. The aim of this study was to investigate whether another release mechanism is involved with HIFU-triggered release from liposomes beside cavitation and temperature. Furthermore, it was studied whether this new release mechanism allows the release of lipophilic compounds. Therefore, both a lipophilic (Nile red) and a hydrophilic (fluorescein) compound were loaded into thermosensitive (TSL) or non-thermosensitive liposomes (NTSL) and the liposomes were subjected both to continuous wave- (CW) and pulsed wave- (PW) HIFU. The mean liposome size varied from 97-139 nm with a PDI ≤ 0.06 for the different formulations. The T_m of the phospholipid bilayer of the TSL was around 42 °C. Approximately 80% of fluorescein was released within 15 min from TSL at temperatures ≥ 42 °C. In contrast, no fluorescein release from NTSL and NR release from both TSL and NTSL was observed at temperatures up to 60 °C. CW-HIFU exposure of TSL resulted in rapid temperature elevation up to 52 °C and subsequently almost quantitative fluorescein release. Fluorescein release from NTSL was also substantial (~64% after 16 min at 20 W). Surprisingly, CW-HIFU exposure (20 W for 16 min) resulted in the release of NR from TSL (~66% of the loaded amount), and this was even higher from NTSL (~78%). PW-HIFU exposure did not result in temperatures above the T_m of TSL. However, nearly 85% of fluorescein was released from TSL after 32 min at 20 W of PW-HIFU exposure, whereas the release from NTSL was around 27%. Interestingly, NR release from NTSL was ~30% after 2 min PW-HIFU exposure and increased to ~70% after 32 min. Furthermore, addition of microbubbles to the liposomes prior to PW-HIFU exposure did not result in more release, which suggests that cavitation can be excluded as the main mechanism responsible for the triggered release of both a hydrophilic and a lipophilic model compound from liposomes. DLS analysis showed that the mean size and PDI of the liposomes did not significantly change after CW- and PW-HIFU exposure. Taken together, it is therefore concluded that neither temperature elevation nor inertial cavitation is essential for the release of both hydrophilic and lipophilic compounds from liposomes. It is assumed that the release originates from radiation force-induced acoustic streaming, causing the liposomes to collide at the walls of the exposure chamber leading to shear forces which in turn results in reversible liposome destabilization and release of both hydrophilic and lipophilic compounds.

INTRODUCTION

The focus in chemotherapy is currently shifting from conventional systemic administration of cytotoxic drugs to more local treatments using for instance drug delivery systems (DDS) [1-8]. Local delivery of an anticancer drug in the tumor ideally results on the one hand in higher efficacy and on the other hand in reduced side effects due to less exposure of healthy tissue to cytotoxic compounds. Nanosized DDS are widely investigated for drug targeting purposes because of their ability to accumulate in the tumor by the enhanced permeability and retention (EPR) effect [9-11]. Frequently studied nanoparticles for drug delivery are liposomes, spherical particles with a phospholipid bilayer surrounding an aqueous core in which hydrophilic drugs can be dissolved whereas lipophilic drugs can be solubilized in the phospholipid bilayer [12]. By introducing phospholipids displaying a gel-to-liquid transition temperature (T_m) around 42 °C such as 1,2-dipalmitoyl-*sn*-glycero-3-phosphocholine (DPPC) in the liposomal bilayer, thermosensitive liposomes (TSL) are prepared, which release hydrophilic compounds present in the aqueous core after exposure to mild hyperthermia [13, 14]. This phase transition is a result of a conformational change of the alkyl chains of the phospholipids, leading to an increase in the volume occupied by the hydrocarbon chains in the membrane and thus an increase in the permeability of the lipid bilayer [15, 16], resulting in liposomal drug release. Clinical trials with a thermosensitive liposome formulation containing doxorubicin (ThermoDox, Celsion corporation, Columbia, MD, USA) in combination with radiofrequency heating-triggered release for the treatment of hepatocellular carcinoma (HCC) are currently underway [17]. Although drug release from different DDS has been modeled [18], few models have considered the release of lipophilic compounds from liposomes [19]. Lipophilic compounds like several taxanes such as paclitaxel [20, 21] and different cisplatin analogues [22, 23] are solubilized in the phospholipid bilayer by van der Waals forces [24]. The interaction between lipophilic compounds and the phospholipid bilayer remains when the T_m is exceeded and therefore these compounds are not released upon heating a liposome formulation above this temperature. Therefore, there is a need for technologies that enable triggered release of lipophilic drugs from liposomes. A recently developed and customized technology for triggered drug release from different DDS is high-intensity focused ultrasound (HIFU) [25-29]. Ultrasound, a sound pressure wave with a frequency higher than 20 kHz, can be focused in a small spatial region in deep tissue, leading to high levels of acoustic energy, which is absorbed by the tissue resulting in local temperature increase. Therefore, HIFU can be used as an external stimulus for local drug release from thermosensitive liposomes at the desired location within the body [5, 30, 31]. However, with relatively long continuous wave- (CW) HIFU exposure, high temperatures are produced, leading to thermal damage and ablation of the affected tissue [32]. In addition to CW-HIFU, pulsed wave- (PW) HIFU can be used for drug release from nanoparticles. PW-HIFU is characterized by emission of ultrasound pulsed during a short time period (typically ~100 μs) followed by a longer period of time without pulse emission (typically ~900 μs), which results in a decrease of temporal average intensities as compared to CW-HIFU [33], and, therefore, thermal effects as associated with CW-HIFU are circumvented [34]. Yet, another effect of ultrasound, especially when using low frequency ultrasound (LFUS), is cavitation; the formation of cavities in a liquid and the subsequent implosion of the cavities which can result in shear forces affecting the nearby tissue [35]. In several

studies, release of lipophilic agents from nanoparticles, such as polymeric micelles [36, 37] and liposomes [38, 39] using LFUS due to the induction of cavitation has been demonstrated. Cavitation, however, may also occur in between the transducer and the focal point with LFUS, leading to unwanted damage of healthy tissue. Additionally, focussing of the ultrasound waves from LFUS is more difficult as compared to high frequency ultrasound, and therefore restricts the use of LFUS for clinical applications [40, 41]. The aim of this study was to investigate whether another release mechanism is involved with HIFU-triggered release from liposomes beside cavitation and temperature. Furthermore, it was studied whether this new release mechanism allows the release of lipophilic compounds. Therefore, both a lipophilic (Nile red) and a hydrophilic (fluorescein) compound were loaded into thermosensitive (TSL) or non-thermosensitive liposomes (NTSL) and the liposomes were subjected both to continuous wave- (CW) and pulsed wave- (PW) HIFU.

MATERIALS AND METHODS

MATERIALS

All chemicals and lipids were commercially available and used as obtained. 1,2-dipalmitoyl-*sn*-glycero-3-phosphocholine (DPPC) and 1,2-dipalmitoyl-*sn*-glycero-3-phospho-ethanolamine-*N*-[methoxy(polyethylene glycol)-2000] (PEG_{2000}-DSPE) were obtained from Lipoid GmbH (Ludwigshafen, Germany). Cholesterol (>99%) and Nile red (Standard Fluka) were supplied by Sigma Aldrich (Steinheim, Germany). 1,2-distearoyl-*sn*-3-glyceryl-phosphatidylcholine (DSPC) was obtained from Avanti Polar Lipids (Alabaster, Alabama, USA). Sodium fluorescein (100 mg mL^{-1}) was obtained from Serb Laboratoires (Paris, France). Slide-A-Lyzer cassettes (MW cut-off 3,5 kDa) were obtained from Pierce (Rockford, IL, USA). Microbubbles (SonoVue, 8 µl mL^{-1}, average size 2-8 µm containing sulfur hexafluoride gas. Shell composition: macrogol 4000, DSPC, DPPG and Palmitic acid) were obtained from Bracco (Milano, Italy).

LIPOSOME PREPARATION

Fluorescein-containing thermosensitive liposomes (F-TSL), Nile red-containing thermosensitive liposomes (NR-TSL), fluorescein-containing non-thermosensitive liposomes (F-NTSL) and Nile red-containing non-thermosensitive liposomes (NR-NTSL) were prepared using a conventional thin-film hydration technique as described previously [42]. The TSL formulations consisted of DPPC, DSPC, cholesterol and PEG_{2000}-DSPE in a molar ratio of 67 : 15 : 13 : 5. The NTSL formulations consisted of DSPC, cholesterol and PEG_{2000}-DSPE in a molar ratio of 56 : 39 : 5 and resembled the FDA-approved Doxil formulation [43] with the modification that the phospholipid HSPC was replaced by DSPC. The lipid concentration of both formulations was 40 mM. Nile red (NR) was introduced into the phospholipid bilayer in a concentration of 125 mmol mol^{-1}. The lipid mixtures were dissolved in ethanol (10 mL) and evaporated to dryness by rotary evaporation under vacuum (Rotavapor R-210, BUCHI Laboratory Equipment, Zurich, Switzerland). The resulting lipid films were further dried under N_2. For F-TSL and F-NTSL, 10 mL sodium fluorescein (25 mg mL^{-1}) was used to hydrate the lipid film. For NR-TSL and NR-NTSL, the lipid film

was hydrated in 10 mL HEPES-buffered saline (HBS; 20 mM HEPES and 135 mM NaCl, pH 7.4). The resulting lipid dispersions were sized with sequential extrusion using a Lipex Extruder (Northern Lipids Inc., Vancouver, Canada) and polycarbonate membrane filters (Poretics Corporation, Livermore, CA) with pore diameters of 600, 400, 200 and 100 nm. Non-encapsulated fluorescein was removed by dialysis against an excess HBS at room temperature using Slide-A-Lyzer cassettes during 48 h with four times a change of buffer.

LIPOSOME CHARACTERIZATION

The average hydrodynamic size and polydispersity index (PDI) of freshly prepared liposomes and liposomes after heat- or HIFU exposure were determined with dynamic light scattering (DLS) using a Malvern ALV CGS-3 system (Malvern Instruments Ltd., Worcestershire, UK). The PDI value ranges from 0 for a monodisperse to 1 for a heterodisperse formulation. Intensity correlation functions were measured using a wavelength of 632.8 nm at a scattering angle of 90°. Size and PDI determination was performed on liposome dispersions before and after HIFU exposure. Differential scanning calorimetry (DSC) measurements were performed in a capillary cell microcalorimeter instrument (MicroCal VP-DSC, Northampton, MA) to determine the phase transition melting temperature (T_m) of the liposomal bilayer. The measurements were performed at temperatures ranging from 25 °C to 60 °C at a heating rate of 1 °C min^{-1} after an equilibration period of 5 min at 25 °C.

RELEASE MEASUREMENTS

To investigate release of the encapsulated compounds from the liposomes in HBS and in HBS:FCS (1:1 v/v) as a result of temperature increase, the different liposome formulations were subjected to different temperatures: 20, 37, 40, 42, 45 and 60 °C up to 15 min using a thermostat-controlled water bath. The release was measured at the exposure temperature as well as after cooling down of the samples to room temperature using a FluoroLog spectrofluorometer (Jobin Yvon Horiba FL3-21, Edison, NJ, USA). Additionally, the fluorescence spectra of free fluorescein and NR exposed to temperatures up to 60 °C for 15 min were taken to verify that changes in fluorescence intensity were not due to thermal degradation of the compounds. For measuring fluorescein release, an excitation wavelength of 494 nm and an emission spectrum in the range of 500-580 nm was used. The release of fluorescein from TSL and NTSL was related to liposomes lyzed with 2% Triton X-100 using the formula: fluorescein (F) released (%) = (F_{post} - F_{pre}) / (F_{lyz} - F_{pre}) x 100%, in which F_{pre} is the fluorescence observed before temperature elevation of HIFU exposure, F_{post} resembles the fluorescence intensity at 525 nm after temperature elevation or HIFU exposure. F_{lyz} corresponds with the fluorescence intensity at 525 nm after the liposomes were lyzed in 2% Triton X-100. When NR is released from the liposomes, it is discharged in the aqueous HBS solution, resulting in quenching [44]. To measure NR release, an excitation wavelength of 550 nm and an emission spectrum in the range of 580-680 nm was used. NR release (%) from TSL and NTSL was calculated using the following formula: NR released (%) = (NR_{pre} - NR_{post}) / (NR_{pre} - NR_{lyz}) x 100%, where NR_{pre} is the fluorescence observed before temperature elevation or HIFU exposure, NR_{post} resembles the fluorescence intensity at 600 nm after temperature elevation or HIFU exposure. NR_{lyz} corresponds with the fluorescence intensity at 600 nm after

the liposomes were lyzed in 2% Triton X-100. Fluorescein release after exposure of the liposomes to CW- and PW-HIFU was measured using a FLUOstar OPTIMA (BMG Labtech, Ortenberg, Germany) with an excitation wavelength of 490 nm and an emission wavelength of 520 nm for fluorescein. For NR release, an excitation wavelength of 550 nm and an emission wavelength of 600 nm was used. Release of both fluorescein and NR was calculated similarly as described above. All experiments were performed in triplicate.

HIFU-TRIGGERED RELEASE STUDIES

For the exposure of the TSL and NTSL to CW- or PW-HIFU, an in-house developed HIFU system was used (Fig. 1), consisting of a single-element transducer (Imasonic, Besançon, France) placed inside a water bath with adjustable temperature and a sample holder. The single-element transducer had an external radius aperture of 120 mm and a focal length of 80 mm. The sinusoidal signal (f = 1.5 MHz) was generated by using AG 1006 amplifier/generator. The dimensions of the focal point were 2 x 2 x 5 mm^3 (at -3 dB). The acoustic output power of the HIFU system was calibrated with a balance measurement [45]. Acoustic powers of 2.5 up to 30 W were used, which corresponds to a peak negative pressure (PNP) of 1.6 and 5.5 MPa, a spatial peak, temporal peak intensity (I_{SPTP}) of 83.4 and 1000.7 W cm^2, a spatial average, temporal average (I_{SATA}) of 7.1 and 84.6 and a mechanical index (MI), which is defined by the following equation: MI = sqrt(PNP) / f, of 0.84 – 1.56, respectively. The sample holder consisted of a silicone-like gasket (Thermo Fisher Scientific, Landsmeer, the Netherlands) sealed on both sides with an ultrasound transparent polyester heat seal membrane (Waters, Acquity UPLC Consumables, Etten-Leur, the Netherlands) and was placed in the focal point. Before HIFU exposure, the sample holder was filled with 0.5 mL of liposome dispersion. The liposome dispersions were degassed in a vacuum desiccator for 24 h prior to HIFU exposure to exclude the possibility for gas nuclei to be present and subsequently eliminate the possibility of cavitation in the sample. The incubation temperature of the sample holder was 37 °C to mimic the *in vivo* situation. Prior to HIFU exposure, the water bath was covered by ultrasound-absorbing material to avoid ultrasound reflection. The temperature at the position of the focal point was measured with a thermocouple fixed in the middle of sample holder filled with degassed liposome dispersion. The samples were subjected to a CW of f = 1.5 MHz at different acoustic powers (0, 2.5, 5, 10, 15, 20, 30 W) for 4 min and to different exposure times (1, 2, 4, 8 and 16 min) at 20 W of acoustic power. In order to exclude the thermal effects associated with CW-HIFU, the liposome formulations were also subjected to PW-HIFU. The liposomes were subjected to a time series of 1, 2, 4, 8, 16 and 32 min at 20 W of acoustic power with a duty cycle of 10% (repeatedly 100 μs 'on-time' and 900 μs 'off-time') and a pulse repetition frequency (PRF) of 1 kHz. Furthermore, microbubbles were added to TSL and NTSL and the liposome dispersions were exposed for 1, 2, 4 and 8 min at 20 W of PW-HIFU.

RESULTS

LIPOSOME PREPARATION AND CHARACTERIZATION

Mean size, PDI and T_m of the liposomes were measured directly after preparation

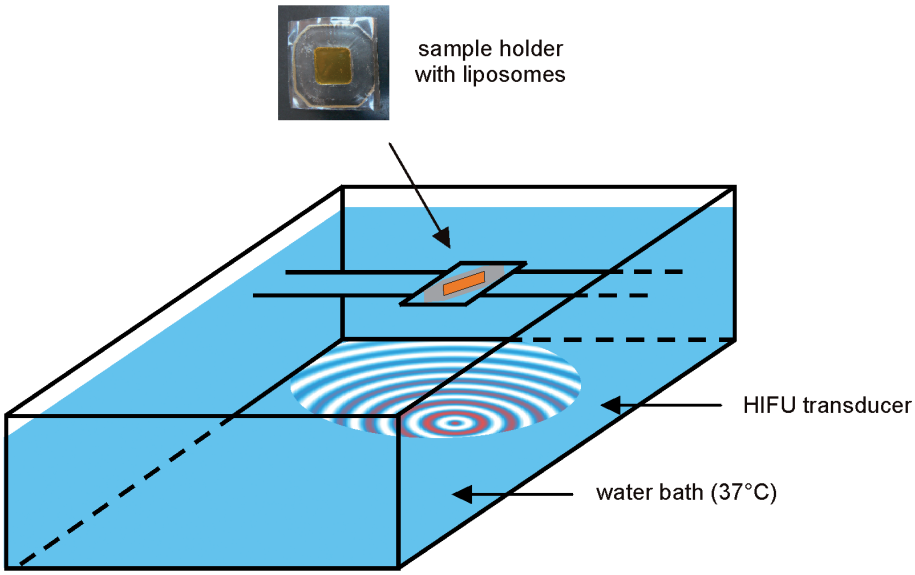

Fig. 1. HIFU system used for ultrasound exposure of the liposome formulations. The sample holder (filled with liposome suspension) was placed in the focal point above the ultrasound transducer. The water bath temperature was 37 °C to mimic the *in vivo* situation.

(Table 1). The liposome formulations had an average size between 97-139 nm and had a small size distribution (PDI ≤ 0.06). DSC analysis showed that the T_m of F-TSL and NR-TSL was 42.1 °C and 42.3 °C, respectively (thermograms not shown), in agreement with literature [46, 47]. For NTSL, as expected, no T_m was detected within the measured temperature range of 25 °C - 60 °C. DLS measurements performed on FCS showed an average size of 21 ± 2 nm with a PDI around 0.48. Addition of FCS to the liposome formulations resulted in a small increase of the PDI (up to 0.32), while the size did not significantly change. This is shown for NR-loaded liposomes (both TSL and NTSL) in Table 2. DLS was measured based on particle volume, so the small serum proteins within FCS did not significantly affect the mean liposomal size, while the PDI was yet increased. Moreover, the mean size and PDI after heating the liposomes in HBS or HBS:FCS (measured at 20 °C) did not significantly change as compared to non-heated liposomes.

TEMPERATURE-TRIGGERED RELEASE OF FLUORESCEIN AND NILE RED FROM TSL AND NTSL

Within 15 min of exposure to 60 °C in HBS and HBS:FCS using a thermostat-controlled water bath, around 80% of the loaded amount of fluorescein from TSL was released (Fig. 2), which is in accordance with previous studies [47]. The emission spectra of both fluorescein release in HBS and HBS:FCS are provided in Fig. 3a and 3b, respectively. When FCS is added to the liposome dispersion, the release of fluorescein from F-TSL is hampered (Fig. 3c) when exposed to 42 °C (T_m of F-TSL) as compared to fluorescein release in HBS alone (Fig. 3a). Maximum release at 42 °C

Table 1: Size, PDI and T_m of the liposome formulations. n/a*) No T_m was not found within the measured temperature range (25 °C to 60 °C). Values are given as mean ± SD, n=3.

Liposome formulation	Size (nm)	PDI	T_m (°C)
F-TSL	133 ± 4	0.02 ± 0.01	42.1 ± 0.1
F-NTSL	97 ± 2	0.05 ± 0.02	n/a*)
NR-TSL	139 ± 5	0.01 ± 0.01	42.3 ± 0.2
NR-NTSL	103 ± 4	0.06 ± 0.02	n/a*)

Table 2. Size (nm) and PDI of FCS and NR-TSL / NR-NTSL after the addition of FCS prior to and after heating.

	NR-TSL Size (nm)	PDI	NR-NTSL Size (nm)	PDI
Freshly prepared	139 ± 5	0.01 ± 0.01	103 ± 4	0.06 ± 0.02
FCS	21 ± 2	0.48 ± 0.02	21 ± 2	0.48 ± 0.02
Fresh + FCS	135 ± 1	0.12 ± 0.04	113 ± 10	0.32 ± 0.02
Post heating + FCS	127 ± 1	0.10 ± 0.06	107 ± 3	0.31 ± 0.01

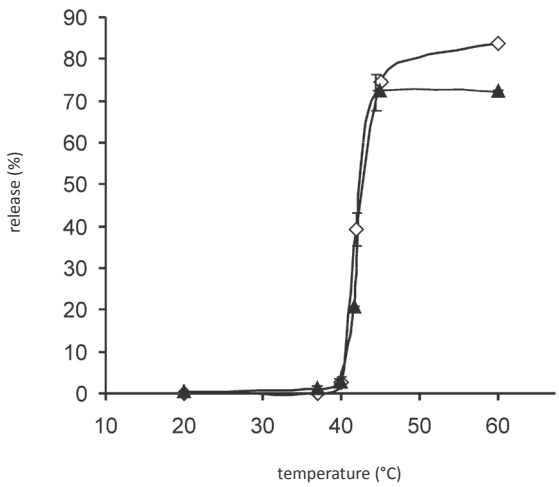

Fig. 2. Release of fluorescein from TSL in HBS (◇) and in HBS:FCS (▲) after 15 min of heating at different temperatures between 20 °C and 60 °C (mean ± SD, n=3).

was observed after 1 h. Exposure of the F-TSL in HBS:FCS to temperatures above the liposomal T_m (Fig. 3b), however, resulted in maximum release within 15 min, which is similar as observed in HBS. As described before, no T_m was found as determined with DSC measurements of F-NTSL, although the T_m of DSPC is around 54-55 °C [48, 49]. This can be explained by the mol fraction cholesterol used for the preparation of

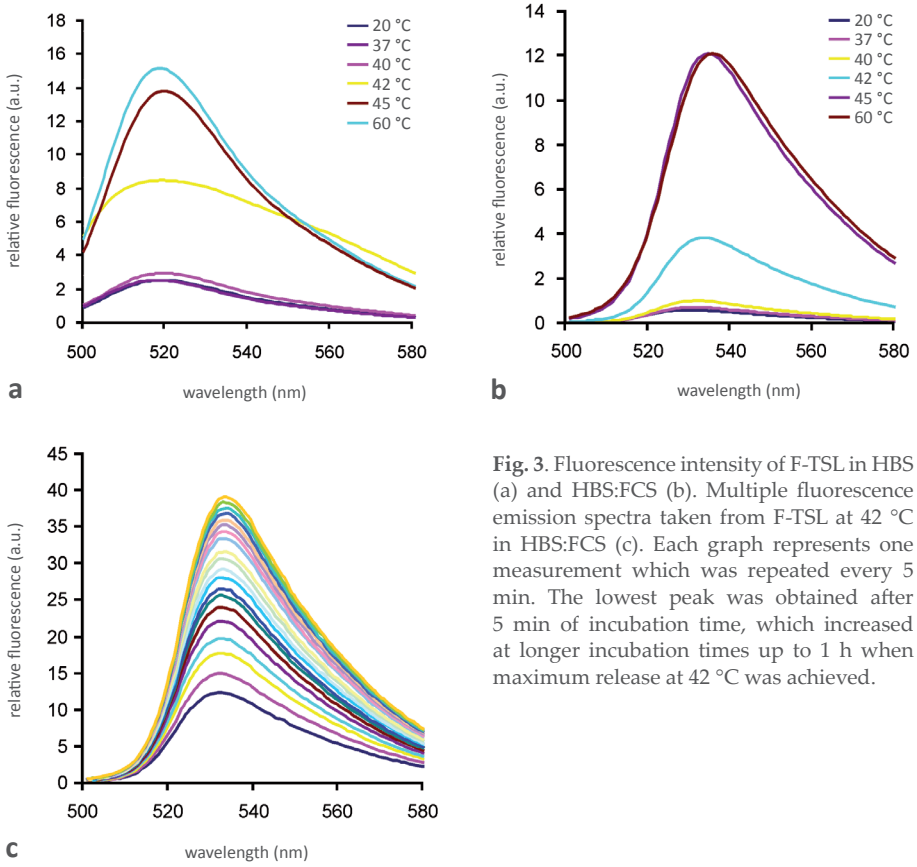

Fig. 3. Fluorescence intensity of F-TSL in HBS (a) and HBS:FCS (b). Multiple fluorescence emission spectra taken from F-TSL at 42 °C in HBS:FCS (c). Each graph represents one measurement which was repeated every 5 min. The lowest peak was obtained after 5 min of incubation time, which increased at longer incubation times up to 1 h when maximum release at 42 °C was achieved.

NTSL, which is 39%. The presence of cholesterol in phospholipid bilayers causes a decrease in enthalpy [50], and, therefore, the T_m is not detected with DSC [51]. Hence, no changes in the fluorescence emission spectra of F-NTSL in HBS are found within the temperature range of 20 °C to 60 °C (Fig. 4a). In the presence of FCS, however, an increase in fluorescence intensity is found at 60 °C (Fig. 4b). Most probably, the serum proteins such as albumin interact with the transient pores which are created when the T_m of the liposomes is exceeded and DSPC undergoes a gel-to-liquid crystalline transition, leading to some fluorescein release from the liposomes. The emission spectra of F-NTSL after HIFU exposure were taken at 20 °C in HBS, so any effect of temperature elevation on the release kinetics instigated by HIFU exposure prior to the fluorescence measurements can be excluded. Fig. 5a shows an increasing decline in fluorescence intensity of NR-TSL upon incubation at elevated temperatures up to 60 °C, measured directly at the elevated temperature. However, when the samples were cooled down prior to measurement, fluorescence intensities were restored to the initial values. It is hypothesized that the phospholipid bilayer in which NR is solubilized is compromised due to the associated conformational changes at and above the liposomal T_m, which allows in- and outflow of the surrounding medium. Consequently, NR is more surrounded with hydrophilic molecules, leading to a decrease in fluorescence

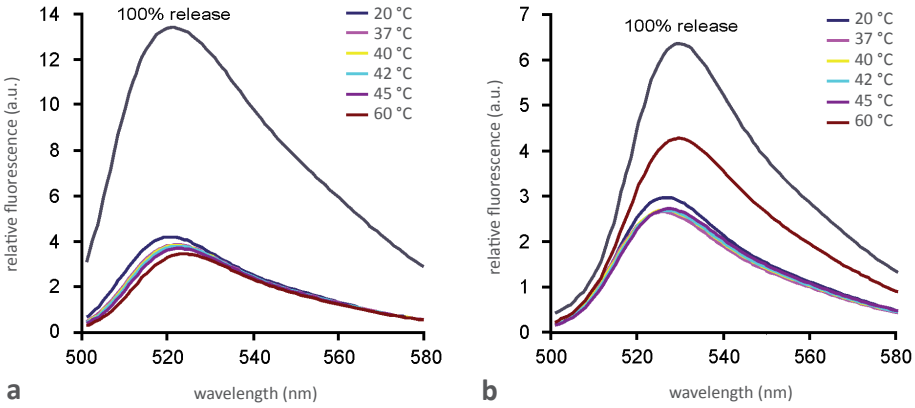

Fig. 4. Fluorescence intensity of F-NTSL at different temperatures in HBS (a) and HBS:FCS compared to Triton X-100 lyzed F-NTSL (100% release) (b), n=3.

intensity due to quenching [52, 53]. In HBS:FCS, the fluorescence was not reduced with increasing temperatures (Fig. 5b) due to the presence of serum proteins, which interact with the liposomal phospholipid bilayer. Subsequently, interaction of hydrophilic molecules with NR is prevented, avoiding a decline in fluorescence. Only at 60 °C, after also exceeding the T_m of DSPC, the fluorescence decreases. The emission spectrum was restored to its initial value when the liposome dispersion was

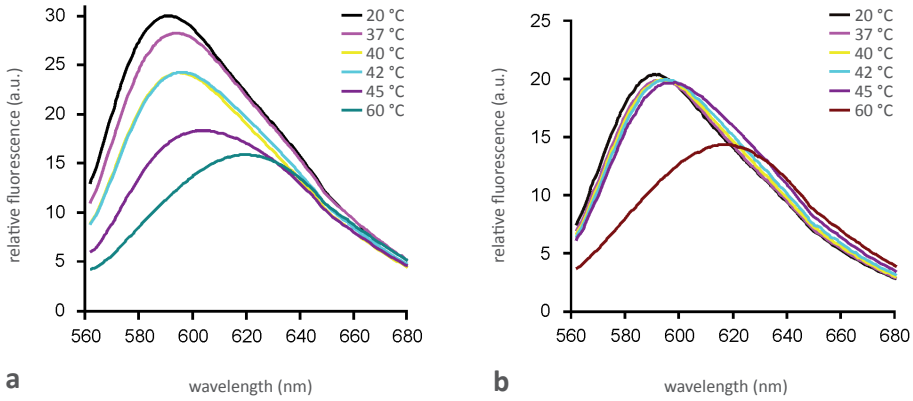

Fig. 5. Fluorescence intensity of NR liposomes at different temperatures in HBS (a) and in HBS:FCS (b), n=3.

cooled down to at 20 °C. Furthermore, incubation of NR-TSL for 2 h at 37 °C did not result in a change in fluorescence, demonstrating that the NR-TSL remained stable and no NR release had occurred. NR-NTSL were exposed to different temperatures in HBS (a) or HBS:FCS (b) and measured directly after heating of the liposomes to the desired temperature. No decrease in fluorescence intensity was observed after temperature elevation up to 45 °C (Fig. 6), since no conformational changes within

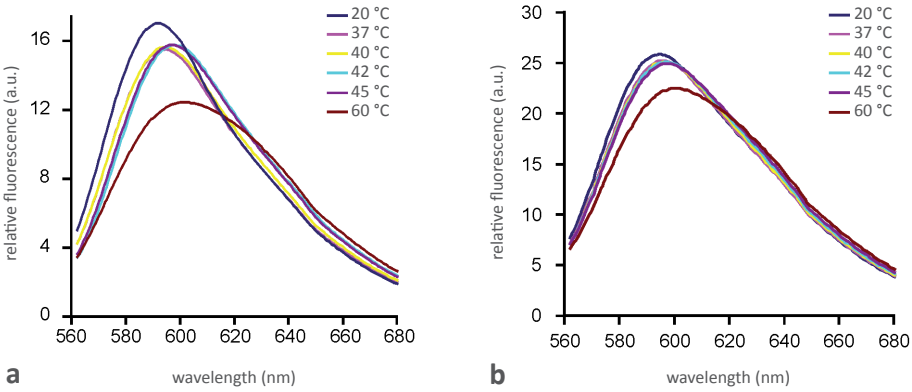

Fig. 6. Fluorescence intensity of NR-NTSL at different temperatures in HBS (a) and HBS:FCS (b), n=3.

the liposomal phospholipid bilayer occur and interaction of hydrophilic molecules with NR is prevented. Only after temperature elevation to 60 °C, thus exceeding the (minor) T_m of DSPC, the fluorescent intensity is somewhat decreased. After the addition of FCS, the difference in fluorescence decrease is less as compared to the fluorescence decrease in HBS alone, probably also due to the interaction of the serum proteins such as albumin interact with the transient pores which are present at 60 °C (Fig. 6b), as described previously. The emission spectrum was restored to its initial value when the liposome dispersion was cooled down to at 20 °C.

TEMPERATURE ELEVATION OF THE LIPOSOMES AT FHE FOCAL SPOT DURING HIFU EXPOSURE

To validate the temperature elevation of the liposome samples during CW- and PW-HIFU exposure, the temperature at the position of the focal point was measured with a thermocouple fixed in the middle of sample holder filled with degassed liposome dispersion. A mean temperature of 44 °C at 4 min of CW-HIFU exposure to 2.5 W and increasing temperatures up to 58 °C at 4 min of HIFU exposure to 20 W (Fig. 7a), which exceeds the T_m of the liposomes. The temperature measured at the focal point raised rapidly to the final temperature and remained stable for the remaining exposure time. A similar release profile is shown after HIFU exposure to 20 W for different time periods, where the temperature in the sample holder raised to ~52 °C after 30 s of exposure time (Fig. 7b), which remained stable after longer exposure times. Exposure of the liposomes to PW-HIFU resulted in a temperature increase of only 2 °C (from 37 °C to 39 °C, Fig. 7b), which excludes temperature as initiator of liposomal release.

CW-HIFU-TRIGGERED RELEASE OF FLUORESCEIN AND NILE RED FROM TSL AND NTSL

Rapid release of fluorescein from TSL incubated at 37 °C was observed after 4 min CW-HIFU exposure to 2.5 W (~80% of the loaded amount was released; Fig. 8a). Thermocouple measurements at the focal spot of the sample holders indicated a rapid

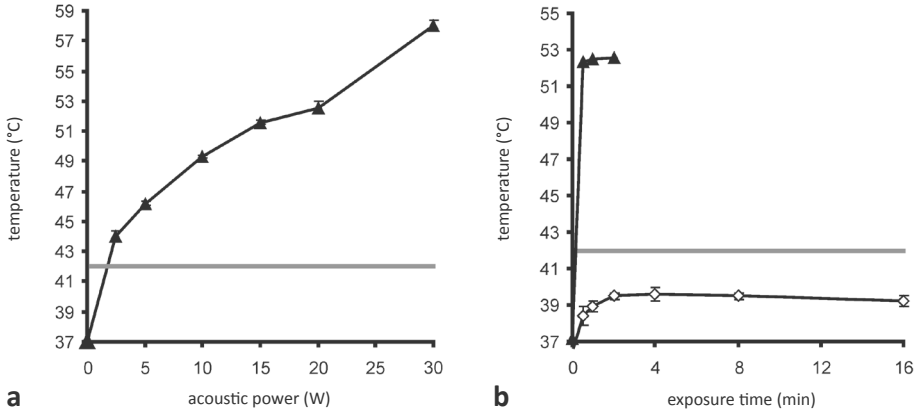

Fig. 7. Temperature ramps of HIFU exposure versus temperature. Exposure of liposomes to CW-HIFU at different acoustic powers (W) for 4 min versus the T_m of the liposomes (a). Exposure of liposomes to 20 W CW-HIFU (▲) and PW-HIFU (◇) for different times (b).

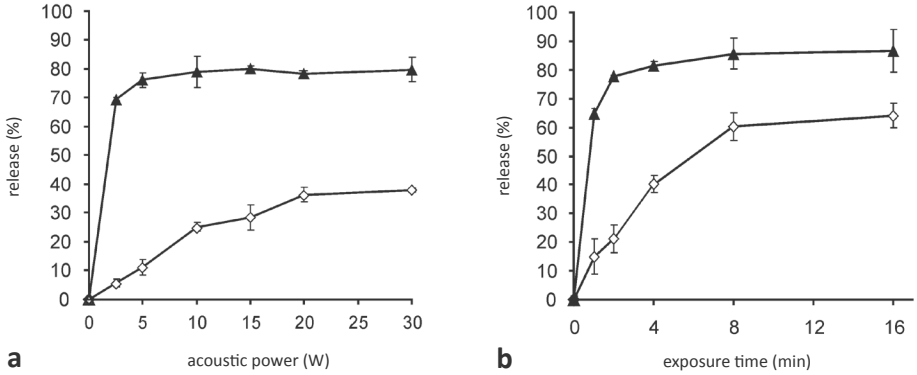

Fig. 8. Release of fluorescein from TSL (▲) and NTSL (◇) after exposure to CW-HIFU. The liposomes were exposed to different acoustic powers for 4 min (a) and to 20 W of acoustic power for different exposure times incubated at 37 °C (b). Values are given as mean ± SD, n=3.

temperature increase from 37 °C to 44 °C (Fig. 7). Exposure of the same formulation for the same time but to a higher dose of 30 W and to 20 W for different time periods up to 16 min resulted in an increase in temperature to 52 °C which was associated with a rapid and almost quantitative fluorescein release (Fig. 8a and b). Furthermore, substantial fluorescein release from NTSL, around 40% of the loaded amount, was observed after exposure to 30 W for 4 min (Fig. 8a) and up to 64% was released after exposure to 20 W for 16 min (Fig. 8b). The release of NR from TSL increased with higher acoustic power (Fig. 9a), reaching ~43% of the loaded amount after exposure to 30 W for 4 min. Fig 9a shows that at similar conditions, an even higher release from NTSL was obtained, reaching ~64% of the loaded amount. Fig. 9b shows that the release NR from TSL after exposure to CW-HIFU at a fixed acoustic power (20 W) increased with time reaching up to 66% of the loaded dose after exposure for 16

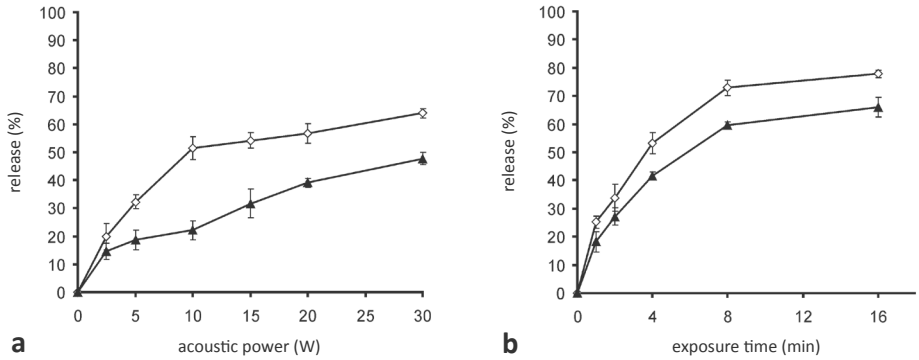

Fig. 9. Release of NR from TSL (▲)and NTSL (◇) incubated at 37 °C after exposure to CW-HIFU. The liposomes were exposed to different acoustic powers (W) for 4 min (a) and exposed to 20 W of acoustic power (W) for different exposure times (b). Values are given as mean ± SD, n=3.

Table 3. Size (nm) and polydispersity index (PDI) of F-TSL / F-NTSL after heating and after CW-HIFU exposure to different acoustic powers.

	F-TSL Size (nm)	PDI	F-NTSL Size (nm)	PDI
Freshly prepared	133 ± 4	0.02 ± 0.01	97 ± 2	0.05 ± 0.02
Post heating	131 ± 3	0.07 ± 0.02	105 ± 1	0.13 ± 0.02
Post HIFU 10 W	127 ± 1	0.07 ± 0.02	104 ± 1	0.14 ± 0.00
Post HIFU 20 W	132 ± 2	0.10 ± 0.06	105 ± 1	0.11 ± 0.02
Post HIFU 80 W	123 ± 1	0.11 ± 0.01	121 ± 4	0.21 ± 0.01
Post HIFU 120 W	118 ± 0	0.14 ± 0.02	113 ± 0	0.16 ± 0.03

min, whereas NTSL showed at the same conditions an even higher release (~78% of the loaded dose). DLS analysis showed that the mean size and PDI of the liposomes did not significantly change after CW-HIFU exposure of the liposomes, as is shown for fluorescein-loaded liposomes (both TSL and NTSL) in Table 3. This confirms that the release of both fluorescein and NR originates from reversible destabilization of the liposomes.

PW-HIFU-TRIGGERED RELEASE OF FLUORESCEIN AND NR FROM TSL AND NTSL

Release of fluorescein from TSL after PW-HIFU exposure at 20 W up to 32 min was substantially higher, ~85%, as compared to ~27% for NTSL (Fig. 10a). During exposure, a mild temperature elevation from 37 °C to ~39 °C (Fig. 7) was measured with the thermocouple. This is around 3 °C lower than the T_m of the TSL and, as a consequence, will not trigger the released of fluorescein from F-TSL. At the same conditions, a higher NR release from NTSL, ~69%, as compared to ~36% for TSL, was observed (Fig. 10b).

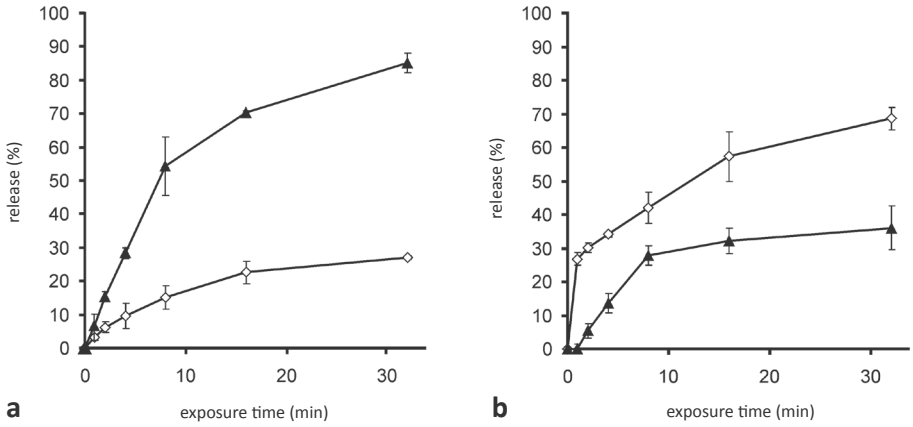

Fig. 10. Release of fluorescein (a) and NR (b) from TSL (▲)and NTSL (◇) incubated at 37 °C after exposure to PW-HIFU (20 W for different times; duty cycle of 10%). Values are given as mean ± SD, n=3.

DISCUSSION

In this study, the involvement of an additional release mechanism from liposomes beside cavitation and temperature associated with HIFU exposure was investigated. Furthermore, the HIFU-triggered release of a lipophilic compound was studied. To discern temperature-induced release from non-temperature effects due to HIFU exposure, both non-temperature sensitive (NTSL) and temperature sensitive (TSL) liposomes containing a hydrophilic compound (fluorescein) or a lipophilic compound (Nile red) were prepared and incubated in a water bath at temperatures ranging between 20 °C and 60 °C. Approximately 80% fluorescein release from TSL was observed within 15 min after exposure to temperatures above the liposomal T_m (≥ 42 °C, Fig. 2). As expected, no release of fluorescein from NTSL was measured. Moreover, NR was not released from both liposome types, most likely due to the strong interaction of NR with the hydrocarbon chains of the phospholipid bilayer by Van der Waals forces [24]. Furthermore, it was demonstrated that the average liposomal size did not significantly change after the addition of FCS and after 15 min of heating to 60 °C, hence no liposome aggregation had occurred. CW-HIFU exposure of F-TSL to 2.5 W of acoustic power incubated at 37 °C resulted in almost complete release within 4 min (Fig 8a), likely because the sample temperature (45 °C) exceeded the T_m of the liposomal bilayer. Furthermore, fluorescein release from NTSL was observed, although the release was slower and less as compared to the release from TSL (Fig. 8). Based on the results from the water bath experiment it is concluded that the fluorescein release from NTSL is not due to the temperature increase, but only due to the ultrasound wave. Surprisingly, CW-HIFU exposure of TSL resulted in ~66% NR release after 16 min of exposure to 20 W, and an even higher release of ~78% from NTSL was observed (Fig. 9). Since no release of NR from both TSL and NTSL after heating in a water bath up to 60 °C was observed and no significant changes in liposome size and PDI before and after HIFU exposure were detected, it can be concluded that HIFU reversibly destabilizes the phospholipid bilayer of the liposomes and weakens NR-lipid interactions, resulting in NR release. The differences in release can

be explained by the liposome composition since the interaction between a lipophilic compound and a phospholipid bilayer is stronger when the bilayer mainly consist of DPPC (TSL) as opposed to DSPC (NTSL) [24, 54]. Fluorescein release from NTSL and NR release from both TSL and NTSL demonstrates that another mechanism than temperature elevation associated with CW-HIFU is responsible for this effect. It is hypothesized that radiation force-induced acoustic streaming causes the liposomes to collide at the walls of the exposure chamber leading to shear forces that destabilize the liposome resulting in release of the loaded compounds [55-57]. CW-HIFU leads to fluorescein and NR release from TSL and NTSL, but also to unwanted heating of the targeted tissue when clinically applied to release cytostatic drugs from liposomes. With PW-HIFU, the same amount of total energy will be generated as compared to CW-HIFU, although a longer total exposure time is needed. In this study it is shown that PW-HIFU only lead to minor temperature increase, from 37 °C to 39 °C. This is due to the short ultrasound exposure (100 μs) followed by a longer period of no ultrasound exposure (900 μs) during which the generated heat dissipated in the surrounding environment. During PW-HIFU the temperature does not exceed the T_m of the liposomal bilayer. Therefore, the observed triggered release of the entrapped compounds is not due to temperature effects. Fluorescein release (~15% of the loaded amount) from TSL was observed after 2 min PW-HIFU exposure, which increased to substantial release (~85% after 32 min). The NTSL formulation used in our study resembles Doxil, a clinically used NTSL formulation (Janssen Biotech, Inc., Horsham, PA, USA), although HSPC was replaced by DSPC and fluorescein was used as a doxorubicin-surrogate. Dromi *et al.* investigated triggered release of doxorubicin *in vivo* with PW-HIFU from ThermoDox [58] and compared the drug release with that from Doxil [33]. The consequential hyperthermia (4 °C to 5 °C) resulted in a significant higher drug deposition in the tumor and reduced tumor growth in ThermoDox-treated mice. Nevertheless, no significant improvement was shown with Doxil-treated mice after PW-HIFU exposure as compared to the non-exposed mice. This was to be expected due to the relatively short PW-HIFU exposure time of 2 min per spot. In our study, only ~5% fluorescein release from NTSL was observed after 2 min PW-HIFU exposure. However, longer exposure times (up to 32 min) resulted in 27% release of the encapsulated compound. These results show that release from NTSL is not due to temperature elevation and confirm that an additional mechanism opposed to temperature elevation or cavitation is responsible for the release. Hence, *in vivo* studies with Doxil and increased PW-HIFU exposure times to achieve higher drug deposition in the tumor and a reduced tumor growth are recommended. In previous studies it was demonstrated that cholesterol can stabilize and rigidify the phospholipid bilayer [59-61]. The TSL investigated in this study contained a three times lower cholesterol concentration as compared to NTSL, which explains the higher HIFU-triggered fluorescein release from TSL as compared to NTSL. The release of NR from NTSL was ~30% after 2 min of exposure time, increasing to ~69% after 32 min. This was higher as compared to TSL (~36%), which is in accordance with the NR release from TSL and NTSL after CW-HIFU exposure. Exposure of microbubbles to PW-HIFU can lead to rapid radial expansion, contraction and the subsequent collapse of the microbubbles within a short exposure period due to the cyclic change of the pressure of an ultrasound field, called inertial cavitation [62, 63]. It can be expected that this phenomenon enhances liposome destabilization and increases the release of entrapped compounds [64]. All liposome samples were degassed prior to CW- or PW-HIFU exposure, minimizing the occurrence of cavitation due to air bubbles

present in the sample. In order to investigate whether HIFU exposure generated cavitation in the liposome samples, they were exposed to PW-HIFU in the presence of sulphur hexafluoride microbubbles. However, no increased release in the presence of microbubbles was observed, even though the microbubbles had collapsed within 1 min of PW-HIFU exposure, which confirms that cavitation was generated. Yet, it was not the most important HIFU-triggered release mechanism from liposomes in this study and points out that the release most likely originates from radiation force-induced acoustic streaming. The resulting shear forces in the sample cause the liposomes to collide at the walls of the exposure chamber leading to shear forces that reversibly destabilize the liposome resulting in release of the loaded compounds.

CONCLUSION

In the present study, for the first time HIFU-triggered release of a lipophilic compound from liposomes is demonstrated. Moreover, it was shown that HIFU exposure resulted in release of a hydrophilic model compound (fluorescein) from non-thermosensitive liposomes. It is concluded that neither temperature elevation nor inertial cavitation is essential for the release of both hydrophilic and lipophilic compounds from liposomes. It is assumed that the release originates from radiation force-induced acoustic streaming, causing the liposomes to collide at the walls of the exposure chamber leading to shear forces which in turn results in reversible liposome destabilization and release of both hydrophilic and lipophilic compounds.

ACKNOWLEDGEMENTS

The authors thank Sander Langereis and Holger Grüll from Philips Research Eindhoven, Department of Biomolecular Engineering, Eindhoven, the Netherlands and Gerben Koning, from the Laboratory of Experimental Surgical Oncology, Erasmus Medical Center, Rotterdam, the Netherlands for valuable discussions. The authors are grateful to Willem van Doesum and Remmert de Roos for their help with the HIFU measurements. This research was financially supported by MediTrans, an Integrated Project funded by the European Commission under the Sixth Framework (NMP4-CT-2006-026668).

REFERENCES

1. Torchilin. Multifunctional nanocarriers. Adv Drug Deliv Rev. 2006;58:1532-55.
2. Allen TM, Cullis PR. Drug delivery systems: entering the mainstream. Science. 2004;303:1818-22.
3. Koning GA, Krijger GC. Targeted multifunctional lipid-based nanocarriers for image-guided drug delivery. Anticancer Agents Med Chem. 2007;7:425-40.
4. Lammers T, Kiessling F, Hennink WE, Storm G. Drug targeting to tumors: principles, pitfalls and (pre-) clinical progress. J Control Release. 2012;161:175-87.
5. Oerlemans C, Bult W, Bos M, Storm G, Nijsen JF, Hennink WE. Polymeric micelles in anticancer therapy: targeting, imaging and triggered release. Pharm Res. 2010;27:2569-89.
6. Kwon IK, Lee SC, Han B, Park K. Analysis on the current status of targeted drug delivery to tumors. J Control Release. 2012;164:108-14.
7. Riehemann K, Schneider SW, Luger TA, Godin B, Ferrari M, Fuchs H. Nanomedicine-challenge and perspectives. Angew Chem Int Ed Engl. 2009;48:872-97.
8. Kim BY, Rutka JT, Chan WC. Nanomedicine. N Engl J Med. 2010;363:2434-43.
9. Greish K. Enhanced permeability and retention of macromolecular drugs in solid tumors: a royal gate for targeted anticancer nanomedicines. J Drug Target. 2007;15:457-64.
10. Maeda H, Wu J, Sawa T, Matsumura Y, Hori K. Tumor vascular permeability and the EPR effect in macromolecular therapeutics: a review. J Control Release 2000;65:271-84.
11. Maeda H. Tumor-selective delivery of macromolecular drugs via the EPR effect: background and future prospects. Bioconjug Chem. 2010;21:797-802.
12. Torchilin VP. Recent advances with liposomes as pharmaceutical carriers. Nat Rev Drug Discov. 2005;4:145-60.
13. Maruyama K, Unezaki D, Takahashi N, Iwatsuru M. Enhanced delivery of doxorubicin to tumor by long-circulating thermosensitive liposomes and local hyperthermia. Biochim Biophys Acta. 1993;1149;209-16.
14. Needham D, Dewhirst MW. The development and testing of a new temperature-sensitive drug delivery system for the treatment of solid tumors. Adv Drug Deliv Rev. 2001;53:285-305.
15. Papahadjopoulos D, Jacobson K, Nir S, Isac T. Phase transitions in phospholipid vesicles. Fluorescence polarization and permeability measurements concerning the effect of temperature and cholesterol. Biochim Biophys Acta. 1973;311:330-48.
16. Yatvin MB, Weinstein JN, Dennis WH, Blumenthal R. Design of liposomes for enhanced local release of drugs by hyperthermia. Science. 1978;202:1290-3.
17. Poon RT, Borys N. Lyso-thermosensitive liposomal doxorubicin: an adjuvant to increase the cure rate of radiofrequency ablation in liver cancer. Future Oncol. 2011;7:937-45.
18. Siepmann J, Siepmann F. Modeling of diffusion controlled drug delivery. J Control Release. 2012;161:351-62.
19. Zeng LK, Wu XY. Modeling the sustained release of lipophilic drugs from liposomes. Applied Physics Letters. 2010;97.
20. Rowinsky EK, Donehower RC. Paclitaxel (taxol). N Engl J Med. 1995;332:1004-14.
21. Guarneri V, Dieci MV, Conte P. Enhancing intracellular taxane delivery: current role and perspectives of nanoparticle albumin-bound paclitaxel in the treatment of advanced breast cancer. Expert Opin Pharmacother. 2012;13:395-406.
22. Okusaka T, Okada S, Nakanishi T, Fujiyama S, Kubo Y. Phase II trial of intra-arterial chemotherapy using a novel lipophilic platinum derivative (SM-11355) in patients with hepatocellular carcinoma. Invest New Drugs. 2004;22:169-76.
23. Yu Y, Lou LG, Liu WP, Zhu HJ, Ye QS, Chen XZ, Gao WG, Hou SQ. Synthesis and anticancer activity of lipophilic platinum(II) complexes of 3,5-diisopropylsalicylate. Eur J Med Chem. 2008;43:1438-43.
24. Zhao L, Feng SS. Effects of lipid chain unsaturation and headgroup type on molecular interactions between paclitaxel and phospholipid within model biomembrane. J Colloid Interface Sci. 2005;285:326-35.

25. de Smet D, Langereis S, van den Bosch S, Gruell H. Temperature-sensitive liposomes for doxorubicin delivery under MRI guidance. J Control Release. 2010;143:120-27.
26. Oerlemans C, Nijsen JF, van Amersfoort M, van Bloois L, Heijman E, Luijten PR, Mali WP, Storm G. A novel approach to identify non-palpable breast lesions combining fluorescent liposomes and magnetic resonance-guided high intensity focused ultrasound-triggered release. Eur J Pharm Biopharm. 2011;77:458-64.
27. Staruch R, Chopra R, Hynynen K. Localised drug release using MRI-controlled focused ultrasound hyperthermia. Int J Hyperthermia. 2011;27:156-71.
28. Ranjan A, Jacobs GC, Woods DL, Negussie AH, Partanen A, Yarmolenko PS, Gacchina CE, Sharma KV, Frenkel V, Wood BJ, Dreher MR. Image-guided drug delivery with magnetic resonance guided high intensity focused ultrasound and temperature sensitive liposomes in a rabbit Vx2 tumor model. J Control Release. 2012;158:487-94.
29. Rapoport N. Ultrasound-mediated micellar drug delivery, Int J Hyperthermia 2012;28:374-85.
30. Marin A, Muniruzzaman M, Rapoport N. Mechanism of the ultrasonic activation of micellar drug delivery. J Control Release. 2001;75:69-81.
31. Deckers R, Moonen CT. Ultrasound triggered, image guided, local drug delivery. J Control Release. 2010;148:25-33.
32. Jolesz FA. MRI-Guided Focused Ultrasound Surgery. Annual Review of Medicine. 2009;60:417-30.
33. Dromi D, Frenkel V, Luk A, Traughber B, Angstadt M, Bur M, Poff J, Xie J, Libutti SK, Li KC, Wood BJ. Pulsed-high intensity focused ultrasound and low temperature-sensitive liposomes for enhanced targeted drug delivery and antitumor effect. Clin Cancer Res. 2007;13;2722-7.
34. Miller DL, Song J. Tumor growth reduction and DNA transfer by cavitation-enhanced high-intensity focused ultrasound *in vivo*. Ultrasound Med Biol. 2003;29:887-93.
35. Apfel RE. Acoustic cavitation: a possible consequence of biomedical uses of ultrasound. Br J Cancer Suppl. 1982;5:140-6.
36. Husseini GA, Pitt WG. The use of ultrasound and micelles in cancer treatment. J Nanosci Nanotechnol. 2008;8:2205-15.
37. Husseini GA, Velluto D, Kherbeck L, Pitt WG, Hubbell JA, Christensen DA. Investigating the acoustic release of doxorubicin from targeted micelles. Colloids Surf B Biointerfaces. 2012;101C:153-5.
38. Schroeder A, Avnir Y, Weisman S, Najajreh Y, Gabizon A, Talmon Y, Kost J, Barenholz Y. Controlling liposomal drug release with low frequency ultrasound: mechanism and feasibility. Langmuir. 2007;23:4019-25.
39. Schroeder A, Honen R, Turjeman K, Gabizon A, Kost J, Barenholz Y. Ultrasound triggered release of cisplatin from liposomes in murine tumors. J Control Release. 2009;137:63-8.
40. Ahmadi F, McLoughlin IV, Chauhan S, ter-Haar G. Bio-effects and safety of low-intensity, low-frequency ultrasonic exposure. Prog Biophys Mol Biol. 2012;108:119-38.
41. Dalecki D. Mechanical bioeffects of ultrasound. Annu Rev Biomed Eng. 2004;6:229-48.
42. Koning GA, Morselt HW, Velinova MJ, Donga J, Gorter A, Allen TM, Zalipsky S, Kamps JA, Scherphof GL. Selective transfer of a lipophilic prodrug of 5-fluorodeoxyuridine from immunoliposomes to colon cancer cells. Biochim Biophys Acta. 1999;1420:153-67.
43. Barenholz Y. Doxil® - The first FDA-approved nano-drug: lessons learned. J Control Release. 2012;160:117-34.
44. Dutta AK, Kamada K, Ohta K. Spectroscopic studies of nile red in organic solvents and polymers. J Photochem Photobiol A: Chem. 1996;93:57-64.
45. Madelin G, Hosten B, Biateau C, Mougenot C, Franconi JM, Thiaudiere E. Comparison of laser interferometry and radiation force method of measuring ultrasonic power. Ultrasonics. 2005;43:769-74.
46. Bikram M, West JL. Thermo-responsive systems for controlled drug delivery. Expert Opin Drug Deliv. 2008;5:1077-91.

47. Djanashvili K, ten Hagen TL, Blange R, Schipper D, Peters JA, Koning GA. Development of a liposomal delivery system for temperature-triggered release of a tumor targeting agent, Ln(III)-DOTA-phenylboronate. Bioorg Med Chem. 2011;19:1123-30.
48. Mabrey S, Sturtevant JM. Investigation of phase transitions of lipids and lipid mixtures by sensitivity differential scanning calorimetry. Proc Natl Acad Sci USA. 1967;73:3862-6.
49. Grudzielanek S, Smirnovas V, Winter R. The effects of various membrane physical-chemical properties on the aggregation kinetics of insulin. Chem Phys Lipids. 2007;149:28-39.
50. Almeida PF, Vaz WL, Thompson TE. Percolation and diffusion in three-component lipid bilayers: effect of cholesterol on an equimolar mixture of two phosphatidylcholines. Biophys J. 1993;64:399-412.
51. McMullen TP, McElhaney RN. Differential scanning calorimetric studies of the interaction of cholesterol with distearoyl and dielaidoyl molecular species of phosphatidylcholine, phosphatidylethanolamine, and phosphatidylserine. Biochemistry. 1997;36:4979-86.
52. Papahadjopoulos D, Jacobson K, Nir S, Isac T. Phase transitions in phospholipid vesicles. Fluorescence polarization and permeability measurements concerning the effect of temperature and cholesterol. Biochim Biophys Acta. 1973;311:330-48.
53. Klymchenko AS, Duportail G, Demchenko AP, Mely Y. Bimodal distribution and fluorescence response of environment-sensitive probes in lipid bilayers. Biophys J. 2004;86:2929-41.
54. Campbell RB, Balasubramanian SV, Straubinger RM. Influence of cationic lipids on the stability and membrane properties of paclitaxel-containing liposomes. J Pharm Sci. 2001;90:1091-105.
55. Hancock HA, Smith LH, Cuesta J, Durrani AK, Angstadt M, Palmeri ML, Kimmel E, Frenkel V. Investigations into pulsed high-intensity focused ultrasound-enhanced delivery: preliminary evidence for a novel mechanism. Ultrasound Med Biol. 2009;35:1722-36.
56. Palmeri ML, Wang MH, Dahl JJ, Frinkley KD, Nightingale KR. Quantifying hepatic shear modulus *in vivo* using acoustic radiation force. Ultrasound Med Biol. 2008;34:546-58.
57. Sarvazyan AP, Rudenko OV, Nyborg WL. Biomedical applications of radiation force of ultrasound: historical roots and physical basis. Ultrasound Med Biol. 2010;36:1379-94.
58. Celsion Corporation, http://celsion.com/docs/pipeline_overview, accessed on 10-10-12.
59. Hartel S, Diehl HA, Ojeda F. Methyl-beta-cyclodextrins and liposomes as water-soluble carriers for cholesterol incorporation into membranes and its evaluation by a microenzymatic fluorescence assay and membrane fluidity-sensitive dyes. Anal Biochem. 1998;258:277-84.
60. Parasassi T, Giusti AM, Raimondi M, Gratton W. Abrupt modifications of phospholipid bilayer properties at critical cholesterol concentrations. Biophys J. 1995;68:1895-1902.
61. Socaciu C, Jessel R, Diehl HA. Competitive carotenoid and cholesterol incorporation into liposomes: effects on membrane phase transition, fluidity, polarity and anisotropy. Chem Phys Lipids. 2000;106:79-88.
62. Ferrara KW. Driving delivery vehicles with ultrasound. Adv Drug Deliv Rev. 2008;60:1097-1102.
63. Yudina A, de Smet M, Lepetit-Coiffé M, Langereis S, Van Ruijssevelt L, Smirnov P, Bouchaud V, Voisin P, Gruell H, Moonen CT. Ultrasound-mediated intracellular drug delivery using microbubbles and temperature-sensitive liposomes. J Control Release. 2011;155:442-8.
64. Ibsen S, Benchimol M, Simberg D, Esener S. Ultrasound mediated localized drug delivery. Adv Exp Med Biol. 2012;733:145-53.

Chapter 4

Chris Oerlemans
Frank Nijsen
Miranda van Amersfoort
Louis van Bloois
Edwin Heijman
Peter Luijten
Willem Mali
Gert Storm

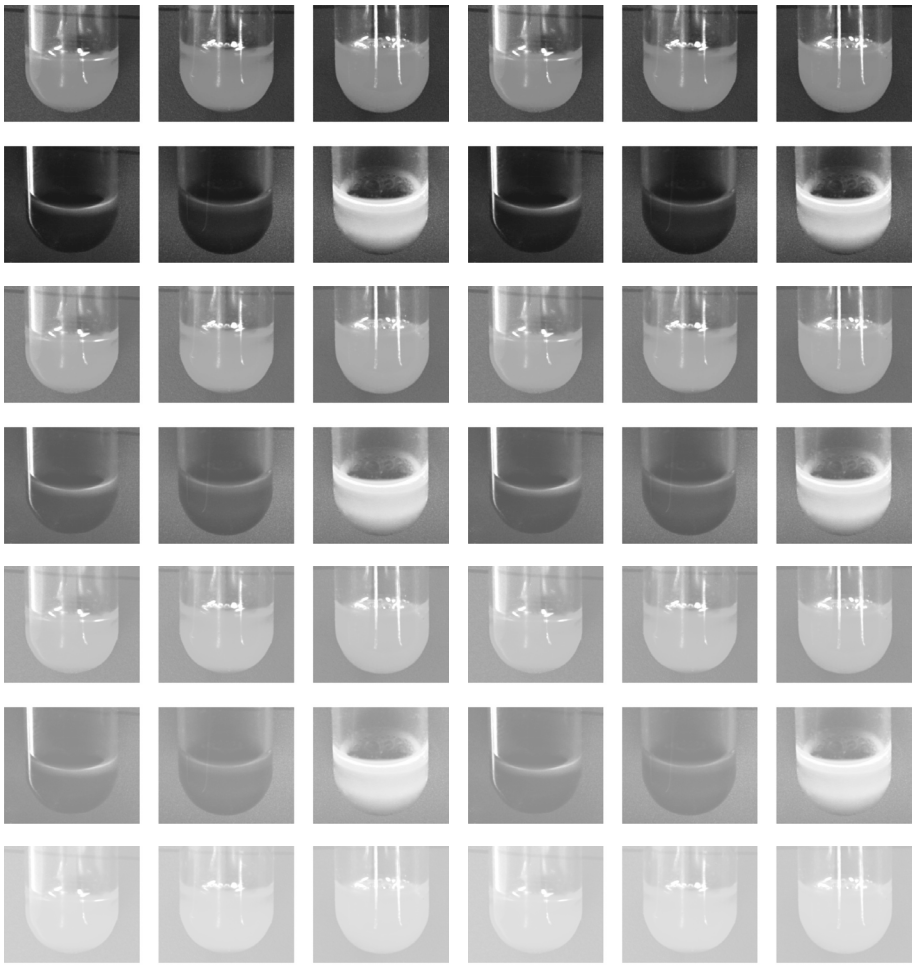

Fluorescent liposomes for MR-HIFU-triggered release and tumor demarcation

European Journal of Pharmaceutics and Biopharmaceutics 77, 458-464
2011

ABSTRACT

The combination of fluorescein-containing liposomes (FCL) and magnetic resonance-guided high intensity focused ultrasound- (MR-HIFU) triggered release is a promising approach for lesion demarcation and more efficient removal of non-palpable breast lesions. Exposure of FCL to ablation temperatures (60 °C) using MR-HIFU would result in palpable, stained tumors, which are more easy to identify during surgical resection. In this study, proof-of-concept concerning fluorescent FCL for MR-HIFU-triggered release and tumor demarcation of non-palpable breast lesions is presented. *Ex vivo* experiments in human blood and porcine muscle tissue showed increased label release from the liposomes, clear fluorescence enhancement and diffusion of the released compound after heating to 60 °C. Next, fluorescein release of FCL was observed after MR-HIFU-mediated mild hyperthermia (42 °C) and ablation temperature (60 °C) for a short period (30 s), which is in line with the clinically relevant MR-HIFU treatment parameters. These results indicate the potential of the FCL as a tool to improve tumor demarcation in patients by MR-HIFU-triggered release. Therefore, this method may offer a new tool for efficient surgical resection of non-palpable breast tumor lesions by enabling proper discrimination between tumor tissue and adjacent healthy tissue.

INTRODUCTION

One of the main difficulties in surgical breast tumor resection is to distinguish non-palpable breast lesions from healthy tissue. Smith-Bindman *et al.* stated after a screening mammography study in the UK and the US that 10-55% of the detected suspicious non-palpable lesions were malignant [1]. These patients must undergo intensive treatments like lumpectomy or mastectomy to ascertain 100% removal of the malignancies. Axillary lymph node dissection and loss of breast tissue severely affects the quality of life of the patients. Hence, it is important to improve lesion demarcation to reduce the removal of healthy tissue. Consequently, there is a need for a method that enables proper discrimination between tumor tissue and adjacent healthy tissue to ensure efficient complete tumor removal. Nowadays, the use of magnetic resonance imaging (MRI) as a non-invasive diagnostic modality for characterization of suspicious breast lesions has become an additional diagnostic tool next to conventional techniques like mammography and ultrasound [2]. A recent clinically available non-invasive technique, that combines MRI with thermal ablation, is magnetic resonance-guided high intensity focused ultrasound (MR-HIFU) [3]. MR-HIFU is able to heat tissue with pinpoint accuracy thereby ablating malignant cells. Temperatures to be reached for this purpose are 60 °C and higher. Currently, clinical trials are performed on MR-HIFU treatment of uterine fibroids and prostate cancer [4, 5]. Extensive preclinical research has been performed to expand the possibilities of this technique to breast tumor treatment [6, 7]. Unfortunately, 100% tumor ablation cannot be guaranteed [6]. Especially for tumors with undefined margins and scattered multiple foci, MR-HIFU-mediated tumor ablation is not suitable [8]. Therefore, surgical resection remains important in the clinical setting. A recent development in anti-cancer therapy is the combination of MR-HIFU and drug-containing nanoparticles like thermosensitive liposomes, which release their content upon application of a heat-trigger around 42 °C [9-12]. Interestingly, the combination of MR-HIFU-mediated ablation and thermosensitive liposomes has not been explored as yet. Although treatment of the lesions with MR-HIFU alone will result in coagulated tissue, which becomes palpable and consequently more easy to identify, visual detection of the malignant areas during surgery will still be difficult. So, it would be beneficial to enable visual discrimination of the lesions from healthy tissue. Margin marking of the lesions with a dye would help to facilitate more efficient lesion resection. An appropriate fluorescent dye for this purpose is fluorescein, since it is already used as a diagnostic tool in combination with ultraviolet (UV) light in a clinical setting and can therefore be safely used in patients [13-15]. Moreover, fluorescein is a self-quenching dye, which means that no fluorescence is detected at high intraliposomal concentration [16]. This has the advantage that the dye can only be detected with UV light after it is being released from the liposomes enabling proper discrimination of the MR-HIFU-treated malignant tissue from the non-treated healthy tissue. The concept of this novel approach to improve efficiency in lesion resection after the MR-HIFU-mediated ablation procedure starts with intravenous administration of fluorescein-containing liposomes (FCL). To ensure a sufficient liposome accumulation at the tumor tissue, it is essential to include cholesterol and poly(ethylene glycol) (PEG) into the liposome formulation for high stability and long circulation, respectively, while the inclusion of a thermosensitive phospholipid such as 1,2-dipalmitoyl-*sn*-glycero-3-phosphocholine (DPPC) enables MR-HIFU-mediated fluorescein release from the liposomes. By virtue of the enhanced permeability and

retention (EPR) effect, liposomes with a size of around 100 nm are able to extravasate from the blood vessels into the tumor tissue [17-21]. Subsequently, the high ablation temperature as applied by MR-HIFU will trigger the FCL to release their dye, which will diffuse throughout the surrounding tumor tissue, resulting in tumor demarcation. In this study, FCL, which are able to release their content after exposure to MR-HIFU-mediated ablation temperatures, are developed, and proof-of-concept is provided for the proposed approach to improve lumpectomy based on a combination of FCL and MR-HIFU.

MATERIALS AND METHODS

MATERIALS

All chemicals and lipids were commercially available and used as obtained. 1,2-dipalmitoyl-*sn*-glycero-3-phosphocholine (DPPC) and 1,2-dipalmitoyl-*sn*-glycero-3-phospho-ethanolamine-*N*-[methoxy(polyethylene glycol)-2000] (PEG_{2000}-DSPE) were obtained from Lipoid GmbH (Ludwigshafen, Germany). Cholesterol (>99%), glutathione (reduced, >99%); Triton X-100 and silicon dioxide (SiO_2, 99%, 0.5-10 μm) were supplied by Sigma Aldrich (Steinheim, Germany). Sodium fluorescein (100 mg mL^{-1}) was obtained from Serb Laboratoires (Paris, France). HMPAO kit was purchased from Ceretec (Amersham, Arlington Heights, IL, USA). ^{99m}Tc-pertechnetate was obtained from a molybdenum-99/technetium-99m generator (Mallinckrodt, Petten, the Netherlands). *N*-(7-nitrobenz-2-oxa-1,3-diazol-4-yl)-1,2-dihexadecanoyl-*sn*-glycero-3-phosphoethanolamine (NBD-PE) was purchased from Invitrogen (Carlsbad, CA, USA). Agarose MP was obtained from Roche Applied Science (Mannheim, Germany).

LIPOSOME PREPARATION

The FCL were prepared with the conventional thin-film hydration technique as described previously [20] and consisted of DPPC, cholesterol and PEG_{2000}-DSPE in a molar ratio of 1.85 : 1 : 0.15. The lipid mixture (100 mM) was dissolved in ethanol (10 mL) and evaporated to dryness by rotary evaporation under vacuum (Rotavapor R-210, BUCHI Laboratory Equipment, Zurich, Switzerland). The resulting lipid film was further dried under N_2 to ensure that all ethanol had evaporated. The lipid film was hydrated with 10 mL fluorescein (100 mg mL^{-1}). For control experiments, ^{99m}Tc-HMPAO- and NBD-PE-containing liposomes were prepared using the same technique. For the ^{99m}Tc-HMPAO-containing liposomes, the lipid film was hydrated with 10 mL glutathione (15.4 mg mL^{-1}). NBD-PE was incorporated with the lipid bilayer to obtain a liposome composition of DPPC, cholesterol, PEG_{2000}-DSPE and NBD-PE in a molar ratio of 1.85 : 1 : 0.15 : 0.03 (NBD-PE 1% of total lipid concentration) at 15 μmol mL^{-1}. The lipid film was hydrated with 10 mL HEPES-buffered saline (HBS; 20 mM HEPES and 135 mM NaCl, pH 7.4). The resulting lipid dispersions were sized with sequential extrusion using a Lipex Extruder (Northern Lipids Inc., Vancouver, Canada) and polycarbonate membrane filters (Poretics Corporation, Livermore, CA, USA) with a pore diameter of 600, 200, 100 nm and 50 nm to obtain liposomes with an average diameter of around 100 nm.

LIPOSOME CHARACTERIZATION

The average hydrodynamic size and polydispersity index (PDI) of the liposomes were determined with dynamic light scattering (DLS) using a Malvern ALV CGS-3 system (Malvern Instruments Ltd., Worcestershire, UK). The PDI value can range from 0 for a monodisperse to 1 for a heterodisperse formulation. Intensity correlation functions were measured using a wavelength of 632.8 nm at a scattering angle of 90°. Non-encapsulated fluorescein or glutathione was removed by dialysis in HBS using Slide-A-Lyzer cassettes with a molecular weight cut-off of 10 kDa (Pierce, Rockford, IL, USA) during 48 h with four times a change of buffer. Dye concentration of FCL was determined by spectrophotometric measurement (UV Mini 1240, Shimadzu Scientific Instruments, Columbia, USA, λ = 490 nm) after lysis of the liposomes using 2% Triton X-100 in HBS. The total phospholipid concentration of the liposomes after extrusion was determined with the phosphate assay as described by Rouser *et al.* [22]. Preformed glutathione-containing liposomes were labeled with ^{99m}Tc-HMPAO as described previously by Phillips *et al.* [23]. Briefly, 740 MBq $^{99m}TcO_4^-$ was added to a lyophilized HMPAO kit. Incubation of 0.5 mL liposomes with 1 mL $^{99m}TcO_4^-$-HMPAO results in a concentration of 14.8 MBq μmol^{-1} lipid. Labeling efficiency of ^{99m}Tc-HMPAO-containing liposomes was determined in the liposome fraction after removal of the non-encapsulated ^{99m}Tc-HMPAO using a PD-10 desalting column (Amersham Biosciences, Uppsala, Sweden) with HBS as eluent. The radioactivity of the liposomes was measured with a VDC-404 dose calibrator (Veenstra Instruments, Joure, the Netherlands). Differential scanning calorimetry (DSC) measurements were performed in a capillary cell microcalorimeter instrument (MicroCal VP-DSC, Northampton, MA) to determine the phase transition melting temperature (T_m) of the liposomes. The experiment was performed at temperatures ranging from 20 °C to 70 °C at a heating rate of 1 °C min^{-1} after an equilibration period of 15 min at 20 °C.

LIPOSOME STABILITY

To investigate liposomal stability, the liposomes were stored at 4 °C for 6 months. Afterwards, three samples of each liposome batch were taken to measure size and PDI. Besides, the three freshly prepared liposome compositions were heated to 60 °C for 180 min to investigate the size distribution and PDI of the liposomes after an extended heating period.

IN VITRO FCL RELEASE STUDIES

For quantitative dye release analysis, the FCL and NBD-PE-containing control liposomes were exposed to different temperatures. Therefore, agarose phantoms (0.5%) were prepared with deionized water in 50 mL BD Falcon tubes. A small cavity was created with a 100 μL pipette tip in the middle of the agarose phantom before the onset of gelation. The remaining cavity after the tip was removed was filled with liposomes containing a total dye concentration of 130 μM. The agarose phantoms were heated to 20, 37, 40, 43, 47 and 60 °C for 30 s using a thermostat-controlled water bath. To study the effect of room and body temperature, the agarose phantoms were exposed to 20 °C and 37 °C for an extended period of 180 min. After heat exposure, the agarose phantoms were stored at 4 °C and dye release was measured with a Photon Imager (Biospace Lab, Paris, France) 24 h after heat exposure to allow the released dye to diffuse throughout the agarose phantoms. Quantitative data (number

of fluorescent counts) was collected and analyzed using M3Vision software (Biospace Lab, Paris, France). FCL and NBD-PE-containing liposomes lysed with 2% Triton X-100 were used as positive control. Agarose phantoms (0.5%) without liposomes were used as negative control.

EX VIVO LIPOSOME RELEASE STUDIES

To determine the feasibility of FCL application in a clinical setting, FCL (800 μM) were mixed with human blood (1 mL : 1 mL) and exposed to 20 °C, 37 °C and 60 °C for 30 s for visual detection of the released dye after heat-triggering. Photographs of the samples were taken under normal light conditions and UV light (350 nm). Additionally, ^{99m}Tc release from liposomes was investigated in porcine muscle tissue using planar nuclear imaging with a dualhead gamma camera (Vertex-MCD, ADAC, Milpitas, CA, USA) before and after heat exposure of the tissue. Two pieces of porcine musculus semitendinosus were obtained from a pig that was previously used as a laboratory animal. The tissue was stored at 7 °C and used within 24 h after the pig was euthanized. The muscle tissues were injected with 1 mL of ^{99m}Tc-HMPAO liposomes of which one was heated to 60 °C using hot air flow and one was kept at room temperature (20 °C), as monitored by a locally placed thermometer. Diffusion of ^{99m}Tc throughout the tissue was allowed for 2 h at room temperature. The acquisition time was 90 s with a count rate of approximately 10,000 cps. The images were acquired in a 256 x 256 matrix with a pixel size of 2.32 mm x 2.32 mm and a 20% window centered around the 140 keV photopeak using a low energy collimator. Posterior and anterior images were fused in one image.

MR-HIFU-TRIGGERED RELEASE STUDY

Agarose phantoms were prepared in polypropylene beakers with 0.5% agarose, 2% SiO_2 and 800 mL deionized water. SiO_2 is added for a higher absorption coefficient of the agarose gel, resulting in better absorption of the ultrasound beam. A small cavity was created in the middle of the agarose phantom with a 2 mL pipette tip, which was inserted in the middle of the agarose before the onset of gelation. After the agarose was cooled down, the pipette tip was removed and the remaining cavity was filled with a mixture of liposomes containing a dye concentration of 800 μM and agarose gel, which was cooled down to 37 °C to prevent premature release from liposomes. After cooling down, more agarose gel (37 °C) was put on top until the cavity was completely covered to prevent scattering of the ultrasound beam during MR-HIFU exposure. The agarose phantoms containing FCL or the control NBD-PE-containing liposomes were heated with the Philips Sonalleve 3 T MR-HIFU system (Philips Healthcare, Helsinki, Finland). This system was used to heat a volume of approximately 1.2 x 1.2 x 5 cm^3 using a 256-element phased-array ultrasound transducer with volumetric heating capabilities and feedback control [24]. The ultrasound field was continuous wave with a frequency of 1.2 MHz. Planning of the target area and temperature mapping during treatment was performed by a 3 T Philips Achieva MRI scanner (Philips Healthcare, Best, the Netherlands). The temperature measurements were performed according to the Proton Chemical Shift (PRF) method [25]. MR phase images of a gradient echo sequence were used to calculate temperature maps. When the spatial temperature in the field-of-view of the first acquired phase image is known (e.g. in equilibrium at room temperature), the temperature distribution in the second acquisition can

be considered as an absolute temperature map. The temperature maps were used as input for the binary feedback loop of the HIFU transducer. The binary feedback loop modulated in real-time the transducer power resulting in a precise control of the temperature in the field-of-view. The MR gradient echo sequence is a dynamic multi-slice sequence with the following parameters: TR/TE = 28/20 ms; flip angle = 19°; matrix = 160 x 99; field-of-view = 400 x 250 mm; voxel size = 2.5 x 2.5 x 7 mm; acquisition time per dynamic scan = 2.5 s. The MR slices were arranged as described by Kohler *et al.* [26]. After a short preheating period (around 30-120 s), the desired temperature of 42 °C and 60 °C was reached and maintained for 30 s. The temperature accuracy was 0.1 °C based on the MR signal intensity [27]. After 24 h of storage at 4 °C, the agarose phantoms were sliced along the midsagittal plane. Dye release from the focal spot was measured with the Photon Imager and analyzed using M3Vision software as described previously. The total dye release after MR-HIFU treatment was compared with FCL or NBD-PE-containing liposomes lyzed with 2% Triton X-100 were used as positive control. Liposome-embedded agarose phantoms, which were not treated with MR-HIFU, were used as negative control.

RESULTS

LIPOSOME PREPARATION AND CHARACTERIZATION

FCL were prepared to determine their implementation as a diagnostic tool in lesion demarcation after MR-HIFU-mediated ablation (Fig. 1). Liposomes containing the lipophilic label NBD-PE were prepared as control liposomes and ^{99m}Tc-HMPAO-containing liposomes were used for *ex vivo* studies (Table 1).

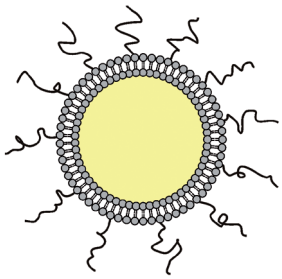

Fig. 1. Schematic representation of the FCL showing a PEG-coated lipid bilayer surrounding an aqueous compartment containing fluorescein.

Table 1. Liposome characteristics

Label	Diamter (nm)	PDI	Dye concentration
Fluorescein	108 ± 1	0.04 ± 0.01	7.1 mg mL^{-1}
NBD-PE	107 ± 2	0.05 ± 0.01	131 μg ml^{-1}
^{99m}Tc-HMPAO	109 ± 2	0.02 ± 0.01	134 MBq mL^{-1}

The average diameter of the liposomes was around 110 nm and the PDI was low in every liposome dispersion (all ≤ 0.05), which indicates a narrow size distribution. Storage of liposomes for 6 months at 4 °C and heating of liposomes to 60 °C for 180 min

did not influence the size distribution of the liposomes, indicating that the liposomes are stable regarding changes in particle size distribution (Fig. 2). DSC measurements confirmed the T_m of the FCL to be at 42 °C, which corresponds with the T_m of DPPC.

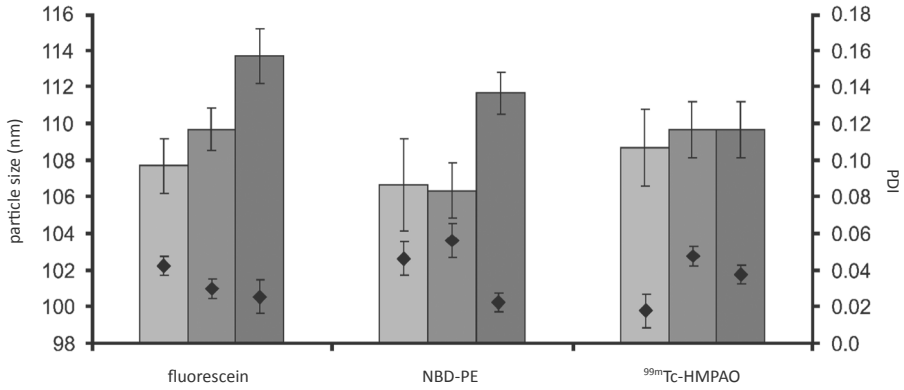

Fig. 2. Liposome size (nm) and PDI (mean ± SD, n=3). Diameter of freshly prepared liposomes (□). Liposome diameter after 180 min of exposure to 60 °C (■). Diameter of liposomes 6 months after storage at 4 °C (■). PDI ± SD is indicated by (◆).

IN VITRO LIPOSOME RELEASE STUDIES

The degree of dye release from FCL exposed to 20, 37, 40, 43, 47 and 60 °C for 30 s is presented in Fig. 3a. Exposure to 43 °C resulted in 38% release, while 68% release was observed after exposure to 60 °C. Exposure to 20 °C and 37 °C, even after an extended exposure period of 180 min, did not result in any detectable release. NBD-PE-containing liposomes exposed to 37 °C and 60 °C for 180 min did not show detectable release of the fluorescent label from liposomes into the agarose phantoms (Fig. 3c), while NBD-PE liberated using 2% Triton X-100 from the liposomal bilayer was able to diffuse throughout the agarose gels. This indicates that the liposomal formulation remains stable after heating. In order to exclude any direct effects of temperature elevation on fluorescence levels of fluorescein, an experiment was performed on fluorescein solubilized in demineralized water. The samples were heated for 15 min from 20 °C up to 60 °C , and emission spectra were measured. No detectable change in the emission spectra was observed at different temperatures (data not shown), hence the increase in fluorescence can exclusively be ascribed to release from the FCL. In Fig. 4, photographs from FCL in human blood exposed to different temperatures for 30 s, taken under normal light conditions (Fig. 4a-c) and 350 nm UV light (Fig. 4d-f), are shown. No visual differences between the samples were observed under normal light conditions. However, under UV light conditions, fluorescence was clearly enhanced after exposure of the FCL to 60 °C (Fig. 4f).

EX VIVO RELEASE STUDIES

Distribution of fluorescein throughout tissue cannot be visualized directly in large tissue samples due to the insufficient tissue penetration depth. Therefore, *ex vivo*

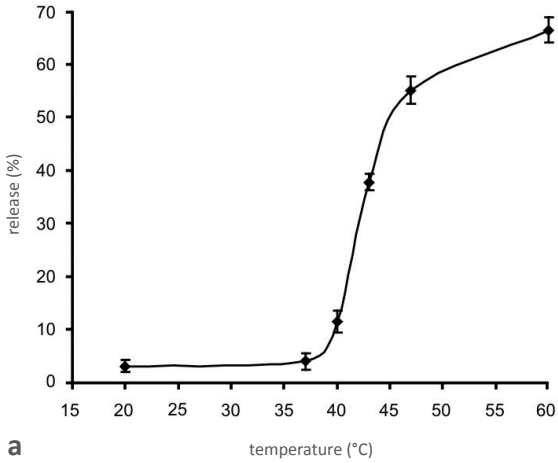

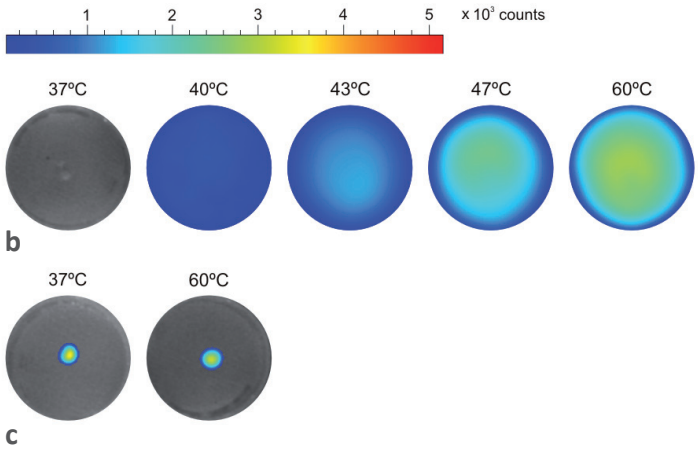

Fig. 3. Percentage of fluorescein release from liposomes after 30 s exposure to different temperatures (mean ± SD, n=3) (a). Fluorescence measurements in FCL-containing phantoms exposed to different temperatures for 30 s (b). Fluorescence of NBD-PE-containing liposomes in agarose phantoms after heat exposure to 37 °C and 60 °C for 30 s (c).

porcine muscle tissue was injected with liposomes labeled with the water-soluble radioisotope ^{99m}Tc (^{99m}Tc-HMPAO-containing liposomes) to evaluate the release properties of the liposome formulation in tissue. Planar nuclear images of the tissue before and after heat exposure (60 °C) are shown in Fig. 5. Fig. 5b indicates the diffusion of ^{99m}Tc in tissue after heat-triggering, which supports the feasibility of MR-HIFU-triggered release from liposomes in tissue. In control tissue, which was not exposed to heat, ^{99m}Tc did not show such enhanced diffusion from the injection spot throughout the tissue (Fig. 5c and d).

MR-HIFU-TRIGGERED RELEASE STUDY

The liposome spot inside the agarose phantoms was treated with MR-HIFU, as is depicted in Fig. 6a. This region of interest (ROI) was heated to 42 °C (T_m of DPPC) and 60 °C (ablation temperature) for 30 s with MR-HIFU. In Fig. 6b and c, the heated liposome spot in the agarose phantom is shown with MRI temperature mapping to

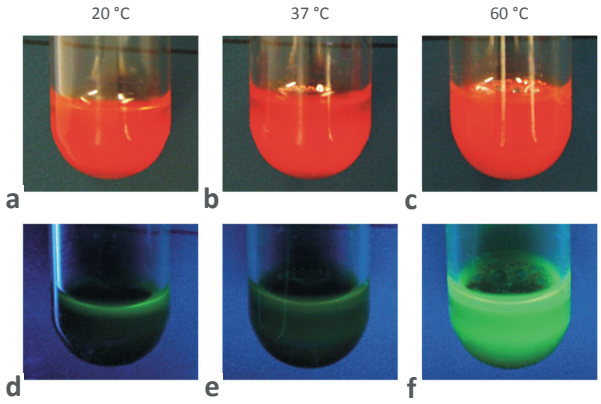

Fig. 4. Photographs from FCL dispersed in human blood. Samples are exposed to 20 °C, 37 °C and 60 °C for 30 s. Photographs taken under normal light conditions (a-c). Photographs taken under 350 nm UV light emission (d-f). Exposure to 20 °C and 37 °C (d and e). After exposure to 60 °C, fluorescence was clearly enhanced (f).

demonstrate the accuracy of the MR-HIFU procedure. MR-HIFU-induced heating to 42 °C resulted in 28% release, whereas 68% release was observed after heating to 60 °C. These results correspond with the heat exposure results that were obtained with a water bath (Fig. 3). MR-HIFU treatment of NBD-PE-containing liposomes did not lead to fluorophore distribution throughout the agarose phantoms, which is also in agreement with the *in vitro* water bath results (see above).

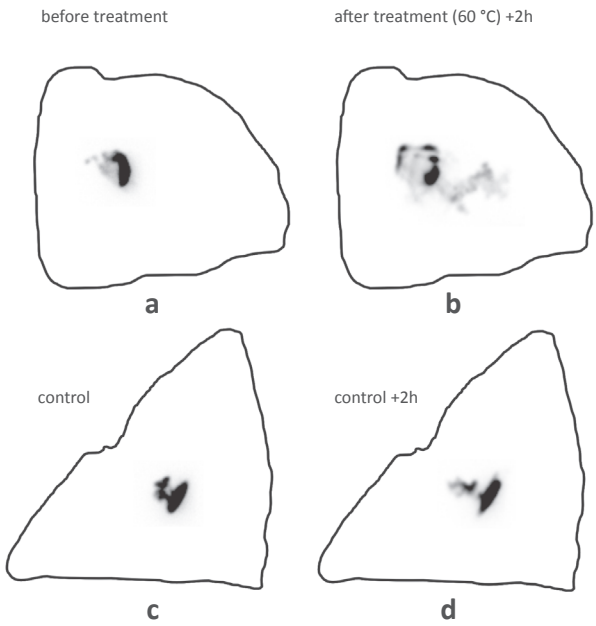

Fig. 5. Planar nuclear images of porcine muscle tissue injected with ^{99m}Tc-HMPAO-containing liposomes. Distribution of ^{99m}Tc in the tissue before and after heat exposure to 60 °C (a and b). Diffusion of ^{99m}Tc throughout the tissue was observed after heat-triggering. In control tissue, such enhanced distribution was not observed (c and d).

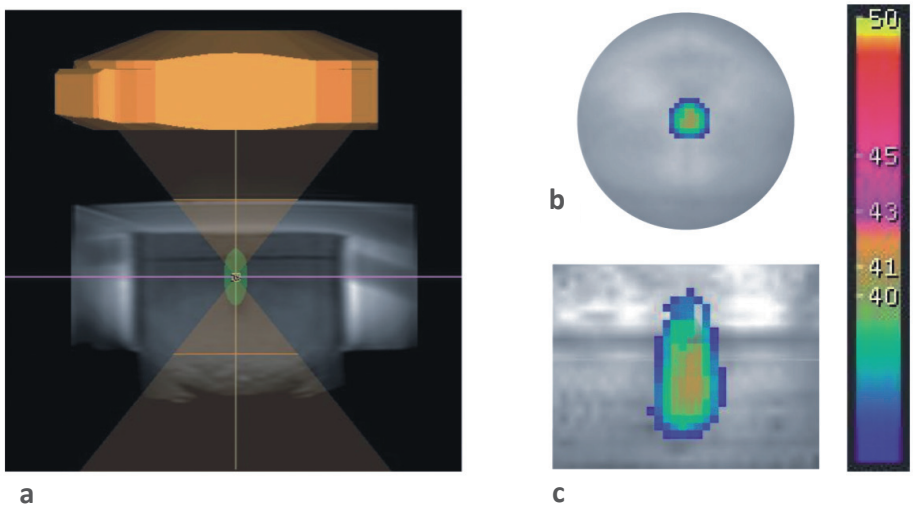

Fig. 6. Schematic drawing of the treatment planning positioned on the MR image of the agarose phantom during MR-HIFU treatment; the intended treatment cell is shown in green (a). Transverse plane of the agarose phantom during the 42 °C treatment, the temperature distribution can be deducted from the color bar (b). Midsagittal plane of the agarose phantom during 42 °C treatment, indicating the heated area and reflecting the treatment cell as prepared during the treatment planning (c).

DISCUSSION

This study was performed to obtain proof-of-concept for the applicability of stable, long-circulating FCL as a tool for tumor demarcation of non-palpable breast lesions after MR-HIFU-mediated ablation. The liposomal size distribution of around 110 nm enables passive tumor targeting facilitated by the EPR effect [17]. A 6-month storage period at 4 °C showed that the FCL did not leak their fluorescent label and are stable regarding changes in particle size distribution. A pharmaceutical acceptable shelf-life is important for usage in a clinical setting and underlines the clinical applicability of the FCL formulation. Temperature-induced fluorescein release from liposomes was investigated by exposure of liposome-embedded agarose phantoms to different temperatures. Exposure of these phantoms to 20 °C and 37 °C did not result in detectable release. Fluorescein release was limited at 40 °C (about 10%) after short exposure times (30 s) while it increased to 68% after 30 s exposure to 60 °C (Fig. 3), illustrating the sensitivity of the liposome formulation for temperature changes above 37 °C. No fluorophore distribution was observed after heating the NBD-PE-containing liposomes to 60 °C, demonstrating the high stability of the liposome formulation. Exposure of FCL dispersed in human blood to 20 °C, 37 °C and 60 °C for 30 s showed a clear enhancement of fluorescence at 60 °C as compared to body temperature (37 °C). The liposomal fluorescein concentration used in these experiments is sufficient for staining in a clinical setting. Due to self-quenching inside the liposomes, fluorescence is only observed when fluorescein is released from the liposomes. This attractive property contributes to efficient lesion demarcation since fluorescence will only be detected around the heated area, which excludes false

positive staining of healthy tissue. Although animal-derived breast tissue or *ex vivo* human mammary tissue may resemble breast tissue in a clinical setting, these tissues, however, do not resemble tumor tissue itself with respect to the tissue consistency. Tumor tissue is often characterized as dense tissue, which is highly vascularized at the tumor periphery. For this reason, muscle tissue was determined to be a suitable alternative for tumor tissue in this setup for *ex vivo* diffusion experiments after heat-triggered liposome release of ^{99m}Tc. *Ex vivo* experiments with porcine muscle tissue injected with ^{99m}Tc-HMPAO showed enhanced distribution of ^{99m}Tc after heating to 60 °C, indicating release and diffusion of ^{99m}Tc. This result additionally confirms the potential applicability of the liposome formulation for lesion demarcation in tissue. To demonstrate the occurrence of temperature-induced release after MR-HIFU-triggering, FCL-embedded agarose phantoms were exposed to MR-HIFU ablation for 30 s. Short ablation temperatures are critical when using MR-HIFU in the body. The short exposure period is in accordance with clinically relevant MR-HIFU parameters [24, 26]. Long heating periods may cause peripheral absorption of heat in non-targeted tissue, yielding the risk of unpredictable thermal lesions [6]. Short exposure of FCL-embedded agarose phantoms to MR-HIFU at 42 °C and 60 °C resulted in dye release kinetics in line with the *in vitro* results obtained with a water bath.

ACKNOWLEDGEMENTS

The authors thank dr. Kristina Djanashvili and dr. Daniel Schüle from the department of Biotechnology, Delft University, the Netherlands, for their help with the DSC measurements. The authors express their gratitude to Lipoid GmbH (Ludwigshafen, Germany) for their generous gift of DPPC. This work is financially supported by MediTrans (an Integrated Project funded by the European Commission).

REFERENCES

1. Smith-Bindman R, Chu PW, Miglioretti DL, Sickles EA, Blanks R, Ballard-Barbash R, Bobo JK, Lee NC, Wallis MG, Patnick J, Kerlikowske K. Comparison of screening mammography in the United States and the United kingdom. JAMA. 2003;290:2129-37.
2. Peters NH, Borel Rinkes IH, Mali WP, van den Bosch MA, Storm RK, Plaisier PW, de Boer E, van Overbeeke AJ, Peeters PH. Breast MRI in nonpalpable breast lesions: a randomized trial with diagnostic and therapeutic outcome – MO. Trials. 2007;8:40.
3. Jolesz FA. MRI-guided focused ultrasound surgery. Annu Rev Med. 2009;60:417-30.
4. Ahmed HU, Zacharakis E, Dudderidge T, Armitage JN, Scott R, Calleary J, Illing R, Kirkham A, Freeman A, Ogden C, Allen C, Emberton M. High-intensity focused ultrasound in the treatment of primary prostate cancer: the first UK series. Br J Cancer. 2009;101:19-26.
5. Zhou XD, Ren XL, Zhang J, He GB, Zheng MJ, Tian X, Li L, Zhu T, Zhang M, Wang L, Luo W. Therapeutic response assessment of high intensity focused ultrasound therapy for uterine fibroid: utility of contrast-enhanced ultrasonography. Eur J Radiol. 2007;62:289-94.
6. Schmitz AC, Gianfelice D, Daniel BL, Mali WP, van den Bosch MA, Image-guided focused ultrasound ablation of breast cancer: current status, challenges, and future directions. Eur Radiol. 2008;18:1431-41.
7. Wu F, ter-Haar G , Chen WR. High-intensity focused ultrasound ablation of breast cancer. Expert Rev Anticancer Ther. 2007;7:823-31.
8. Wu F, Wang ZB, Cao YD, Chen WZ, Bai J, Zou JZ, Zhu H. A randomised clinical trial of high-intensity focused ultrasound ablation for the treatment of patients with localised breast cancer. Br J Cancer. 2003;89:2227-33.
9. Langereis S, Keupp J, van Velthoven JL, de Roos IH, Burdinski D, Pikkemaat JA, Gruell H. A temperature-sensitive liposomal ^{1}H CEST and ^{19}F contrast agent for MR image-guided drug delivery. J Am Chem Soc. 2009;131:1380-1.
10. Kennedy JE. High-intensity focused ultrasound in the treatment of solid tumours. Nat Rev Cancer. 2005;5:321-7.
11. Frenkel V, Etherington A, Greene M, Quijano J, Xie J, Hunter F, Dromi S, Li KC. Delivery of liposomal doxorubicin (Doxil) in a breast cancer tumor model: investigation of potential enhancement by pulsed-high intensity focused ultrasound exposure. Acad Radiol. 2006;13:469-79.
12. de Smet M, Langereis S, den Bosch SV. Gruell H. Temperature-sensitive liposomes for doxorubicin delivery under MRI guidance. J Control Release. 2009;143:120-7.
13. Bennett TJ, Barry CJ. Ophthalmic imaging today: an ophthalmic photographer's viewpoint - a review. Clin Experiment Ophthalmol. 2009;37:2-13.
14. Paraskevas LR, Halpern AC, Marghoob AA. Utility of the Wood's light: five cases from a pigmented lesion clinic. Br J Dermatol. 2005;152:1039-44.
15. Winter ML, Ellis MD, Snodgrass WR. Urine fluorescence using a Wood's lamp to detect the antifreeze additive sodium fluoresce: a qualitative adjunctive test in suspected ethylene glycol ingestions. Ann Emerg Med. 1990;19:663-7.
16. Lakowicz JR, Malicka J, D'Auria S, Gryczynski I. Release of the self-quenching of fluorescence near silver metallic surfaces. Anal Biochem. 2003;320:13-20.
17. Greish K. Enhanced permeability and retention of macromolecular drugs in solid tumors: a royal gate for targeted anticancer nanomedicines. J Drug Target. 2007;15:457-64.
18. Maeda H, Wu J, Sawa T, Matsumura Y, Hori K. Tumor vascular permeability and the EPR effect in macromolecular therapeutics: a review. J Control Release. 2000;65:271-84.
19. Harrington KJ, Mohammadtaghi S, Uster PS, Glass D, Peters AM, Vile RG, Stewart JS. Effective targeting of solid tumors in patients with locally advanced cancers by radiolabeled pegylated liposomes. Clin Cancer Res. 2001;7:243-54.
20. Koning GA, Morselt HW, Velinova MJ, Donga J, Gorter A, Allen TM, Zalipsky S, Kamps JA, Scherphof GL. Selective transfer of a lipophilic prodrug of 5-fluorodeoxyuridine from immunoliposomes to colon cancer cells. Biochim Biophys Acta. 1999;1420:153-67.

21. Li CJ, Miyamoto Y, Kojima Y, Maeda H. Augmentation of tumour delivery of macromolecular drugs with reduced bone marrow delivery by elevating blood pressure. Br J Cancer. 1993;67:975-80.
22. Rouser G, Fleischer S, Yamamoto A. Two dimensional then layer chromatographic separation of polar lipids and determination of phospholipids by phosphorus analysis of spots. Lipids. 1970;5:494-6.
23. Phillips WT, Rudolph AS, Goins B, Timmons JH, Klipper R, Blumhardt R. A simple method for producing a technetium-99m-labeled liposome which is stable *in vivo*. Int J Rad Appl Instrum. 1992;B19:539-47.
24. Enholm JK, Kohler MO, Quesson B, Mougenot C, Moonen CT, Sokka SD. Improved volumetric MR-HIFU ablation by robust binary feedback control. IEEE Trans Biomed Eng. 2010;57:103-13.
25. Ishihara Y, Calderon A, Watanabe H, Okamoto K, Suzuki Y, Kuroda K, Suzuki Y. A precise and fast temperature mapping using water proton chemical shift. Magn Reson Med. 1995;34:814-23.
26. Kohler MO, Mougenot C, Quesson B, Enholm J, Le BB, Laurent C, Moonen CT, Ehnholm GJ. Volumetric HIFU ablation under 3D guidance of rapid MRI thermometry. Med Phys. 2009;36:3521-35.
27. Senneville BD, Mougenot C, Moonen CT. HIFU treatment of mobile organs under MR control. Int J Hyperthermia. 2005;21:515-31.

Chapter 5

Chris Oerlemans
Peter Seevinck
Gerrit van de Maat
Hassan Boulkhrif
Chris Bakker
Wim Hennink
Frank Nijsen

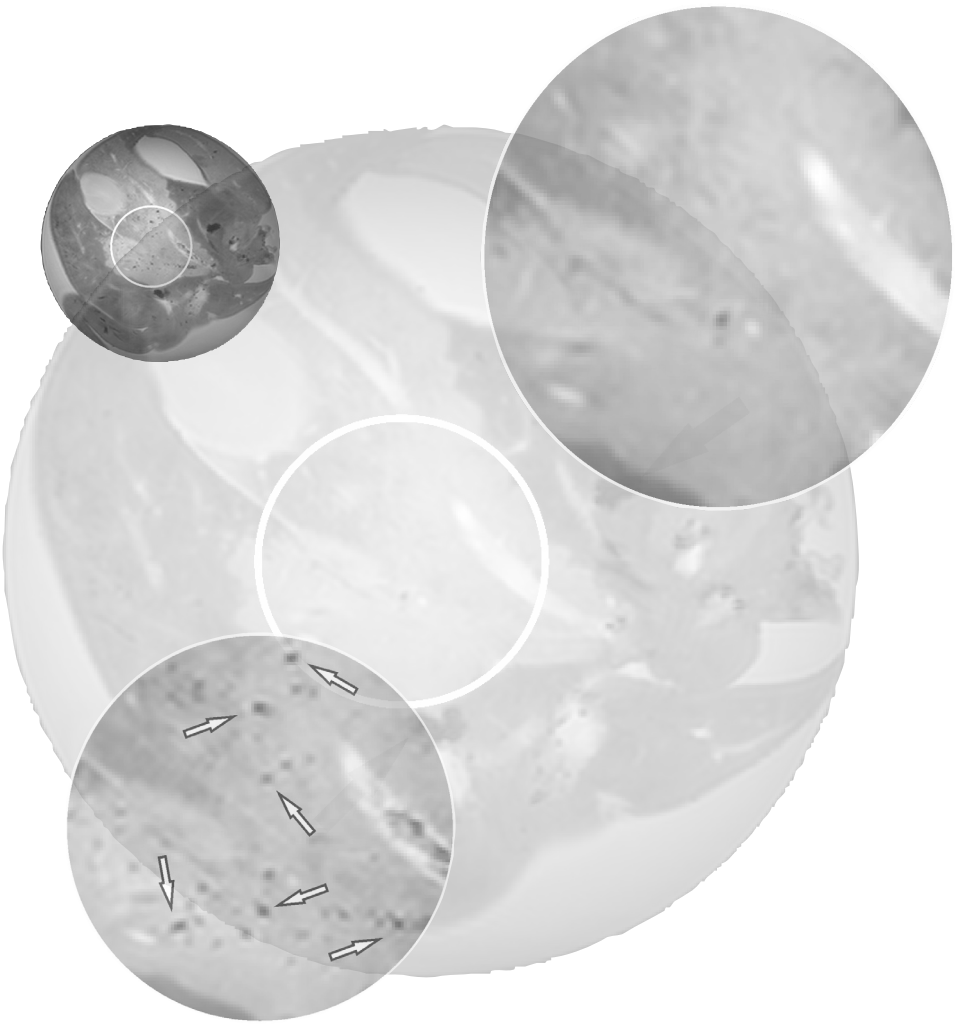

Alginate-lanthanide microspheres for MRI-guided embolotherapy

Acta Biomaterialia 9, 4681-4687
2013

ABSTRACT

In cancer therapy, a promising treatment option to accomplish a high tumor-to-normal-tissue ratio is endovascular intervention with microsized particles, such as embolotherapy. In this study, alginate microspheres (ams) were prepared with the JetCutter technique, which is based on cutting a sodium alginate solution jet stream into small droplets of uniform size which are then crosslinked with different lanthanides or iron-III, resulting in microspheres of a predefined size which can be visualized by magnetic resonance imaging (MRI). The microspheres were investigated for their size and morphology (light microscopy and scanning electron microscopy analysis), cation content and MRI properties. The lanthanide-ams formulations, with a uniform size of 250 μm and a cation content between 0.72-0.94%, showed promising results for MR imaging. This was further demonstrated for Ho^{3+}-crosslinked alginate microspheres (Ho^{3+}-ams), the most potent microsphere formulation with respect to MR visualization, allowing single sphere detection and detailed microsphere distribution examination. Intravascular infusion of Ho^{3+}-ams by catheterization of *ex vivo* rabbit and porcine liver tissue and assessment of the procedure with MRI clearly showed accumulation and subsequently embolization of the targeted vessels, allowing accurate monitoring of the microsphere biodistribution throughout the tissue. Therefore, the different alginate-lanthanide microsphere formulations developed in this study show great potential for utilization as image-guided embolotherapy agents.

INTRODUCTION

In cancer chemotherapy, treatment techniques aimed at local drug delivery are gaining increasing interest. Ideally, successful tumor targeting will lead to a high tumor-to-normal-tissue ratio, enhancing treatment efficacy while toxicity and side effects are reduced [1, 2]. A promising treatment option for efficient tumor targeting is embolotherapy, in which microsized particles are administered selectively into the tumor-feeding artery by catheterization. During this procedure, a catheter is advanced intra-arterially to the desired location. Using radiopaque contrast medium, the procedure can be performed under fluoroscopy guidance. When the tumor-feeding artery is reached with the catheter, the microsized particles are infused. As a result, the blood flow is reduced or completely obstructed, which causes a lack of nutrients and oxygen and eventually leads to necrosis of the affected tissue. Different embolization agents, such as polyvinyl alcohol embolization particles and tris-acryl gelatin embolization microspheres, have been developed and are currently utilized for various indications, such as treatment of uterine fibroids, arteriovenous malformations and hypervascularized tumors [3, 4]. Furthermore, embolization microspheres can also be exploited as a carrier of therapeutic agents, e.g. drug-eluting beads, which have been used recently in transarterial chemo-embolization [5-7]. These microspheres enabled visualization with fluoroscopy and X-ray computed tomography (CT) imaging, which would allow 'real-time' image guidance of the transcatheter embolization procedure [8, 9]. However, these ionizing radiation-based imaging techniques lack soft tissue contrast, which is important for tumor identification. The possibility to non-invasively assess the biodistribution of microspheres in conjunction with the local anatomy is of major importance, because it allows for superior treatment monitoring as well as validation of the targeting efficiency. Recently, our group demonstrated proof-of-concept of an embolization particle based on alginate containing a magnetic resonance imaging (MRI) contrast agent (Ho^{3+}) [10]. MRI is a promising modality for image-guided embolotherapy and biodistribution assessment of microspheres within the patient due to its relatively high spatial and temporal resolution and superior soft tissue contrast properties [11] as compared to CT, which allows visualization of lower quantities of the contrast agent and improves localization with respect to soft tissue target organs. After intra-arterial infusion of microspheres, clustering and accumulation of the microspheres within the tissue can occur, which may lead to saturation of the MR signal, especially when using high-field MRI and microspheres with a high magnetic susceptibility. Therefore, alginate microspheres with a low susceptibility may be more suitable for the quantification of higher microsphere concentrations. Alginate, the main component of these microspheres, is a biocompatible hydrophilic polysaccharide consisting of alternating (1,4)-linked β-D-mannuronic (M) acid and α-L-guluronic acid (G) units and can interact with different cations, resulting in the formation of a hydrogel [12]. Alginate hydrogels have been widely investigated in the biomedical research field and have subsequently been successfully employed as matrix devices for the loading and release of drugs [13-17] and growth factors [18-21], as well as for the entrapment of cells [22-25]. The development of different microsized spherical particles which have the potential to be used, for instance, as drug carriers and additionally can be visualized with MRI will offer a great improvement in minimally invasive transcatheter embolization therapy. In this comparative study, different lanthanides were investigated for their ability to form alginate-based MRI-detectable

microspheres, exploiting the paramagnetic behavior of the lanthanides [26-28]. All microsphere formulations were characterized with light microscopy, scanning electron microscopy (SEM) and complexometric cation content analysis. Extensive qualitative and quantitative MRI assessment of the microsphere formulations was of particular interest. Furthermore, *ex vivo* embolization studies with rabbit and porcine liver were performed and the possibility of 'single sphere detection' was explored, which would allow detailed microsphere biodistribution examination.

MATERIALS AND METHODS

MATERIALS

All chemicals and polymers were from commercial sources and were used as obtained. Sodium alginate (Protanal LF 240 D, Ph. Eur.) was a generous gift from FMC Biopolymer Ltd. (Girvan, Ayrshire, UK). Calcium(II) chloride dihydrate (≥99.0%), ferric(III) chloride hexahydrate (≥98%), gadolinium(III) chloride hexahydrate (99%), dysprosium(III) chloride hexahydrate (99.9%), Eriochrome Black T (ACS reagent), 1,10-phenanthroline (≥99%), ammonium iron(II) sulphate hexahydrate (Mohr's salt, ACS reagent; 99%) and sodium chloride (ACS reagent, ≥99.8%) were obtained from Sigma Aldrich (Steinheim, Germany). Holmium(III) chloride hexahydrate (99.9%), ytterbium(III) chloride hexahydrate (99.9%), thulium(III) chloride hexahydrate (99.9%), europium(III) chloride hexahydrate (99.9%) and terbium(III) chloride hexahydrate (99.9%) were purchased from Metall rare earth Ltd. (Shenzhen, China). Agarose MP was obtained from Roche Applied Science (Mannheim, Germany). Nitric acid (65%), potassium nitrate (99.9%), ethylene dinitrilotetraacetic acid (EDTA; >99.0%), xylenolorange (Ph. Eur. 99.9%), hydroxylamine hydrochloride (≥96%) and manganese(II) chloride tetrahydrate (ACS reagent) were obtained from Merck (Darmstadt, Germany). Sodium hydroxide (99.9%) was purchased from Riedel-de Haën (Seelze, Germany), Magnesium(II) chloride hexahydrate was obtained from Boom Lab (Meppel, the Netherlands).

ALGINATE MICROSPHERE PREPARATION

An important advantage of alginate gels is their ease of preparation, allowing the formation of gels with different shapes and sizes [29]. The JetCutter technique allows for the preparation of monodisperse alginate microspheres (ams) (Fig. 1), as previously described by Prusse *et al.* [30], resulting in the preparation of spherical particles with a predetermined size which can be utilized as embolization agents [10, 31, 32]. The JetCutter uses a mechanical cutting step in combination with a jet of fluid, which is pressed through a nozzle with a small diameter to create identical cylindrical segments that will become spherical due to the surface tension of the fluid [10]. In order to produce ams with the JetCutter, sodium alginate was dissolved in demineralized water under magnetic stirring at a concentration of 2% (w/v). Subsequently, the alginate solution was processed with the JetCutter using a nozzle diameter of 120 μm and a rotor speed set to 5000 rpm. The JetCutter was equipped with a cutting tool consisting of 120 wires with a diameter of 100 μm. An alginate flow rate of 0.12 mL s^{-1} was used to prepare microspheres with a target size of around 250 μm. The droplets were collected into various solutions containing 25 mM concentrations of the

chloride salts of alkaline earth metals ($CaCl_2$), transition metals ($FeCl_3$) or lanthanides ($HoCl_3$, $GdCl_3$, $DyCl_3$, $YbCl_3$, $TmCl_3$, $EuCl_3$ and $TbCl_3$). Ca^{2+}- and Fe^{3+}-ams were used as control formulations, as Ca^{2+} is often used for alginate hydrogel formation [29] and Fe^{3+} is frequently used in non-lanthanide-based MRI contrast agents [33, 34]. All droplets were allowed to crosslink for 2 h under gentle magnetic stirring. After three washing steps with demineralized water to remove excess cations, the microspheres were collected and stored in demineralized water at room temperature. In order to determine the influence of the crosslinking time and crosslinking solution concentration on cation content, the ams were also allowed to crosslink for 2 up to 24 h or to crosslink in a 100 mM crosslinking solution.

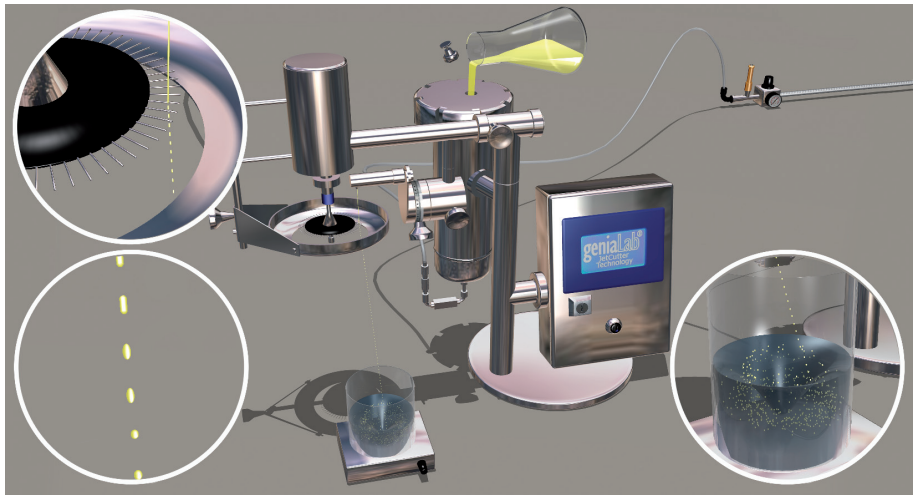

Fig. 1. The JetCutter system used in this study to prepare monodisperse ams with different crosslinking agents. The cutting disk cuts the alginate jet stream into small cylinders (top left). The cylinders become spherical when falling down (bottom left). When the droplets come into contact with the crosslinking solution, microspheres are formed (bottom right).

LIGHT MICROSCOPY

Morphological examination of the formed ams was performed using light microscopy (magnification 10 x 10). To calculate the mean size, the diameters of 25 randomly selected microspheres were determined. Size distribution was calculated as the coefficient of variation (C.V.), which is defined as the ratio between the standard deviation and the mean. A C.V. of less than 5% is the commonly accepted definition of monodispersity [35].

SCANNING ELECTRON MICROSCOPY

For SEM analysis of the surface morphology of the different ams, they were subjected to critical point drying, which allows the examination of the microspheres under vacuum. Therefore, freshly prepared microspheres were centrifuged at 3000 rpm for 2 min and subsequently subjected to dehydration steps for 5 min each in an increasing series of ethanol (30%, 50%, 70%, 80%, 90%, 96% and 100%). Next,

ethanol was replaced by acetone in three consecutive steps (50%, 67% and 100%). The microspheres were then transferred into a beaker glass filled with 100% acetone and microporous specimen capsules (Sigma Aldrich, Steinheim, Germany), equipped with filter paper and subsequently the microspheres were dried using a critical point dryer (Baltec corporation, Canonsburg, PA, USA). Then, the samples were mounted on an aluminum stub and coated with a 6 nm layer of platinum. SEM micrographs were obtained using an FEI FEG-SEM XL30 microscope (FEI Company, Eindhoven, the Netherlands) at a voltage of 5 kV.

COMPLEXOMETRIC CATION CONTENT ANALYSIS

To determine the cation content of the ams, different complexometric analyses were performed. For the lanthanide-ams, a complexometric titration was performed as previously described by Zielhuis *et al.* [10] with minor modifications. Briefly, 250 mg of ams was collected by filtration of the ams through a 20 μm sieve to remove the excess water. Next, the ams were broken down in 10 mL of nitric acid (65%) at 100 °C for 30 min. Hexamethylenetetramine (5 g) and xylenol-orange (50 mg, 1:100 mixture in potassium nitrate) were added and the resulting solution was brought to pH 5 using 10 MNaOH. The solution was titrated with 10 mM EDTA until a color change from pink to yellow was observed. For Ca^{2+}-ams, after the destruction of the microspheres the pH was brought to 10 and Eriochrome Black T indicator (1:10 mixture in NaCl) was added to the sample. $MgCl_2$ (1 mM) was added as an indicator blank. The resulting solution was titrated until a color change from red to blue was observed. All titrations were performed in triplicate. For Fe^{3+}-ams, the 1,10-phenanthroline colorimetric method described by Talelli *et al.* [36] was used. Briefly, an excess of hydroxylamine hydrochloride solution (100 mg mL^{-1} in ammonium acetate buffer, pH 4) was added to reduce Fe^{3+} to Fe^{2+}, followed by the addition of 1,10 phenanthroline (6 mg mL^{-1} in ammonium acetate buffer, pH 4) to form an orange-red complex of tris(1,10-phenanthroline) iron(II). The absorbance of the samples was measured at 910 nm using an ultraviolet-visible spectrophotometer (Shimadzu UV/VIS 2450 spectrophotometer, Shimadzu Suzhou Instruments, Kyoto, Japan). The concentration of iron(II) was calculated using a calibration curve obtained using Mohr's salt solution in HCl 0.01 N in a concentration range of 0-10 μg mL^{-1}. All measurements were performed in triplicate.

EX VIVO EMBOLIZATION PROCEDURE WITH HO^{3+}-AMS

Rabbit and porcine liver were used for an *ex vivo* embolization procedure to mimic potential *in vivo* imaging applications. Therefore, the organs were flushed with heparin solution to prevent coagulation of blood in the tissue and subsequently with a solution of 0.16 mM $MnCl_2 \cdot 4H_2O$ in demineralized water to reduce the longitudinal relaxation rate (T_1) of the water and to mimic the relaxation properties of tissue [37]. Next, a catheter (Abbocath-T I.V. Catheter 20 g x 1.25'', Hospira Inc., Lake Forest, IL, USA) was introduced in the hepatic artery of the rabbit liver, while a 4F straight catheter (Merit Medical Europe, Maastricht-Airport, the Netherlands) was introduced in the hepatic artery in the porcine liver. Next, 50 mg of Ho^{3+}-ams dispersed in 5 mL (rabbit liver) or in 50 mL (porcine liver) of $MnCl_2 \cdot 4H_2O$-doped demineralized water (see above) was administered. Magnetic resonance imaging (MRI) was performed prior to and after administration of the microspheres to determine the biodistribution

of the microspheres in the tissue. Due to the very low $MnCl_2 \cdot 4H_2O$ concentration and the quick transformation of the liquid agarose to a solid gel state, interference with the microspheres by Mn^{2+} is negligible.

MAGNETIC RESONANCE IMAGING

To investigate the sensitivity of MRI for the different microsphere formulations, gel phantoms in glass tubes (length = 93 mm; inner diameter = 11 mm) were prepared with 1% agarose in a solution of 0.16 mM $MnCl_2 \cdot 4H_2O$ in demineralized water. A homogeneously distributed concentration series of ams from 0 to 200 μg mL^{-1} (cation weight) was prepared for each microsphere formulation. MRI was performed using a 1.5 and 3 T clinical MR scanner (Intera, Achieva, respectively, Philips Healthcare, Best, the Netherlands). The sample tubes were positioned parallel to the B_0 field in an eight-element head coil in the MR scanner. The sensitivity of MRI for a particulate agent is determined by the r_2* relaxivity of the agent (in s μg^{-1} mL^{-1}), which represents the change in the effective proton transverse relaxation rate (R_2* in s^{-1}) per unit concentration (in μg mL^{-1}). The R_2* relaxation rate characterizes the rate of mono exponential MR signal decay due to transverse relaxation, according to the formula: $S(t) = S(0) \cdot \exp(-R_2^* \cdot t)$, where S(t) and S(0) are the MRI signal at time t and 0, respectively. To determine the r_2* relaxivity of the ams, the R_2* relaxation rates of the concentration series were measured using a 3-D multiple gradient echo sequence with the following imaging parameters: echo time and spacing = 4.0 ms, 21 echoes, repetition time = 200 ms, field of view (FOV) = 144 × 96 × 22 mm^3, acquired and reconstructed voxel size of 1 × 1 × 2 mm^3, two signal averages and a 60° flip angle. For single sphere detection at 3 T, similar imaging parameters were used, apart from an echo time and spacing of 3.0 ms and an acquired voxel size of 0.5 x 0.5 x 1 mm^3, reconstructed to a voxel size of 0.25 x 0.25 x 0.5 mm^3. Linear regression of the R_2* values as a function of the concentration provides the r_2* relaxivity. The relaxivity r_2* was calculated from transverse images using the method described by Seevinck *et al.* [11]. For MR imaging of *ex vivo* rabbit liver (measured at 3 T), identical MRI parameters were used for the single sphere detection scan as described previously. For porcine liver (measured at 3 T), a 3-D multiple gradient echo sequence was used with an echo time and echo spacing of 4.6 ms (water and fat in-phase), 15 echoes, repetition time of 150 ms, FOV of 224 × 224 × 130 mm^3 with an acquired voxel size of 1 × 1 × 2 mm^3 reconstructed to 0.5 x 0.5 x 2 mm^3 and a 45° flip angle.

RESULTS

LIGHT MICROSCOPY

Table 1 shows the average sizes and C.V. of the ams crosslinked with different cations. Ca^{2+}-ams showed an average size of 281 μm, while the trivalent cation-ams displayed an average size of around 250 μm, which has been demonstrated to be an optimal size for embolization, since microspheres of this size will embolize the tumor or will be in close proximity to the tumor margin [38, 39]. Since the C.V. was < 5%, the different microspheres can be considered monodisperse (Table 1). All preparation parameters were kept identical, hence any size variation between the Ca^{2+}-ams (divalent) and trivalent cation-ams is solely attributable to the nature of the crosslinking agents

(further discussed under 'Complexometric cation content analysis'). Fig. 2 shows representative light microscopy photographs of microsphere formulations crosslinked for 2 h with an alkaline earth metal- (Ca^{2+}), transition metal- (Fe^{3+}) and lanthanide (Ho^{3+}) crosslinking agent, respectively. These pictures demonstrate that the different microsphere formulations are spherical in shape and display a uniform size.

Table 1. Size (mean diameter) and C.V. of the different alginate microsphere formulations.

Crosslinking agent	Size (μm ± C.V.)	Crosslinking agent	Size (μm ± C.V.)
Ca^{2+}	281 ± 3	Dy^{3+}	248 ± 3
Fe^{3+}	249 ± 4	Ho^{3+}	253 ± 1
Eu^{3+}	250 ± 4	Tm^{3+}	252 ± 4
Gd^{3+}	250 ± 2	Yb^{3+}	246 ± 3
Tb^{3+}	248 ± 3		

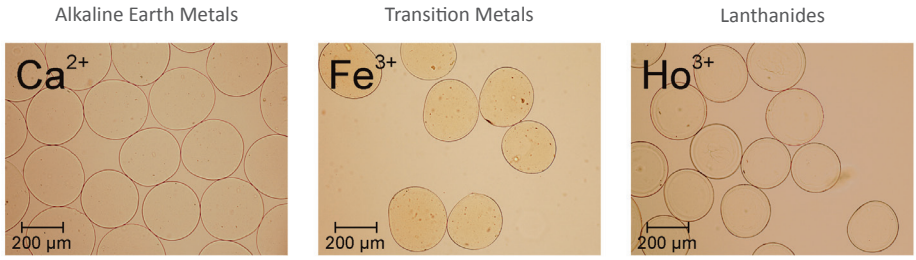

Fig. 2. Light microscopy pictures from representative microsphere formulations comprising alkaline earth metal-, transition metal- and lanthanide-ams magnification 10 x 10).

SCANNING ELECTRON MICROSCOPY (SEM)

Fig. 3a shows SEM images of critical-point dried Ca^{2+}-, Fe^{3+}- and Ho^{3+}-ams. The surface morphology of the ams is shown in Fig. 3b (magnification 35,000x). Ca^{2+}-ams showed a tightened smooth surface, while trivalent cation-ams (transition metals and lanthanides) displayed a much more irregular shaped surface morphology: Fe^{3+}-ams showed wrinkled, 'coralline' surface characteristics, whereas all lanthanide-ams showed a 'knitting pattern' structure. The morphological differences between divalent- and trivalent cation-ams can be explained by the geometrical structures for chelation between the functional groups and the inter-diffused cations; a planar geometry for the divalent cation-crosslinked alginates, and a non-planar geometrical structure for trivalent cation-crosslinked alginates [40, 41], resulting in a smooth or more irregular shaped surface, respectively.

COMPLEXOMETRIC CATION CONTENT ANALYSIS

Fig. 4a shows the cation content (w/w) of the different microsphere formulations which varied from 0.33% (Ca^{2+}) up to 0.94% (Yb^{3+}). Cesaro *et al.* reported that the

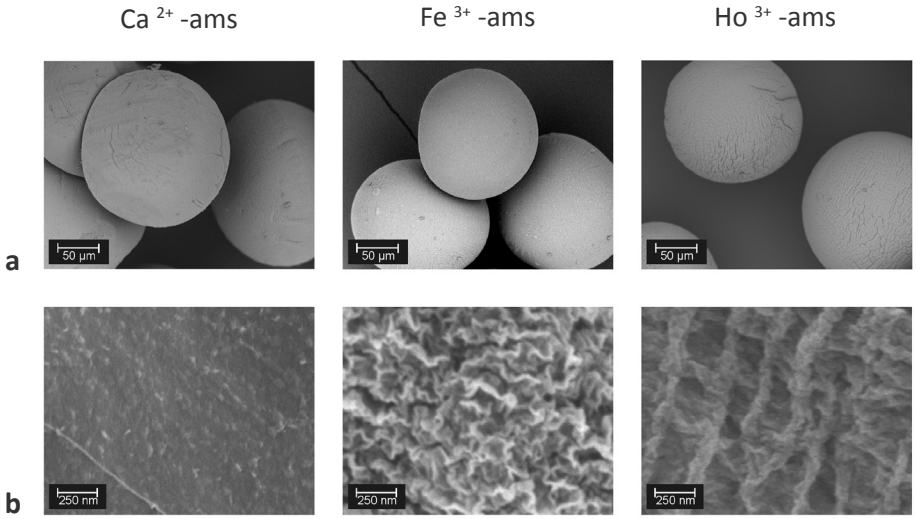

Fig. 3. SEM images of critical-point-dried ams (a). Note that the microsphere size is reduced in some extent, which is due to critical point drying, resulting in the loss of water. Surface morphology of ams (b).

strength of cation crosslinking of the alginate chains is related to release of structured water that hydrates both the ion and the uronic moieties [42]. The stronger the interactions between cations and uronic moieties, the more water is released. For the divalent Ca^{2+}-ams, this may explain the somewhat larger size (281 µm) compared to the microspheres crosslinked with the different trivalent cations (all around 250 µm). Longer crosslinking times (up to 24 h) or a higher cation concentration in the crosslinking solution (up to 4x higher) did not result in significantly higher cation concentrations within the microspheres (data not shown). This can be explained by the cation - monomer (G or M) unit ratio (Fig. 4b), indicating that all binding sites for lanthanides were filled (ratio 1:2). Zaafarany *et al.* stated that lanthanide ions are restricted to crosslinking via only intermolecular association in their alginate complexes for geometrical reasons [41], which may explain the ratio of one lanthanide cation per two monomer units, which is half the ratio as compared to Ca^{2+} and Fe^{3+} - monomer ratio. This 1:1 ratio for Ca^{2+} and Fe^{3+} cations is likely caused by a difference in valence (divalent for Ca^{2+} cations versus trivalent for lanthanides) and ionic radius, which is much smaller for Fe^{3+} as compared to lanthanides [43]. Lanthanides contain a much larger ionic radius, therefore a ratio of one lanthanide cation per two monomer units was observed. Due to the relatively low lanthanide concentrations within the microspheres, toxicity of the microspheres is expected to be low. For example, administration of 1 g of microspheres (a regular amount for embolization) to a 50 kg patient, would result in a total lanthanide concentration of around 0.001 mmol kg^{-1}, which is in the same order as FDA-approved Gd-chelates for MR imaging where concentrations of around 0.1 mmol kg^{-1} are administered and a dissociation up to 1% of the total administered dose is observed [44].

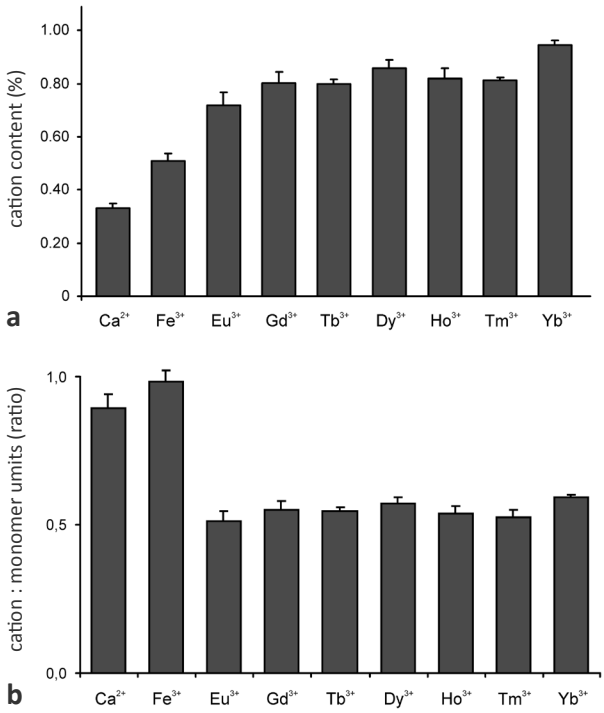

Fig. 4. Cation content (% w/w) of ams (a). Ratio of cation versus monomer units (mol mol^{-1}) (b). Values are provided as mean + SD, n = 3.

MAGNETIC RESONANCE IMAGING

The increase of the effective transverse relaxation rate (R_2*) as a function of cation concentration was measured for each alginate microsphere formulation using an ROI analysis. Linear calibration curves were found for measurements at 1.5 as well as at 3 T ($R^2 > 0.95$ for each formulation). Fig. 5 shows the R_2* for the 0 to 400 μg mL^{-1} Ho^{3+}-ams concentration series measured at 3 T. The standard deviation (SD) clearly increases with cation content, which is to be expected. Furthermore, saturation of R_2* occurs for concentrations higher than 200 μg mL^{-1}. Knowing the size of the acquired voxel volumes (1 x 1 x 2 mm = 2 μL), the size and volume of the analyzed ROI (111 voxels, 0.222 mL) and the average diameter of the microspheres (250 μm), it can be calculated that for cation concentrations of 2, 5, 10, 20, 50, 100, 200 μg mL^{-1}, each voxel

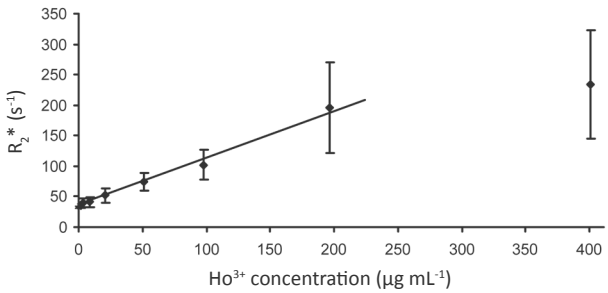

Fig. 5. R_2* relaxation rate (s^{-1}) versus Ho^{3+} concentration of ams measured at 3 T. The solid line is a least squares fit to the data points which are given as mean ± SD in the ROI of 111 voxels. The slope represents the relaxivity (r_2*).

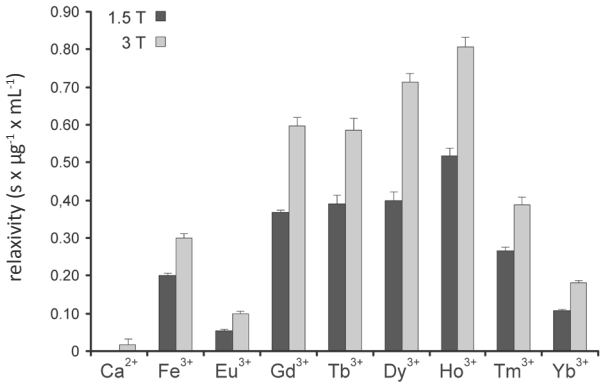

Fig. 6. Relaxivity (r_2*) of the different alginate microsphere formulations at 1.5 and 3 T. Values are provided as mean + SD, n=3.

on average contains 0.06, 0.15, 0.30, 0.59, 1.49, 2.47 and 5.95 microspheres, and each ROI approximately 7, 17, 33, 66, 165, 330 and 660 microspheres, respectively. At low concentrations, that means that most voxels by far do not contain any microspheres, leaving the SD unaffected as compared to the bare medium. When increasing the concentration, more and more voxels will contain one or more microspheres, which is determined by randomness, increasing the signal variation over the entire ROI and as result the SD of the mean R_2^* value. Fig. 6 shows the relaxivity (r_2*) of the different microsphere formulations at both 1.5 T and 3 T. At 3 T, the relaxivity was higher as compared to 1.5 T, as was expected since in a higher magnetic field the paramagnetic microspheres induce stronger magnetic field distortions. No MR signal decay enhancement was observed with Ca^{2+}-ams, which was expected regarding its non-paramagnetic nature. From Fig. 6, it can be concluded that the lanthanide-ams, and especially Ho^{3+}-ams are most potent as MR contrast agents, followed by Dy^{3+}, Gd^{3+} and Tb^{3+}, which can be explained by their paramagnetic behavior. The differences in relaxivity between the alginate-lanthanide microsphere formulations can be explained by the differences in susceptibility between the lanthanides. Ho^{3+}-ams showed the highest relaxivity at both 1.5 and 3 T and were therefore used for further assessment with MRI. In Fig. 7, the fourth echo of the multi-gradient echo series (echo time 12 ms) of the Ho^{3+}-ams concentration series is shown. The expected number of microspheres in a single slice of the 2, 5, 10 and 20 µg mL^{-1} Ho^{3+} concentration series was calculated, taking into account tube diameter and slice thickness, providing theoretical microsphere quantities of 2.3, 5.8, 11.7 and 23.4, respectively. These estimations resemble an equivalent number of microspheres as compared to the black

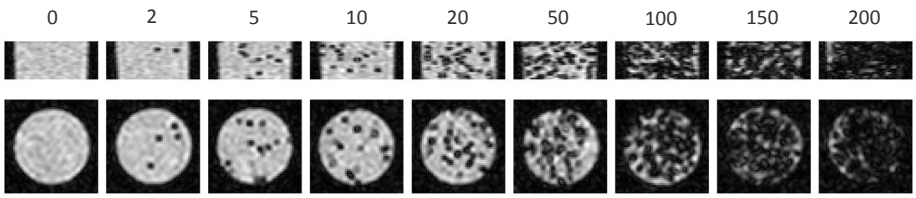

Fig. 7. Detection of Ho^{3+}-ams in a phantom concentration series (cation concentration in µg mL^{-1}) by high resolution T_2^*-weighted 3-D gradient echo MR imaging, measured at 3 T. Sagittal plane (above) and transversal plane (below). Individual microspheres can be clearly detected at Ho^{3+} concentrations up to 20 µg mL^{-1}.

spots detected on the high resolution MR images of the phantom setup in Fig. 7, confirming the possibility to visualize individual microspheres at low concentrations up to 20 μg mL^{-1} in a clinical setup. At higher microsphere concentrations (above 20 μg mL^{-1}), MR signal decay enhancement was widely distributed throughout the phantom and, therefore, the microspheres cannot be distinguished individually anymore with the used imaging parameters.

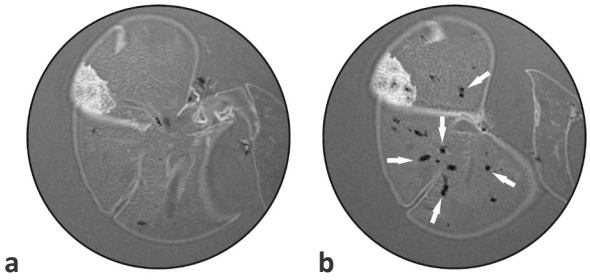

Fig. 8. T_2^*-weighted gradient echo MR images of rabbit liver tissue before (a) and after (b) intravascular infusion of microspheres in the hepatic artery, measured at 3 T. The white arrows indicate signal voids which represent clusters of microspheres.

Fig. 8 shows an MR image of *ex vivo* rabbit liver before and after microsphere administration. The Ho^{3+}-ams were heterogeneously distributed as a result of the administration method (intravascular infusion), leading to accumulation of microspheres and subsequently embolization of the targeted vessels. The larger signal voids consisting of overlapping signal losses at several positions, which were not present in the images prior to administration, are expected to be clusters of microspheres (white arrows). As a result, quantification based on single sphere detection, as observed in Fig. 7 at concentrations ≤ 20 μg mL^{-1}, will not be possible in situations with clustered microspheres. However, *in vivo* quantification of the

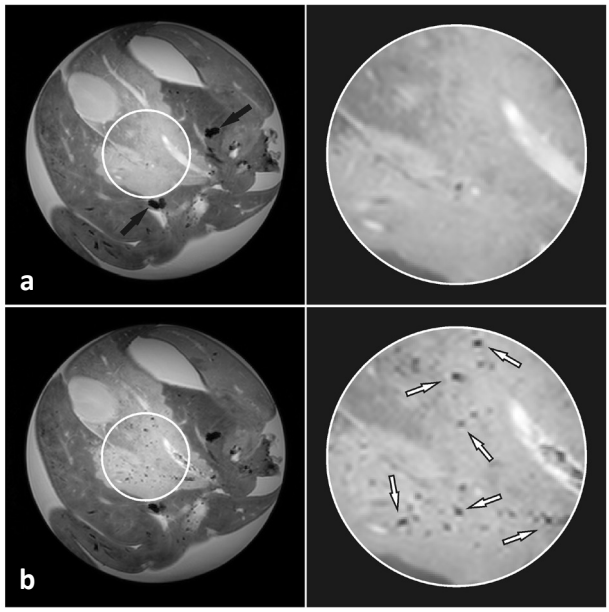

Fig. 9. T_2^*-weighted gradient echo MR images of porcine liver tissue before (a) and after (b) the administration of Ho^{3+}-ams introduced via selective lobular catheterization, measured at 3 T (white arrows show some examples of Ho^{3+}-ams). The larger spots showing signal decay (already visible before microsphere administration) are likely caused by the presence of blood clots or air bubbles within the tissue (black arrows). Images on the right are excerpt from (a) and (b) with a magnification of 3x.

administered microsphere dose in a specific ROI may well be possible when based on R_2* relaxation rate changes rather than single sphere measurements, analogous to the ROI analysis performed to construct the calibration curves. Clinically, it is desirable to reduce scan times as much as possible which, however, also results in lower image resolution and will therefore further complicate single sphere detection *in vivo*. Nonetheless, when MRI-guided embolotherapy becomes clinical practice, monitoring of the administration procedure along with the assessment of the resulting biodistribution of the microspheres will be of primary importance. MR images of *ex vivo* porcine liver before and after intravascular microsphere infusion taken at a lower, clinically more realistic resolution, are presented in Fig. 9. Although image resolution is too low to discriminate single spheres, the MR signal decay at several positions within the tissue after microsphere administration is clearly enhanced. This lead to reduced signal intensities and allowed for accurate monitoring of the microsphere distribution throughout the tissue, which opens a wide range of innovative and dedicated clinical applications in embolotherapy.

CONCLUSION

In this study, the preparation and characterization of different monodisperse alginate microsphere formulations as well as their feasibility for MRI-guided embolotherapy was demonstrated. Monodisperse ams were prepared with the JetCutter technique using nine different cations. Especially the lanthanide-ams formulations showed promising results for MR imaging and can be detected individually at low, non-clustered homogeneously distributed concentrations, as demonstrated for Ho^{3+}-ams, allowing detailed microsphere biodistribution examination, despite the low holmium concentration within the microspheres. Due to the relatively low lanthanide concentrations within the microspheres, toxicity of the microspheres is expected to be low, although *in vivo* studies are necessary to validate the toxicity profile and long-term stability. Intravascular infusion of Ho^{3+}-ams by catheterization of *ex vivo* tissue and assessment of the procedure with MRI showed that accumulation and subsequently embolization of the targeted vessels with Ho^{3+}-ams was clearly observed, allowing accurate monitoring of the microsphere biodistribution throughout the tissue. After intra-arterial infusion of microspheres, clustering and accumulation of the microspheres within the tissue can be expected, which may lead to saturation of their effect on the T_2*-weighted MR signal, complicating the assessment of the amount of microspheres administered based on local R_2* values. This phenomenon is more prominent with contrast agents with a higher susceptibility and, furthermore, will increase with higher field strength (Fig. 5). The different alginate-lanthanide microsphere formulations as developed in this study allow the selection of the most suitable microsphere formulation for the specific clinical task and magnetic field strength. These newly developed alginate-lanthanide microsphere formulations offer specific real-time feedback of the clinical procedure and therefore show great potential for utilization as image-guided embolotherapy agents.

ACKNOWLEDGEMENTS

The authors thank Chris Schneijdenberg en Wally Mϋller, BioMolecular Imaging, Faculty of Science, Utrecht University, the Netherlands, for their help with the SEM, Ulrich Jahnz, GeniaLab® Biotechnologie, Braunschweig, Germany, for the JetCutter system, FMC Biopolymers and in particular Frederike Huissoon, IMCD Benelux B.V., for their generous gift of Protanal LF 240D.

REFERENCES

1. Varde NK, Pack DW. Microspheres for controlled release drug delivery. Expert Opin Biol Ther. 2004;4:35-51.
2. Peer D, Karp JM, Hong S, Farokhzad OC, Margalit R, Langer R. Nanocarriers as an emerging platform for cancer therapy. Nat Nanotechnol. 2007;2:751-60.
3. Spies JB, Allison S, Flick P, McCullough M, Sterbis K, Cramp M, Bruno J, Jha R. Polyvinyl alcohol particles and tris-acryl gelatin microspheres for uterine artery embolization for leiomyomas: results of a randomized comparative study. J Vasc Interv Radiol. 2004;15:793-800.
4. Ginat DT, Saad WE, Turba UC. Transcatheter renal artery embolization: clinical applications and techniques. Tech Vasc Interv Radiol. 2009;12:224-39.
5. Lammer J, Malagari K, Vogl T, Pilleul F, Denys A, Watkinson A, Pitton M, Sergent G, Pfammatter T, Terraz S, Benhamou Y, Avajon Y, Gruenberger T, Pomoni M, Langenberger H, Schuchmann M, Dumortier J, Mueller C, Chevallier P, Lencioni R. Prospective randomized study of doxorubicin-eluting-bead embolization in the treatment of hepatocellular carcinoma: results of the PRECISION V study. Cardiovasc Intervent Radiol. 2010;33:41-52.
6. Pawlik TM, Reyes DK, Cosgrove D, Kamel IR, Bhagat N, Geschwind JF. Phase II trial of sorafenib combined with concurrent transarterial chemoembolization with drug-eluting beads for hepatocellular carcinoma. J Clin Oncol. 2011;29:3960-7.
7. Lewis AL, Dreher MR. Locoregional drug delivery using image-guided intra-arterial drug eluting bead therapy. J Control Release. 2012;161;338-50.
8. Dreher MR, Sharma KV, Woods DL, Reddy G, Tang Y, Pritchard WF, Chiesa OA, Karanian JW, Esparza JA, Donahue, Levy EB, Willis SL, Lewis AL, Wood BJ. Radiopaque drug-eluting beads for transcatheter embolotherapy: experimental study of drug penetration and coverage in Swine. J Vasc Interv Radiol. 2012;23:257-64.
9. Sharma KV, Dreher MR, Tang Y, Pritchard W, Chiesa OA, Karanian J, Peregoy J, Orandi B, Woods D, Donahue D, Esparza J, Jones G, Willis SL, Lewis AL, Wood BJ. Development of 'imageable' beads for transcatheter embolotherapy. J Vasc Interv Radiol. 2010;21:865-76.
10. Zielhuis SW, Seppenwoolde JH, Bakker CJ, Jahnz U, Zonnenberg BA, van het Schip AD, Hennink WE, Nijsen FJ. Characterization of holmium loaded alginate microspheres for multimodality imaging and therapeutic applications. J Biomed Mater Res A. 2007;82:892-8.
11. Seevinck PR, Seppenwoolde JH, de Wit TC, Nijsen JF, Beekman FJ, van het Schip AD, Bakker CJ. Factors affecting the sensitivity and detection limits of MRI, CT, and SPECT for multimodal diagnostic and therapeutic agents. Anticancer Agents Med Chem. 2007;7:317-34.
12. George M, Abraham TE. Polyionic hydrocolloids for the intestinal delivery of protein drugs: alginate and chitosan-a review. J Control Release. 2006;114:1-14.
13. Sugawara S, Imai T, Otagiri M. The controlled release of prednisolone using alginate gel. Pharm Res. 1994;11:272-7.
14. Pasparakis G, Bouropoulos N. Swelling studies and *in vitro* release of verapamil from calcium alginate and calcium alginate-chitosan beads. Int J Pharm. 2006;323:34-42.
15. Misirli Y, Ozturk E, Kursaklioglu H, Denkbas EB. Preparation and characterization of Mitomycin-C loaded chitosan-coated alginate microspheres for chemoembolization. J Microencapsul. 2005;22:167-78.
16. Takka S, Acarturk F. Calcium alginate microparticles for oral administration: I: Effect of sodium alginate type on drug release and drug entrapment efficiency. J Microencapsul. 1999;16:275-90.
17. Acarturk F, Takka S. Calcium alginate microparticles for oral administration: II. Effect of formulation factors on drug release and drug entrapment efficiency. J Microencapsul. 1999;16:291-301.

18. Mumper RJ, Hoffman AS, Puolakkainen PA, Bouchard LS, Gombotz WR. Calcium-Alginate Beads for the Oral Delivery of Transforming Growth Factor-Beta(1) (Tgf-Beta(1)) - Stabilization of Tgf-Beta(1) by the Addition of Polyacrylic-Acid Within Acid-Treated Beads. J Control Release. 1994;30:241-51.
19. Gu F, Amsden B, Neufeld R. Sustained delivery of vascular endothelial growth factor with alginate beads. J Control Release. 2004;96:463-72.
20. Huwer H, Winning J, Vollmar B, Rissland J, Welter C, Schafers HJ, Menger MD. Microvascularization and ventricular function after local alginate-encapsulated angiogenic growth factor treatment in a rat cryothermia-induced myocardial infarction model. Microvasc Res. 2001;62:211-4.
21. Hao X, Silva EA, Mansson-Broberg A, Grinnemo KH, Siddiqui AJ, Dellgren G, Wärdell E, Brodin LA, Mooney DJ, Sylvén C. Angiogenic effects of sequential release of VEGF-A165 and PDGF-BB with alginate hydrogels after myocardial infarction. Cardiovasc Res. 2007;75:178-85.
22. Schwinger C, Koch S, Jahnz U, Wittlich P, Rainov NG, Kressler J. High throughput encapsulation of murine fibroblasts in alginate using the JetCutter technology. J Microencapsul. 2002;19:273-80.
23. Maguire T, Novik E, Schloss R, Yarmush M. Alginate-PLL microencapsulation: effect on the differentiation of embryonic stem cells into hepatocytes. Biotechnol Bioeng. 2006;93:581-91.
24. Moustafa T, Girod S, Tortosa F, Li R, Sol JC, Rodriguez F, Bastide R, Lazorthes Y, Sallerin B. Viability and functionality of bovine chromaffin cells encapsulated into alginate-PLL microcapsules with a liquefied inner core. Cell Transplant. 2006;15:121-33.
25. Hwang YS, Cho J, Tay F, Heng JY, Ho R, Kazarian SG, Williams DR, Boccaccini AR, Polak JM, Mantalaris A. The use of murine embryonic stem cells, alginate encapsulation, and rotary microgravity bioreactor in bone tissue engineering. Biomaterials. 2009;30:499-507.
26. Aime S, Castelli DD, Crich SG, Gianolio E, Terreno E. Pushing the sensitivity envelope of lanthanide-based magnetic resonance imaging (MRI) contrast agents for molecular imaging applications. Acc Chem Res. 2009;42:822-31.
27. Norek M, Peters JA. MRI contrast agents based on dysprosium or holmium. Prog Nucl Magn Reson Spectrosc. 2011;59:64-82.
28. Bottrill M, Kwok L, Long NJ. Lanthanides in magnetic resonance imaging. Chem Soc Rev. 2006;35:557-71.
29. Matricardi P, Meo CD, Coviello T, Alhaique F. Recent advances and perspectives on coated alginate microspheres for modified drug delivery. Expert Opin Drug Deliv. 2008;5:417-25.
30. Prusse U, Dalluhn J, Breford J, Vorlop KD. Production of spherical beads by JetCutting. Chemical Engineering & Technology. 2000;23:1105-10.
31. Becker TA, Kipke DR, Brandon T. Calcium alginate gel: a biocompatible and mechanically stable polymer for endovascular embolization. J Biomed Mater Res. 2001;54:76-86.
32. Becker TA, Kipke DR. Flow properties of liquid calcium alginate polymer injected through medical microcatheters for endovascular embolization. J Biomed Mater Res. 2002;61:533-40.
33. Nakamura H, Ito N, Kotake F, Mizokami Y, Matsuoka T. Tumor-detecting capacity and clinical usefulness of SPIO-MRI in patients with hepatocellular carcinoma. J Gastroenterol. 2000;35:849-55.
34. Long CM, van Laarhoven HW, Bulte JW, Levitsky HI. Magnetovaccination as a novel method to assess and quantify dendritic cell tumor antigen capture and delivery to lymph nodes. Cancer Res. 2009;69:3180-7.
35. Takeuchi S, Garstecki P, Weibel DB, Whitesides GM. An axisymmetric flow-focusing microfluidic device. Advanced Materials. 2005;17:1067-72.
36. Talelli M, Rijcken CJ, Lammers T, Seevinck PR, Storm G, van Nostrum CF, Hennink WE. Superparamagnetic iron oxide nanoparticles encapsulated in biodegradable thermosensitive polymeric micelles: toward a targeted nanomedicine suitable for image-guided drug delivery. Langmuir. 2009;25:2060-7.

37. Seppenwoolde JH, Nijsen JF, Bartels LW, Zielhuis SW, van het Schip AD, Bakker CJ. Internal radiation therapy of liver tumors: qualitative and quantitative magnetic resonance imaging of the biodistribution of holmium-loaded microspheres in animal models. Magn Reson Med. 2005;53:76-84.
38. Lee KH, Liapi E, Vossen JA, Buijs M, Ventura VP, Georgiades C, Hong K, Kamel I, Torbenson MS, Geschwind JF. Distribution of iron oxide-containing Embosphere particles after transcatheter arterial embolization in an animal model of liver cancer: evaluation with MR imaging and implication for therapy. J Vasc Interv Radiol. 2008;19:1490-6.
39. Lencioni R, de BT, Burrel M, Caridi JG, Lammer J, Malagari K, Martin RC, O'Grady E, Real MI, Vogl TJ, Watkinson A, Geschwind JF. Transcatheter treatment of hepatocellular carcinoma with doxorubicin-loaded DC bead (DEBDOX): technical recommendations. Cardiovasc Intervent Radiol. 2011;35;980-5.
40. Hassan RM. Alginate polyelectrolyte lonotropic gels. XIII geometrical aspects for chelation in metal alginate complexes related to their physico-chemical properties. Polymer International. 1993;31:81-6.
41. Zaafarany I, Khairou K, Hassan R. Physicochemical studies on some crosslinked trivalent metal-alginate complexes especially the electrical conductivity and chemical equilibrium related to the coordination geometry. High Performance Polymers. 2010;22:69-81.
42. Cesaro A, Delben F, Paoletti S. Interaction of divalent-cations with polyuronates. Journal of the Chemical Society-Faraday Transactions I. 1988;84:2573-84.
43. DeRamos CM, Irwin AE, Nauss JL, Stout BE. ^{13}C NMR and molecular modeling studies of alginic acid binding with alkaline earth and lanthanide metal ions. Inorganica Chimica Acta. 1997;256:69-75.
44. Wedeking P, Kumar K, Tweedle MF. Dissociation of gadolinium chelates in mice: relationship to chemical characteristics. Magn Reson Imaging. 1992;10:641-8.

Chapter 6

Chris Oerlemans
Peter Seevinck
Maarten Smits
Chris Bakker
Wim Hennink
Frank Nijsen

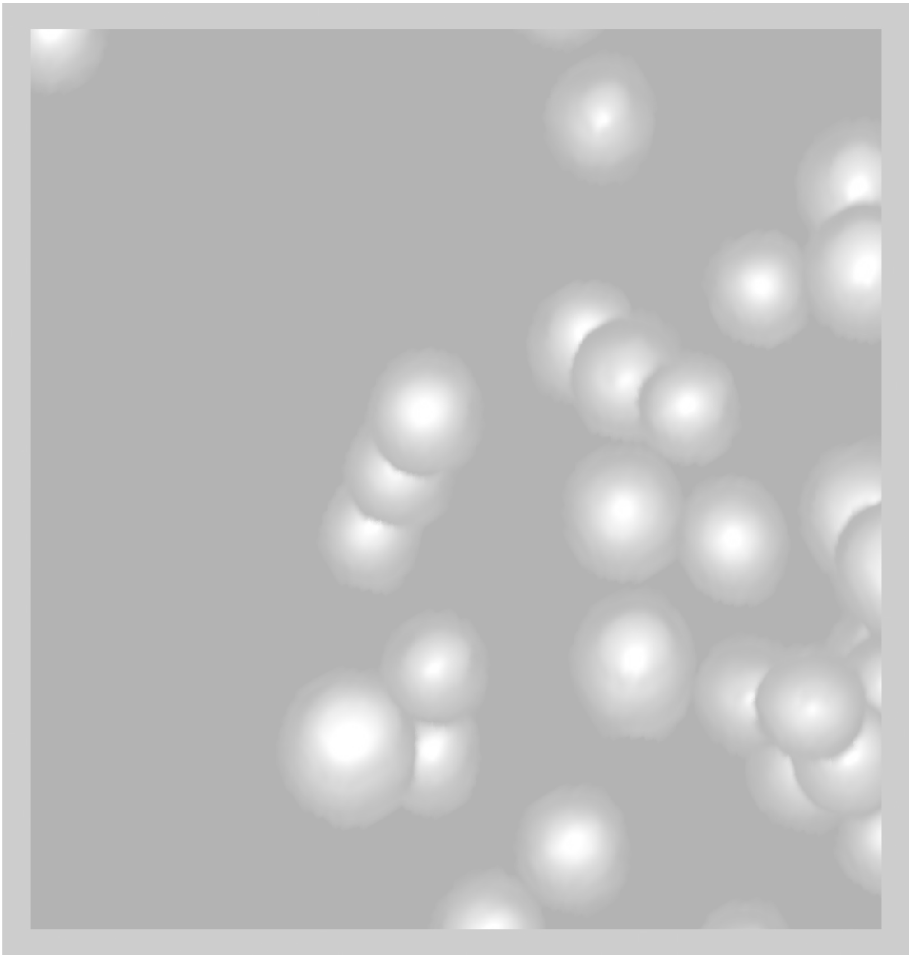

Microspheres for fluoroscopy-guided embolotherapy and multimodality imaging

Submitted

ABSTRACT

Embolotherapy is a minimally invasive transcatheter technique aiming at reduction or complete obstruction of the blood flow by infusion of micro-sized particles in order to induce tumor regression. A major drawback of the currently commercially available and clinically used microspheres is that they cannot be detected *in vivo* with medical imaging techniques, impeding intra- and post-procedural feedback. It can be expected that real-time monitoring of microsphere infusion and post-procedural imaging will result in a more safe, efficient and successful treatment. In this study, a novel microsphere formulation has been developed that can be visualized with fluoroscopy, X-ray computed tomography (CT) and magnetic resonance imaging (MRI). The microspheres were prepared with the JetCutter technique and consist of alginate (matrix-forming polymer), holmium (crosslinking- and MRI contrast agent), lipiodol (radiopaque contrast agent) and Pluronic F-68 (surfactant). The mean size (± SEM) of the hydrated holmium-lipiodol alginate microspheres (Ho-lip-ams) was 570 ± 12 μm with a holmium content of 0.38 ± 0.01% (w/w). Stability studies showed that the microspheres remained intact during incubation for two weeks in fetal calf serum (FCS) at 37 °C. The inclusion of lipiodol in the microspheres rendered excellent visualization capabilities for fluoroscopy and CT, whereas the holmium ions, which keep the alginate network together, also allow MR imaging. In this study it was shown that single sphere detection was possible by fluoroscopy, CT and MRI. The Ho-lip-ams were visualized in real-time during infusion in a porcine kidney using fluoroscopy, and post-procedural, the deposition of the microspheres was examined with fluoroscopy, (cone beam rotational) CT and MRI. The different imaging modalities showed similar deposition patterns of the microspheres within the organ. The combination of intra-procedural visualization, multimodality imaging for patient follow-up and the possibility of quantification offers a new and promising method for more safe, efficient and successful embolization treatment.

INTRODUCTION

Embolotherapy, i.e. intra-arterial injection of embolic agents, has gained an important position in the treatment of a wide variety of conditions affecting different organs of the human body, such as uterine fibroids, arteriovenous malformations (AVM), as well as kidney and liver tumors. Embolotherapy is a minimally invasive transcatheter technique aiming at reduction or complete obstruction of the blood flow by infusion of micro-sized particles of a predefined size in order to induce tumor regression. Several bland embolotherapy agents are commercially available and clinically used, ranging from heterodisperse, irregularly shaped, polyvinyl alcohol (PVA) particles [1] to spherically shaped and uniformly sized microspheres such as Embosphere [2-5] (BioSphere Medical, Rockland, USA), Embozene [6-8] (CeloNova BioSciences, San Antonio, USA) and LC beads [9] (Biocompatibles, Farnham, UK). These microspheres with a size range of 40-1300 μm are introduced into the feeding artery of the tissue via fluoroscopy-guided catheterization and result in uniform artery occlusion with a predictable penetration depth [10, 11]. More recently, microspheres that can be loaded with drugs, i.e. drug-eluting beads (DEB) [12] (Biocompatibles, Farnham, UK), which contain doxorubicin (DEBDOX) [13] or irinotecan (DEBIRI) [14] are commercially available for clinical treatment of liver cancer patients. A major drawback of the currently clinically available bland- and chemo-microspheres, however, is that they cannot be visualized *in vivo* with medical imaging techniques. Consequently, microspheres that can be detected with multiple imaging modalities such as fluoroscopy, computed tomography (CT) and magnetic resonance imaging (MRI) are highly needed and open the possibility to perform real-time monitoring during administration, post-treatment biodistribution assessment and dosimetry. X-ray imaging offers the opportunity of real-time monitoring the microsphere infusion with fluoroscopy, providing direct feedback for the interventional radiologist, and subsequent rapid post-procedural assessment with CT. MRI provides relatively high spatial and temporal resolution and superior soft tissue contrast properties as compared to CT [15]. This allows visualization of smaller quantities of the contrast agent and detection of the microspheres relative to the targeted tissue while exposure to non-target tissue of the patient to ionizing radiation is avoided. Therefore, a microsphere formulation that can be simultaneously visualized by X-ray and MRI techniques, is expected to increase both the safety (less non-targeted delivery) and the efficacy (adequate delivery in the target regions) of embolotherapy procedures. The purpose of this study was to develop a multimodal imageable microsphere formulation for embolotherapy and to investigate its multimodality imaging properties in an *in vitro* and *ex vivo* model. Therefore, microspheres were prepared with alginate, lipiodol, which renders X-ray visibility and holmium, a paramagnetic element which renders it an MRI-contrast agent.

MATERIALS AND METHODS

MATERIALS

All chemicals and polymers were of commercial sources and were used as obtained. Sodium alginate (Protanal LF 240 D, Ph. Eur.) was a generous gift from FMC Biopolymer Ltd. (Girvan, Ayrshire, UK). Pluronic F-68 was obtained from Sigma

Aldrich (Steinheim, Germany). Holmium(III) chloride hexahydrate ($HoCl_3 \cdot 6H_2O$; 99.9%) was purchased from Metall rare earth Ltd. (Shenzhen, China). Lipiodol, a radiopaque contrast agent composed of iodinated ethyl esters of fatty acids from poppy seed oil with a total iodine content of 37% (w/w) [16], which is frequently used for transarterial (chemo)embolization procedures (TAE/TACE) [17], was purchased from Guerbet (Lipiodol Ultrafluide, Guerbet, Aulnay-Sous-Bois, France). Agarose multipurpose (MP) was obtained from Roche Applied Science (Mannheim, Germany). Manganese(II) chloride tetrahydrate ($MnCl_2 \cdot 4H_2O$; ACS reagent), nitric acid (65%), ethylene dinitrilotetraacetic acid (EDTA; >99.0%), potassium nitrate (99.9%) and xylenol-orange (Ph. Eur. 99.9%) were obtained from Merck (Darmstadt, Germany). Sodium hydroxide (99.9%) was purchased from Riedel-de Haën (Seelze, Germany).

ALGINATE MICROSPHERE PREPARATION

For the preparation of alginate microspheres, the JetCutter technique was used [18], resulting in spherical particles with a predetermined size. Briefly, sodium alginate was dissolved in demineralized water under magnetic stirring at a concentration of 2% (w/v). Subsequently, lipiodol or poppy seed oil was added to the alginate solution under vigorous stirring to prepare a 1:1 alginate : oil (w/w) emulsion. 1% (w/v) Pluronic F-68 was added as a surfactant to stabilize the emulsion. Next, the alginate-oil emulsion was processed with the JetCutter which was equipped with a cutting tool consisting of 40 wires with a diameter of 100 µm. A nozzle diameter of 250 µm was used and the rotor speed was set to 4000 rpm. The droplets were hardened into solutions containing 25 mM of the chloride salt of holmium to form holmium-lipiodol alginate microspheres (Ho-lip-ams) and holmium-poppy seed oil alginate microspheres (Ho-pso-ams). The preparation of Ho-lip-ams is illustrated in Fig. 1. Non-ethiodized poppy seed oil was used as control. The alginate microspheres were allowed to crosslink for 2 h under gentle magnetic stirring. After three washing steps

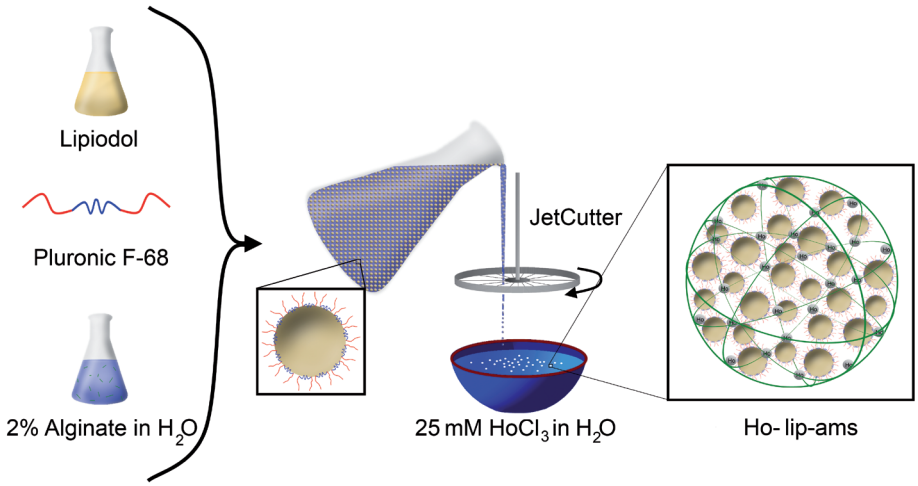

Fig. 1. Schematic drawing of Ho-lip-ams preparation. Lipiodol and water for injection are emulsified with Pluronic F-68. Next, the emulsion is processed with the JetCutter. The formed droplets fall into the holmium chloride solution resulting in the formation of Ho-crosslinked alginate microspheres entrapping lipiodol emulsified droplets (Ho-lip-ams).

with demineralized water to remove excess cations, the microspheres were collected and stored in demineralized water at room temperature.

MICROSPHERE CHARACTERIZATION

Morphological examination and size distribution of Ho-pso-ams and Ho-lip-ams were investigated with light microscopy (magnification 4 x 10). To calculate the average size and its distribution, the diameters of 100 randomly selected microspheres were determined. For the determination of the total holmium content of the Ho-lip-ams, 500 mg of Ho-lip-ams was collected by filtration using a 20 μm sieve to remove excess water. Next, the microspheres were destroyed in 10 mL of nitric acid (65%) at 100 °C for 30 min. All samples were diluted in 2% nitric acid and measured on a Varian 820 MS (Varian, the Netherlands) with a detection limit of 0.1 ng mL^{-1} holmium using standard holmium reference material (CertiPUR Holmium ICP Standard, traceable to SRM from NIST, Merck, Darmstadt, Germany). To investigate the stability of Ho-lip-ams, microsphere samples (400 mg) were incubated in test tubes containing 10 mL fetal calf serum (FCS) and 5% penicillin/streptomycin to prevent bacterial and fungal growth. The test tubes were continuously shaken at 37 °C for 14 consecutive days. After 4 h and every 24 h, the test tubes were centrifuged, and 1 mL of the supernatant was collected for microscopic examination and holmium content determination with inductively coupled plasma mass spectrometry (ICP-MS) analysis. The measurements were performed in duplicate.

IN VITRO PHANTOMS CONTAINING ALGINATE MICROSPHERES

For *in vitro* imaging of the Ho-pso-ams and Ho-lip-ams, a concentration series was prepared. The microspheres were embedded in agarose gel phantoms (1% w/w) containing 0.16 mM $MnCl_2$ to mimic the MRI relaxation properties of tissue as described previously [19]. The microsphere concentration in the sample tubes ranged from 0 to 196 mg mL^{-1}.

INTRA-ARTERIAL HO-LIP-AMS INFUSION IN A PORCINE KIDNEY

A porcine kidney from a 30 kg weighing female pig that was previously used as laboratory animal, was used to perform an *ex vivo* embolization procedure and mimic potential *in vivo* imaging applications. All experimental protocols and procedures applied on the pig prior to our *ex vivo* experiments were approved by the local experimental animal welfare committee and conform to national and European regulations for animal experimentation. The kidney was flushed with heparin solution to prevent coagulation of blood in the tissue and subsequently with 0.16 mM $MnCl_2$ in demineralized water to reduce the longitudinal relaxation rate (T_1) of the water and to mimic the relaxation properties of tissue [19]. Next, the left renal vein and artery were ligated and the organ was extirpated. A catheter (Abbocath - T I.V. Catheter 20 g x 1.25'', Hospira Inc., Lake Forest, IL, USA) was placed selectively in the inferior segmental renal artery and fixated with a suture. The kidney was placed in a plastic bucket and fixated to the sides of the bucket. A 30 cm flushing line connected to a three-way stopcock was connected to the catheter. Then, a 10 mL syringe was filled with 42 mg of Ho-lip-ams dispersed in water for injection and connected to the three-way stopcock for infusion. The microspheres were brought into suspension

by cautiously shaking the syringe and administered through the catheter system into the kidney under subtraction fluoroscopy at 70 kV using a digital flat panel fluoroscopy system (Allura Xper FD, Philips Healthcare, Best, the Netherlands). After the procedure, the catheter was flushed with 50 mL solution of 0.16 mM $MnCl_2$ in demineralized water to ensure complete microsphere infusion.

RESULTS AND DISCUSSION

MICROSPHERE CHARACTERIZATION

A representative micrograph of Ho-lip-ams is shown in Fig. 2. The emulsified lipiodol is visible as small droplets of a size range around 10-80 μm dispersed in the alginate matrix. The mean size (± SEM) of the Ho-lip-ams was 570 ± 12 μm, which is a clinically appropriate diameter for embolotherapy [20]. The size of the microspheres, however, is not limited to this range and can be tailored to fit a specific embolotherapy strategy by adjusting the settings of the JetCutter, enabling microsphere sizes between 120 μm to 3 mm [21].

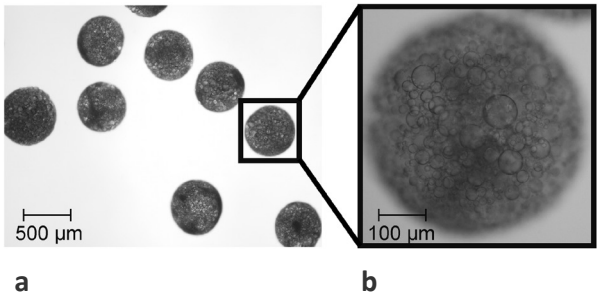

Fig. 2. Micrographs of Ho-lip-ams (magnification 40 x 10) (a), and 200 x magnification of a single Ho-lip-ams which shows the lipiodol emulsified droplets within the microspheres (b).

The holmium content of the Ho-lip-ams was 0.38 ± 0.01% (w/w). Inductively coupled plasma mass spectrometry (ICP-MS) measurements of fetal calf serum (FCS) in which Ho-lip-ams were incubated at 37 °C for two weeks showed a holmium dissociation of 10.8 ± 1.1%. This release was reached already after one day, while no further leakage was observed up to two weeks of exposure time, hence the holmium-alginate matrix of the Ho-lip-ams remained intact. Meanwhile, slow lipiodol release from the holmium-alginate matrix was observed over time (Fig. 3). This observation is worth further investigation, since lipiodol is frequently used for transarterial chemoembolization (TACE) procedures in combination with a chemotherapeutic agent such

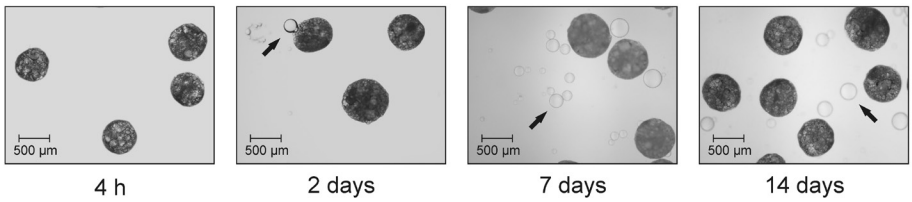

Fig. 3. Micrographs of Ho-lip-ams after 4h, 2 days, 7 days and 14 days of incubation in FCS (magnification 4 x 10). The black arrows indicate small lipiodol droplets.

as doxorubicin or cisplatin [22, 23]. Due to the relatively low holmium content within the Ho-lip-ams, and the slow release of holmium in time, toxicity of the microspheres is expected to be relatively low. To illustrate, FDA-approved gadolinium-chelates, which are frequently used for MRI diagnostics, are administered in concentrations of 0.1 mmol kg^{-1}, from which 1% is dissociated [24]. Holmium is a lanthanide comparable to gadolinium, and for a 100 kg patient receiving 1 g of microspheres (a regular amount for embolization), a total holmium concentration of 250 nmol kg^{-1} would be administered to the patient, which is 4 times lower as compared to the 1% of dissociated gadolinium from gadolinium-chelates and even 40 times lower when taken into account the dissociated holmium percentage from Ho-lip-ams.

MULTIMODALITY IMAGING OF ALGINATE MICROSPHERE PHANTOMS

The radiopaque Ho-lip-ams were clearly visible with CT, CBCT and MRI (Fig. 4). MRI confirmed the spatial Ho-lip-ams distribution as observed with CT. These images demonstrated single sphere detection with both imaging modalities. Ho-pso-ams were not detected with CBCT and CT imaging, due to the absence of radiopaque iodine within the microspheres. 3-D rendering of CT images illustrates the spatial distribution of the Ho-lip-ams as individual microspheres throughout the agarose phantoms (Fig. 5).

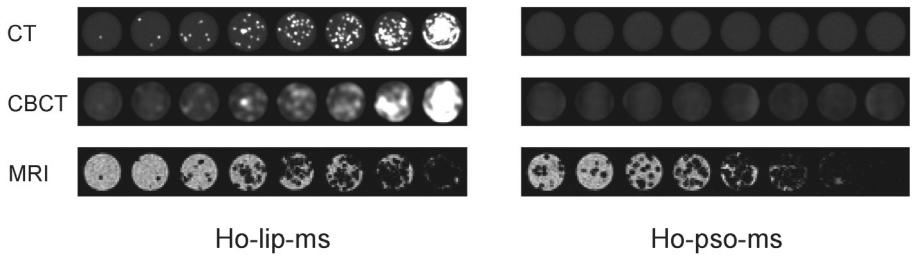

Fig. 4. Transverse images of a concentration series of Ho-lip-ams and Ho-pso-ams. The Ho-lip-ams can be depicted as single spheres using multimodality imaging (CT, CBCT and MRI). For Ho-pso-ams, only MRI allows for microsphere visualization due to the absence of radiopaque lipiodol. MR images are taken from the third echo (TE = 14.2 ms).

The sensitivity of X-ray CT (in HU mg^{-1} mL^{-1}) for the Ho-lip-ams and Ho-pso-ams is shown in Fig. 6. As expected, Ho-lip-ams had superior CT imaging properties as compared to Ho-pso-ams (a sensitivity increase ~60 times was observed at 80 kV). These results confirm the findings of Fig. 4.

HO-LIP-AMS INFUSION IN A PORCINE KIDNEY

Ho-lip-ams were clearly visible under digital subtraction fluoroscopy during administration via a catheter into an *ex vivo* porcine kidney (Fig. 7). An embolization procedure with the currently used non-imageable microspheres is continued until a desired embolization endpoint is reached or reflux of contrast material into non-target vessels is observed [16]. Intra-procedural imaging of an embolization procedure would facilitate direct feedback of the microsphere administration and may therefore enable the possibility to modify the intervention and defining desirable embolization

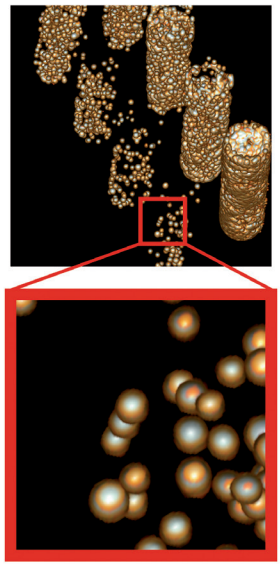

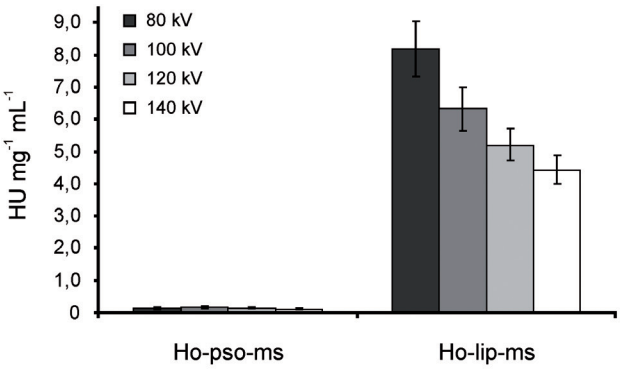

Fig. 5. Ho-lip-ams depicted as single spheres with 3-D CT assessment (left).

Fig. 6. CT sensitivity (in HU mg^{-1} mL^{-1}) of Ho-pso-ams and Ho-lip-ams (top).

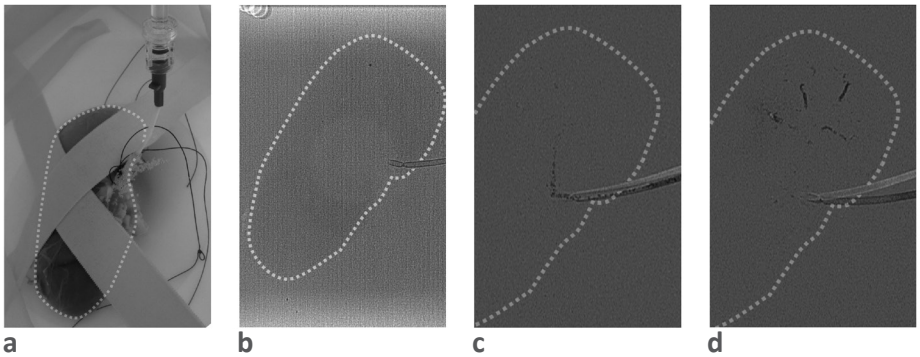

Fig. 7. Fluoroscopy-guided infusion of Ho-lip-ams in a porcine kidney. The kidney, which is delineated by the dotted line in this figure, was fixated to the inside of a plastic box and a catheter was inserted in the inferior segmental renal artery (a). Fluoroscopy of the kidney before microsphere infusion (b). Digital subtraction fluoroscopy of kidney during the embolization procedure (c, d).

endpoints [25]. After the procedure, multimodality imaging was performed to determine the distribution of the microspheres in the kidney. Selective embolization of the inferior renal segment was achieved (Fig. 8). The fluoroscopy (Fig. 8a), CBCT (Fig. 8b), CT (Fig. 8c) and MR (Fig. 8d) images show a similar microsphere distribution and indicate that all four modalities are appropriate for Ho-lip-ams visualization. Post-procedural imaging of the embolization procedure allows determination of bead distribution relative to the targeted tissue and enables dosimetry. The Ho-lip-ams comprises of components all in compliance with the requirements of the European Pharmacopoeia. This may be advantageous when CE marking of the new formulation

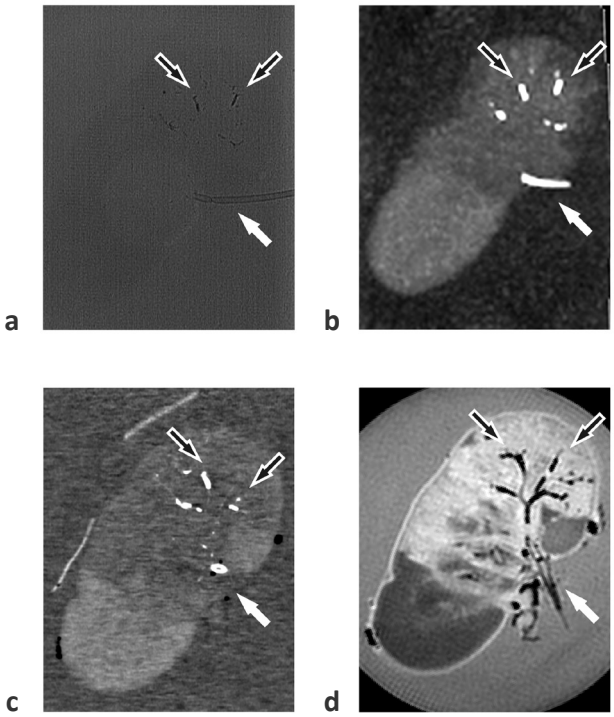

Fig. 8. Multimodal images of a porcine kidney after infusion of Ho-lip-ams. Fluoroscopy (a), CBCT (b), CT (c) and MRI (third echo, TE = 2.9 ms) (d). The black arrows indicate the clusters of microspheres deposited in the tissue. The white arrows show the catheter position on the different modalities.

is considered. Yet, it is important to realize that the microspheres first have to be thoroughly tested on cell cultures and that long-term *in vivo* toxicity tests have to be performed before clinical implementation can be achieved.

CONCLUSION

In the present study, a new microsphere formulation for multimodality image-guided embolotherapy is presented. The materials used for microsphere preparation and consequently the expected low toxicity indicates great potential for clinical implementation. The combination of intra-procedural visualization, multimodality imaging for patient follow-up and the possibility of quantification offers a new and promising method for more safe, efficient and successful embolization treatment.

REFERENCES

1. Derdeyn CP, Moran CJ, Cross DT, Dietrich HH, Dacey Jr. RG. Polyvinyl alcohol particle size and suspension characteristics. AJNR Am J Neuroradiol. 1995;16:1335-43.
2. Biosphere medical, http://www.biospheremed.com/products/embosphere.cfm, accessed on 10-30-12.
3. Spies JB, Benenati JF, Worthington-Kirsch RL, Pelage JP. Initial experience with use of tris-acryl gelatin microspheres for uterine artery embolization for leiomyomata. J Vasc Interv Radiol. 2001;12:1059-63.
4. Spies JB, Allison S, Flick P, McCullough M, Sterbis K, Cramp M, Bruno J, Jha R. Polyvinyl alcohol particles and tris-acryl gelatin microspheres for uterine artery embolization for leiomyomas: results of a randomized comparative study. J Vasc Interv Radiol. 2004;15:793-800.
5. Spies JB, Cornell C, Worthington-Kirsch R, Lipman JC, Benenati JF. Long-term outcome from uterine fibroid embolization with tris-acryl gelatin microspheres: results of a multicenter study. J Vasc Interv Radiol. 2007;18:203-7.
6. CeloNova BioSciences, http://www.celonova.com/index.php?q=node/29, accessed on 10-30-12.
7. Stampfl S, Stampfl U, Bellemann N, Sommer CM, Thierjung H, Radeleff B, Lopez-Benitez R, Berger I, Kauffmann GW, Richter GM. Biocompatibility and recanalization characteristics of hydrogel microspheres with polyzene-F as polymer coating. Cardiovasc Intervent Radiol. 2008;31:799-806.
8. Stampfl U, Sommer CM, Bellemann N, Holzschuh M, Kueller A, Bluemmel J, Gehrig T, Shevchenko M, Kenngott H, Kauczor HU, Radeleff B. Multimodal visibility of a modified polyzene-F-coated spherical embolic agent for liver embolization: feasibility study in a porcine model. J Vasc Interv Radiol. 2012;23:1225-31.
9. Biocompatibles Ltd., http://www.biocompatibles.com/products/lcbead, accessed on 10-30-12.
10. Rasuli P, Hammond I, Al-Mutairi B, French GJ, Aquino J, Hadziomerovic A, Goulet S, Jolly EE. Spherical versus conventional polyvinyl alcohol particles for uterine artery embolization. J Vasc Interv Radiol. 2008;19:42-6.
11. Chiesa AG, Hart WR. Uterine artery embolization of leiomyomas with trisacryl gelatin microspheres (TGM): pathologic features and comparison with polyvinyl alcohol emboli. Int J Gynecol Pathol. 2004;23:386-92.
12. Biocompatibles Ltd., http://www.biocompatibles.com/products/dcbead, accessed on 10-30-12.
13. Lewis AL, Holden RR. DC Bead embolic drug-eluting bead: clinical application in the locoregional treatment of tumours. Expert Opin Drug Deliv. 2011;8:153-69.
14. Lewis AL, Holden RR, Chung ST, Czuczman T, Kuchel T, Finnie J, Porter S, Foster D. Feasibility, safety and pharmacokinetic study of hepatic administration of drug-eluting beads loaded with irinotecan (DEBIRI) followed by intravenous administration of irinotecan in a porcine model. J Mater Sci Mater Med. 2013;24:115-27.
15. Seevinck PR, Seppenwoolde JH, de Wit TC, Nijsen JF, Beekman FJ, van het Schip AD, Bakker CJ. Factors affecting the sensitivity and detection limits of MRI, CT, and SPECT for multimodal diagnostic and therapeutic agents. Anticancer Agents Med Chem. 2007;7:317-34.
16. Lewis AL, Dreher MR. Locoregional drug delivery using image-guided intra-arterial drug eluting bead therapy. J. Control Release. 2012;161:338-50.
17. Lewandowski RJ, Geschwind JF, Liapi E, Salem R. Transcatheter intraarterial therapies: rationale and overview. Radiology 201;259:641-57.
18. Prusse U, Dalluhn J, Breford J, Vorlop KD. Production of spherical beads by JetCutting. Chemical Engineering & Technology. 2000;23:1105-10.

19. Seppenwoolde JH, Nijsen JF, Bartels LW, Zielhuis SW, van het Schip AD, Bakker CJ. Internal radiation therapy of liver tumors: qualitative and quantitative magnetic resonance imaging of the biodistribution of holmium-loaded microspheres in animal models. Magn Reson Med. 2005;53:76-84.
20. Biosphere medical, http://www.biospheremed.com/publication_files/MR02-033-RevF-Embosphere.pdf, accessed on 10-30-12.
21. Genialab GmbH, http://www.genialab.com/TechJetCutter.php, accessed on 10-30-12.
22. Lo CM, Ngan H, Tso WK, Liu CL, Lam CM, Poon RT, Fan ST, Wong J. Randomized controlled trial of transarterial lipiodol chemoembolization for unresectable hepatocellular carcinoma. Hepatology 2002;35:1164-71.
23. Llovet JM, Real MI, Montana X, Planas R, Coll S, Aponte J, Ayuso C, Sala M, Muchart J, Sola R, Rodes J, Bruix J. Arterial embolisation or chemoembolisation versus symptomatic treatment in patients with unresectable hepatocellular carcinoma: a randomised controlled trial. Lancet 2002;359:1734-9.
24. Wedeking P, Kumar K, Tweedle MF. Dissociation of gadolinium chelates in mice: relationship to chemical characteristics. Magn Reson Imaging. 1992;10:641-8.
25. Sharma KV, Dreher MR, Tang Y, Pritchard W, Chiesa OA, Karanian J, Peregoy J, Orandi B, Woods D, Donahue D, Esparza J, Jones G, Willis SL, Lewis AL, Wood BJ. Development of 'imageable' beads for transcatheter embolotherapy. J Vasc Interv Radiol. 2010;21:865-76.

Chapter 7

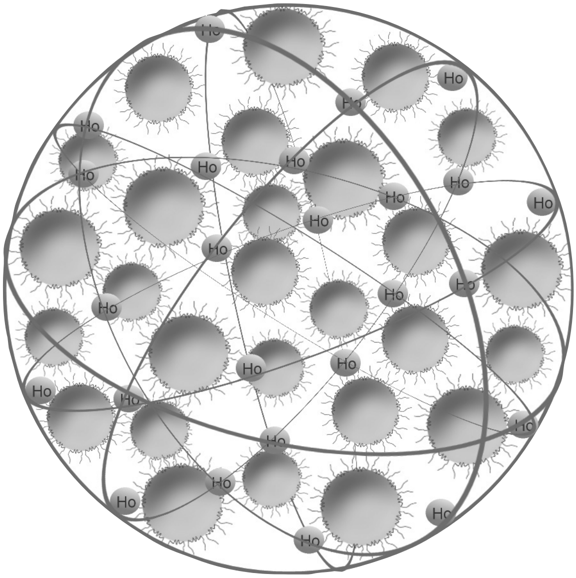

Summary and future directions

SUMMARY

Great process has been made during the last decades to overcome cancer. However, this disease still remains one of the leading causes of death worldwide. A multitude of therapeutic approaches has been proposed for different cancer types, including systemic chemotherapy, tumor resection, tumor ablation, external beam radiation therapy, immunotherapy, radiofrequency ablation (RFA), gene therapy and inhibition of angiogenesis. An important role is reserved for targeted therapies, where tumors are treated locally, thereby preventing damage to the surrounding healthy tissue [1, 2]. Local therapy can be achieved in different ways. For example, nanocarriers can be loaded with chemotherapeutic compounds and systemically administered into the blood stream. By encapsulation of the drugs in these carriers, their solubility and stability can be improved. The drugs incorporated in the nanoparticles also have improved pharmacokinetics. Finally, due to the enhanced permeability and retention (EPR) effect [3], the nanoparticles will accumulate in and around tumor tissue, resulting in a better efficacy and reduced systemic toxicity of the loaded drug. Although there has been emphasis on nanosized carriers, also microparticles offer excellent opportunities for targeted drug delivery. Embolotherapy involves the administration of microparticles with a size between 15-1200 μm into the tumor-feeding artery by catheterization [4]. The microspheres lodge in the tumor feeding artery and thereby block the blood flow, causing a lack of nutrient and oxygen supply to the tumor which finally leads to necrosis of the tumor tissue. Beside targeted therapy with nano- and microparticles, local tumor therapy can also be achieved by external modalities, such as high-intensity focused ultrasound (HIFU), which enables accurate ablation of malignant tissue. Next to tumor ablation, HIFU is also able to trigger drug release from nanocarriers such as polymeric micelles and liposomes to improve treatment outcome. In this dissertation, several new drug delivery systems for targeted cancer therapy are investigated and described. Targeted approaches and combinations of the different strategies are demonstrated both *in vitro* and *ex vivo*.

Chapter 2 reviews the current status of polymeric micelles in anticancer therapy. Micelles are colloidal particles with a size around 5-100 nm and are under investigation as drug delivery systems for hydrophobic drugs. Currently, five micellar formulations for anticancer therapy are under clinical evaluation. Furthermore, future perspectives for micellar drug delivery are discussed. Micellar drug delivery systems can be

optimized in different ways: targeting moieties which specifically recognize tumor cells can be attached to the micelles to increase the selectivity for tumor cells and enhance intracellular drug delivery. Imaging agents can be anchored to the micelles to allow *in vivo* tracking of the particles using different modalities such as MRI, CT and SPECT. Furthermore, pH-, thermo-, ultrasound-, or light-sensitive block copolymers enable controlled micelle dissociation and triggered drug release. This results in a higher drug concentration at the tumor site and improves the efficacy. The combination of these approaches will further improve specificity and efficacy of micelle-based drug delivery and brings the development of a 'magic bullet' a major step forward.

Chapter 3 (I) provides new insights into triggered release of a lipophilic compound (Nile red, NR) from non-crosslinked (NCL) and core-crosslinked (CCL) micelles exposed to continuous wave- (CW) HIFU and pulsed wave- (PW) HIFU high-intensity focused ultrasound (HIFU). After 4 min exposure to 20 W CW-HIFU, almost complete NR release (~85%) from NCL was achieved. CW-HIFU exposure of CCL resulted in less release as compared to NCL. Furthermore, a slightly higher NR release was observed from CCL micelles with 4% methacrylation compared to those with 13% methacrylation. No differences in NR release from NCL micelles between PW- and CW-HIFU were observed when equal amounts of acoustic energy were deposited. Addition of microbubbles to the micelle dispersions prior to HIFU exposure did not result in more NR release, indicating that inertial cavitation is not the main release mechanism of NR from the micelles. This was confirmed with dynamic light scattering (DLS) and gel permeation chromatography (GPC), which indicated that no changes in size distribution of the micelles and no degradation of the polymer chains had occurred after HIFU exposure. Therefore, it is hypothesized that the polymeric micelles are temporally destabilized upon HIFU exposure due to radiation force-induced shear forces, leading to NR release on demand.

Chapter 3 (II) describes a promising concept for local drug delivery using CW- and PW-HIFU to trigger the release of a hydrophilic (fluorescein) and lipophilic (Nile red, NR) model compound from thermosensitive liposomes (TSL) and non-thermosensitive liposomes (NTSL). The mean liposome size was 97-139 nm with a small polydispersity index (PDI) ≤ 0.06 and a melting transition of the lipid bilayer of TSL around 42 °C. Exposure of the TSL to CW-HIFU exposure resulted in rapid temperature elevation up to 53 °C and subsequently almost quantitative fluorescein release since the T_m of the liposomal bilayers was exceeded. Fluorescein release from NTSL was also substantial (~64% after 16 min at 20 W). Surprisingly, the release of NR from TSL was ~66%, and this was even higher from NTSL (~78%). Nearly 85% of fluorescein release was observed after PW-HIFU exposure of TSL for 32 min at 20 W, whereas under the same conditions the release of fluorescein from NTSL was around 27%. Interestingly, NR release from NTSL was ~30% after 2 min of PW-HIFU exposure, increasing to ~70% after 32 min. In this study, HIFU-triggered release of a lipophilic compound from liposomes was reported for the first time. It is discussed that the release originates from radiation force-induced acoustic streaming which in turn results in reversible liposome destabilization and release of both hydrophilic and lipophilic compounds.

Chapter 4 presents a novel approach to identify non-palpable breast lesions combining fluorescent liposomes and MR-HIFU-triggered release. In this approach, fluorescein-containing liposomes (FCL) are administered into the blood stream. Due to the EPR effect, the liposomes will passively accumulate in the tumor tissue. Subsequently, exposure of the FCL localized in the tumor to ablation temperatures using HIFU would then result in palpable, fluorescently-stained tumors, which are more easy to identify during surgical resection. *Ex vivo* experiments in human blood and porcine muscle tissue showed increased release from the liposomes, clear fluorescence enhancement and diffusion of the released compound after heating to 42 °C and 60 °C for a short period (30 s), which is in line with the clinically relevant MR-HIFU treatment parameters. Therefore, this method may offer a new tool for efficient surgical resection of non-palpable breast tumor lesions by enabling proper discrimination between tumor tissue and adjacent healthy tissue.

Chapter 5 reports on the development of alginate-lanthanide microspheres for magnetic resonance imaging (MRI)-guided embolotherapy. Embolotherapy, or endovascular intervention with microsized particles has gained an important position in the treatment of a wide variety of conditions affecting different organs of the human body, such as uterine fibroids, arteriovenous malformations (AVM), kidney and liver tumors. Alginate microspheres (ams) were prepared with the JetCutter technique, which is based on cutting a sodium alginate solution jet stream into small droplets of uniform size which are then crosslinked with different lanthanides or iron-III, resulting in microspheres of a predefined size which can be visualized by MRI. The lanthanide-ams formulations had a uniform size of 250 μm and a cation content between 0.72-0.94% (w/w). The different lanthanide-ams were visualized with MRI on both 1.5 and 3 T. The highest relaxivity was found for Ho^{3+}-ams. Further investigation of Ho^{3+}-ams using MRI showed that the microspheres could be depicted as single spheres. Intravascular infusion of Ho^{3+}-ams by catheterization of *ex vivo* rabbit as well as porcine liver tissue and assessment of the procedure with MRI clearly showed accumulation and subsequently embolization of the targeted vessels, allowing accurate monitoring of the microsphere distribution over the tissue. Therefore, these alginate-lanthanide microsphere formulations show great potential for utilization as image-guided embolotherapy agents.

Chapter 6 is dedicated to the development of alginate-lipiodol microspheres to allow multimodality imaging during and after embolotherapy. An important drawback of the current clinically available microspheres, is that they cannot be detected *in vivo* with medical imaging techniques, impeding intra- and post-procedural feedback. Real-time monitoring of microsphere infusion and post-procedural imaging is expected to result in a more safe, efficient and successful treatment. A novel microsphere formulation is proposed that can be visualized with fluoroscopy, X-ray computed tomography (CT) and magnetic resonance imaging (MRI). The microspheres were prepared with the JetCutter technique and consist of alginate, holmium, lipiodol and Pluronic F-68. The mean size (± SEM) of the holmium-lipiodol alginate microspheres (Ho-lip-ams) was 570 ± 12 μm with a holmium content of 0.38 ± 0.01% (w/w). Stability studies showed that the microspheres remained intact during incubation for two weeks in fetal calf serum at 37 °C. The inclusion of lipiodol in the microspheres rendered excellent visualization capabilities for fluoroscopy and (cone beam) CT, whereas the holmium ions, which keep together the alginate network,

also allow MR imaging. Single sphere detection was possible by fluoroscopy, CT and MRI. The Ho-lip-ams were distinguished in real-time during infusion in a porcine kidney using fluoroscopy. Similar deposition patterns of the microspheres within the organ were observed with fluoroscopy, (cone beam) CT and MRI. The combination of intra-procedural visualization, multimodality imaging for patient follow-up and the possibility of quantification offers a new and promising method for more safe, efficient and successful embolotherapy.

FUTURE DIRECTIONS

Local cancer therapy has proven its value over the last years. Several liposome formulations are clinically approved and used for the treatment of i.e. multiple myeloma, ovarian cancer, metastatic breast cancer and AIDS-related Kaposi's sarcoma [5]. Five micelle formulations are now in clinical trials for different cancer types such as breast cancer, adenocarcinoma of oesophagus, gastroesophageal junction and stomach, pancreatic cancer and non-small-cell lung carcinoma (NSCLC) [6]. Microspheres have gained an important position in embolotherapy for the treatment of a wide variety of conditions affecting different organs of the human body, such as uterine fibroids, arteriovenous malformations (AVM), kidney and liver tumors. However, efficacy of these drug delivery systems can still be improved. Preclinical research has been conducted to develop more efficient drug delivery. For instance, targeting ligands can be attached to the particles, enabling binding to receptors found on cancer cells, which is believed to result in increased particle accumulation in the tumor tissue. However, the total amount of particles that accumulate in the tumor tissue depends only on the EPR effect and the circulation half life. Attachment of targeting ligands to particles might adversely affect the circulation kinetics [5] and may therefore even decrease the amount of drug that is deposited in the tumor. Therefore, attaching targeting moieties to nanoparticles is only useful to achieve improved retention and intracellular delivery. Moreover, active targeting is an attractive approach to reach metastasis. Loading of the particles with imaging ligands allows visualization of the treatment to predict the outcome of the therapy. This contributes to the treatment efficiency and gives insight into the prospect of novel cancer therapies. Conversely, the circulation kinetics may be adversely affected when the imaging moieties are attached to the surface of the particle. Furthermore, high concentrations of contrast agents may result in toxic side effects [7-9]. Triggered drug release from particles, for instance by temperature elevation or high-intensity frequency ultrasound (HIFU), is non-invasive and can be locally applied at the tumor site, and is therefore an attractive method to obtain a higher drug efficacy. On the other hand, particle adjustment to increase their susceptibility to destabilization is required, which makes the particles less stable, also in the circulation. Therefore, there is a need for stable particles that yet provide the possibility of triggered drug release. It should also be taken into account that triggered release in clinical practice requires an extra treatment step: the patient has to undergo a HIFU procedure to locally heat the nanocarriers, leading to higher costs and more inconvenience for the patient. It is therefore imperative that advances for improved drug delivery and efficacy have to be carefully conducted, taking into account the possible adverse effects concerning circulation kinetics and stability. In this dissertation, evidence of a new triggered release mechanism from liposomal and micellar formulations is presented. For clinical translation, the model compounds used in these studies can be replaced by a variety of chemotherapeutic compounds to tumor tissue such as alkylating agents like cisplatin and cyclophosphamine, taxanes like paclitaxel, anthracycline antibiotics such as doxorubicin, as well as different antimetabolites like 5-fluorouracil or different pyrimidines for the treatment of multiple cancer types. Particularly for breast cancer, the combination between tumor ablation and HIFU-triggered liposomal release may lead to more efficient treatment, especially by replacing the clinically approved fluorescent dye fluorescein [10, 11] by several drugs specifically used to treat breast cancer, such as tamoxifen, anastrozole or letrozole for hormone-dependent tumors and cyclophosphamide, doxorubicin or

epirubicin for non-hormone-dependent tumors. Besides nanoparticles, novel bland embolization microspheres crosslinked with a variety of lanthanide elements for MR imaging are proposed in this dissertation. Moreover, the development of holmium-crosslinked alginate microspheres containing the radiopaque contrast agent lipiodol, allowing both röntgen- and MR imaging for more safe and controlled embolization therapy, is described. The main component of these microspheres is alginate, which is a linear copolymer with homopolymeric blocks of (1-4)-linked β-D-mannuronate and α-L-guluronate residues, and is used for several biomedical applications, varying from the preparation of dental impressions and food additives, to the encapsulation of (stem) cells or antibodies [12]. The versatility of alginate and the imaging opportunities obtained with the different microsphere formulations developed in this disquisition offer numerous possibilities for advanced cancer therapy. For instance, the microspheres can be loaded with different therapeutic agents, depending on the purpose of the therapy. A suspension of lipiodol and cisplatin or doxorubicin is already clinically used for transarterial chemoembolization (TACE) [13]. In our research, slow lipiodol release from a holmium-alginate matrix was observed, which offers the possibility of controlled drug release from a multimodal imageable microsphere formulation. Long-term prospects would include the combination of nano- and microparticles: nanoparticles can be encapsulated in microparticles to enable a more efficient targeted therapy. It is envisioned that after intra-arterially administration of biodegradable microspheres, the nanoparticles are released from the microspheres over time and accumulate in the tumor tissue with a higher efficiency as compared to systemic nanoparticles administration. Another prospect includes the encapsulation of stimuli-responsive nanoparticles in non- (or slowly) degradable microparticles. For example, thermosensitive liposomes loaded with both a contrast agent and a chemotherapeutic compound can be encapsulated in holmium-alginate microspheres. HIFU can be applied as an external trigger for local release of the contrast agent and the drug. MR imaging enables intra-procedural feedback of the embolization procedure, while MR thermometry and -imaging allows monitoring of the HIFU exposure and release procedure. Intra- and post-procedural monitoring of the treatment with multimodality imaging is crucial to verify whether the therapy is successfully executed and facilitates the possibility for optimization of future treatments. For clinical translation, the particles have to be further investigated in terms of toxicity, safety and efficacy in *in vivo* models. Moreover, it should be taken into account that medical implementation is only possible when particle preparation takes place under good manufacturing practice (GMP). In conclusion, the different particles as developed in this dissertation show encouraging results for future clinical implementation, and bring the prospect of combined therapies a step forward. The particles can be tailored in various ways, enabling the development of personalized medicine where the therapy can be adjusted to the needs of the individual patient. For these combined therapies, the main focus is to design imageable drug delivery systems, which also allow drug release 'on command', resulting in a high efficacy with a significant decrease in toxicity and side effects. Merging the platforms of nano- and microsparticle-based drug delivery combined with triggered drug release and multimodality imaging facilitates interdisciplinary integration of both preclinical and clinical research and brings the prospect of the 'magic bullet' a major step forward.

REFERENCES

1. Peer D, Karp JM, Hong S, Farokhzad OC, Margalit R, Langer R. Nanocarriers as an emerging platform for cancer therapy. Nat Nanotechnol. 2007;2:751-60.
2. Varde NK, Pack DW. Microspheres for controlled release drug delivery. Expert Opin Biol Ther. 2004;4:35-51.
3. Maeda H. Macromolecular therapeutics in cancer treatment: The EPR effect and beyond. J Control Release. 2012;164:138-44.
4. Biosphere medical, http://www.biospheremed.com/publication_files/MR02-033-RevF-Embosphere.pdf, accessed on 10-30-12.
5. Lammers T, Kiessling F, Hennink WE, Storm G. Drug targeting to tumors: principles, pitfalls and (pre-) clinical progress. J Control Release. 2012;161:175-87.
6. Oerlemans C, Bult W, Bos M, Storm G, Nijsen JF, Hennink WE. Polymeric micelles in anticancer therapy: targeting, imaging and triggered release. Pharm Res. 2010;27:2569-89.
7. Minchin RF, Martin DJ. Nanoparticles for molecular imaging - an overview. Endocrinology 2010;151:474-81.
8. Spencer AJ, Wilson SA, Batchelor J, Reid A, Rees J, Harpur E. Gadolinium chloride toxicity in the rat. Toxicol Pathol. 1997;25:245-55.
9. Perazella MA. Current status of gadolinium toxicity in patients with kidney disease. Clin J Am Soc Nephrol. 2009;4:461-9.
10. Dollery CT, Hodge JV, Engel M. Studies of the retinal circulation with fluorescein. Br Med J. 1962;2:1210-5.
11. Bennett TJ, Barry CJ. Ophthalmic imaging today: an ophthalmic photographer's viewpoint - a review. Clin Experiment Ophthalmol. 2009;37:2-13.
12. Oerlemans C, Seevinck PR, van de Maat GH, Boulkhrif H, Bakker CJ, Hennink WE, Nijsen JF. Alginate-lanthanide microspheres for MRI-guided embolotherapy. Acta Biomater. 2013;9:4681-7.
13. Lewandowski RJ, Geschwind JF, Liapi E, Salem R. Transcatheter intraarterial therapies: rationale and overview. Radiology. 2011;259:641-57.

Chapter 8

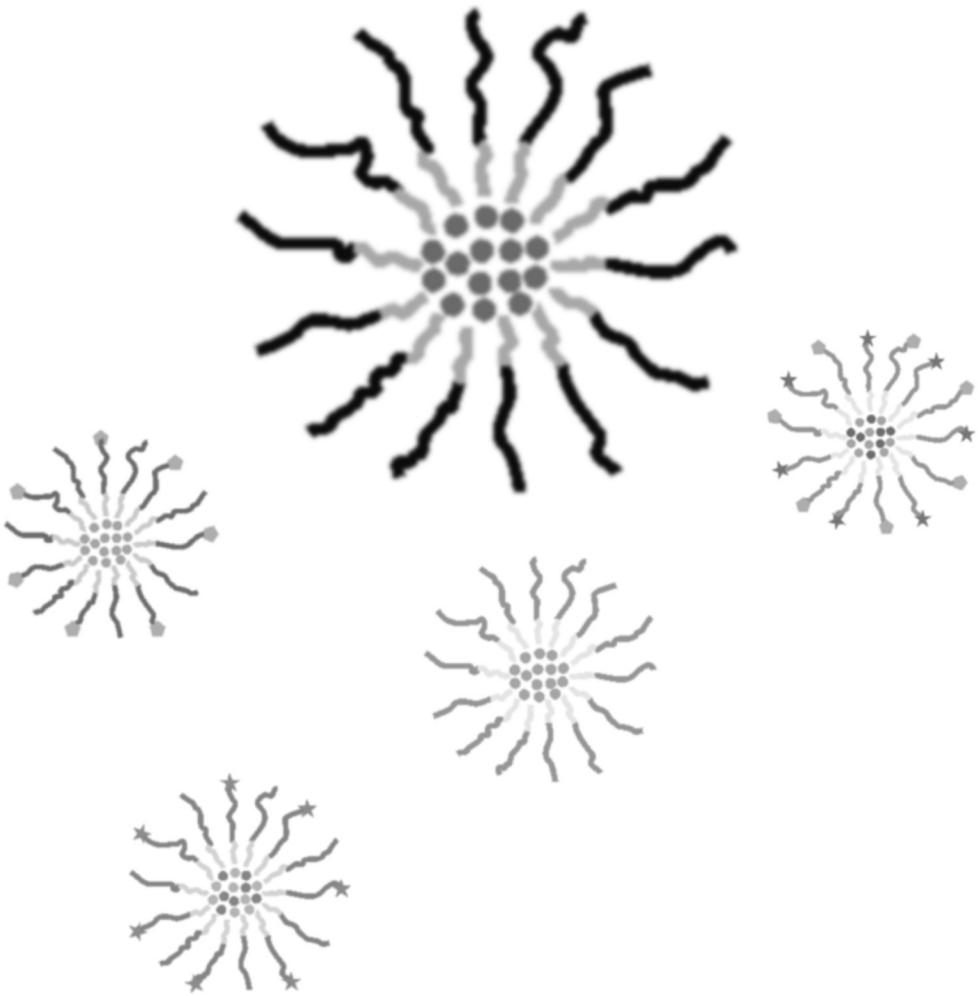

Samenvatting in het Nederlands

INLEIDING

De afgelopen decennia is er aanzienlijke progressie geboekt in het onderzoek naar de behandeling van kanker. Desondanks blijft kanker nog steeds een van de meest voorkomende doodsoorzaken ter wereld. Voor verschillende typen kanker worden momenteel verscheidene behandelmethoden toegepast, zoals chemotherapie, tumorresectie, tumorablatie, radiotherapie, immunotherapie, radiofrequente ablatie (RFA), gentherapie en inhibitie van angiogenese. Een belangrijke ontwikkeling die momenteel wordt onderzocht is het lokaal behandelen van tumoren, waardoor de efficiëntie van de behandeling toeneemt, terwijl schade aan het omliggende weefsel wordt beperkt of zelfs voorkomen wordt. Lokale therapie kan op verschillende manieren worden bewerkstelligd, bijvoorbeeld met behulp van nanodeeltjes, deeltjes met een diameter van slechts enkele tientallen tot honderden nanometers die kunnen worden geladen met cytostatica. Door het inkapselen van de medicijnen in nanodeeltjes kan de oplosbaarheid, de stabiliteit en de farmacokinetiek worden verbeterd. Naast nanodeeltjes kunnen ook micropartikels worden gebruikt voor lokale therapie door de partikels te gebruiken voor embolisatie. Micropartikels zijn een factor duizend groter dan nanodeeltjes en kunnen het bloedvat afsluiten (emboliseren), wat een tekort aan voedingsstoffen en zuurstof voor de tumor tot gevolg heeft. Dit leidt tot necrose van het tumorweefsel. Naast doelgerichte therapieën met nano- of microdeeltjes, kan lokale tumortherapie ook worden bewerkstelligd met externe, non-invasieve technieken, zoals bijvoorbeeld met hoge-intensiteit gefocusseerde echografie (HIFU). Hierbij worden geluidsgolven in een klein gebied gefocusseerd waardoor er een lokale verhoging van de temperatuur ontstaat, die in de kliniek zelfs kan oplopen tot ongeveer 60 °C. Deze techniek kan worden gebruikt om tumorweefsel te ableren. Naast tumorablatie, kan HIFU ook worden gebruikt voor gecontroleerde afgifte van medicijnen uit nanodeeltjes zoals polymere micellen en liposomen.

NANOTECHNOLOGIE IN KANKERTHERAPIE

In 1986 is door Japanse wetenschappers ontdekt dat de vaatstructuur in tumoren anders is dan in gezond weefsel. De oorzaak hiervoor is dat wanneer de tumoren een bepaalde grootte bereiken (er wordt uitgegaan van ongeveer 200 mm), diffusie van zuurstof en voedingsstoffen naar de tumorcellen niet meer toereikend is. Tumoren zijn hierdoor genoodzaakt om verschillende stoffen, waaronder groeifactoren

aan te maken die resulteren in angiogenese, oftewel het aanmaken van nieuwe bloedvaten. Bij tumorcellen is dit proces echter verstoord, waardoor de vaatstructuur abnormaliteiten vertoond. Hierbij moet gedacht worden aan endotheelcellen die niet enkellaags gerangschikt zijn, de afwezigheid van glad spierweefsel en een groter lumen. De Japanse onderzoekers zagen dat door deze 'lekke' vaten kleine partikels van enkele honderden nanometer (nm) in het tumorweefsel terechtkwamen en daar vanwege de afwezigheid van een effectieve lymfatische drainage op de plek bleven. Dit fenomeen werd daarom het 'enhanced permeability and retention' (EPR) effect genoemd. Deze ontdekking heeft de deuren geopend voor de introductie van nanopartikels voor de behandeling van kanker. Immers, wanneer deze kleine partikels een cytostaticum bevatten, dan kan de tumor veel gerichter worden aangepakt, zelfs wanneer deze partikels intraveneus worden toegediend. Voorbeelden van zulke medicijndragers, ook wel 'drug delivery systems' (DDS) genoemd, zijn liposomen en polymere micellen. Liposomen zijn kleine vetbolletjes van ongeveer 50 tot 200 nm in diameter, bestaande uit een fosfolipide bilaag die een waterige kern omsluit, In de kern van een liposomen kan een waterminnend (hydrofiel) stofje worden gebracht, terwijl een vetminnend (lipofiel) stofje in de bilaag kan worden opgelost. Micellen hebben een grootte van ongeveer 5 tot 100 nm en bestaan uit amfifiele verbindingen, oftewel verbindingen die zowel een hydrofiel als een lipofiel gedeelte bevatten. Als deze monomeren in een hydrofiele omgeving worden gebracht, dan vindt aggregatie plaats en ontstaan micellen doordat de lipofiele gedeeltes van de monomeren zich afkeren van het hydrofiele medium. Wanneer dit proces plaatsvindt in de aanwezigheid van een lipofiel stofje, dan wordt deze ingesloten in de micellen. Zowel liposomen als micellen kunnen technologisch zo worden vervaardigd dat ze specifieke eigenschappen krijgen, waarbij gedacht kan worden aan de mogelijkheid tot 'triggered release', zodat de nanopartikels het ingesloten stofje vrijgeven bij een externe trigger. Voorbeelden van een externe trigger zijn temperatuursverhoging, blootstelling aan ultrageluid, blootstelling aan licht van een specifieke golflengte en pH veranderingen. Tevens kunnen de nanopartikels worden uitgerust met een 'targeting ligand', oftewel moleculen zoals antilichamen die specifiek binden aan tumorcellen met als doel een efficiëntere afgifte van cytostatica te bewerkstelligen. Ook zijn er voorbeelden bekend van liposomen die kunnen worden afgebeeld via medische beeldvormende technieken zoals computertomografie (CT) en magnetische resonantie beeldvorming (MRI). Op deze manier is men in staat om de uitkomst van de therapie in kaart te brengen en kan de therapie worden geoptimaliseerd.

EMBOLISATIETHERAPIE

Embolisatietherapie behelst het via een katheter inbrengen van micropartikels in een arterie, zodat de bloedtoevoer wordt geblokkeerd en zuurstof en nutriënten het tumorweefsel niet meer kunnen bereiken. In de oncologie wordt deze therapie voornamelijk toegepast bij niertumoren, primaire levertumoren en colorectale levermetastasen, omdat de nier en de lever gemakkelijk kunnen worden bereikt via een katheter. Daarnaast worden levermetastasen voor ongeveer 90% van bloed voorzien door de arteria hepatica (leverslagader), terwijl dit bij het gezonde leverweefsel met name wordt aangevoerd via de poortader. Ook de micropartikels kunnen worden uitgerust met cytostatica, waardoor naast embolisatie van het bloedvat, de tumor tevens via medicijnen behandeld wordt, wat de kans groter maakt dat de tumor verdwijnt. Dit wordt ook wel transarteriële chemo-embolisatie ofwel TACE

genoemd. Daarnaast kunnen microsferen radioactief worden gemaakt (zoals SIR-Spheres zijn voorzien van radioactief yttrium-90 en holmium-PLLA-microsferen van het radioactieve element holmium-166), zodat levermetastasen binnen in het lichaam kunnen worden bestraald (radio-embolisatie). Een bijkomend voordeel van holmium is dat dit element kan worden gedetecteerd via een MRI scan. Radioactief holmium kan tevens via nucleaire beeldvormingstechnieken (SPECT) worden gedetecteerd, zodat goed in de gaten kan worden gehouden of de behandeling verloopt volgens plan. Het aspect 'beeldvorming' wordt steeds belangrijker in de oncologie gezien de toename van minimaal-invasieve therapieën. Terwijl bij tumorresectie een goed beeld kan worden gevormd van de behandeling tijdens de operatie, is die mogelijkheid niet aanwezig bij embolisatietherapie. Beeldvorming van de behandeling is alleen mogelijk via röntgen-doorlichting met behulp van additionele contrastmiddelen aangezien de micropartikels zelf niet zichtbaar zijn. Het onderzoek beschreven in dit proefschrift heeft geleid tot de ontwikkeling van verschillende microsferen welke zowel met MRI alsmede met CT/röntgen-doorlichting kunnen worden afgebeeld. Deze ontwikkelingen dragen bij aan een verbetering van de huidige behandelingsmethoden door de mogelijkheid tot het 'live' kunnen volgen van de procedure, wat zal leiden tot succesvollere behandelingen en een betere prognose de patiënt, doordat de observatie van de patiënt, ook na de behandeling, optimaal is.

Hoofdstuk 2 geeft een uitgebreid overzicht van de huidige status van polymere micellen in zowel preklinisch als klinisch onderzoek. Hedendaags worden vijf typen micellen geschikt geacht voor de behandeling van patiënten. NK012 is een type micel dat een camptothecine-analoog bevat en in klinische fase 2-onderzoek verkeerd voor de behandeling van borstkanker. Tevens wordt NK105, een type micel dat het cytostaticum paclitaxel bevat, onderzocht in fase-2 onderzoek voor de behandeling van maagkanker. SP1049C (fase 3) bevat doxorubicine en wordt onderzocht op geschiktheid voor de behandeling tegen adenocarinomen in de slokdarm, maagklep en maag. NC-6004 bevindt zich in fase 1/2 onderzoek voor de behandeling van verscheidene solide tumoren, terwijl Genexol-PM reeds in fase 4 verkeerd en dus is geregistreerd als geneesmiddel tegen borstkanker. Tevens wordt Genexol-PM onderzocht voor toepassingen bij vele andere soorten tumoren. Daarnaast wordt in dit hoofdstuk beschreven welke modificaties kunnen worden aangebracht bij micellen die potentieël kunnen leiden tot efficiëntere drug afgifte. Liganden die specifiek binden aan tumorcellen kunnen worden gebruikt voor een meer doeltreffende behandeling, terwijl contrastmiddelen kunnen worden toegevoegd aan micellen om ze met medische beeldvormende technieken te volgen in het lichaam. Een belangrijk aspect bij micellen is het gecontroleerd laten vrijgeven van het cytostaticum. Hiervoor kunnen de micellen op een specifieke manier worden aangepast zodat ze gevoelig worden voor temperatuursverhoging, ultrageluid (HIFU), pH-veranderingen, UV- of infrarood licht. Het ultieme doel is om de verschillende modificaties met elkaar te verenigen, zodat we steeds dichterbij de ontwikkeling van de 'magische kogel' geraken.

Hoofdstuk 3 (I) beschrijft nieuwe inzichten in de vrijgifte van een lipofiele stof (Nile red, NR) vanuit polymere micellen waarbij de polymeerketens onderling zijn gekoppeld (CCL) en micellen waarbij dit niet het geval is (NCL) door middel van zowel continue golf-hoge intensiteit gefocusseerd ultrasoon geluid (CW-HIFU) en gepulseerde golf-HIFU (PW-HIFU). Na 4 minuten blootstelling aan 20 W CW-HIFU

was bijna alle NR vrijgegeven uit de NCL micellen (~85%). Blootstelling van CCL micellen aan 20 W CW-HIFU gedurende 4 minuten resulteerde in veel minder NR vrijgifte. Tevens was de vrijgifte van NR uit CCL micellen met een lagere mate van polymerisatie met methacrylaat (4%) iets hoger in vergelijking met CCL micellen met een hogere mate van methacrylaat polymerisatie (13%). Er werden geen verschillen in NR vrijgifte gezien uit NCL micellen na CW- en PW-HIFU blootstelling op pH 5. Toevoegen van microbubbels aan de micellen resulteerde niet in meer NR vrijgifte uit de micellen. Dit toont aan dat cavitatie, een effect wat met HIFU wordt geassocieerd, niet het belangrijkste vrijgifte mechanisme is van NR uit de micellen. Dit is geverifieerd met experimenten waarbij de grootte van de micellen is gemeten (dynamic light scattering, DLS) en experimenten waarbij de samenstelling van de polymeren waaruit de micellen bestaan is onderzocht voor en na HIFU blootstelling (gel permeation chromatography, GPC). Er is hierbij geen verandering in micelgrootte of degradatie van de polymeren waargenomen. Dit suggereert dat de polymere micellen tijdelijk worden gedestabiliseerd door blootstelling aan HIFU, wat leidt tot de vrijgifte van NR.

Hoofdstuk 3 (II) rapporteert over de vrijgifte van zowel hydrofiele en lipofiele stoffen vanuit thermosensitieve (TSL) alsmede uit non-thermosensitieve liposomen (NTSL) onder invloed van HIFU. De TSL en NTSL bevatten de hydrofiele stof fluoresceïne of de lipofiele stof Nile red (NR). De liposomen hadden een gemiddelde diameter van 97-139 nm met een lage polydispersiteit index (PDI) ≤ 0.06. De fase-overgang temperatuur (T_m) van de TSL was rond 42 °C. Blootstelling van de TSL aan CW-HIFU resulteerde in een snelle temperatuurstoename naar 53 °C, waardoor nagenoeg de volledige hoeveelheid aan fluoresceïne werd vrijgegeven aangezien de T_m was overschreden. Daarentegen werd ook een substantiële hoeveelheid fluoresceïne vrijgegeven uit NTSL (~64% na 16 min op 20 W). Verrassend was de observatie dat de vrijgifte van NR uit TSL rond de 66% lag, en zelfs nog hoger was vanuit NTSL (~78%). Bijna 85% fluoresceïne werd vrijgegeven na 32 min blootstelling van de TSL aan PW-HIFU, terwijl dit 27% was bij NTSL. Een belangrijke observatie was dat rond 30% NR werd vrijgegeven vanuit NTSL na 2 minuten PW-HIFU blootstelling, wat opliep tot ongeveer 70% na 32 minuten. Dit is de eerste studie die rapporteert over HIFU-geïnduceerde vrijgifte van een lipofiele stof vanuit liposomen. Het wordt aangenomen dat HIFU blootstelling resulteert in tijdelijke destabilisatie van de liposomen, die tijdens deze periode van destabilisatie hun stoffen vrijgeven. Deze bevindingen leiden tot nieuwe inzichten in HIFU-geïnduceerde vrijgifte van stoffen vanuit liposomen en tonen aan dat hyperthermie en cavitatie niet de enige mechanismen van vrijgifte zijn door middel van HIFU blootstelling. Deze inzichten kunnen bijdragen aan het ontwikkelen van methodes voor efficiëntere afgifte van cytostatica rondom tumoren.

In **hoofdstuk 4** wordt de ontwikkeling van fluoresceïne-bevattende thermosensitieve liposomen (FCL) voor tumor demarcatie tijdens borsttumorresectie beschreven. Via CW-HIFU kan de temperatuur in de borst op de plek van een aanwezige non-palpabele tumor binnen korte tijd zeer lokaal worden verhoogd tot ongeveer 60 °C, zodat eiwit-denaturatie plaatsvindt en de borsttumor palpabel en dus voelbaar wordt voor de chirurg om het resterende tumorweefsel operatief te verwijderen. De FCL kunnen vooraf aan de HIFU-blootstelling intraveneus worden toegediend, waarna ze middels het EPR effect in en om het tumorweefsel terechtkomen. Er wordt geen fluorescentie gedetecteerd als de fluorescente stof binnenin de liposomen zit,

echter wanneer de het weefsel wordt verhit en de fluorescente stof vrijkomt uit de liposomen, licht de tumor op onder een UV lamp. Op deze manier wordt specifiek de tumor gedemarkeerd. De chirurg kan vervolgens de tumor efficiënt verwijderen, terwijl het gezonde weefsel zoveel mogelijk gespaard blijft.

Hoofdstuk 5 beschrijft de ontwikkeling van alginaat microsferen welke gebruikt kunnen worden als embolisatiepartikel. De microsferen uit deze studie zijn gemaakt via de JetCutter techniek en bevatten een lanthanide (europium, gadolinium, terbium, dysprosium, holmium, thulium of ytterbium), waardoor de microsferen kunnen worden afgebeeld met behulp van MRI. De microsferen hadden een gemiddelde diameter van 250 μm en een lanthanide gehalte van 0.72-0.94%. De verschillende typen microsferen zijn onderzocht op de mate van zichtbaarheid via MRI, waaruit is gebleken dat de microsferen met holmium uiteindelijk het beste zichtbaar waren. De microsferen konden zelfs als indiviuele bolletjes worden afgebeeld. In een lever van een konijn en in de nier van een varken is met deze microsferen een katheterisatie-procedure nagebootst en is aangetoond dat de distributie van de microsferen accuraat kan worden gevolgd in weefsel, wat 'real-time' terugkoppeling van de klinische procedure mogelijk maakt en dus tot een grotere slagingskans van de embolisatie therapie kan leiden.

In **hoofdstuk 6** wordt een nieuw type microsfeer gepresenteerd welke geschikt is voor multimodale beeldvorming. Het nieuwe type microsfeer, bestaande uit alginaat, lipiodol, holmium en Pluronic F-68 kon zowel met behulp van röntgenstraling (CT) door de encapsulatie van lipiodol als röntgencontrastmiddel, en MRI, door de aanwezigheid van holmium, als individuele microsferen worden afgebeeld in fantomen. De gemiddelde diameter van de microsferen was 570 μm met een holmium concentratie van 0.38%. De microsferen bleven stabiel na incubatie voor twee weken in serum op 37 °C. Tijdens een *ex vivo* experiment met een varkensnier, waarbij via katheterisatie de microsferen zijn toegediend, kon de procedure intra-proceduraal met fluoroscopie 'live' worden gevolgd, terwijl tevens de distributie van de microsferen via alle gebruikte medische beeldvormende technieken, te weten fluoroscopie, (cone beam) CT en MRI konden worden afbeeeld. De combinatie van intra-procedurale detectie en multimodale beeldvorming biedt de mogelijkheid tot goede nazorg voor de patient en kan daardoor resulteren in een veiligere, efficientere en meer succesvolle behandeling.

Chapter 8

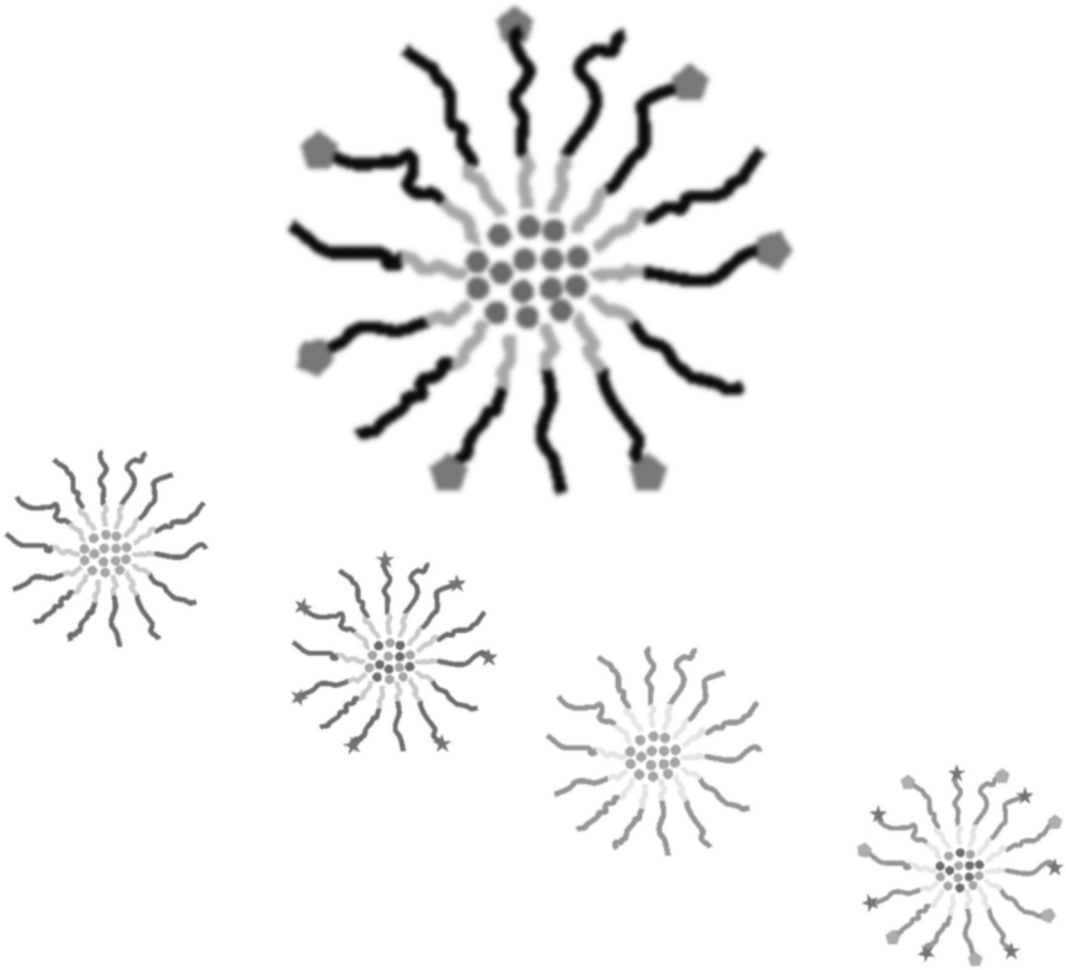

ARTICLES

Oerlemans C., Bult W., Bos M., Storm G., Nijsen J.F.W., Hennink W.E. Polymeric micelles in anticancer therapy: targeting, imaging and triggered release. Pharmaceutical Research 27, 2569-2589 (2010).

Oerlemans C., Nijsen J.F.W., van Amersfoort M., van Bloois L., Heijman E., Luijten P.R., Mali W.P.Th.M., Storm G. A novel approach to identify non-palpable breast lesions combining fluorescent liposomes and magnetic resonance-guided high intensity focused ultrasound-triggered release. European Journal of Pharmaceutics and Biopharmaceutics 77, 458-464 (2011).

Oerlemans C., Seevinck P.R., van de Maat G.H., Boulkhrif H., Bakker C.J.G., Hennink W.E., Nijsen J.F.W. Alginate-lanthanide microspheres for MRI-guided embolotherapy. Acta Biomaterialia 9, 4681-4687 (2013).

Oerlemans C., Deckers R.H.R., Storm G., Hennink W.E., Nijsen J.F.W. Evidence for a new mechanism behind HIFU-triggered release from liposomes. Journal of Controlled Release. In press (2013).

Deckers R.H.R., Paradissis A., **Oerlemans C.**, Talelli M., Storm G., Hennink W.E., Nijsen J.F.W. New insights into the HIFU-triggered release from polymeric micelles. Submitted.

Oerlemans C., Seevinck P.R., Smits M.L.J., Hennink W.E., Van den Bosch M.A.A.J., Bakker C.J.G., Nijsen J.F.W. Alginate-lipiodol microspheres for fluoroscopy-guided embolotherapy and multimodality imaging. Submitted.

ABSTRACTS

Oerlemans C., Nijsen J.F.W., van den Bosch M.A.A.J., van Bloois L., Luijten P.R., Storm G. Dye-containing liposomes for heat-triggered release. EuroNanoMedicine, Bled, Slovenia, September 28-30, 2009.

Oerlemans C., Nijsen J.F.W., van Amersfoort M., van Bloois L., Heijman E., Luijten P.R., Storm G. A novel approach to identify non-palpable breast lesions combining fluorescent liposomes and MRgHIFU-triggered release. MediTrans Third Annual meeting, Saarbrücken, Germany, March 19-22, 2010.

Oerlemans C., Nijsen J.F.W., van Amersfoort M., van Bloois L., Heijman E., Luijten P.R., Storm G. A novel approach to identify non-palpable breast lesions combining fluorescent liposomes and MRgHIFU-triggered release. 8th International Conference and Workshop on Biological Barriers - *in vitro* Tools, Nanotoxicology, and Nanomedicine, Saarbrücken, Germany, March 22-27, 2010.

Oerlemans C., Nijsen J.F.W., van Amersfoort M., van Bloois L., Heijman E., Luijten P.R., Mali W.P.Th.M., Storm G. A novel approach to identify non-palpable breast lesions combining fluorescent liposomes and MR-HIFU. MediTrans Final Meeting, Sant Feliu de Guixols, Spain, October 28-30, 2010.

Lorenzato C.S., **Oerlemans C.**, Nijsen J.W.F., Moonen C.T., Bos C. MRI *in vitro* setup for studying contrast agent effect in inhomogeneous environment. The International Society for Magnetic Resonance in Medicine (ISMRM) 21st Annual Meeting & Exhibition, Salt Lake City, Utah, USA, April 20-26, 2013.

AWARDS

Best oral presentation at the MediTrans PhD student oral presentation competition October 30, 2010, Sant Feliu de Guixols, Spain.

Chapter 8

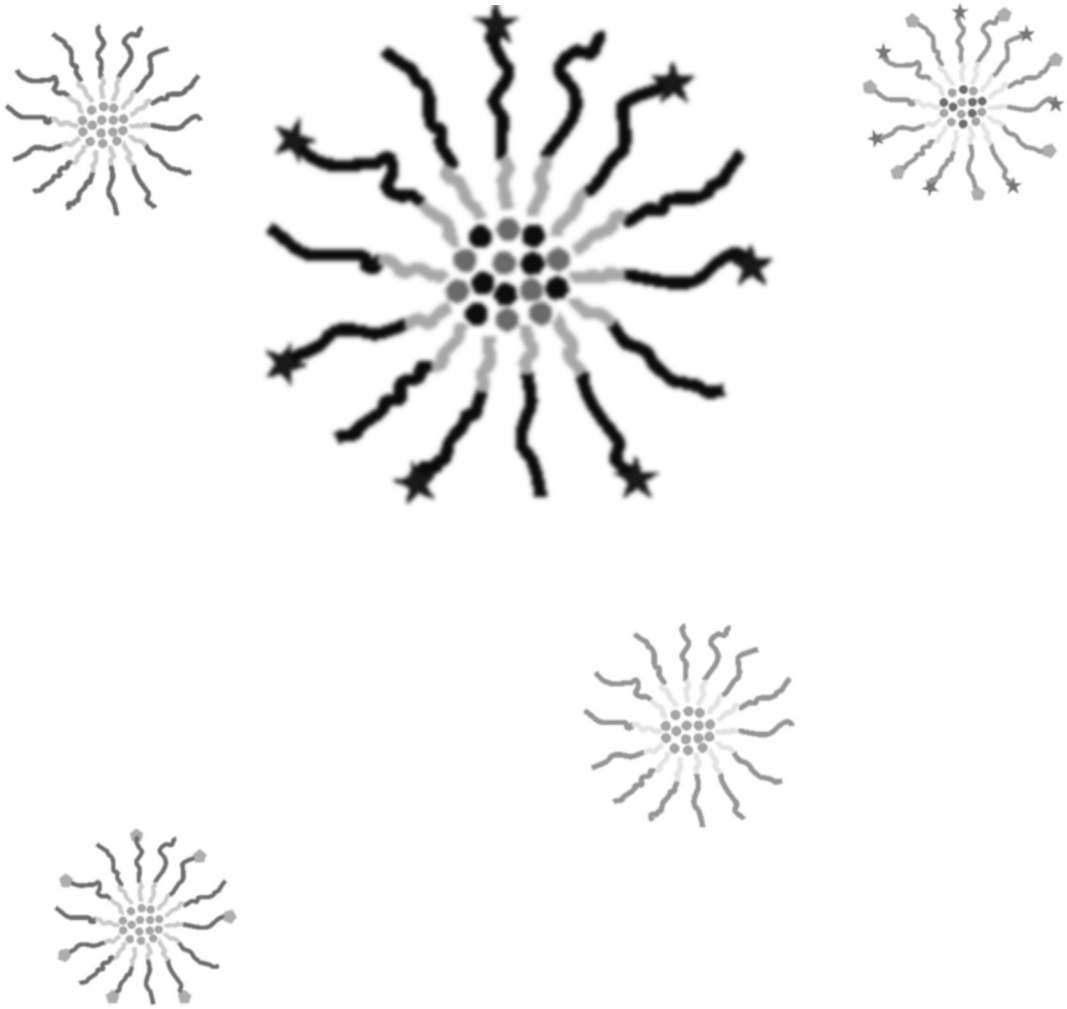

M. van Amersfoort (Miranda) — Department of Medical Oncology, University Medical Center Utrecht (UMCU), Utrecht, The Netherlands

C.J.G. Bakker (Chris) — Department of Radiology and Nuclear Medicine, University Medical Center Utrecht (UMCU), Utrecht, The Netherlands

H. Boulkhrif (Hassan) — Department of Radiology and Nuclear Medicine, University Medical Center Utrecht (UMCU), Utrecht, The Netherlands

L. van Bloois (Louis) — Department of Pharmaceutics, Utrecht Institute for Pharmaceutical Sciences, Utrecht University, Utrecht, The Netherlands

M. Bos (Mariska) — Department of Radiology and Nuclear Medicine, University Medical Center Utrecht (UMCU), Utrecht, The Netherlands

H. Boulkhrif (Hassan) — Department of Radiology and Nuclear Medicine, University Medical Center Utrecht (UMCU), Utrecht, The Netherlands

W. Bult (Wouter) — Department of Pharmacy, University Medical Centre Groningen (UMCG), Groningen, The Netherlands.

R.H.R. Deckers (Roel) — Image Sciences Institute, University Medical Center Utrecht (UMCU), Utrecht, The Netherlands

W.E. Hennink (Wim) — Department of Pharmaceutics, Utrecht Institute for Pharmaceutical Sciences, Utrecht University, Utrecht, The Netherlands

E. Heijman (Edwin) — Department of Biomedical Engineering, Philips Research Europe, Eindhoven, The Netherlands

P.R. Luijten (Peter) — Department of Radiology and Nuclear Medicine, University Medical Center Utrecht (UMCU), Utrecht, The Netherlands

G.H. van de Maat (Gerrit) — Department of Radiology and Nuclear Medicine, University Medical Center Utrecht (UMCU), Utrecht, The Netherlands

W.P.Th.M. Mali (Willem) — Department of Radiology and Nuclear Medicine, University Medical Center Utrecht (UMCU), Utrecht, The Netherlands

J.F.W. Nijsen (Frank) — Department of Radiology and Nuclear Medicine, University Medical Center Utrecht (UMCU), Utrecht, The Netherlands

P.R. Seevinck (Peter) — Department of Radiology and Nuclear Medicine, University Medical Center Utrecht (UMCU), Utrecht, The Netherlands

M.L.J. Smits (Maarten) — Department of Radiology and Nuclear Medicine, University Medical Center Utrecht (UMCU), Utrecht, The Netherlands

G. Storm (Gert) — Department of Pharmaceutics, Utrecht Institute for Pharmaceutical Sciences, Utrecht University, Utrecht, The Netherlands

M. Talelli (Marina) — Department of Pharmaceutics, Utrecht Institute for Pharmaceutical Sciences, Utrecht University, Utrecht, The Netherlands

Chapter 8

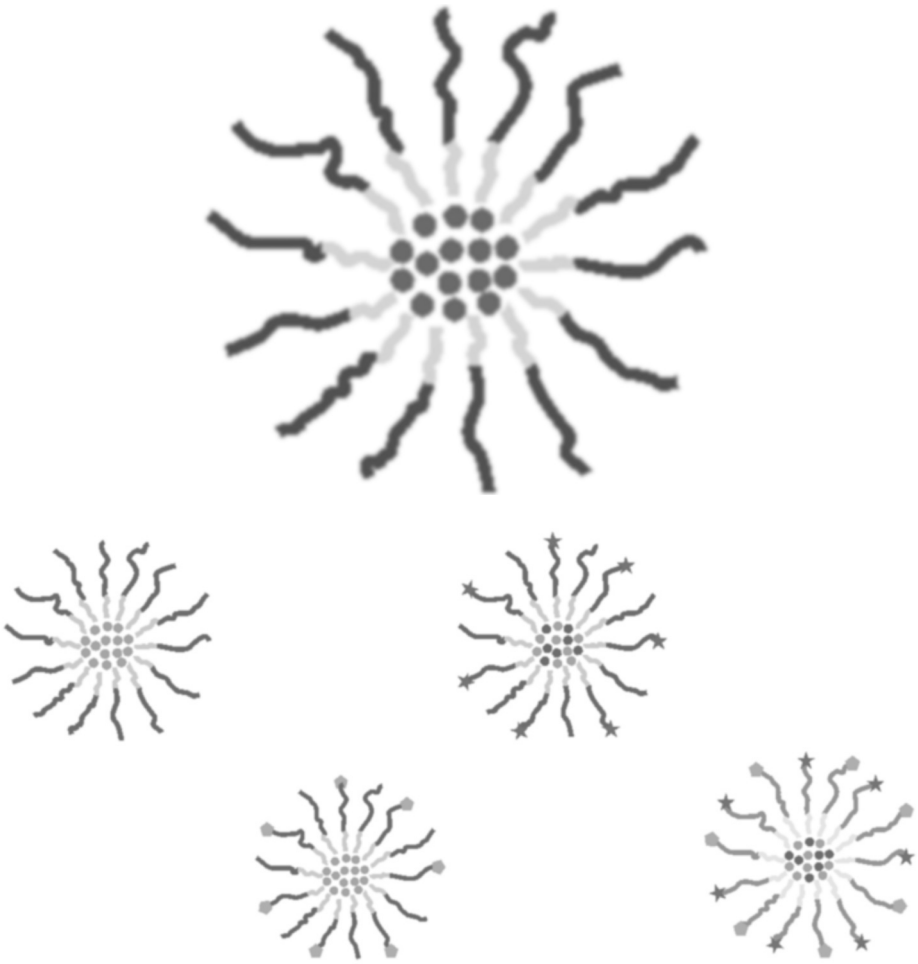

Samenvatting in het Nederlands
List of publications
List of affiliations
Curriculum Vitae
Dankwoord

Chris Oerlemans was born on July 31, 1983 in a village called Kapelle in the heart of Zeeland, the Netherlands. He finished his secondary school in 2001 at the Sint Willibrordcollege (now: Ostrea College) in Goes. After graduation, he started with the bachelor study biology at Wageningen University and Research centre (WUR). During his master, he specialized in cell biology, meanwhile two theses and one internship were performed. His first thesis at the Department of Toxicology (WUR) was titled 'Effects of airborne particulate matter on early apoptosis in cardiomyocytes'. His second thesis at the Department of Nutrition, Metabolism and Genomics (Division of Human Nutrition, WUR) was titled: 'Effects of inflammatory mediators on the expression of nuclear receptors in the liver'. His internship was performed at Numico Research B.V., where he contibuted to the development of a clinical food for cancer patients. In June 2008, he started his PhD project at the Department of Radiology and Nuclear Medicine and the Image Sciences Institute (ISI) of University Medical Center Utrecht (UMCU), in close cooperation with Utrecht Institute of Pharmaceutical Sciences (UIPS), Utrecht University, which resulted in the publication of several papers in scientific journals and the dissertation as presented here. Currently, he works as a postdoc in the research group Image-guided Molecular Interventions of prof. Chrit Moonen and is committed to the HIFU-CHEM project under the Center for Translational Molecular Medicine (CTMM) consortium, investigating MR-HIFU triggered release of doxorubicin from thermosensitive liposomes and its effect on tumor growth and pharmacokinetics.

Chris Oerlemans is geboren op 31 juli 1983 in het Zeeuwse dorp Kapelle, ook wel 'de bloesem van Zeeland' genoemd. In 2001 heeft hij het voortgezet wetenschappelijk onderwijs (VWO) afgerond aan het Sint Willibrordcollege (tegenwoordig: Ostrea College) te Goes. Hierna is hij begonnen met de studie biologie aan Wageningen Universiteit en Research centre (WUR). In 2002 heeft hij zijn propedeuse gehaald en in 2004 zijn bachelordiploma. Zijn masterdiploma celbiologie werd behaald in 2007. Tijdens de masterfase heeft hij twee afstudeervakken gevolgd en een stage afgerond. Zijn eerste afstudeervak is uitgevoerd bij de vakgroep Toxicologie (WUR) waarbij hij de invloed van fijnstof en ultrafijnstof (afkomstig van uitlaatgassen van auto's en uitstoot van de industrie) op de ontsteking van alveolaire macrofagen en het indirecte effect hiervan op geprogrammeerde celdood (apoptose) van de hartspiercellen heeft onderzocht. Zijn tweede afstudeervak heeft plaatsgevonden aan de vakgroep Nutrition, Metabolism and Genomics (leerstoelgroep Humane

Voeding, WUR), waarbij via genexpressie gekeken is naar ontstekingsreacties in de lever bij verschillende diëten (vetarm en vetrijk) en de invloed van een nieuw voedingscomponent op deze ontstekingsreacties. Zijn stage heeft hij uitgevoerd bij Numico Research te Wageningen (tegenwoordig: Danone Research) waarbij hij heeft meegewerkt aan de ontwikkeling van klinische voeding voor het verhogen van de weerstand bij kankerpatiënten. In juni 2008 is hij gestart met zijn promotie-project bij de Afdeling Radiologie en Nucleaire Geneeskunde van het Universitair Medisch Centrum Utrecht (UMCU) en het Image Sciences Institute (ISI) in nauwe samenwerking met het Utrechts Utrecht Institute of Pharmaceutical Sciences (UIPS) van Universiteit Utrecht, wat heeft geresulteerd in de publicatie van verscheidene artikelen in wetenschappelijke tijdschriften en het proefschrift wat hier voor u ligt. Momenteel werkt hij als postdoc bij de onderzoeksgroep Image-guided Molecular Interventions onder leiding van prof. Chrit Moonen en is hij betrokken bij het HIFU-CHEM project onder het Center for Translational Molecular Medicine (CTMM) consortium waarbij hij onderzoek verricht aan thermosensitieve liposomen geladen met doxorubicine voor MR-HIFU-getriggerde vrijgifte en het effect op tumorgroei.

Chapter 8

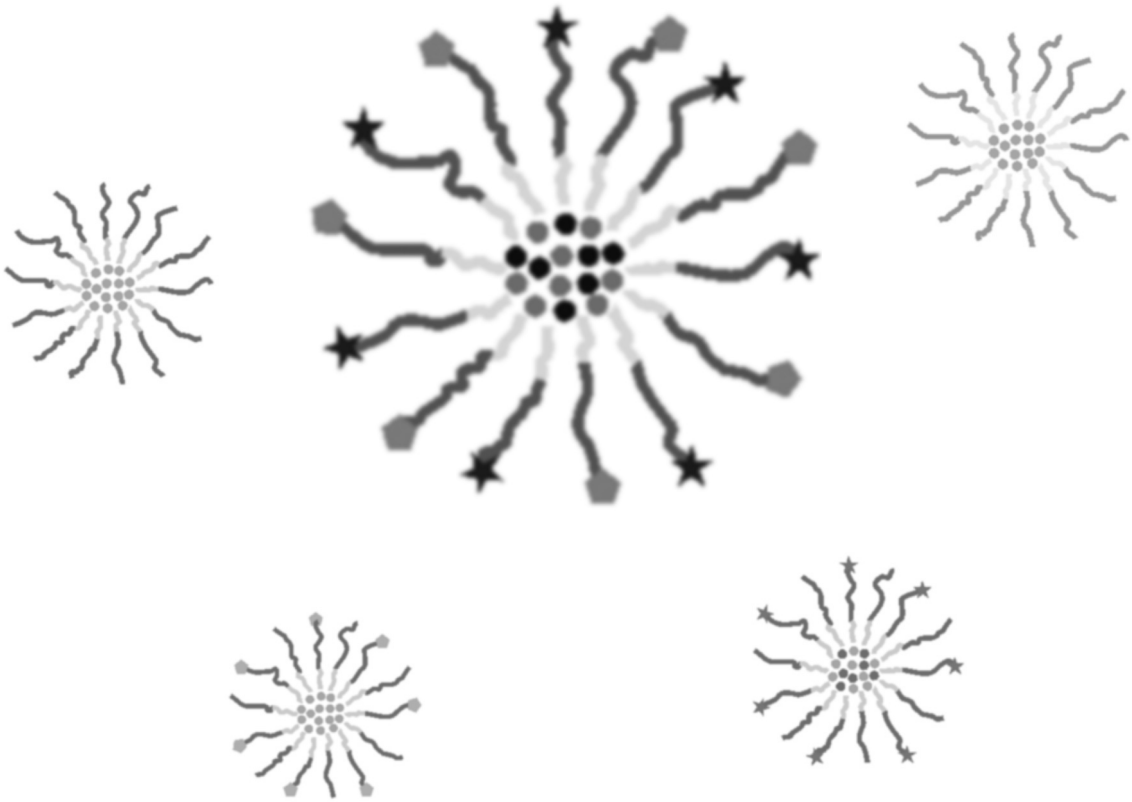

Samenvatting in het Nederlands
List of publications
List of affiliations
Curriculum Vitae
Dankwoord

Vijf jaar geleden heb ik de kans gekregen een wetenschappelijk promotieonderzoek uit te voeren. De eerlijkheid gebiedt mij te zeggen dat ik, als Wageningse bioloog, nog nooit van een liposoom, micel of microsfeer had gehoord alvorens te beginnen aan dit avontuur in het UMC Utrecht. Gelukkig werd mijn enthousiasme na mijn aanstelling verder aangewakkerd door de bezieling van mijn collega's en vooral van mijn (co)promotoren. Derhalve wil ik een aantal mensen hartelijk danken voor hun ondersteuning tijdens mijn promotieonderzoek.

Allereerst gaat mijn dank uit naar mijn promotoren en copromotor. Zij hebben het mogelijk gemaakt dit proefschrift te vervaardigen en te mogen verdedigen.

Prof. dr. Luijten, beste Peter, jij hebt mij het vertrouwen gegeven door mij als bioloog een medisch/farmaceutisch gerichte promotie uit te laten voeren. Je heb altijd een vinger aan de pols gehouden, ondanks dat we inhoudelijk niet helemaal in hetzelfde vakgebied zaten. Mede dankzij jou mag ik nu nog twee jaar verder als postdoc in het HIFU-CHEM project van CTMM.

Prof. dr. ir. Hennink, beste Wim, ergens 'makkelijk mee wegkomen' is bij jou niet aan de orde, en terecht. Ik heb je directheid leren waarderen, en al hebben de grote hoeveelheden teruggezonden versies van manuscripten mij de nodige zweetdruppels gekost: ik ben je zeer erkentelijk. Ik ben onder de indruk van je gestructureerdheid, je kennis en professionaliteit; door jouw ondersteuning heb ik mijn promotieonderzoek succesvol kunnen voltooien: bedankt!

Dr. Nijsen, beste Frank, jij hebt mijn promotietraject zijn uiteindelijke vorm gegeven en op de voet gevolgd. We waren het niet altijd eens over de te volgen route, maar dat krijg je natuurlijk met zo'n eigenwijze promovendus. Ik heb veel van je geleerd, vooral een 'hands-on' mentaliteit. Die was bij mij in het begin slechts 'latent' aanwezig, maar ik heb wel gezien dat je in plaats van plannen achter het bureau ook direct het lab in kunt gaan om tot mooie resultaten te komen; de befaamde 'quick-and-dirty' methode. Je hebt mij zeer vrij gelaten in de invulling van mijn onderzoek zodat ik mij zelf heb kunnen ontwikkelen tot zelfstandig onderzoeker.

Daarnaast had dit proefschrift nooit kunnen worden gedrukt zonder een positieve beoordeling van de beoordelingscommissie.

Prof. dr. Storm, beste Gert, vanaf het begin af aan was je betrokken bij mijn onderzoek. Jij hebt mijn eerste wetenschappelijk publicatie mogelijk gemaakt. Naast coauteurschappen bij meerdere publicaties, ben je uiteindelijk ook degene die mede mijn proefschrift heeft beoordeeld, waarvoor dank. Als er iemand positief gestemd is, dan ben jij het wel! Dat zal de sfeer voor de komende twee jaar dat we met elkaar blijven samenwerken alleen maar ten goede komen.

Prof. dr. Moonen, beste Chrit, nadat ik je al enkele keren had ontmoet op congressen vanwege onze gezamelijke betrokkenheid bij het MediTrans project, besloot je in 2011 samen met je onderzoeksgroep te verhuizen van Bordeaux naar Utrecht. Voor het UMC, maar tevens voor mij, een erg prettige stap. Want naast het feit dat je op het gebied van HIFU als autoriteit mag worden gezien en het UMC hiermee wereldwijd mee op de kaart hebt gezet, heb je mij de kans gegeven om postdoc bij je groep te worden voor de komende twee jaar op het gebied van HIFU-triggered drug release. Daarvoor ben ik je zeer erkentelijk.

Prof. dr. van den Bosch, beste Maurice, ik heb je leren kennen toen je nog niet de positie van professor had. Gelukkig ben je nog even toegankelijk als voorheen. Door jouw kennis en kunde op het gebied van interventieradiologie, en met name embolisatie, heeft de Holmium Research Group een flinke boost gekregen en zijn de 'holmium bollen' inmiddels verheven tot speerpunt van het UMC. Tevens ben je nauw betrokken bij het HIFU-onderzoek en dicht je de kloof tussen het wetenschappelijke onderzoek en de directe klinische toepasbaarheid, exact wat een universitair medisch centrum nodig heeft: met z'n allen werken aan een betere prognose voor patiënten.

Prof. dr. Grüll, beste Holger, meermaals ben ik te gast geweest in jullie lab. Wat een professionaliteit en wat een grote hoeveelheid aan apparatuur is bij jullie aanwezig op de High Tech Campus in Eindhoven! Ik heb mijn ogen uitgekeken. Het werk beschreven in Hoofdstuk 4 had nooit voltooid kunnen worden zonder de hulp van jullie vakgroep, en ook de vruchtbare discussie's hebben hun vruchten afgeworpen in het onderzoek. De gastvrijheid en openheid van jullie groep vind ik zeer te waarderen. Ik heb dan ook met veel plezier samengewerkt. Hopelijk kunnen we dit in de toekomst voortzetten.

Prof. dr. Jiskoot, beste Wim, wij hebben elkaar leren kennen tijdens een van mijn eerste cursussen op het gebied van farmaceutische wetenschappen, de 'advanced drug delivery and drug targeting' cursus, waarvoor ik een week in Leiden verbleef. Erg praktisch zo'n stoomcursus in het begin van mijn PhD-project! Een mooie week in Leiden, welke ik zeer heb gewaardeerd. Bedankt dat je mijn manuscript wilden beoordelen. Wellicht komen we elkaar vaker tegen in de nabije toekomst.

Ook tijdens de dagelijkse werkzaamheden heb ik natuurlijk met een aantal mensen een mooie tijd beleefd.

Dr. Van het Schip, beste Fred, helaas kwam ik te laat bij de groep voor jou om mij als copromotor te kunnen begeleiden. Je zou immers bij mijn promotie reeds de pensioengerechtigde leeftijd hebben bereikt. Desalniettemin kon ik altijd bij je binnenlopen voor vragen en berkeningen met betrekking tot chemie. Ik wens je veel geluk in je nieuwe levensfase.

Dr. Vente, beste Maarten, de wandelende radioembolisatie-encyclopedie, maar bovenal: vriend. Met name in mijn derde jaar, toen we kamergenoten waren, hebben we veel 'kennis gedeeld', of zoals de grote baas Frank het vaak (uiteraard onterecht) formuleerde: ouwehoeren. Helaas heb jij uiteindelijk gekozen om elders aan de slag te gaan, maar gelukkig hebben we nog altijd contact gehouden en spreken we nog regelmatig af om een goudgele rakker te nuttigen. De volgende nemen we op de promotie. Ik ben vereerd jou als paranimf aan mijn zijde te hebben tijdens de verdediging van mijn proefschrift.

Dr. Heijenbrok, beste Frank, we kennen elkaar nog geen jaar, maar als kamergenoten leer je elkaar natuurlijk al snel goed kennen. Gelukkig delen we eenzelfde gevoel voor humor, want wat hebben we (naast natuurlijk het harde werken!) gelachen met elkaar. Laten we zeggen dat dit samen te vatten is als een avondje cabaret van Javier Guzman, waar we dan ook rond het verschijnen van dit proefschrift naar toe gaan. Ook jou bedank ik hartelijk voor de ondersteuning tijdens de verdediging van mijn proefschrift.

Dr. Bult, beste Wouter, onze eerste kennismaking was tijdens het Biomaterials congres in Amsterdam. En dat terwijl ik nog niet eens officieel in dienst was. Frank kon enkele dagen van het congres niet aanwezig zijn, dus mocht ik als 'Dr. Nijsen' op het congres rondlopen; die promotie had ik dus al snel voor elkaar. Uiteindelijk hebben wij zo'n 3 jaar samen opgetrokken en heb je mij wegwijs gemaakt in het UMC en vooral bij Farmacie. Na je promotie vertrok je naar het UMC Groningen om te starten met de opleiding voor ziekenhuisapotheker. Daar heb je het nu prima naar je zin, met inmiddels het gehele plaatje van 'huisje, boompje, beestje' compleet. Dank voor je hulp, gezelligheid en humor.

Dr. Seevinck, beste Peter, met jou als 'MRI-maatje' heb ik vele uren achter de scanner doorgebracht met allerhande rariteiten, waaronder agarose-gels met microsferen, maar ook levers van konijnen en varkens. Gelukkig kon ook jij mijn gevoel voor humor waarderen, al kon je de herhaling van grappen, of het maken van de grappen terwijl jij intensief geconcentreerd was scanparameters in te voeren, niet altijd op waarde schatten. Tja, dat krijg je als ik tot 23:00 stil op een stoel moet blijven zitten… Toch konden we ook serieus onderzoek doen, waarbij onze samenwerking heeft geresulteerd in mooie publicaties, en er ligt nog meer in het verschiet de komende jaren!

Dr. Zonnenberg, beste Bernard, jij hebt mij een aantal mooie ideeën gegeven voor mijn onderzoek. Ik heb hier een deel van ter harte genomen en inmiddels zoals je weet mooie 'bollen' gemaakt. Helaas was er geen tijd genoeg om ze te beladen, maar ik blijf nog even, dus wie weet…

Dr. Bakker, beste Chris, wij hebben vooral intensief contact gehad rondom de ontwikkeling van de 'nieuwe' microsferen. Je hebt er zelfs voor gezorgd dat er een mooi apparaat op het lab van Nucleaire Geneeskunde kwam te staan om deze microsferen te kunnen maken. Daar ben ik je dankbaar voor. Ik heb je leren kennen als een kundige onderzoeker die precies en gedetailleerd te werk gaat. Ook de manuscripten waarvan je coauteur bent werden kritisch door jou bekeken. Ik heb je bijdrage hieraan, maar vooral je prettige persoonlijkheid als aangenaam ervaren.

Naast de 'theoretische' begeleiding, was ik natuurlijk nergens zonder de praktische begeleiding op het lab. De helden van het lab zijn zonder twijfel **Remmert de Roos** van het nucleaire lab in het UMC en **Louis van Bloois** en **Mies van Steenbergen** van het farmaceutisch lab. Zonder dit 'gouden trio', bij wie ik altijd terecht kon, had mijn onderzoek nooit kunnen slagen. Heren: hulde!

Ik kon niet daadwerkelijk alle experimenten zelf uitvoeren, dus gelukkig hebben 'mijn' studenten die ik tijdens mijn promotieonderzoek heb mogen begeleiden mij hiermee prima kunnen helpen. **Mariska Bos**, jij was de eerste student die ik heb mogen begeleiden en je hebt een uitgebreide literatuurstudie uitgevoerd over micellen en liposomen. Voor mij vormde jouw scriptie een mooie aanzet voor het schrijven van een review-artikel over micellen, waar jij dan ook coauteur van bent geworden en wat inmiddels al meer dan 100 maal (!) is geciteerd. **Hassan Boulkhrif**, de 'bollenmaker', inmiddels afgestudeerd apotheker en ondertussen alweer derdejaars student geneeskunde. Ook jouw bijdrage en in het bijzonder je eigen inzicht heeft geleid tot een coauteurschap op een publicatie. Naast het harde werken hebben we samen ontzettend veel gelachen op het lab en zijn we vrienden geworden. Erg leuk dat we nog regelmatig bij elkaar over de vloer komen. Binnenkort weer een happie eten in Nieuwegein? **Leida Reijnders**, vreemd hoe de verhoudingen soms kunnen liggen: een 10 jaar jonger kereltje moest jou begeleiden voor je wetenschappelijke stage. Inmiddels ben je alweer ver gevorderd in je studie geneeskunde en komen we elkaar nog regelmatig tegen aangezien je samen met Bernard een nieuw project aan het opzetten bent. Erg leuk dat je zo enthousiast bent geworden voor wetenschappelijk onderzoek. **Willem van Doesum**, jij mag inmiddels wel 'HIFU-expert' genoemd worden voor het uren achtereen op samples 'schieten'. Ondertussen mocht je als dierenarts-in-opleiding ook honden en katten behandelen met intratumorale holmium-microsferen-injecties. Een drukke, maar mooie tijd.

Binnen de onderzoeksschool ImagO en met name het Image Sciences Institute (ISI) heb ik de nodige kennis opgedaan van allerhande algoritmes, wiskundige formules en beeldreconstructies voor beeldverwerking van (met name) MRI-scans. Tevens heb ik de gelegenheid gekregen om voor deze groep meerdere malen mijn onderzoek te presenteren en mensen hierdoor te enthousiasmeren voor nano- en microdeeltjes. Hiervoor wil ik de hele groep bedanken, en met name **prof. dr. Max Viergever,** voor het bieden van deze mogelijkheid. Enkele promovendi die rond dezelfde tijd als ik zijn begonnen bij het ISI en tevens betrokken waren bij het onderzoek naar de holmium-microsferen wil ik graag in het bijzonder bedanken voor de mooie tijd: **Gerrit van de Maat, Hendrik de Leeuw** en **Mattijs Elschot**.

In de loop der tijd heb ik verschillende kamergenoten zien komen en gaan; naast mijn twee paranimfen wil ik graag **dr. Gerard Krijger** en **Bo van Leeuwen** bedanken voor de gezelligheid op de kamer.

Gedurende mijn promotietraject hebben naast de medewerkers van mijn afdeling(en) een aantal mensen van andere afdelingen binnen het UMC, maar tevens buiten het UMC, mij geholpen om zelfstandig onderzoeker te worden. Met betrekking tot mijn eerste publicatie (Hoofdstuk 4 van dit proefschrift) wil ik graag **dr. Patrick Derksen**, **Eva Vlug, Ron Schackmann**, **Livio Kleij** en **Miranda van Amersfoort** van de Afdeling Medische Oncologie, en **dr. Kristina Djanashvili**, **dr. Joop Peters** en **dr. Daniel**

Schühle van de Afdeling Biotechnologie van de TU Delft bedanken. Daarnaast heb ik zeer prettig samengewerkt met **prof. dr. Holger Grüll**, **dr. Sander Langereis, dr. Edwin Heijman, dr. Jeroen Pikketmaat, dr. Mariska de Smet, dr. Anke de Vries en Nicole Hijman** van de Afdeling Biomedical Engineering van TU Eindhoven en Philips Research Eindhoven. De elektronenmicroscopie afbeeldingen (Hoofdstuk 5) waren niet mogelijk geweest zonder de hulp van **dr. Wally Müller** en **Chris Schneijdenberg** van de Afdeling Biomolecular Imaging van Universiteit Utrecht.

Ondanks het feit dat ik verbonden was aan de Divisie Beeld en de knapste koppen binnen deze divisie dagelijks met multimodale beeldvorming werken, zijn de beste kwaliteit plaatjes nog altijd te verkrijgen via de Afdeling Fotografie. **Roy Sanders**, bedankt voor het opmaken van mijn posters voor congressen en **Karin van Rijnbach**, jou ben ik dankbaar voor het verzorgen van de lay-out van mijn proefschrift.

A special thanks goes out to **Mr. Kerry Randolph** from Phoenix, Arizona, USA, who has been so kind to create the cover of my thesis, including the wonderful optical illusion. Many thanks to you Kerry!

De *ex vivo* nieren, levers en andere organen van zowel varkens als konijnen zijn verkregen via het Gemeenschappelijk Dierenlaboratorium (GDL). In het bijzonder wil ik hiervoor **Nico Attevelt**, **Hester de Bruin** en **Anja van der Sar** bedanken.

Natuurlijk zijn er nog veel meer mensen die een bedankje verdienen. Ik kwam dagelijks in contact met de **medewerkers van Nucleaire Geneeskunde** en dan met name de **laboranten** en de **klinisch fysici**. Ook wil ik de **medewerkers** en in het bijzonder de **promovendi** van **Farmacie** bedanken voor de gezelligheid op en rond het lab.

Ik heb de kans gekregen om mij verder te ontwikkelen en bekwamen in het wetenschappelijk onderzoek in mijn huidige betrekking als postdoc bij de vakgroep 'Image-guided Molecular Intervantions' (kortweg 'de HIFU-groep' genoemd) onder leiding van **prof. dr. Chrit Moonen** en **dr. Clemens Bos**. Ik ben jullie dankbaar dat ik deze kans heb gekregen. Tevens wil ik **dr. Roel Deckers** bedanken. Al voordat ik postdoc bij de HIFU groep was geworden, hebben wij intensief samengewerkt aan de ontwikkeling van liposomen en micellen in combinatie met HIFU-triggered release, wat uiteindelijk tot twee gezamenlijke artikelen heeft geleid (Hoofdstuk 3 van dit proefschrift).

Bovenal wil ik **mijn familie** bedanken. Naast mijn **ooms**, **tantes**, **neefjes** en **nichtjes**, die waarschijnlijk nooit echt begrepen waar ik het over had als ik over mijn onderzoek begon, gaat mijn dank speciaal uit naar mijn lieve **oma** en (in gedachten) **opa Smid**, mijn zus **Marcella** en mijn zwager **Henjo**. Ik weet dat jullie trots zijn. **Pa** en **ma**, zonder jullie had ik dit onderzoek nooit kunnen voltooien. Ik wil jullie bedanken voor jullie steun en interesse, maar vooral jullie geduld tijdens het aanhoren van mijn frustraties over het onderzoek. Deze horde is nu genomen, de volgende horde is meer persoonlijk van aard. Jullie weten waar ik het over heb. En jullie weten dat ook dit goed komt. Ik houd van jullie.